Physico-Chemical and Microfluidic Approaches Toward Engineering Oscillating and Communicating Chemical Droplets

Kristian Torbensen

Université Pierre et Marie Curie

Ecole doctorale 388 : Chimie-Physique et Chimie Analytique de Paris Centre

Laboratoire PHENIX, UMR CNRS 8234, Equipe Colloïdes Inorganiques

Physico-Chemical and Microfluidic Approaches Toward Engineering Oscillating and Communicating Chemical Droplets

Par Kristian TORBENSEN

Thèse de doctorat de Chimie-Physique

Dirigée par Ali ABOU-HASSAN

Présentée et soutenue publiquement le 28 septembre 2016

Devant un jury composé de :

Mme. TAYLOR Annette	Professeur des Universités Université de Sheffield (Angleterre)	Rapporteur
M. BARET Jean-Christophe	Professeur des Universités Université de Bordeaux	Rapporteur
M. BAIGL Damien	Professeur des Universités UPMC Sorbonne Universités	Examinateur
M. GAMBY Jean	Chargé de Recherche au CNRS Université Paris Sud	Examinateur
Mme BROCHARD WYART Françoise	Professeur des Universités UPMC Sorbonne Universités	Examinateur
Mme CABUIL Valérie	Professeur des Universités UPMC Sorbonne Universités	Examinateur
M. ROSSI Federico	Professeur des Universités Université de Salerno (Italie)	Examinateur
M. ABOU-HASSAN Ali	Maître de Conférences, HDR	Directeur de thèse

Acknowledgements

First, I would like to thank my supervisor, Dr. Ali Abou-Hassan, for accepting me as his first Ph.D. student. It has been a pleasure to meet and work with such a dedicated person. I wish you all the best for the future.

I would also like to thank the jury members, in particular Annette Taylor and Jean-Christophe Baret, for judging my work and taking their time to come to Paris for my defence.

I also thank Sandra Ristori and Federico Rossi for our fruitful collaboration.

I also thank the entire group of the Phenix Laboratory at Université Pierre et Marie Curie, it has been a pleasure to be here.

I would like to thank the Phenix Laboratory and the doctoral school Université Pierre et Marie Curie for financing my Ph.D. education.

Finally, I would like to thank the city of Paris. It is, as Ernest Hemingway put it, a moveable feast that I will bring with me for the rest of my life.

To my dear Parents

Table of Contents

General Introduction

Generation, propagation and reception of (bio/chemical) information between individual organisms are the keystone of many intelligent communicating systems and are ubiquitous in Nature. Colonies of fireflies synchronize their flashes, and contraction and expansion of heart muscles are few examples among others, where bio/chemical signals generated by synchronized sources produce a cooperative behaviour. The objective of this thesis is to yield a proof of concept of a microchemical system, capable of produce and stock chemical information within individual microsized chemical reactors (microreactors), to generate, propagate and control the chemical communication and synchronization between individual microreactors. For this purpose, micrometric liposomes encapsulating chemical reactions, could serve as individual microreactors and vehicles of chemical information (communication). Encapsulating an oscillating reaction such as the Belousov-Zhabotinsky reaction in liposomes arranged in a network, would allow for spatio-temporal analysis of the propagation of chemical information, and the occurrence of cooperative effects due to synchronization of individual chemical communication sources. However, several obstacles must be overcome to achieve this goal, both in understanding the physico-chemical phenomena of communicative networks, but also in developing a reliable platform allowing for generating homogeneous and stable liposomes. It is the scope of this thesis to address these issues, providing understanding and knowhow, in order to engineer and develop liposome-based communicative networks. Microfluidics has proved suitable for generating monodisperse liposomes, and was hence chosen as the liposome engineering platform.

An example of propagation and reception of bio-chemical communication can be found in the neural cellular network present in all mammals. Propagation of information between nerve cells proceeds *via* the release of neurons, the messenger molecules, from vesicles in the pre-synaptic cell, as illustrated in Figure 1A. The neurons diffuse across the synaptic cleft and reach the post-synaptic cell, where they bind to target specific receptors. The neuron binding induce a conformational change in the receptors, giving rise to a signal being passed on via the post-synaptic cell. The neuron-receptor binding is irreversible, meaning that the neurons can be released from the receptor, diffuse back to the pre-synaptic cell, and be reincorporated in the pre-synaptic vesicles. To mimic such a communicative network of *in-vivo* cells, one needs to engineer an *in-vitro* system constituting a network of cell-like structures (shell-core structures) capable of releasing and taking up messenger molecules, as illustrated in Figure 1B. The pertinent issues here are, first, the capability of the cell membranes to hold and encapsulate chemical species constituting a reaction activated, or deactivated, by specific molecules, *i.e.,* the messenger molecules, while at the same time allowing these specific messenger molecules to permeate the membranes, in order to diffuse from one cell to another within the network. Second, the encapsulated chemical reaction must, as mentioned above, be of a kind sensitive to small perturbations in the concentrations of specific molecules, *i.e.,* the messenger molecules, in order to change, *e.g.,* in an activating (proceeding) or deactivating (ceasing) manner.

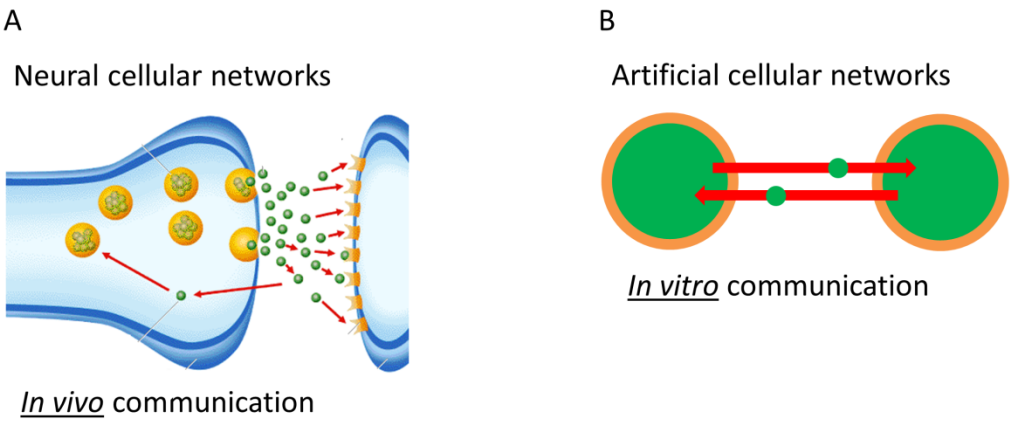

Figure 1. A) Communicative natural neural cellular network proceeding via diffusion of neurons between synaptic cells. B) Artificial communicative network of cell-like structures (shell-core structures) capable of releasing and taking up messenger molecules governing the state of an encapsulated chemical reaction.

To follow the aforementioned biomimicking approach, liposomes are chosen as the shell-core structures constituting the artificial cellular network. Liposomes are minute spherical sacs of phospholipids, the latter constituting the main part of cell membranes in all mammals. Due to their amphiphilic nature, phospholipids can self–assemble into globular bilayer structures encapsulating an aqueous core, as illustrated in Figure 2, hereby resembling natural cells. Encapsulating liposomes can be engineered using water-in-oil-in-water (w/o/w) emulsions as templates. Using microfluidics, the latter can be generated uniformly and with a high throughput. To obtain liposomes, the middle oil phase is subsequently removed. The entire process of generating encapsulating liposomes is illustrated in Figure 3. Finally, the Belousov-Zhabotinsky reaction was chosen as the chemical system to be encapsulated. This reaction oscillates over time, with the oscillation periods being governed by intermediates capable of crossing phospholipid membranes, as hence able to diffuse between individual liposomes arranged in a network. The above mentioned issues will be addressed in individual chapters in the thesis manuscript. Altogether, they will describe a multiscale approach with the overall objective to study the collective behaviour in a network of microreactors, or artificial cells, in a bio/chemical approach mimicking natural cellular networks.

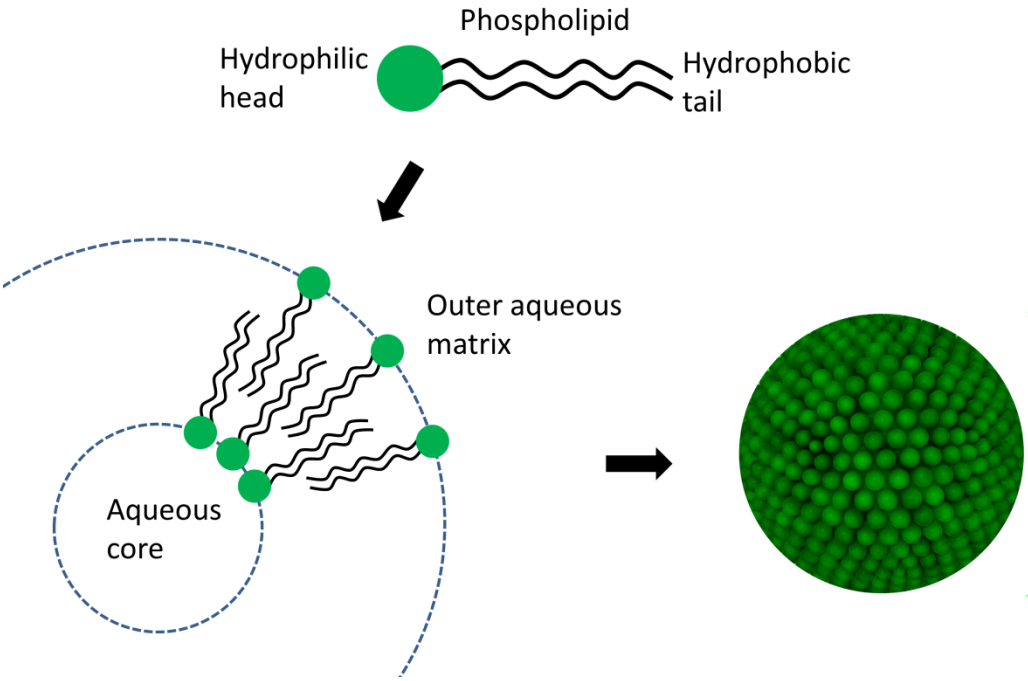

Figure 2. Illustration showing the principal of the self-assembly of amphiphilic phospholipids into globular structures encapsulating an aqueous core.

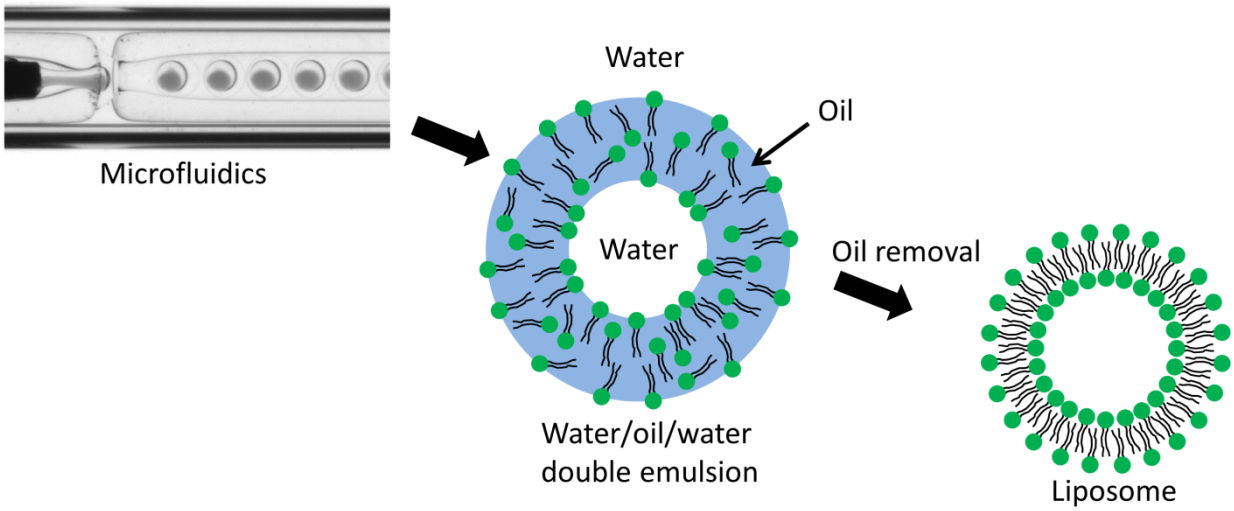

Figure 3. Illustration showing the principal of liposome formation by phospholipid membrane self-assemble *via* solvent removal from w/o/w double emulsions.

The thesis consists of five chapters, of which two have been accepted for publication and two have been submitted, each dealing with its own specific subject related to the formation of BZ-encapsulating liposomes. In some chapters, additional relevant experiments are described, that should serve as supplement to a "complete" chapter. In general, the main strategy was to understand the nature of chemical communication from a bottom-up approach, that is, to start with understanding the interaction of the BZ-reaction with lipid-based membranes, encapsulate and study the BZ-reaction in simple emulsions with lipid-based membranes, proceed to double emulsions for eventually to end up with liposomes. As the thesis deals with several different subjects, such as microfluidics, reaction-diffusion systems, physical chemistry and soft matter, it has brought its

author an insight into many interesting fields of chemistry, and trying to link these together has been both learning, exciting and challenging. The thesis does not contain a bibliographic part as such. Since we were invited to write a review article on chemical communication in microfluidic based droplet networks, this part will serve as the literature study. Below is a short description of each chapter, providing an overview of the content of this thesis. Each chapter in the thesis will have its own short introduction. Finally, the conclusions from each chapter are resumed, and an overall conclusion and perspectives are given. It is my hope, that the reader will enjoy reading it, as much as I enjoyed writing it.

Chapter I give an introduction to the Belousov-Zhabotinsky reaction. This is followed by an invited review article on microfluidic generated droplet based communicative networks, submitted to *Lab on a Chip*. The state-of-the-art within droplet based chemical communication is reviewed, providing an overview of the works and results. Also, this chapter serve as the bibliographic part of the thesis.

Chapter II deals with the interaction of the Belouvsov-Zhabotinsky reaction on phospholipid membranes in bulk solution. The BZ-reaction contains both charged species and organic molecules that can affect the properties of lipid membranes, such as the lammellarity. Small angle x-ray scattering (SAXS) is used to investigate these interactions, together with the effect of dopants, such as cholesterol, on lipid membranes. Furthermore, the effect of lipid membranes on the oscillatory behaviour of the BZ-reaction is described. This chapter is published in *Journal of Physical Chemistry B*.

Chapter III starts with an investigation on the influence of polyvinyl alcohol (PVA) on the BZ-reaction in bulk solutions. Since PVA is later used as a viscosity modulator for BZ-encapsulation by microfluidics, a sustainable oscillating system in the presence of PVA is sought. Chapter III also describes a communicative 1D network of simple emulsions droplets, stabilized by lipid membranes, encapsulating the Belousov-Zhabotinsky reaction. It is investigated, how various dopant molecules, *e.g.,* cholesterol affects the chemical communication between the droplets, by changing the lipid membrane properties. This part has been submitted to the *Journal of Physical Chemistry Letters*. Furthermore, an attempt to inhibit the BZ-reaction by illumination in the presence of a photosensitizer is described.

Chapter IV describes a reliable and easy-to-assemble coaxial microfluidic device for the generation of double emulsions, to serve as templates for liposomes. The versatility of the device is demonstrated by generating monodisperse double emulsions with different oil shell thicknesses, by manipulating the flow rates and the device geometry. This part is published in *Journal of Flow Chemistry*. The device is used to encapsulate and optimize the stability of double emulsions encapsulating the BZ-reaction. Also reported in this chapter are the attempts to produce liposomes upon solvent removal from double emulsions.

Chapter V reports on a peculiar phenomenon observed upon changing the composition of the oil phase in double emulsions. Under flow, certain double emulsions deformed, and eventually exhibited "tip-streaming", by which smaller double emulsions were formed. As this process removes some of the solvent from the oil phase, it is suggested that this method might allow for the formation of liposomes. Since only sparse literature exist on this topic regarding double emulsions, methodologies relating to tip-streaming of simple emulsion drops are adopted for understanding this phenomenon. However, by doing so, several pitfalls might arise. The content of this chapter is thus very much open for discussion.

Chapter I: Bibliography

I.1. Introduction

In this first part of this chapter, the Belousov Zhabotinsky reaction will be introduced. A short description of its main characteristic and features are provided. In the second part, chemical approaches to generate reaction-diffusion systems exhibiting chemical communication between microreactors will be reviewed. Such systems, consisting of confined volumes of the oscillatory Belousov-Zhabotinsky reaction arranged in various geometries, have proven a significant tool for modelling bio-physical networks and communicative pathways between microreactors. The review article has been submitted to *Lab on a Chip*.

I.2. Introduction to the oscillating Belousov-Zhabotinsky reaction

Until few decades ago, chemical oscillations were thought to be exotic reactions of merely theoretical interest. Now known to govern an array of physical and biological processes, these oscillations are being studied by several groups with various scientific expertise, from physics to biology. Among others, one of the most promising applications of chemical oscillators is their use as "signal transmitter/receiver", where reaction intermediates can be exchanged among different units to probe and study complex communication networks, or new forms of chemical computing. Here we will sketch the basic features of the Belouzov-Zhabothinsky reaction, and its use in communication tasks.

The Belousov-Zhabotinsky (BZ) reaction belongs to a class of chemical reactions exhibiting non-equilibrium thermodynamics. It constitutes a reacting chemical system, in which the concentration of one or more compounds exhibits periodic changes, resulting in the establishment of an autocatalytic nonlinear chemical oscillator. The BZ reaction essentially consists of an oxidation of an organic substrate (generally malonic acid) by bromate ions in a strongly acidic medium and in the presence of a redox catalyst (ferroin, cerium sulphate, ruthenium complexes, etc.). Figure 1 briefly summarizes the basic mechanism responsible for the onset of the oscillations in the concentration of some key intermediates, together with a typical spectrophotometric time-series. In addition to temporal oscillations, one of the most attractive feature of far from equilibrium chemical systems is their ability to generate patterns and shapes, either moving, pulses and waves, or stationary Turing structures, starting from a spatially homogeneous reactive medium, a phenomenon known as symmetry breaking. Thanks to these peculiarities, chemical oscillators have long been regarded as possible models for biologically and physiologically related open questions, such as morphogenesis, cardiac pathologies, calcium signalling dynamics, etc.

A further step in complex systems modelling has been achieved by combining the BZ reaction with self-assembled amphiphilic matrices, such as micelles, vesicles, emulsions. Current major research lines on the BZ-type oscillators, involve network dynamics, where the interest is focused on the emergence of collective behaviour when several single oscillators are coupled together, either locally or globally, through the exchange of chemical intermediates.

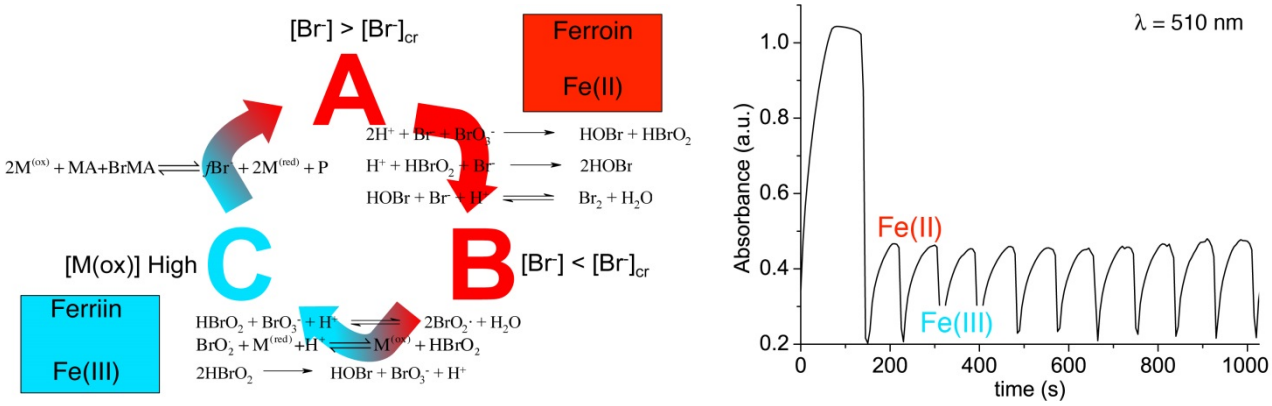

Figure 1. Left panel describes the oscillating mechanism of the BZ reaction: Three key steps are the basic backbone of a much more complex kinetic mechanism. Briefly, the concentrations of Br^- and the oxidized form of the catalyst act as switchers among the three processes, (A) Br^- ions are consumed to yield bromine and bromous acid $HBrO_2$, (B) the autocatalytic species $HBrO_2$ oxidize the catalyst and (C) the catalyst is reduced by the organic substrate to yield Br^- and restart the cycle. The squares in the corners illustrate the colour and redox state changes of the catalyst (ferroin). Right panel: A spectrophotometric time-series (absorbance maximum of ferroin) illustrates well the temporal oscillatory behaviour of the reaction.

The appearance of complex temporal or spatio-temporal phenomena has been observed in arrays of BZ micro droplets, lattices or bulk systems of catalyst-loaded resin microparticles. The dynamical behaviour of the system and/or the pattern selection is generally determined by the type and magnitude of the coupling strength; which is a function of the experimental parameters such as reagent concentration, stirring and illumination.

During each oscillatory cycle, the BZ-reaction produces several chemical intermediates having different physico-chemical properties (charge, hydrophobicity, etc.). Some of them act as oscillations inhibitors, like Br^- or Br_2, which bring the system in a reduced state preventing the formation of the autocatalytic species. On the contrary, activators like $HBrO_2$ or the catalyst promote oscillations. When single oscillators are physically separated by a barrier, or by a solvent immiscible with water, the intermediates can be used as messengers to deliver chemical information among different single units. By exploiting the different properties of the intermediates, it is possible to choose the barriers in order to have a specific type of coupling (global, inhibiting or activating) and the corresponding feedback on the oscillating mechanisms.

Another important issue for controlling the communication dynamics in networks of chemical oscillators is the way the signal leaves one unit to reach its neighbours. For example, messenger molecules can target a specific area or they can uniformly spread in the surrounding environment, depending on the dynamical behaviour of the chemical oscillator inside a single

compartment (see Figure 2). One of the crucial parameters influencing the global dynamics of the BZ-reaction is the medium homogeneity. In the absence of any macroscopic concentration gradients, the system oscillates uniformly in space (homogeneous oscillations). On the contrary, when spatial gradients are present, the BZ behaves as a reaction-diffusion system generating fronts, pulses or waves.

When the BZ system is confined in a vesicle, when no stirring is possible, the critical parameter responsible for the homogeneity of the system is the size of the vesicle, *i.e.,* its diameter $\emptyset$. Therefore, if the time of diffusive mixing within a single droplet, $t=\emptyset^2/2D$ (with $D \approx 1\times10^{-5}$ cm^2/s, the typical diffusion coefficient of aqueous species), is smaller than the period of oscillation T, an individual BZ vesicle can be considered homogeneous.

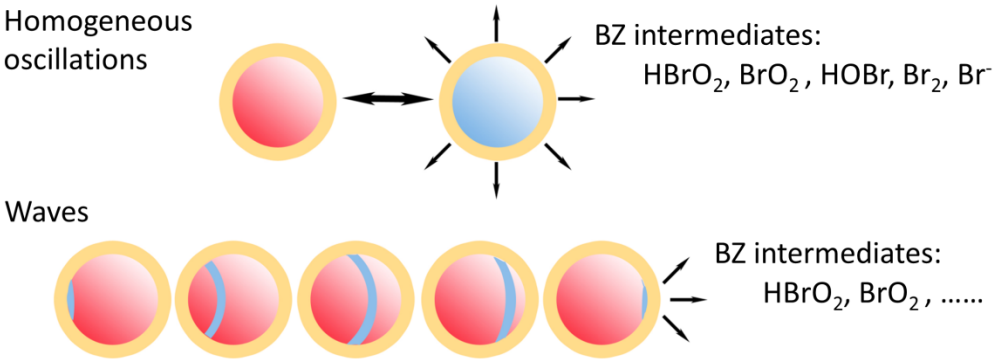

Figure 2. BZ intermediates (chemical signals) are released from each single vesicle in a fashion that depends on the spatio-temporal dynamics of the confined oscillator. If the system oscillates homogeneously, chemical intermediates do not have any preferential release direction. If a pulse is triggered in a precise point, the signal will follow the direction of the wave propagation to reach a specific target area.

As sketched in Figure 2, the type of dynamical behaviour inside the droplet dictates the directionality of the signal propagation outside the membrane. Bulk oscillations generate an isotropic distribution of the BZ intermediates in the inner aqueous phase, which, in turn, may cross the amphiphilic barriers in each point of the membrane. Pulses or chemical waves, on the contrary, are directional signals propagating along a straight line, which can be controlled to deliver information to a precise target.

In the following part, the BZ-reaction used for the generation and study of communicative networks is reviewed.

I.3. Chemical information and dynamics of droplet emulsions in networks of Belousov-Zhabotinsky micro-oscillators produced by microfluidics

Kristian Torbensen,[a] *Federico Rossi,*[b] *Sandra Ristori,*[c] *and Ali Abou-Hassan*[a]*

[a]Sorbonne Universités, UPMC Univ Paris 06, UMR 8234, Laboratoire PHysico-chimie des Electrolytes, Nanosystèmes InterfaciauX (PHENIX), 4 place Jussieu - case 51, 75252 Paris cedex 05 – France

[b]Department of Chemistry and Biology, University of Salerno, Via Giovanni Paolo II 132, Fisciano (SA), Italy

[c]Department of Earth Sciences & CSGI, University of Florence, Via della Lastruccia 3, 50019 Sesto Fiorentino, Firenze, Italy

ABSTRACT:

Chemical communication is ubiquitous in nature. Synchronization of dynamic elements is a widespread phenomenon with biological, physical and chemical importance. Such synchronization, *via* chemical communication, can be described as a reaction-diffusion system where messenger molecules diffuse from one element to trigger a reaction in another. In this Focus Paper, we review a number of articles reporting various approaches to generate reaction-diffusion model systems exhibiting chemical communication between microreactors using microfluidics. These systems consist of micro compartments containing the oscillatory Belousov-Zhabotinsky reaction. Arranged in different configurations, these communicative microreactors serve to mimic various types of bio-physical networks, aiding to comprehend the concept of chemical communication.

INTRODUCTION:

The generation, propagation and reception of bio/chemical information between individual organisms are the keystones of many intelligent communicating systems.[1] The transmission of a signal at the level of an individual generator-receptor couple is for example the basis for the bio/chemical signal transmission in neural synaptic communication.[2, 3] The propagation of a signal wave-front among different individual sources is then associated with the synchronization of the

sources and the observation of cooperative phenomena.[4] Such cooperative effects are ubiquitous in nature: The cooperative and synchronous flashing in colonies of fireflies, in cardiac pathologies related to the heart muscles cooperative contraction/expansion, in morphogenesis, calcium signalling dynamics, decentralized bacterial quorum sensing, etc.[1, 2] Specifically, in cell populations, a variety of dynamical behaviours have been reported, ranging from a single synchronization state to multiple synchronization states, which reflect different degrees of communication.[5] At the extremities, synchronization in nature occurs, on the smallest scale, as simultaneously moving electrons in superconductors, and at the largest scale, as planetary systems hurled by gravitational synchrony.[6] At the level of unicellular organisms, cooperation and synchronization occurs *via* chemical communication based on a chemical messenger diffusion/reaction which extends over a wide range of time and length-scales.[7, 8] Inside a cell, within trans-membrane protein machines, chemical communication is restricted to the nanometer scale. However, in many other examples, chemical reagents are able to cross biological membranes and be transported to their target by diffusion over larger distances in an aqueous environment. For instance, the nervous system involves micron-scale chemical communication during synaptic communication from neurons to axons.[9] Diffusion of chemical reagents over even longer distances (hundreds of micrometers and more) in the extracellular solution is believed to be responsible of the large-scale collective behaviours of colonies of unicellular organisms. Comprehending such long-range chemical communication is also important for the development of biomimetic networks, new forms of chemical computing or attempts toward artificial human-like nervous systems.[10] In this field of research, the biomimetic approach often concerns artificial compartments emitting chemical signals.

Synchronized and cooperative behaviour are also widely exploited in our everyday life through information and communication technology (ICT). The most fascinating novelties in modern science consist of using biological paradigms for developing new technologies. One of the most interesting is the bio/chemical-information and communication technology (bio/chemical-ICT),[9-11] which aims at extending the well-known field of ICT, classically based on the transmission of electrical or electromagnetic signals, to the bio/chemical world of molecules.[12, 13] In a biomimetic approach, it has been proposed to carry chemical information into individual encapsulated microchemical reactors and to propagate chemical information between them. Such biomimetic naturally occurring information processes can provide a basis for unconventional computing strategies. For example, the development of microchemical-ICT tools, such as a

microchemical-computer, is amenable from the control of the spreading of chemical information wave-front between individual microreactors. By mimicking hardware computing platforms, the individual encapsulated microchemical reactors should be guided in a geometrically constrained media (channels) to different logical or counting gates obtained from the geometrical arrangement of microreactors.[10, 12, 14]

More than a conceptual microchemical computer, other fundamental and applied objectives are sought through the development of such a chemical-ICT. Among them, it is proposed to generate and control the synchronisation and the propagation of chemical information from individual microreactors. This approach should mimic and then help understanding fine level of chemical communications involved in more complex systems, such as living organisms. Microfluidics is here an excellent choice of means to fabricate bio mimicking microreactors; droplet-based microfluidics is a powerful tool for encapsulating biological entities and chemical reagents in artificial micro-compartments with monodisperse size, mostly constituted by water in oil microdroplets.[15-18] They are generally used for the high through-put screening of reactions for their ability to compartmentalize materials in libraries of isolated chemical micro-reactors.[19] As in nature, chemical communication plays an essential role in these artificial micro-reactors, and is obtained in various modalities, either within the encapsulated entities, between the interior and the outside of the compartment (partition), or between neighbouring compartments. The leakage (or partitioning) of chemical information from individual microreactor within a network, to its external environment has been detected and modelled. Communication between compartments can be explained by the generation of intermediates that allow for the spatio-temporal propagation of chemical information. This phenomenon eventually leads to the production of collective behaviours such as coupling and synchronization, which is promising for the development of complex communication in droplet networks.

An extensive general review on the potentiality of "active" droplets outside of equilibrium, from nano- to millimetre sized scale, has been recently published.[20] In this review, we focus on a biomimetic model of chemical communication proceeding *via* a reaction/diffusion pathway. In particular, we will make an overview of a non-equilibrium chemical system, specifically the autocatalytic Belousov-Zhabotinsky (BZ) oscillating reaction,[21, 22] encapsulated or confined in nano- or micro sized compartments. The BZ reaction is driven by the oxidation of an organic substrate, e.g. malonic acid, by bromate in an acidic solution in the presence of a catalytic specie in the form of an organo-metal complex such as ferroin (a phenanthroline-iron(II) complex). Due to

the chromogenic and redox activity of its ferroin catalyst and the generation and consumption of both excitatory and inhibitory intermediates, the BZ reaction is a pertinent model to illustrate the complexity of communication in chemical systems. The compartmentalization of the BZ reaction in individual nano- and microreactors, microparticles, vesicles, polymersomes, or aqueous microdroplets, has been used as a model system to investigate short and long-range chemical communication between microreactors configured in various configurations, from linear arrays to network with intricate geometries and multiple connections.[7, 23-36] The communication between individual compartments is then explained by the generation and diffusion of the excitatory/inhibitory intermediates, which serve as messenger molecules for the spatio-temporal propagation of chemical information. For a more thoroughly review on the BZ reaction, we encourage the reader to consult these articles.[37-41]

Numerous investigations of the BZ reaction in bulk solution have been published since it was first described in details,[42] and various wave patterns propagating in solution have been reported. In such systems, the wave propagation is governed by a locally initiated signal transmission, causing the signal to suffer from diffusion broadening. To deliberately uni-direct a propagating wave signal, Ginn et *al*.[43] fabricated a microfluidic device where two BZ containing chambers were connected *via* a microchannel, see Figure 1.

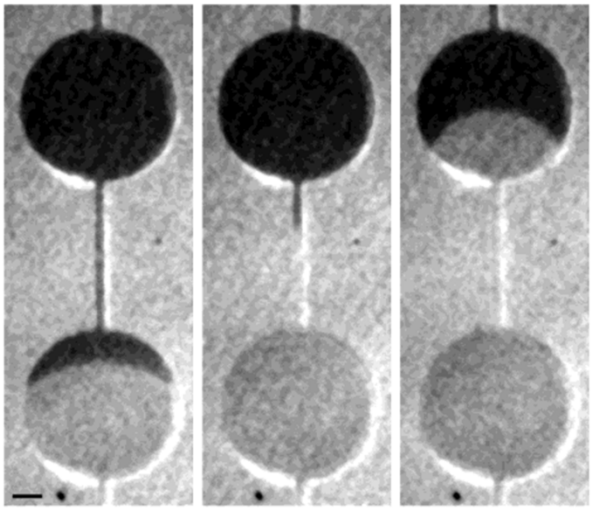

Figure 1. Oxidation wave traveling through a BZ system in a patterned microreactor. The channel has a height of 80 μm and a width of 50 μm. The circular portion of the reactor has a diameter of 1 mm, and the length of the reference bar (A) is 200 μm. Initial BZ concentrations are 1.50 M H_2SO_4, 0.15 M 1,4 cyclohexanedione, 0.10 M $NaBrO_3$, and 3.1 mM ferroin. The snapshots are separated by 10 s. Reprinted from ref.43 with permission of the American Chemical Society.

In the following sections, we will review different reports having attempted to optimize and quantify the chemical communication between networks of microoscillators. In the scope of this journal, the emphasis will be on systems elaborated using microfluidics. However, other approaches to describe chemically communicating systems will be explored. It exist a conspicuous literature[44-49] on theoretical approaches to describe communicative networks of diffusively coupled oscillators; in the framework of micro-sized confined systems, Vanag et *al*.[50-52] analysed numerically the coupling between micro oscillators for both homogeneous and heterogeneous systems, *i.e.,* systems in which both activator and inhibitor of the oscillators can diffuse freely or are coupled *via* messenger molecules, respectively. Holley et *al.*[53] modulated propagating waves in oscillating vesicles connected in various networks. The influence of the spatial geometry, network connectivity and interacting waves was investigated with the purpose of generating logic gates. Also, the influence of microfluidic entrapment on the kinetics of autocatalytic reaction was recently investigated.[54]

The BZ reaction confined in simple reactor networks as a model oscillatory system*:*

Coupled compartmentalized oscillators have been generated and studied by Toiya et *al.*,[25] The microfluidic device, shown in Figure 2A, was employed to generate BZ containing aqueous droplets separated by octane. The authors here showed the experimental significance of the geometric restrictions of the BZ containing droplets; to obtain a homogeneous system within each droplet, the period of oscillation was required to be less than the time of diffusive mixing in the droplet. To observe any coupling between droplets, the same restriction concerns the time of diffusion *via* the droplet spacing medium. The oscillation dynamics was found to be rather sensitive to the concentration of the BZ component malonic acid (MA); at higher concentrations, anti-phase oscillation between neighbouring droplets was observed. For intermediate and smaller concentrations of MA, the system reached stationary *Turing* patterns, occurring after a few anti-phase oscillation periods or immediately, respectively. Bearing in mind that MA is involved in the generation of the BZ inhibitor bromine, a relative hydrophobic molecule capable of partitioning in the oil phase, these observations lead the authors to speculate whether this intermediate specie was responsible for the communication between the droplets. Indeed, by adding a scavenger for bromine to the organic phase separating the BZ droplets, communication ceased to occur, and the droplets

oscillated independently. The analysis was based on space-time plots constructed from time-series of images, as shown in Figure 3A. Computer simulation based on the FKN-model, including the BZ excitatory specie bromine dioxide radical, lead the authors to the conclusion that for the experimental conditions applied here, the inhibitory coupling by bromine was dominant. In order to investigate these findings on a more quantitative basis, Delgado *et al.*[31] exploited the photosensitivity of an additional co-catalyst to trigger the production of bromide within individual drops, thus inhibiting oscillations within the drops exposed to light. Figure 2B shows the microfluidic device used to generate arrays of micro oscillators. Experimentally it was shown that such a drop with high bromide concentration positioned in the center of a 1D array of in-phase oscillators, emitted, upon ceasing illumination, a sufficient amount of bromide to cause neighbour drops to display out-of-phase coupling. Eventually, this caused the fraction of in-phase drops to decay monotonically, resulting in the entire array to oscillate out-of-phase. The perturbation of the in-phase oscillation was furthermore found to depend on the initial concentration of MA in the drops; higher concentrations resulted in weaker coupling and thus prolonging the time to attain anti-phase synchrony with a phase shift of exactly 180°. Numerical simulations based on an open system, *i.e.,* the drops surveyed being positioned far from the boundaries, confirmed these findings. Restricting the number of oscillating drops by applying boundary conditions set by non-oscillating drops, and setting the initial phase of the surveyed drops by external light forcing, the authors observed the same general out-of-phase behaviour. However in this case, due to the influence of the close by boundaries, the out-of-phase behaviour deviated slightly from the ideal 180° anti-phase synchrony.

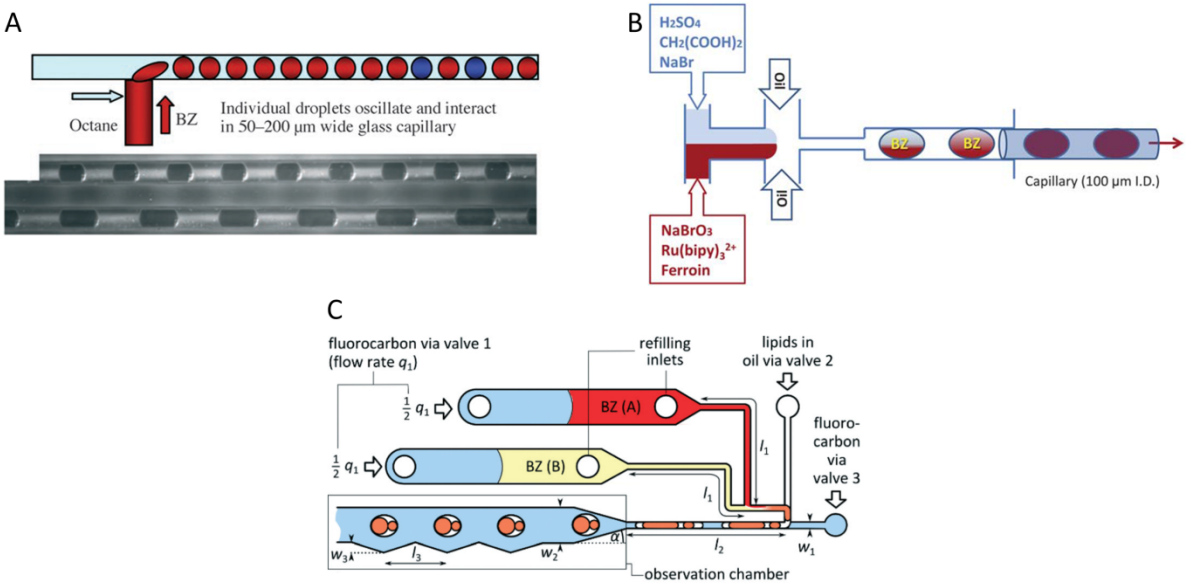

Figure 2. (A) Schematic representation of the microfluidic device. Red droplets correspond to the reduced form of the catalyst (ferroin), blue droplets to the oxidized form (ferrin). Below: Snapshot of two capillaries with droplets. BZ droplets with convex surfaces are dark due to ferroin. Horizontal length of the frame and inner diameter (ID) of the capillary are 4.8 mm and 150 mm, respectively. Reproduced from ref.25 Copyright© 2008 Wiley-VCH Verlag GmbH & Co. KGaA. Reproduced with permission. (B) Schematic drawing of the microfluidic PDMS device drop generator. At left, two different aqueous streams containing complementary reactants of the BZ solution are injected into the drop generator (light blue and red). The streams merge and co-flow down a central channel, meeting two perpendicular oil flows that generate BZ droplets in a nozzle. The co-flow of the BZ solution is preserved immediately after the drops are formed, but complete mixing takes place in less than 1 s. A glass capillary (100 mm ID) was inserted in the PDMS chip a few millimetres downstream from the nozzle to collect the BZ droplets. Reproduced from ref.31 with permission from the Royal Society of Chemistry. (C) Layout of channels on the microfluidic chip. The fluorocarbon phase supplied via valve 1 pushes BZ components A and B. The 'refilling inlets' were closed during the operation of the valves. The opening angle of the inlet to the observation chamber was $\alpha \approx 30°$. This smooth widening prevented fragmentation of the larger drops. The notches at the sidewall of the chamber served as traps for the capsules, allowing for their immobilization during monitoring of the progress of reactions. The lengths of the channels were $l1 = 17$ mm and $l2 = 9.5$ mm. The widths of the inlet and outlet channels at all three T-junctions were equal to $w1 = 0.3$ mm and their depths $h1 = 0.3$ mm. The width of the chamber was $w2 = 2$ mm, the depth was $h2 = 2$ mm, and the sizes of the notches were $w3 = 0.3$ mm by $l3 = 2$ mm. Reproduced from ref.35 with permission from the Royal Society of Chemistry.

Li *et al*.[33] confirmed the role of the BZ intermediate bromine as the main messenger specie in the inhibitory coupling between BZ drops. By increasing the initial bromate concentration, and decreasing the MA concentration in the BZ drops, excitatory coupling leading to in-phase synchrony between neighbour drops was observed, see Figure 3B. Thus, in these conditions, the inter-droplet diffusion of the excitatory intermediate bromate dioxide radical plays a significant role. Based on finite element analysis, the authors suggested a theoretical model for the coupling strength between BZ drops separated by fluorinated oil, as the ratio between the diffusive flux and the consumption of the inhibitor specie bromine. The transition from weak to strong coupling transforms the dynamical phase behaviour from out-of-phase to in-phase. The possibility of cross-diffusion, *i.e.,* diffusion of one specie induced by a concentration gradient of another, has been investigated for other BZ species.[29, 55] In a microemulsion, cross-diffusion coefficients were established for various species like bromine, bromide, ferroin, bromate, etc.[29, 55, 56] These results suggest that a more complex diffusion-reaction pattern is occurring in the communication pathway

between BZ droplets (see also Vanag et *al*.[57] for a complete overview on the effects of cross-diffusion on pattern formation). Moreover, cross-diffusion can also generate hydrodynamic motions, if the dimensions of the reactor allow for bulk movements, thus potentially affecting the information delivery among single oscillators.[58-60] More complex synchronization patterns, shown in Figure 4A, were observed for higher order (1.5D and 2D) arrays.[28] Okano *et al*.[26, 30] studied the phase synchronization of a 2D array of BZ cell elements in a gel matrix. Using an external light source to locally trigger the photosensitive BZ reaction, the authors described the correlation between the illumination time and coherent resonance within the cell array. It was also established that larger arrays were more sensitive to external perturbations. Tompkins *et al*.[61] employed 1- and 2D arrays of BZ drops suspended in oil to test the Turing model for morphogenesis.[62] By tuning the coupling strength via drop size and MA concentration, the authors were able to generate the spatiotemporal chemical structures predicted by Turing. Due to the heterogeneity of the experimental setup, *i.e.,* the diffusion of trigger molecules between BZ drops occurs through an oil phase, in contrast to the homogeneously coupled cells employed in Turing's prediction, an additional structure was found. Tompkins *et al*.[34] also investigated the evolution of the phase difference between BZ drops in different constellations as illustrated in Figure 4B. They demonstrated the ability to perturb the phase differences by setting different boundary conditions, e.g. applying constant concentration or non-flux boundaries to their system. In order to model neurotransmission signalling, which is typically unidirectional and occurs *via* discrete pulses of mass exchange in contrast to continuous mass diffusion, Horvath *et al*.[63] performed an experiment with pulse-coupled oscillators. The coupling strength between two oscillators was controlled by varying the concentration of the inhibitor specie bromide in one oscillator as a function of the oscillatory signal in the other. By adjusting the time delay, analogue to the delay in neurotransmitter release due to signal transduction, between signal and bromine concentration variation, different resonance patterns were observed. A similar method was employed by Weiner *et al*.,[64] Holz *et al*.[65] and Fukuda *et al*.,[23] conducting experiments and numerical simulations on the pacemaker entrainment of a 1D arrangement of ion-exchange beads loaded with a BZ catalyst, and submerged in a catalyst free BZ solution. It was demonstrated how the signal wave induced by the pacemaker bead propagated along a chain of beads, and that the propagation strongly depended on the inter-bead distance, with a critical distance beyond which no entrainment occurs. The same experimental system extended to a 2D array[24] led to equivalent conclusions.

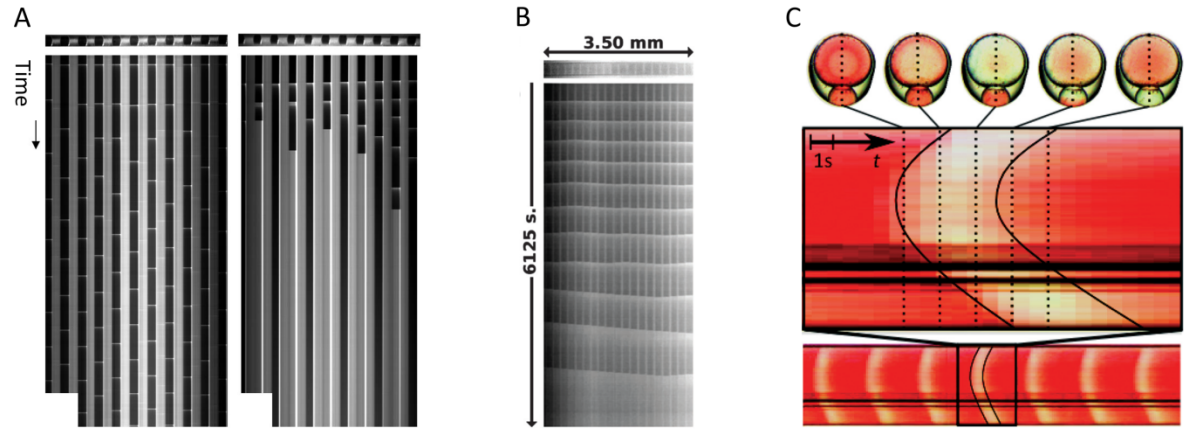

Figure 3. Examples of space-time plots obtained by stacking consecutive images of the droplet arrays shown top-most in each image. (A) Anti-phase oscillations with spikes of oxidation of ferroin seen as light horizontal lines across BZ droplets and (left) stationary Turing structures with alternating oxidized and reduced states evolving from an initial oscillatory state. Horizontal lengths of the frame and the capillary ID are 4.8 mm and 150 mm, respectively; the total times are 5200 s (right) and 10 800 s (left), respectively. Patterns extend to the left and right of the segments shown. Reproduced from ref.25 Copyright© 2008 Wiley-VCH Verlag GmbH & Co. KGaA. (B) In-phase patterns: photographs of drops in capillary and (below) Space-time plots. Droplet diameter is 150 μm and the distance between droplets is 36 μm. Reproduced from ref.33 with permission of the Royal Society of Chemistry. (C) Cuts of the snapshots of a BZ-doublet along the dotted lines (top) collected on a single time-plot (middle and bottom). One can notice the parabolic shape of the white stripe representing the chemical wave of the oxidized catalyst expanding from the center of the larger droplet (the black solid lines are guide to the eye) because in the center, the concentration of activator first exceeds the threshold for selfexcitation. The wave propagates outwards, passes through the facet between the droplets and propagates through the small drop. The long-time dynamics can be inferred from a stack containing multiple sequences of oscillations (bottom). Reproduced from ref.35 with permission of the Royal Society of Chemistry.

Resin beads were also employed in a stirred bulk solution by Taylor et *al.*[7] Here, they investigated the oscillating behaviour as a function of stirring rate and bead density. Upon decreasing the stirring rate, and thus the exchange rate between the beads, a gradual decrease in both oscillation amplitude and period was observed. Below a threshold stirring rate, the beads became totally desynchronized. Increasing the bead density, which correspond to a stronger coupling, resulted in synchronized oscillation. In another work by Taylor et *al.*,[66] the same system was applied to demonstrate how clusters of synchronized oscillators can emerge within a group of oscillating beads. The authors found coherence between the coupling strength and the number of clusters in a group; high exchange rate of the BZ inhibitor bromide resulted in several clusters, while a homogeneous system, i.e. a single cluster, was observed for a high exchange rate of the activator bromous acid. This is in line with previous findings for coupled BZ droplets; weak

coupling, i.e. inhibitory coupling, usually generate desynchronized oscillators, and conversely for strong excitatory coupling. Similar results were also obtained with hydrogels[67] and micrometre sized inorganic clay particles;[68] gels and particles were functionalized with ruthenium and/or ferroin and employed to study the global behaviour of a network of independent oscillators arranged in various geometries.

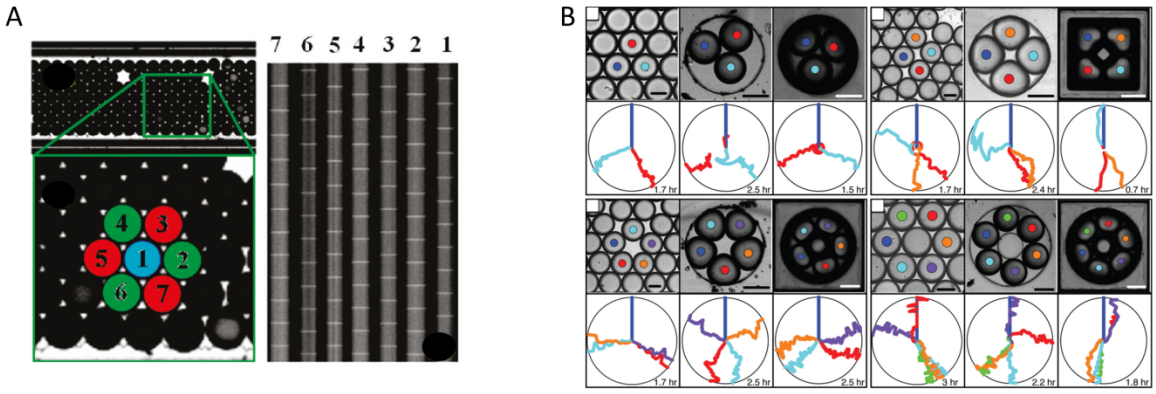

Figure 4. (A) Three-phase oscillatory clusters in a 2D configuration of BZ drops. Drop diameter is 128 μm. Initial concentrations: $[H_2SO_4]$ = 0.08 M, $[NaBrO_3]$ = 0.29 M, [MA] = 0.64 M, [Ferroin] = 3 mM, [NaBr] = 0.01 M, and $[Ru(bpy)_3]$=1.2 mM. Reproduced from ref.28 Copyright© 2010, American Chemical Society. (B) Network patterns observed from ring networks of three, four, five, and six members with constant-concentration and no-flux boundary conditions. Top: Images of the networks with the oscillating drops colour coded as below. All scale bars are 100 μm. Bottom: Radial-phase-time plots of the networks above. Left: Circular networks with constant-concentration boundary conditions implemented *via* optical isolation in close-packed drops. Only the colour coded drops are oscillatory; the other drops are optically inhibited. Middle: Circular networks with constant-concentration boundary conditions implemented in thin PDMS with optically inhibited drops in surrounding channels. The surrounding channels are not shown. Right: Circular networks with no-flux boundary conditions implemented in etched silicon. Reprinted with permission from ref.34 Copyright© 2015, American Institute of Physics.

Chemical communication between BZ droplets via surfactant bilayers:

As described above, for microreactors separated by an oil film, bromine is the main messenger molecule diffusing between the microreactors, thus promoting inhibitory coupling as the most frequent phenomenon. However, for microreactors brought into close contact, where coalescence is avoided by adding a surfactant to the oil phase, nanometer thick bilayers between the microreactors are formed. This facilitates mass transfer of less hydrophobic molecules, such as the BZ activator bromine dioxide radical, between the micoreactors. Thutupalli *et al*.[27, 69] demonstrated

this by generating BZ drops suspended in oil containing the surfactant monoolein. When drops were separated by even a small volume of oil, the coupling remained inhibitory, whereas drops in contact only separated by a monoolein bilayer exhibited excitatory in-phase synchrony, see Figure 5A. This was neatly demonstrated for both 1- and 2D arrays of microreactors. Rossi et *al*.[36] showed how chemical coupling of BZ microemulsions, locally separated by a phospholipid bilayer, eventually transformed an initial out-of-phase synchrony into excitatory in-phase synchrony *via* trans bilayer diffusion of bromous acid. A schematic illustration of this messenger pathway is shown in Figure 5B. Guzowski *et al*.[35] encapsulated pairs of BZ droplets in an oil drop containing phospholipids, see Figure 2C. At the contact point, a lipid bilayer membrane was formed between the droplets. They demonstrated how resonance between chemical oscillators depends on the relative volumes of the droplets; smaller drops eventually became in-phase synchronized with the larger ones by excitatory coupling, see Figure 3C.

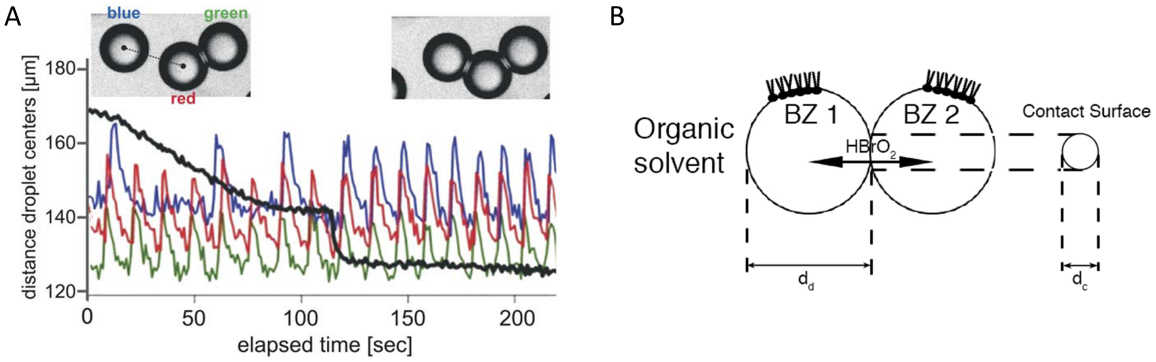

Figure 5. (A) Effect of membrane formation upon the phase coupling of chemical oscillators. The blue, red, and green traces represent the transmittance of the three droplets shown in the insets as a function of time. The black curve shows, on the same time axis, the distance of the 'blue' from the 'red' droplet (measured center-to-center). Clearly, the oscillations couple in phase as soon as the membrane is formed (jump in the black curve), but not before. Reproduced from ref.27 with permission of the Royal Society of Chemistry. (B) Sketch of a double emulsion system where two droplets are in touch. d_d is the droplet diameter and d_c is the diameter of the contact surface between two droplets, which has been approximated to a circle.

Chemical communication between BZ encapsulating liposomes:

Tomasi *et al.*[32] described, for the first time, the encapsulation of the BZ reaction encapsulated in liposomes by employing a flow focusing microfluidic device (see figure 6A). This

novel system provided the opportunity to study chemical communication between cell-like structures composed of a 1,2-dimyristoyl-*sn*-glycero-3-phosphocholine (DMPC) membrane, in a purely aqueous environment (see Figure 6B). This implied a high extent of partitioning of all the BZ species, some of them capable of crossing the phospholipid membrane, thus allowing exploring chemical communication pathways in a different environment with respect to the water-in-oil micro-droplets. In this case, the microfluidic technique granted the best experimental method to obtain giant-sized (100 – 300 μm) liposomes in the presence of the acidic and oxidizing medium of the BZ reaction. Other techniques of liposome formation, such as the *droplet transfer method*,[70, 71] were effective for the formation of millimetre sized water-in-oil emulsions, but failed when droplets were dispersed in an aqueous medium. By using electrochemical techniques, it was possible to characterize the behaviour of the oxy-bromine intermediates at the interface between a hydrophilic and a hydrophobic medium, both in the presence and in the absence of a lipid membrane.[32, 72] The main outcome was the unambiguous identification of brominated species as the messenger molecules between different compartments; this, together with numerical simulations, allowed to assess the activatory-type coupling which carried the signal transmission through oxidation waves at the points of contact between different liposomes. A typical pulse transmission is depicted in the Figure 6B. The liposomes generated by means of microfluidic techniques represent an interesting system to study the influence of the membranes on the communication dynamics in the network of chemical oscillators. In fact, to control the chemical communication, the membranes could be engineered to be selectively permeable to specific messenger molecules.[73] In practice, by using different dopants to be intercalated into the DMPC lipid bilayers, it was possible to tune some of the membranes properties, such as the lamellarity, the permeability and the local curvature, that, in turn, may influence the signal–transmission. Specifically, the effect on the membranes structure of dopants like cholesterol, myristic acid, sodium tetradecyl sulphate and tetradecylamine was studied by Small Angle X-ray Scattering and the role of each dopant on the oscillatory dynamics was investigated for micro-sized water/lipid/oil simple emulsions.[74] The introduction of bilayer intercalating species brought about new dynamical regimes with respect to the pure DMPC membranes, where, for simple emulsions, it was found a mostly inhibitory-type coupling, with alternate droplets oscillating with the same periods and phase. The presence of the bromine-scavenger cholesterol induced the formation of weakly phase-coupled patterns, while, the presence of the anionic surfactant, sodium dodecyl sulphate, promoted a strongly coupled system with the presence of phase-lock states between alternate oscillators.

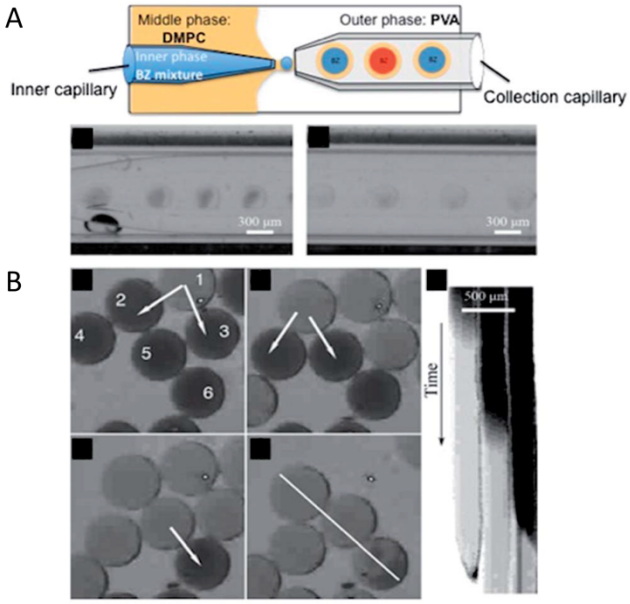

Figure 6. (A) Cartoon showing the coaxial microfluidic device and schematizing the encapsulation process. (B) Formation of the BZ/O/W double emulsions in the microfluidic device at the entrance (below left) of the collection capillary and (below right) at the exit of the collection capillary, time elapsed 80 s. (B) The pulse transmission across the touching liposomes after solvent evaporation. White arrows indicate the direction of pulse propagation. (Left): Image showing the space–time plot of liposomes 2, 5, 6 along the white bar. (B) Consecutive images showing a wave front propagating through three liposomes, along with the corresponding space-time plot. Reproduced from ref.32 with permission of the Royal Society of Chemistry.

CONCLUSION:

Chemical approaches to generate reaction-diffusion systems exhibiting chemical communication between microreactors have been reviewed. Systems consisting of confined volumes of the oscillatory Belousov-Zhabotinsky reaction arranged in various geometries have proven a significant tool for modelling bio-physical networks and communication pathways. The pertinent chemical species responsible for the chemical communication in these systems are, mainly, the inhibitory bromine and the excitatory bromine dioxide radical. However, other ionic species, such as Br^- and $HBrO_2$ may play an important role. Since their concentrations are governed by the experimental conditions, various coupling patterns are achievable, *i.e.,* the phase shift between different oscillators is tuneable. In this respect, membranes and surfactants confining the microreactors play a significant role; they can promote preferential communication pathways or act

as specific scavengers for messenger molecules, thus allowing a fine-tuning of the general dynamical properties of the chemical oscillators networks. Droplet arrays separated by an organic medium represent a valuable tool for investigating the motion of chemical species through long distances, compared to the molecular scale, and for engineering coupled aqueous domains. The applications of such systems are not entirely defined yet, though they are considered as prototypes for many innovative and technically sophisticated devices. However, the most challenging configurations are those in which both the internal and external compartments (where signal emitters are produced and exchanged) encompass an aqueous medium. Semipermeable membranes surrounding oils or water droplets also represent a boundary region whose properties are still being investigated. In general, due to their "soft" nature, the means to study compartments separated by mono or multishell amphiphilic membranes without perturbation are limited and often indirect. Thus, only a broad range of physico-chemical biological and computational methods can afford extensive understanding of communication within networks of chemically coupled oscillators confined in liquid domains. Finally, using microfluidics to produce and organize liquid droplets into arrays, offers an exceptional instance for technical control, as well as a versatile platform, though conventional techniques must be adapted to these particular configurations.

REFERENCES:

1. S. H. Strogatz, *Sync: How Order Emerges From Chaos In the Universe, Nature, and Daily Life* Hachette Books; Reprint edition (April 14, 2004), 2004.
2. I. Z. Kiss and J. L. Hudson, *Aiche Journal*, 2003, **49**, 2234-2241.
3. I. R. Epstein and B. Xu, *Nat Nano*, 2016, **11**, 312-319.
4. K. Showalter and I. R. Epstein, *Chaos*, 2015, **25**, 097613.
5. G. Ghoshal, A. P. Muñuzuri and J. Pérez-Mercader, *Scientific Reports*, 2016, **6**, 19186.
6. S. H. Strogatz, *Sync: The Emerging Science of Spontaneous Order* Penguin, New Ed (29 avril 2004).
7. A. F. Taylor, M. R. Tinsley, F. Wang, Z. Huang and K. Showalter, *Science*, 2009, **323**, 614-617.
8. I. R. Epstein, *Chemical Communications*, 2014, **50**, 10758-10767.
9. M. W. Barnett and P. M. Larkman, *Practical Neurology*, 2007, **7**, 192-197.
10. A. Adamatzky, J. Holley, P. Dittrich, J. Gorecki, B. De Lacy Costello, K.-P. Zauner and L. Bull, *Biosystems*, 2012, **109**, 72-77.
11. J. Holley, A. Adamatzky, L. Bull, B. De Lacy Costello and I. Jahan, *Nano Communication Networks*, 2011, **2**, 50-61.
12. P. L. Gentili, *RSC Adv.*, 2013, **3**, 25523-25549.
13. *Advances in Artificial Life, Evolutionary Computation and Systems Chemistry*, Springer International Publishing, Cham, 2016.
14. P. H. King, J. C. Corsi, B.-H. Pan, H. Morgan, M. R. R. de Planque and K.-P. Zauner, *Biosystems*, 2012, **109**, 18-23.
15. N. Shembekar, C. Chaipan, R. Utharala and C. A. Merten, *Lab on a Chip*, 2016, **16**, 1314-1331.
16. D. J. Collins, A. Neild, A. deMello, A.-Q. Liu and Y. Ai, *Lab on a Chip*, 2015, **15**, 3439-3459.
17. S.-Y. Teh, R. Lin, L.-H. Hung and A. P. Lee, *Lab on a Chip*, 2008, **8**, 198-220.
18. M. T. Guo, A. Rotem, J. A. Heyman and D. A. Weitz, *Lab on a Chip*, 2012, **12**, 2146-2155.
19. H. Song, D. L. Chen and R. F. Ismagilov, *Angewandte Chemie International Edition*, 2006, **45**, 7336-7356.
20. S. Lach, S. M. Yoon and B. A. Grzybowski, *Chemical Society Reviews*, 2016, DOI: 10.1039/C6CS00242K.
21. B. P. Belousov, *A periodic reaction and its mechanism»*, Sbornik Referatov po Radiatsonno Meditsine, Moscow, 1958.
22. A. M. Zhabotinsky, *Proc. Acad. Sci. USSR,* , 1964, **157**, 392-395.
23. H. Fukuda, N. Tamari, H. Morimura and S. Kai, *The Journal of Physical Chemistry A*, 2005, **109**, 11250-11254.
24. H. Fukuda, H. Morimura and S. Kai, *Physica D: Nonlinear Phenomena*, 2005, **205**, 80-86.
25. M. Toiya, V. K. Vanag and I. R. Epstein, *Angewandte Chemie International Edition*, 2008, **47**, 7753-7755.
26. T. Okano and K. Miyakawa, *Phys Rev E*, 2009, **80**, 026215.
27. S. Thutupalli, S. Herminghaus and R. Seemann, *Soft Matter*, 2011, **7**, 1312-1320.
28. M. Toiya, H. O. González-Ochoa, V. K. Vanag, S. Fraden and I. R. Epstein, *The Journal of Physical Chemistry Letters*, 2010, **1**, 1241-1246.
29. F. Rossi, V. K. Vanag and I. R. Epstein, *Chemistry – A European Journal*, 2011, **17**, 2138-2145.
30. T. Okano, A. Kitagawa and K. Miyakawa, *Phys Rev E*, 2007, **76**, 046201.
31. J. Delgado, N. Li, M. Leda, H. O. Gonzalez-Ochoa, S. Fraden and I. R. Epstein, *Soft Matter*, 2011, **7**, 3155-3167.
32. R. Tomasi, J.-M. Noel, A. Zenati, S. Ristori, F. Rossi, V. Cabuil, F. Kanoufi and A. Abou-Hassan, *Chem. Sci.*, 2014, **5**, 1854-1859.

33. N. Li, J. Delgado, H. O. Gonzalez-Ochoa, I. R. Epstein and S. Fraden, *Phys Chem Chem Phys*, 2014, **16**, 10965-10978.
34. N. Tompkins, M. C. Cambria, A. L. Wang, M. Heymann and S. Fraden, *Chaos*, 2015, **25**, 064611.
35. J. Guzowski, K. Gizynski, J. Gorecki and P. Garstecki, *Lab on a Chip*, 2016, **16**, 764-772.
36. A. Z. F. Rossi, S. Ristori, J-M. Noel, V. Cabuil, F. Kanoufi and A. Abou-Hassan, *Int. J. Unc. Comp.*, 2015, **11 (1)**, 23-36.
37. R. J. Field, *Journal of Chemical Education*, 2000, **77**, 450.
38. I. R. Epstein and K. Showalter, *The Journal of Physical Chemistry*, 1996, **100**, 13132-13147.
39. A. F. Taylor, *Progress in Reaction Kinetics and Mechanism*, 2002, **27**, 247-325.
40. L. Sciascia, F. Rossi, C. Sbriziolo, M. L. T. Liveri and R. Varsalona, *Phys Chem Chem Phys*, 2010, **12**, 11674-11682.
41. J. J. Tyson, *Frontiers in Mathematical Biology*, 1994, **100**, 569-587.
42. A. M. Zhabotinsky, *Proc. Acad. Sci. USSR Chem. Sect.*, 1964, **157, 4**.
43. B. T. Ginn, B. Steinbock, M. Kahveci and O. Steinbock, *The Journal of Physical Chemistry A*, 2004, **108**, 1325-1332.
44. K. Bar-Eli, *The Journal of Physical Chemistry*, 1984, **88**, 3616-3622.
45. M. Rosenblum and A. Pikovsky, *Contemporary Physics*, 2003, **44**, 401-416.
46. Y. Kuramoto, *Physica A: Statistical Mechanics and its Applications*, 1981, **106**, 128-143.
47. M. N. Stolyarov, V. A. Romanov and E. I. Volkov, *Phys Rev E*, 1996, **54**, 163-169.
48. M. Dolnik and I. R. Epstein, *Phys Rev E*, 1996, **54**, 3361-3368.
49. Y. Kuramoto, *Chemical oscillations, waves, and turbulence*, Springer Science & Business Media, 2012.
50. V. K. Vanag and I. R. Epstein, *Phys Rev E*, 2011, **84**, 066209.
51. A. I. Lavrova and V. K. Vanag, *Phys Chem Chem Phys*, 2014, **16**, 6764-6772.
52. V. K. Vanag and I. R. Epstein, *The Journal of Chemical Physics*, 2003, **119**, 7297-7307.
53. , !!! INVALID CITATION !!!
54. R. Niedl, I. Berenstein and C. Beta, *Phys Chem Chem Phys*, 2016, **18**, 6451-6457.
55. F. Rossi, V. K. Vanag, E. Tiezzi and I. R. Epstein, *The Journal of Physical Chemistry B*, 2010, **114**, 8140-8146.
56. V. K. Vanag, F. Rossi, A. Cherkashin and I. R. Epstein, *Journal of Physical Chemistry B*, 2008, **112**, 9058-9070.
57. V. K. Vanag and I. R. Epstein, *Phys Chem Chem Phys*, 2009, **11**, 897-912.
58. M. A. Budroni, *Phys Rev E*, 2015, **92**.
59. M. A. Budroni, L. Lemaigre, A. De Wit and F. Rossi, *Phys Chem Chem Phys*, 2015, **17**, 1593-1600.
60. M. A. Budroni, J. Carballido-Landeira, A. Intiso, A. D. Wit and F. Rossi, *Chaos: An Interdisciplinary Journal of Nonlinear Science*, 2015, **25**, 064502.
61. N. Tompkins, N. Li, C. Girabawe, M. Heymann, G. B. Ermentrout, I. R. Epstein and S. Fraden, *PNAS*, 2014, **111**, 4397-4402.
62. A. M. Turing, *Philosophical Transactions of the Royal Society of London B: Biological Sciences*, 1952, **237**, 37-72.
63. V. Horvath, P. L. Gentili, V. K. Vanag and I. R. Epstein, *Angewandte Chemie International Edition*, 2012, **51**, 6878-6881.
64. J. Weiner, R. Holz, F. W. Schneider and K. Bar-Eli, *The Journal of Physical Chemistry*, 1992, **96**, 8915-8919.
65. R. Holz and F. W. Schneider, *The Journal of Physical Chemistry*, 1993, **97**, 12239-12243.
66. A. F. Taylor, M. R. Tinsley, F. Wang and K. Showalter, *Angewandte Chemie*, 2011, **123**, 10343-10346.
67. M. L. Smith, K. Heitfeld, C. Slone and R. A. Vaia, *Chem Mater*, 2012, **24**, 3074-3080.
68. F. Rossi, S. Ristori, N. Marchettini and O. L. Pantani, *J. Phys. Chem. C*, 2014, **118**, 24389-24396.
69. S. Thutupalli and S. Herminghaus, *The European Physical Journal E*, 2013, **36**, 1-10.

70. P. Stano, T. P. de Souza, P. Carrara, E. Altamura, E. D'Aguanno, M. Caputo, P. L. Luisi and F. Mavelli, *Mech Adv Mater Struc*, 2015, **22**, 748-759.
71. S. Pautot, B. J. Frisken and D. A. Weitz, *Langmuir*, 2003, **19**, 2870-2879.
72. T. J. Stockmann, J.-M. Noël, S. Ristori, C. Combellas, A. Abou-Hassan, F. Rossi and F. Kanoufi, *Analytical Chemistry*, 2015, **87**, 9621-9630.
73. K. Torbensen, F. Rossi, O. L. Pantani, S. Ristori and A. Abou-Hassan, *The Journal of Physical Chemistry B*, 2015, **119**, 10224-10230.
74. K. Torbensen, S. Ristori, F. Rossi and A. Abou-Hassan, *Submitted*, 2016.

Chapter II: Interaction of the Belousov-Zhabotinsky Reaction with Phospholipid Engineered Membranes

II.1. Introduction

This chapter deals with the interaction of the Belousov-Zhabotinsky reaction with phospholipid engineered membranes. Bearing in mind the objective of this thesis, such interactions must be well understood in order to develop a reliable platform for generating BZ-encapsulating liposomes. In a bulk study, the lipid bilayer interaction with the BZ-reaction is investigated using small angle x-ray scattering (SAXS), and UV-vis spectroscopy, addressing bilayer penetration and ordering/disordering phenomena. This work is published in *Journal of Physical Chemistry B*.

II.2. Interaction of the Belousov-Zhabotinsky Reaction with Phospholipid Engineered Membranes

Kristian Torbensen,[a≠] *Federico Rossi,*[b≠] *Ottorino L. Pantani,*[c] *Sandra Ristori,*[d]*

and Ali Abou-Hassan[a]*

[a]Sorbonne Universités, UPMC Univ Paris 06, UMR 8234, Laboratoire Physico-chimie des Electrolytes, Nanosystèmes InterfaciauX (PHENIX), 4 place Jussieu - case 51, 75252 Paris cedex 05, France

[b] Department of Chemistry and Biology, University of Salerno, Via Giovanni Paolo II 132, Fisciano (SA), Italy

[c]Department of Agrifood Production and Environmental Sciences, University of Florence, P.le delle Cascine 28, 50144 Firenze, Italy

[d]Department of Earth Sciences & CSGI, University of Florence, Via della Lastruccia 3, 50019 Sesto Fiorentino, Firenze, Italy

ABSTRACT:

Compartmentalized in liposome arrays, the Belousov-Zhabotinsky (BZ) oscillatory reaction might represent a good model for biochemical networks. In order to engineer such liposomes we used small angle X-ray scattering (SAXS) to study the effect of individual BZ reactant as well as of the entire BZ mixture on the structural properties of lipid layer(s) formed by 1,2-Dimyristoyl-sn-glycero-3-phosphocholine (DMPC) phospholipids in aqueous media. These properties were compared with those of lipid layers doped with myristic acid (Myr-A), sodium tetradecylsulfate (STS), and cholesterol (CHOL). In parallel, the effect on the BZ reaction exerted by doped DMPC liposomes was investigated by UV-visible spectroscopy, followed by image analysis of the recorded time series. SAXS experiments showed that chemical species involved in the BZ reaction bring small changes to the internal structure of DMPC bilayers. However, ferroin can reduce the liposome lamellarity by being adsorbed on the surface of lipid-layers. Also, the presence of charged dopants such as STS and TA tends to reduce the lamellarity of liposomes, while CHOL brings marked

changes in the BZ system due to chemical reaction with oxidant species. In particular, an increase of the oscillation frequency is observed when the BZ reaction is carried out in the presence of CHOL-DMPC liposomes. For this behavior, a possible explanation supported by numerical simulations is bromination of CHOL double bonds by BZ intermediates.

INTRODUCTION:

The spatio-temporal propagation of chemical species is an important phenomenon for cell signaling[1] and has comprehensive applications in fields ranging from information technology to molecular computing.[2] Chemical oscillators are an example of signal emitters which, if confined in micro-domains, can be used to model complex processes such as cell communication. In this context, a major prerequisite to mimic the structure of a biological cell is to elaborate aqueous micro compartments surrounded by phospholipid membranes. These compartments must encapsulate chemical reactions whose time and space progression is governed by periodic fluctuations in the concentration of chemical species, which can act as activatory or inhibitory messengers and reach different compartments through the outside medium. A good candidate for signal generator is the Belousov-Zhabotinsky (BZ) reaction, a robust chemical oscillator in which an organic substrate (malonic acid) is oxidized by bromate in the presence of a redox catalyst, such as ferroin, $Fe(o\text{-}phen)_3^{2+}$. This system has been extensively used to model communication among droplets dispersed in organic media[3] and has shown to be compatible with phospholipid lamellar phases.[3b,4] Recently, we reported for the first time the successful encapsulation of the BZ reaction inside giant liposomes and emulsions obtained with microfluidics.[5,6] In particular, by using a flow-focusing microfluidic device, we produced BZ liposomes with a diameter of 250-300 μm, surrounded by 1,2-Dimyristoyl-sn-glycero-3-phosphocholine (DMPC) bilayers, dispersed in an aqueous medium containing polyvinyl alcohol (PVA) as viscosity modulator. This configuration had not previously been investigated. Our works showed that the passage of excitatory signals between BZ compartments (most probably the autocatalytic activator $HBrO_2$) is a key step for communication and, therefore, that the $HBrO_2$ permeability through the lipid shell is of paramount importance. We also showed that limitations to observing sustained oscillations may be due to liposome short-term stability, since different stress and strains from the inside (e.g. CO_2 production), or from the outer phase (viscosity and osmotic gradients) can impair the lipid layer.

Engineering stable and communicating liposomes requires a fine-tuning of the physico-chemical properties of the confining membranes, such as lamellarity and permeability. In order to shed light on these questions, here we carried out the structural characterization of membranes with different composition in the presence of BZ reagents using Small Angle X-ray Scattering (SAXS). In addition, we investigated the effect of membrane composition on the BZ oscillatory behavior using UV-visible spectroscopy. The aim of this work is to obtain insight into the BZ-phospholipid membrane interaction, which will be beneficial for engineering stable liposomes to encapsulate the BZ oscillator for the study of chemical communication.

A first important question concerns the location of the BZ catalyst; i.e. assessing whether the amphipathic ferroin interacts with the lipid bilayers and, in that case, to which extent the interaction occurs is a relevant issue for the analysis of the BZ behavior in membrane-confined environments. In particular, the sorption of ferroin may influence the liposome lamellarity, which should have pronounced effects both on the interaction among BZ species and on the bilayer permeability. Matosevic et al.[7] used confocal microscopy imaging to investigate the lamellarity of giant liposomes where fluorescence-labeled lipids had been inserted in the confining membranes. In the present case, the redox activity of the encapsulated BZ system did not allow such investigation; consequently we used Small Angle X-ray Scattering (SAXS) as a non-interfering method to obtain information on the lipid membrane organization. SAXS has proven to be a valuable tool for studying the properties and organization of lipid bilayers, and has been extensively used for the investigation on the uptake of guest molecules by vesicles, lamellar phases and other phospholipid self-assemblies.[8,9] In particular, SAXS provides a direct method to establish whether a lipid mixture generates rigid or soft bilayers, and to determine if a repeat distance among stacked bilayers exists. The absorption of molecules/ions on the bilayer surface and the penetration of exogenous species within the hydrophobic region can deeply influence these properties. Moreover, the ordering/disordering effect brought about by the interaction with external agents can be monitored by comparing the electron density profile of pure and composite bilayers.

EXPERIMENTAL DETAILS:

Sodium bromate, malonic acid (MA), cholesterol (CHOL), myristic acid (Myr-A), sodium tetradecylsulfate (STS), polyvinyl alcohol (PVA; Mw = 10 kDa), tetradecylamine (TA) and sulfuric acid (96 %) were all purchased from Sigma-Aldrich and used without further purification. Ferroin was synthesized by adding 1.10-phenanthrolin to an aqueous solution of iron(II) sulfate in the stoichiometric ratio 3:1. Both chemicals were purchased from Sigma-Aldrich. 1,2-Dimyristoyl-sn-glycero-3-phosphocholine (DMPC) was purchased by Avanti Polar Lipids, Inc.

SMALL ANGLE X-RAY SCATTERING:

SAXS measurements were performed at the ID02 beamline of the ESRF (Grenoble, France). The samples were injected into 1.5 mm inner diameter quartz capillary tubes, and the scattered beam intensity I(q) was recorded as a function of the moment transfer $q = (4\pi/\lambda)\sin\theta$ (where 2θ is the scattering angle). The q-range covered was 0.030 - 3.21 nm^{-1}. Normalization and background subtraction were carried out with standard procedures.[10] I(q) diagrams were fitted with the Global Analysis Program (GAP version 1.3), written by Dr Georg Pabst,[11,12] which allows to obtain structural details of lipid membranes and electron densities in the polar/apolar regions (see SI for details). The samples were prepared by mixing the lipids and the BZ reactants with water, vigorous vortexing and homogenization in an ultrasonic bath for 5 minutes.

UV-VIS SPECTROSCOPY:

The absorption spectra were recorded with an Agilent 8453 Diode Array UV-vis spectrophotometer. The measurements were performed in a total volume of 1.5 mL in a 10 mm quartz cuvette at constant magnetic stirring (~ 300 rpm).

RESULTS AND DISCUSSION:

Figure 1 shows a comparison among the SAXS diagrams of pure DMPC (1% w/w), DMPC + ferroin ([ferroin] = 2.5×10^{-3} M), and in the presence of MA and BrO_3^- at working concentration similar to when the BZ reaction is performed, i.e. [MA] = 0.15 M, [BrO_3^-] = 0.18 M. The SAXS intensity profile in Figure 1 of the DMPC/water system shows two distinct Bragg peaks originating from the oligolamellar lipid-layer stacking of the liposomes.[13] Upon addition of ferroin, i.e. the autocatalytic species in the BZ reaction, the disappearance of both Bragg peaks indicates a transformation of the lipid-layers from oligolamellar to monolamellar. Such a transformation can be caused by ferroin adsorption at the liposome surface, at which the positive charge of the ferroin induces electrostatic repulsion between the lipid bilayers, thus favoring monolamellar liposomes. No further major changes of the intensity profile were observed by addition of MA and BrO_3^-.

These results were supported by fitting the SAXS diagrams (see SI for details). The fits indicated that, in the pure DPMC system, about 40% of the bilayers were stacked into oligolamellar structures with a thickness of 38.6 Å and an average of three repeat elements with a lamellar repeating distance of 65 Å, while no bilayer stacking was retained after ferroin addition. Again, the addition of the BZ species MA and BrO_3^- brought about only minor changes to the DMPC membranes in terms of bilayer thickness and electron density distribution (see table SI1).

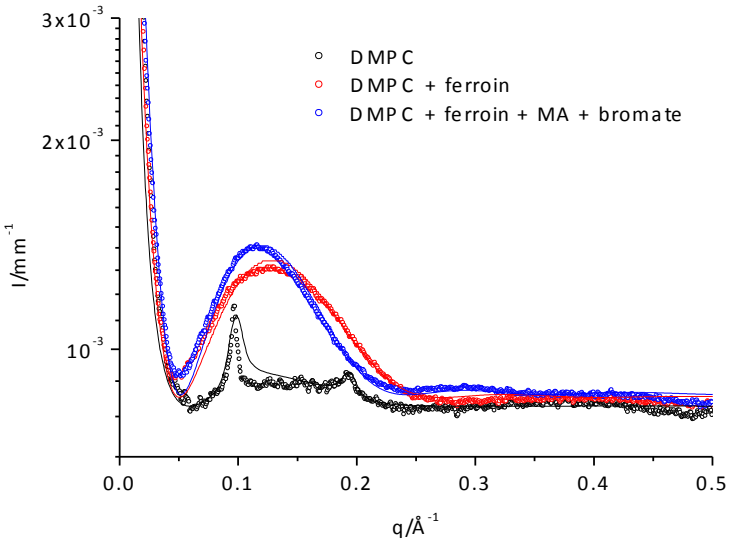

Figure 1. Experimental (symbols) and fitted (continuous lines) SAXS intensity profiles obtained for DMPC in pure water (1% w/w) and in the presence of ferroin with or without the BZ reactants malonic acid and BrO_3^- (see text and SI for details).

The surface charge of model liposomes was determined by Zeta-potential measurements. These liposomes were prepared and homogenized by extrusion, but have the same composition as those reported in Figure 1. Upon sorption of ferroin on DMPC aggregates, the surface charge increased significantly from -5 ± 2 to 11 ± 2 mV (see table SI2), thus supporting the hypothesis of ferroin adsorption on the surface of lipid layers. The effects induced by ferroin and other BZ components on the bilayer are shown in Figure 2, where the electron density profiles reconstructed from the fitting of each SAXS curve are reported.

When additional BZ species are present in solution, a broadening of the polar region at ~ 20 Å from the bilayer center is observed, indicating a penetration of these species in the bilayer which results in an increased distance between DMPC head groups.

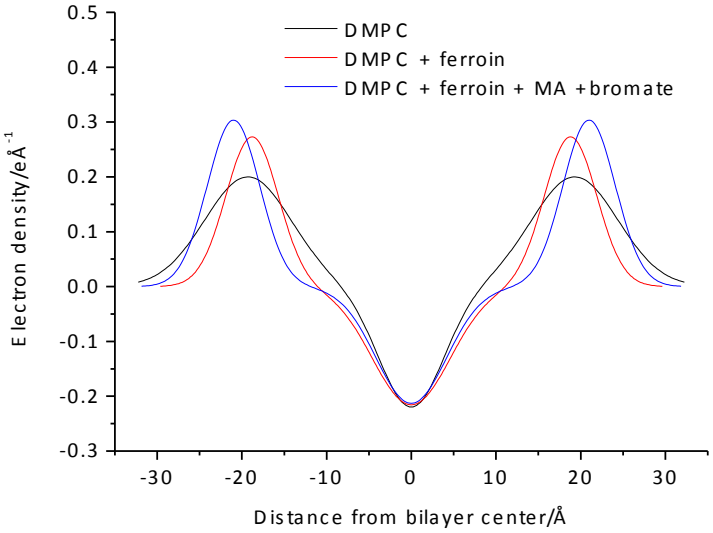

Figure 2. Electron density profiles obtained from fitting the SAXS intensity diagrams reported in Figure 1. See SI for more details.

The phosphocholine (PC) polar head is known to keep its zwitterionic character in a wide range of pH; however, it has been shown that relevant protonation of PC lipids occurs at pH lower than ≈ 2,[14] which is the typical value for BZ reaction. Thus, to mimic the conditions of the BZ environment, the interactions between lipid bilayers and BZ components were also studied in acidic solution, i.e. in the presence of H_2SO_4. Figure 3 shows a comparison between the SAXS diagrams of the whole BZ system and the same system without ferroin. In this latter case, the SAXS diagrams are dominated by the sharp peaks of Bragg reflections, which mask the form factor of the bilayers

and complicate the evaluation of the degree of lamellarity. It is also important to note that the SAXS intensity profiles of DMPC in the presence of H_2SO_4 and the oxidant BrO_3^- was similar to that of DMPC in pure water. Indeed no changes were observed even after several hours, which evidence the stability of DMPC lipids in the acidic and oxidant conditions of the BZ reaction.

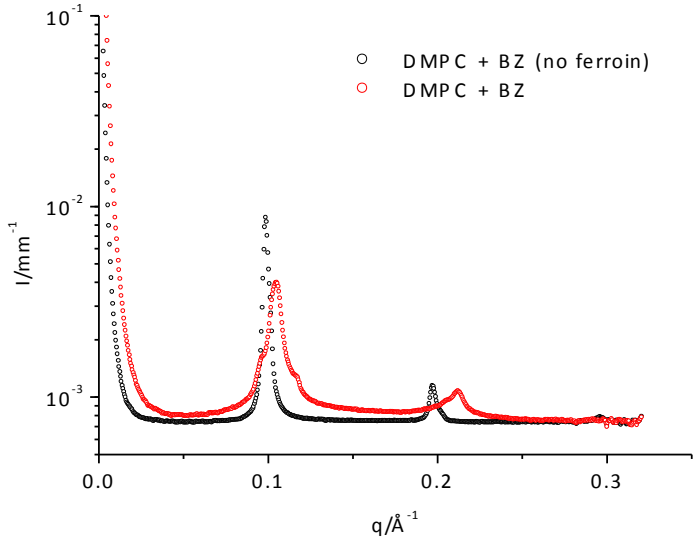

Figure 3. SAXS intensity profiles of DMPC in pure water (1% w/w) in the presence of the entire BZ system (red) and the BZ system without the catalyst ferroin (black).

However, the position of the first order reflections at q_{max} = 1.05 10^{-2} $Å^{-1}$ and q_{max} = 9.9 10^{-2} $Å^{-1}$, corresponding to a bilayer spacing ($2\pi/ q_{max}$) of 63.5 Å for BZ with ferroin and 59.8 Å for BZ without ferroin, shows the capability of ferroin to increase the mean distance between bilayers, in agreement with its location on the bilayer surface. Noteworthy, the slight increase of the Zeta-potential from 11 ± 3 to 18 ± 2 mV upon addition of the whole set of BZ reactants, can be caused by the acid catalyzed oxidation of ferroin to ferrin by BrO_3^-, thus introducing further positive charges at the liposome surface.

As mentioned above, an efficient way of tuning the physico-chemical properties of liposomes is to vary the local curvature of their lipid bilayers,[15,16] which results in increased flexibility in response to a stress, such as swelling or shrinking. Amphiphiles with a molecular shape, i.e. packing parameter, different from the main lipid components, can be inserted in the bilayer with the purpose of changing the spontaneous local curvature.[17] In particular, we used myristic acid (Myr-A) to build mixed DMPC-Myr-A bilayers. This choice was motivated by Myr-A

having the same hydrocarbon chain as DMPC, but a different head group. The SAXS intensity profile of the mixed DMPC/Myr-A (80/20 mol/mol) in water is shown in Figure 4. This profile, given by two Bragg peaks and an underlying bilayer form factor, indicate that oligolamellar and monolamellar structures coexist in solution, as discussed above. Since a multilamellar structure can be an obstacle for efficient chemical communication,[18] we doped the lipid mixture by inserting additional, charged, amphiphiles to obtain the desired lamellarity reduction. These doping components were the negative tetradecylsulfate (STS, sodium salt) and tetradecylamine (TA), the latter having a $pK_a = 10.62$[19] and thus positively charged at neutral or acidic pH. The SAXS diagrams of doped bilayers (5% mol/mol of charged amphiphile) are reported in Figure 4: the diminution (for TA) or the complete disappearance of the Bragg peaks (for STS), demonstrate the reduced lamellarity due to the presence of the dopants.

Rigidity and lateral inhomogeneity in bilayers are usually varied by adding sterols, naturally present in many biological membranes. In particular, cholesterol (CHOL) is a major constituent of the cell plasma membranes in higher organisms[20]. In DMPC/CHOL mixed bilayers we observed the expected rigidifying effect[21,13]; the presence of BZ reactants CHOL induced further marked changes, as shown in figure 5. In fact, the SAXS diagrams presented both a strong maxima displacement and broadening of Bragg peaks upon CHOL insertion in the DMPC bilayers. This effect was attributed to a chemical reaction between oxidant species and the CHOL double bond (*vide infra*). In turn, this showed that BZ species with oxidant capability penetrate below the polar head region, in agreement with the hypothesis previously based on the electron density profiles.

The influence of several surfactants, including lipid phases, on the BZ kinetic and dynamic behavior has been widely investigated. For unstirred solutions, e.g. thin liquid films, the behavior of a BZ/DPPC reaction-diffusion lamellar system was found to change from pacemaker structures and traveling waves to Turing patterns on increasing phospholipid concentrations.[4] For BZ/anionic amphiphile systems forming micelles in stirred solutions, such as BZ/sodium dodecyl sulfate,[22] an increased oscillation frequency was observed. These phenomena were proposed to originate from sequestering of pertinent BZ components or intermediates. Cationic, anionic and zwitterionic surfactants have also been reported to perturb the temporal characteristics of BZ reactions.[23]

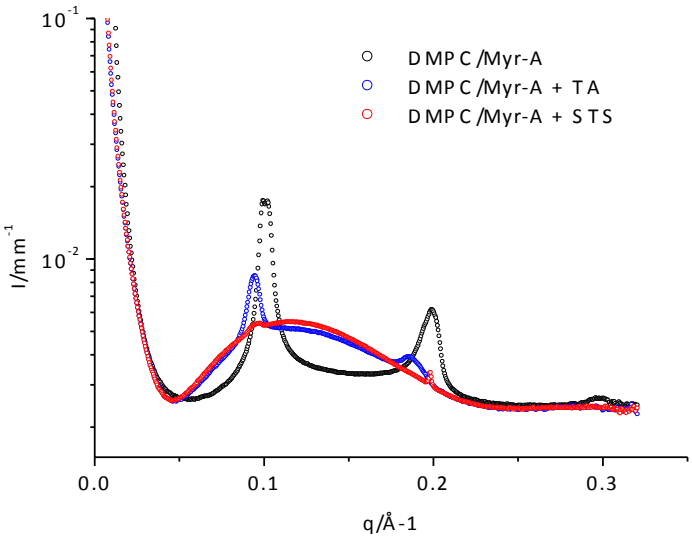

Figure 4. SAXS intensity profiles of DMPC/Myr-A 80/20 molar ratio (black), DMPC/Myr-A/TA 75/20/5 molar ratio (blue) and DMPC/Myr-A/STS 75/20/5 molar ratio (red). All the three systems where measured in presence of the entire set of BZ reagents.

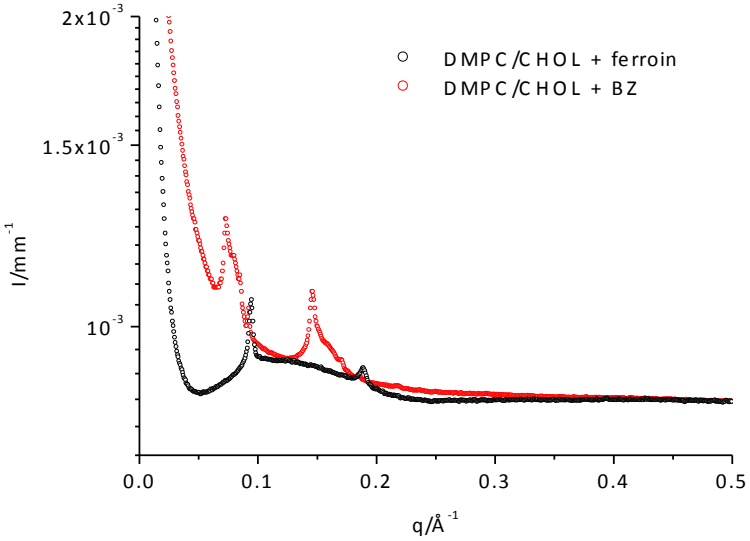

Figure 5. SAXS intensity diagrams of the lipid mixtures DMPC/CHOL 80/20 mol/mol in the presence of ferroin (red) and of all BZ reactants (black). The position of the first Bragg peak was q_{max} = 9.95 10^{-2} $Å^{-1}$ and q_{max} = 7.38 10^{-2} $Å^{-1}$, respectively, which corresponded to a bilayer spacing of 66 Å and 85 Å.

The effect on the BZ reaction exerted by the doped DMPC liposomes considered in this work was investigated by time dependent UV-visible spectroscopy, followed by image analysis of the recorded time series. The composition of the BZ/lipids mixtures investigated was the same as

for the SAXS measurements. In general, time series were monitored for 20 min in a 1.5 mL solution under stirring (see SI for details) and the oscillation frequencies were extracted by measuring the time periods between consecutive ferroin absorption peaks.

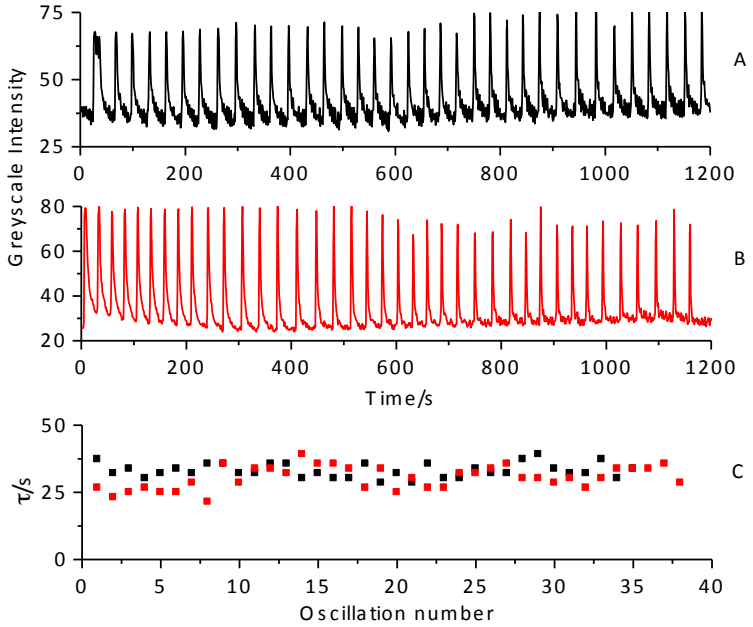

Figure 6. A) BZ reaction in pure aqueous solution (black). B) BZ reaction in 1% w/w DMPC/water (red). C) Comparison between the oscillation periods of the two systems. Data recorded under constant stirring.

Figure 6 shows the comparison between a BZ reaction in pure water (Panel A) and in the presence of 1% w/w DMPC (Panel B). The analysis of the oscillation period (τ) (Panel C) reveals no major changes between the two systems, with $\tau = 34 \pm 3$ s in pure water and $\tau = 32 \pm 3$ s in the presence of the lipids. The shape of the frequency profile is maintained throughout the entire time period of recording, indicating a homogeneous system even in the presence of the liposomes. Likewise, as the reaction cycles proceed, there is no indication of membrane sequestering of intermediates, e.g. the BZ inhibitor Br^- or the activator $HBrO_2$. Furthermore, the increased viscosity of the reaction solution upon addition of DMPC seems not to affect the oscillation frequency and, due to the stirring, the BZ reaction in the bulk will henceforth be considered under kinetic control. The increased lamellarity obtained by introducing Myr-A in DMPC bilayers, as observed by SAXS measurements (Figure 4), had no pronounced effect on the BZ oscillatory dynamics.

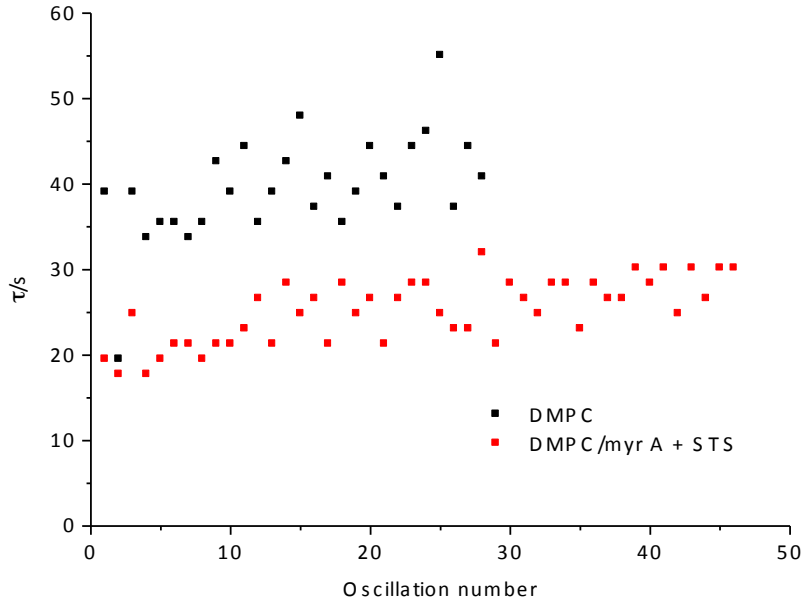

Figure 7. Oscillation periods recorded for BZ in pure aqueous solution (■) and in DMPC-Myr-A-STS/aqueous phase in molar fractions of 0.80:0.15:0.05, respectively, giving a total concentration of 1% w/w (■). Data recorded under constant stirring.

In fact, the oscillation frequencies for the BZ/DMPC system in the presence of various concentrations of Myr-A (up to 40% molar fraction) did not vary significantly and only small variations of the oscillation period, like in the case of pure DMPC, were detected. Indeed, if sequestering of some BZ components or intermediates was significant, a more pronounced effect would have been observed for the Myr-A induced oligolamellar system, thus confirming the findings for the pure DMPC system.

Upon addition of even a small amount (5% molar fraction) of the anionic species STS to the DMPC-Myr-A liposomes, a decrease in lamellarity was observed by SAXS measurements, as displayed in Figure 4. Concomitantly, a significant increase in the BZ oscillation frequency was observed for a similar bulk solution (Figure 7) which is in line with previous findings reported for pure anionic micellar systems consisting of sodium dodecylsulfate.[22] A direct comparison between the two systems is difficult, since micelles are highly dynamical objects, whose time of breaking/reassembling is in the order of a few milliseconds, whereas lipid bilayers are kinetically stabilized structures, which may experience undulation or stacking, but no fragmentation over periods of days. The only feature in common between micelles and liposomes is the internal structuring into polar and non-polar regions. Moreover, the STS hydrophobic moiety is a linear

alkane with the anionic hydrophilic head group exposed directly to the bulk solution; STS has a branched alkane chain with the sulfate group positioned near the center, thus constituting a bulkier molecule. The geometry of the STS, together with its net charge, explains the decrease in lamellarity upon STS-doping of the DMPC-Myr-A system since the sulfate group will be incorporated below the polar heads in the lamellar structure. In micelles, the introduction of a charged species alters the partition of BZ intermediates and, in particular, a major role was played by the partition of ferroin and bromomalonic acid (BrMA) in the hydrophobic core of the SDS aggregates.[22] This causes an increase in the reaction rate of the ferroin oxidation, known as Process C in the FKN model.[24,25] The net negative charge brought about by STS molecules over the lipid membranes seems, in this case, to promote the same effect as shown in Figure 7 , i.e. the positively charged ferroin is likely partitioned in the membrane bilayers. However, it is difficult to assess the effect of STS towards BrMA, the latter bearing no net charge. A further investigation, based on Br Anomalous SAXS experiments, is planned to shed light on the distribution of brominated species in the dispersed lipid/surfactant phase.

The addition of CHOL to the DMPC liposomes had a similar catalytic effect on the oscillation frequency with respect to the STS (Figure 8). In this case, however, the increase of the oscillation frequency is caused not only by the changes in the bilayer properties but, most probably, by chemical interaction between CHOL and BZ intermediates, e.g. bromination of the CHOL double bond by a bromine addition reaction.[26] Indeed, bromine is known to be a "secondary" inhibitor for the BZ oscillation mechanism, since it is directly related with the primary inhibitor bromide, Br^-, through the equilibrium (reaction (1))[25, 27]

$$Br^- + HOBr + H^+ \rightleftharpoons Br_2 + H_2O \qquad (1)$$

Reaction (1) takes place after the autocatalytic step when $[Br^-]$ is high.

The decrease of the oscillation periods observed is due to a loss of Br_2 through the interaction with CHOL, which, in turn, causes a faster decrease of the inhibitory specie Br^-, thus shortening the recovery period between the two autocatalytic stages.[26] In order to confirm this mechanism, numerical simulations have been performed by using the CO.PA.SI. software.[27] Several models are known to be able to reproduce the dynamical regime of the BZ reaction, however quantitative matching between simulations and experimental data is generally difficult and often it requires the tuning of one or more kinetic constants.[28]

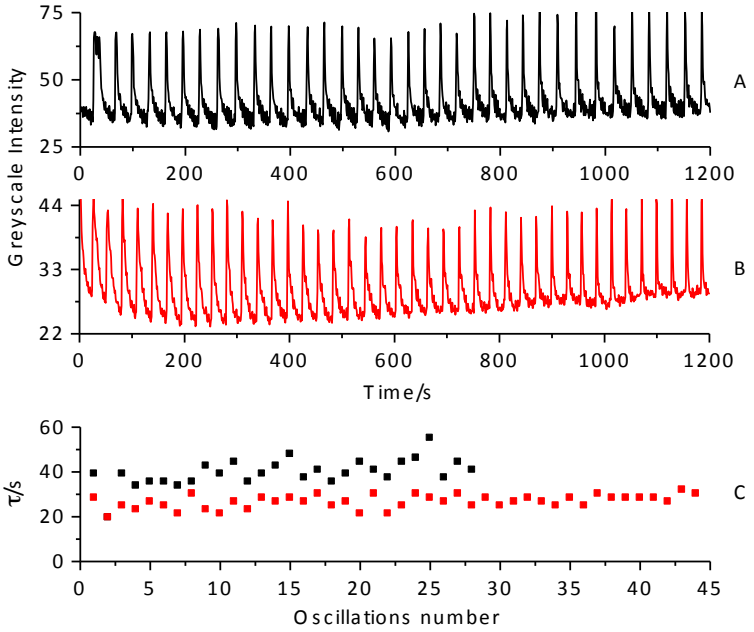

Figure 8. A) BZ reaction in pure aqueous solution (black). B) BZ reaction in a DMPC-CHOL/aqueous phase (red). C) Comparison between the oscillation periods of the two systems. Data recorded under constant stirring.

Here we followed different strategies in order to explore the possibility that the bromination of cholesterol is responsible for the observed oscillation frequency increase. First, we used a standard model (Model A) for the ferroin catalyzed BZ reaction,[29,30] to which a bromination reaction was added (reaction (2), see SI for more information)

$$Br_2 + CHOL \xrightarrow{K} Br_2 - CHOL \qquad (2)$$

In this case we chose a kinetic rate constant K = 340 $M^{-1}s^{-1}$. The K value was obtained through a best fitting procedure of the simulated data on the experimental time-series. In fact the kinetic constant of cholesterol bromination, to the best of our knowledge, has never been measured. However, halogen addition on the double bond of olefins is a well-known reaction and the kinetic parameters have been measured for a broad range of organic species.[31,32] The value of the second order constant was found to vary to a large extent, depending on the structure of the organic molecule and on the substituents attached to the double bonds ($\sim 1 \times 10^{-2}$ $M^{-1}s^{-1}$ – 1×10^{6} $M^{-1}s^{-1}$). Therefore, the constant, K, used in our simulations seems to be reliable. Figure 9 shows the simulated frequency trend for a BZ reaction in the absence (black squares) and in the presence of 6 mM cholesterol, i.e. the highest concentration used in our experiments. The qualitative and

quantitative behavior of the effect of cholesterol addition is well reproduced as an increasing trend of the oscillation frequency can be observed.

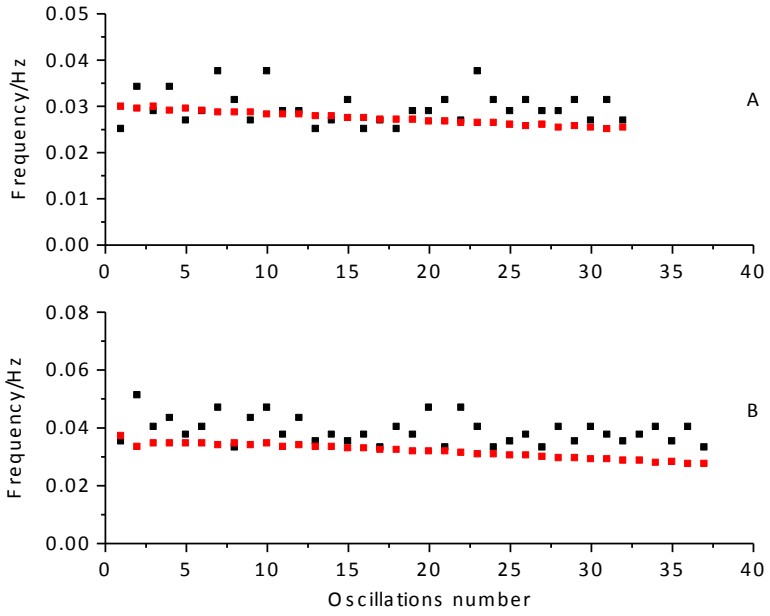

Figure 9. Experimental (■) and simulated (■) oscillation frequencies for: A) BZ in pure aqueous solution. B) BZ in DMPC-CHOL/aqueous phase with [cholesterol] = 6 mM, K = 134 $M^{-1}s^{-1}$.

We also tried to measure the kinetic constant of reaction (2) in our experimental conditions (See SI for more information). The measure of K in a water solution, however, present several difficulties, due to the high volatility of Bromine, the low solubility of CHOL and the precipitation of secondary products, like Br_2 – CHOL. Such effects are not evident in a full BZ reaction, probably because the membranes themselves help the solubilization of the precipitates and the concentration of the Br_2 is rather low.

We decided to study reaction (2) in an organic solvent commonly used for this purpose, namely the Methyl-*tert*-butyl ether (MTBE). In this case, the second order kinetic constant was found to be significantly lower than that found by the fitting procedure and it was K = 0.129 $M^{-1}s^{-1}$. By inserting this constant in Model A, we obtained a good quantitative match with the experimental frequency of the second half of the reaction (from ~ 400 s), in the presence of [CHOL] = 6 mM (see the red circles in Figure 10).

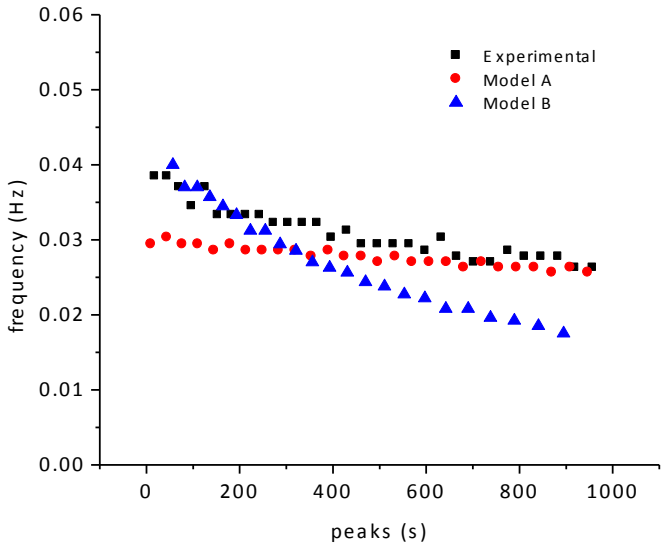

Figure 10. Experimental (■) and simulated (● Model A and ▲ Model B) oscillation frequencies for: BZ in DMPC-CHOL/aqueous phase with [CHOL] = 6 mM. K = 0.129 $M^{-1}s^{-1}$.

However, the first half of the reaction was poorly simulated and we tried another model (model B) developed by Striziak and coworkers to reproduce more complex dynamical regimes of the BZ reaction (Chaos, Mixed mode oscillations, etc.).[33,34] Substianlly, the two models are very similar, except that in Model B the reactions for the bromination of the Malonic Acid are included in the kinetic scheme (see the above references for all the details). The blue triangles in Figure 10 show that in the presence of [CHOL] = 6 mM, Model B reproduces quantitatively the first experimental oscillations.

CONCLUSION:

We investigated the interaction between both DMPC liposomes and liposomes doped with cholesterol, myristic acid, tetradecylsulfate and tetradecylamine, and the species involved in the BZ reaction by using small angle X-ray scattering (SAXS) and UV-visible spectrophotometry. Upon addition of ferroin (the BZ catalyst) the SAXS intensity profiles showed significant reduction of the liposome lamellarity, while the electron density profiles obtained from the fitting of SAXS diagrams indicated that ferroin is located on the liposome surface. In the acidic/oxidant set of BZ reactants, the coexistence of oligolammellar and monolamellar liposomes was observed. In particular, by using myristic acid as dopant, this coexistence could be shifted in favor of

monolamellar liposomes upon addition of tetradecylsulfate and tetradecylamine. Small changes in the lamellar spacing between lipid bilayers were induced by the BZ system, e.g. in pure DMPC liposomes the shift was from of 59.8 Å to 63.5 Å. The ensemble of these structural data evidenced a partial penetration of the BZ species within the lipid bilayers.

The DMPC liposomes produced in this work were shown to exert only small perturbations to the BZ oscillating behavior. However, liposomes doped with either tetradecylsulfate or cholesterol had a catalytic effect on the oscillating frequency due to membrane partitioning of the BZ catalyst or removal of inhibitor species, respectively. The latter hypothesis was also confirmed by numerical simulations. These findings, together with ongoing Br-Anomaluos SAXS measurements on the same systems, can prove valuable for the engineering of communicative networks based on encapsulated oscillating reactions.

ASSOCIATED CONTENT:

Supporting Information. Fitting of SAXS diagrams, Zeta potential of extruded liposomes and kinetic model for numerical simulation of the BZ reaction.

This material is available free of charge via the Internet at http://pubs.acs.org.

Corresponding Authors

* E-mail: ali.abou_hassan@upmc.fr; E-mail: Sandra.ristori@unifi.it

Author Contributions

≠ These authors contributed equally to this work.

Acknowledgments. We thank the ESRF (Grenoble) for beam-time allocation and the staff of the ID02 beam-line for valuable technical assistance.

REFERENCES:

1. Ruiz-Mirazo, K.; Briones, C.; de la Escosura, A., Prebiotic Systems Chemistry: New Perspectives for the Origins of Life. *Chemical Reviews* **2014,** *114* (1), 285-366.
2. (a) Pikovsky, A., Michael Rosenblum,; Kurths., J., *Synchronization: A Universal Concept in Nonlinear Sciences*. Cambridge University Press: 2001; (b) Horvath, V.; Gentili, P. L.; Vanag, V. K.; Epstein, I. R., Pulse-Coupled Chemical Oscillators with Time Delay. *Angew. Chem. Int. Ed.* **2012,** *51* (28), 6878-6881; (c) Gentili, P. L., Small steps towards the development of chemical artificial intelligent systems. *RSC Adv.* **2013,** *3* (48), 25523-25549.
3. (a) Vanag, V. K.; Epstein, I. R., Pattern Formation in a Tunable Medium: The Belousov-Zhabotinsky Reaction in an Aerosol OT Microemulsion. *Physical Review Letters* **2001,** *87* (22), 228301; (b) Rossi, F.; Ristori, S.; Rustici, M.; Marchettini, N.; Tiezzi, E., Dynamics of pattern formation in biomimetic systems. *Journal of Theoretical Biology* **2008,** *255* (4), 404-412; (c) Toiya, M.; González-Ochoa, H. O.; Vanag, V. K.; Fraden, S.; Epstein, I. R., Synchronization of Chemical Micro-oscillators. *J. Phys. Chem. Lett.* **2010,** *1* (8), 1241-1246; (d) Epstein, I. R., Coupled chemical oscillators and emergent system properties. *Chem. Commun.* **2014,** *50* (74), 10758-10767; (e) Tompkins, N.; Li, N.; Girabawe, C.; Heymann, M.; Ermentrout, G. B.; Epstein, I. R.; Fraden, S., Testing Turing's theory of morphogenesis in chemical cells. *PNAS* **2014,** *111* (12), 4397-4402.
4. Magnani, A.; Marchettini, N.; Ristori, S.; Rossi, C.; Rossi, F.; Rustici, M.; Spalla, O.; Tiezzi, E., Chemical Waves and Pattern Formation in the 1,2-Dipalmitoyl-sn-glycero-3-phosphocholine/Water Lamellar System. *Journal of the American Chemical Society* **2004,** *126* (37), 11406-11407.
5. Tomasi, R.; Noel, J.-M.; Zenati, A.; Ristori, S.; Rossi, F.; Cabuil, V.; Kanoufi, F.; Abou-Hassan, A., Chemical communication between liposomes encapsulating a chemical oscillatory reaction. *Chem. Sci.* **2014,** *5* (5), 1854-1859.
6. F. Rossi, A. Z., S. Ristori, J-M. Noel, V. Cabuil, F. Kanoufi and A. Abou-Hassan, COBRA at Unconventional Computation and Natural Computation 2013. *Int. J. Unc. Comp.* **2015,** *11* (1), 23-36.
7. Matosevic, S.; Paegel, B. M., Layer-by-layer cell membrane assembly. *Nat. Chem.* **2013,** *5* (11), 958-963.
8. P. Lindler, T. Z. E., *Neutrons, X-rays and Light. Scatterning Methods Applied to Soft Condensed Matter*. North Holland Press, Amsterdam: 2002.
9. Kučerka, N.; Nieh, M.-P.; Pencer, J.; Harroun, T.; Katsaras, J., The study of liposomes, lamellae and membranes using neutrons and X-rays. *Curr. Opin. Colloid Interface Sci.* **2007,** *12* (1), 17-22.
10. Almeida, P. F. F.; Vaz, W. L. C.; Thompson, T. E., Lateral diffusion in the liquid phases of dimyristoylphosphatidylcholine/cholesterol lipid bilayers: a free volume analysis. *Biochemistry* **1992,** *31* (29), 6739-6747.
11. Khelashvili, G.; Pabst, G.; Weinstein, H.; Harries, D., Cholesterol Orientation and Tilt Modulus in DMPC Bilayers. *J. Phys. Chem. B* **2010,** *114*, 7524-7534.
12. Th. Zemb, P. L. e., *Neutron, X-rays and light scattering methods applied to soft condensed matter*. North Holland Press, Amsterdam: 2002.
13. Pabst, G.; Katsaras, J.; Raghunathan, V. A.; Rappolt, M., Structure and Interactions in the Anomalous Swelling Regime of Phospholipid Bilayers†. *Langmuir* **2003,** *19* (5), 1716-1722.

14. Teixeira, V. H.; Vila-Viçosa, D.; Baptista, A. M.; Machuqueiro, M., Protonation of DMPC in a Bilayer Environment Using a Linear Response Approximation. *J. Chem. Theory Comput.* **2014,** *10* (5), 2176-2184.
15. Chapman, D., Phospholipid bilayers physical principles and models. Gregor Cevc and Derek Marsh (Eds), John Wiley and Sons Ltd. xvi + 442 pages, £73.35 (1987). *Cell Biochemistry and Function* **1988,** *6* (2), 147-148.
16. Lipowsky, R., The conformation of membranes. *Nature* **1991,** *349* (6309), 475-481.
17. Teixeira, C. V.; Blanzat, M.; Koetz, J.; Rico-Lattes, I.; Brezesinski, G., In-plane miscibility and mixed bilayer microstructure in mixtures of catanionic glycolipids and zwitterionic phospholipids. *Biochimica et Biophysica Acta (BBA) - Biomembranes* **2006,** *1758* (11), 1797-1808.
18. J.F. Nagle, S. T.-N., *Structure and interaction of lipid bilayers: role of fluctuations*. 2001.
19. Haynes, W. M., Handbook of Chemistry and Physics, 95th Edition. CRC Press: 2014.
20. K. Simons, E. I., How cells handle cholesterol. *Science & Government Report* **2000,** *290*, 1721-1726.
21. G. Pabst, R. K., B. Pozo-Navas, M. Rappolt, K. Lohner, P. Laggner, Structural analysis of weakly ordered membrane stacks. *J. Appl. Cryst* **2003,** *36*, 1379-1388.
22. Rossi, F.; Lombardo, R.; Sciascia, L.; Sbriziolo, C.; Liveri, M. L. T., Spatio-Temporal Perturbation of the Dynamics of the Ferroin Catalyzed Belousov–Zhabotinsky Reaction in a Batch Reactor Caused by Sodium Dodecyl Sulfate Micelles. *J. Phys. Chem. B* **2008,** *112* (24), 7244-7250.
23. (a) Rossi, F.; Varsalona, R.; Liveri, M. L. T., New features in the dynamics of a ferroin-catalyzed Belousov–Zhabotinsky reaction induced by a zwitterionic surfactant. *Chemical Physics Letters* **2008,** *463* (4–6), 378-382; (b) Paul, A., Observations of the Effect of Anionic, Cationic, Neutral, and Zwitterionic Surfactants on the Belousov–Zhabotinsky Reaction. *J. Phys. Chem. B* **2005,** *109* (19), 9639-9644; (c) Jahan, R. A.; Suzuki, K.; Mahara, H.; Nishimura, S.; Iwatsubo, T.; Kaminaga, A.; Yamamoto, Y.; Yamaguchi, T., Perturbation mechanism and phase transition of AOT aggregates in the Fe(II)[batho(SO3)2]3 – catalyzed aqueous Belousov–Zhabotinsky reaction. *Chemical Physics Letters* **2010,** *485* (4–6), 304-308.
24. Noyes, R. M.; Field, R.; Koros, E., Oscillations in chemical systems. I. Detailed mechanism in a system showing temporal oscillations. *Journal of the American Chemical Society* **1972,** *94* (4), 1394-1395.
25. Field, R. J.; Koros, E.; Noyes, R. M., Oscillations in chemical systems. II. Thorough analysis of temporal oscillation in the bromate-cerium-malonic acid system. *Journal of the American Chemical Society* **1972,** *94* (25), 8649-8664.
26. (a) Steinbock, O.; Müller, S. C., Radius-Dependent Inhibition and Activation of Chemical Oscillations in Small Droplets. *J. Phys. Chem. A* **1998,** *102* (32), 6485-6490; (b) Budroni, M. A.; Rossi, F., A Novel Mechanism for In-Situ Nucleation of Spirals Controlled by the Interplay Between Phase Fronts and Reaction-Diffusion Waves in an Oscillatory Medium. *J. Phys. Chem. C* **2015**.
27. Hoops, S.; Sahle, S.; Gauges, R.; Lee, C.; Pahle, J.; Simus, N.; Singhal, M.; Xu, L.; Mendes, P.; Kummer, U., COPASI—a COmplex PAthway SImulator. *Bioinformatics* **2006,** *22* (24), 3067-3074.
28. Taylor, A. F., MECHANISM AND PHENOMENOLOGY OF AN OSCILLATING CHEMICAL REACTION. *Progress in Reaction Kinetics and Mechanism* **2002,** *27* (4), 247-325.
29. Benini, O.; Cervellati, R.; Fetto, P., Experimental and mechanistic study of the bromomalonic acid/bromate oscillating system catalyzed by [Fe(phen)3]2+. *Int. J. Chem. Kinet.* **1998,** *30* (4), 291-300.
30. Rossi, F.; Ristori, S.; Marchettini, N.; Pantani, O. L., Functionalized Clay Microparticles as Catalysts for Chemical Oscillators. *J. Phys. Chem. C* **2014,** *118* (42), 24389-24396.

31. Burgess, A. E.; Latham, J. L., Kinetics of fast brominations: A potentiometric study. *Journal of Chemical Education* **1969,** *46* (6), 370.
32. Yates, K.; McDonald, R. S.; Shapiro, S. A., Kinetics and mechanisms of electrophilic addition. I. Comparison of second- and third- order brominations. *The Journal of Organic Chemistry* **1973,** *38* (14), 2460-2464.
33. Strizhak, P. E.; Khavrus', V. A.; Goncharenko, M. M.; Ivashchenko, T. S., Kinetic scheme for a ferroin-catalyzed belousov-zhabotinskii reaction with compound-period transient states. *Theoretical and Experimental Chemistry* **1998,** *34* (3), 138-143.
34. Kalishin, E. Y.; Goncharenko, M. M.; Khavrus, V. A.; Strizhak, P. E., Periodic, Mixed-Mode, and Chaotic Regimes in the Belousov–Zhabotinskii Reaction Catalyzed by Ferroin. *Kinetics and Catalysis* **2002,** *43* (2), 233-244.

Supporting Information

Interaction of the Belousov-Zhabotinsky Reaction with Phospholipid Engineered Membranes

Kristian Torbensen,[a] *Federico Rossi,*[b] *Ottorino L. Pantani,*[c] *Sandra Ristori,*[d]***

and Ali Abou-Hassan[a]***

[a] Sorbonne Universités, UPMC Univ Paris 06, UMR 8234, Laboratoire Physico-chimie des Electrolytes, Nanosystèmes InterfaciauX (PHENIX), 4 place Jussieu - case 51, 75252 Paris cedex 05 – France

[b] Department of Chemistry and Biology, University of Salerno, Via Giovanni Paolo II 132, Fisciano (SA), Italy

[c] Department of Agrifood Production and Environmental Sciences, University of Florence, P.zle Cascine 28, 50144 Firenze, Italy

[d] Department of Earth Sciences & CSGI, University of Florence, Via della Lastruccia 3, 50019 Sesto Fiorentino, Firenze, Italy

SAXS EXPERIMENTS AND CURVE FITTING:

Fitting of SAXS diagrams

The GAP software models the SAXS intensity profiles of bilayer-based structures by the following equation:

$$I(q) = \frac{(1 - N_{diff})\, S(q)P(q) + N_{diff}\, P(q)}{q^2} \qquad (1)$$

where N_{diff} is the fraction number of positionally uncorreraled bilayers (i.e. those forming non interacting vesicles), *S(q)* is the structure factor defining the spatial distribution of scatteres and describing the inter-particle interactions and *P(q)* is the absolute square of the bilayer form factor. In this work, a structure factor obtained by a modified Caillé theory[1, 2] was chosen to model the bilayer interactions when quasi-Bragg peaks were evidenced in the intensity profiles. The electron density is modelled in the GAP software by a three-Gaussians profile,[3] representing the polar head groups, placed at ± z_H, and the hydrocarbon core. The standard deviation of these electron distributions are σ_H and σ_C, respectively. The terminal methyl group in the bilayer center corresponds to the minimum of the electron density profile, as sketched in scheme SI1. The amplitude (always negative) of the hydrophobic tails with respect to the headgroup is termed ρ_H.

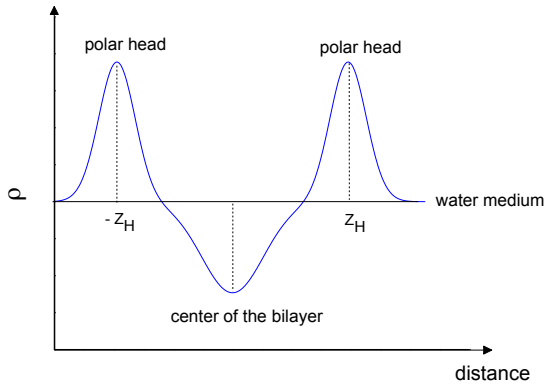

Scheme SI1. Electron density profile as a function of the distance from the bilayer center, modeled by the sum of three gaussian distributions.

In summary, the best fit parameters used in this fitting procedure were: The lamellar repeating distance, *d* (for systems presenting Bragg peaks); the average number of bilayers per scattering domain (*N*) and the fraction of positionally uncorrelaed bilayers (N_{diff}); the Gaussian distributin center of the polar heads electron density profile (z_H) and its standard variation width (σ_H); the Gaussian distribution center and standard variation of the hydrophobic core (z_C and σ_C , respectively), the amplitude (always negative) of the hydrophobic tails Gaussian relative to the headgroup Gaussian (ρ_C) and the fluctuation Caillé parameter (η) related to the bilayer bending rigidity.

The best-fit valus which describe the structure and the electron density of DMPC lamellar phases in water and in different dispersing media are reported in table SI1. For all systems the

total lipid content was kept constant at 1% w/w.

The electron density profiles of plain a DMPC bilayer in the presence of different water soluble species and bilayer components are shown in figure SI1 and SI2, respectively. For these profiles, normalization was performed with respect to the absolute value of the DMPC bilayer center, i.e. 0.2 e/Å. This choice was motivated by the following considerations: (i) ferroin is absorbed on the surface (see main text) and it is not expected to inflence the bilayer center electron density; (ii) the bilayer absorption of small water molecules should bring very little effct to the elctron density of this highly hydrophobic region; (ii) myr A carry the same chian as DMPC, therefore the bilayer interior of plain DMPC, DMPC-myr A and DMPC-myr A-STS bilayer should be very close to one another.

Table SI1. Structural and electron density parameters

System composition and dispersing medium	d (Å)	N	z_H (Å)	σ_H (Å)	σ_C (Å)	ρ_C (Å)	η	N_{diff}
DMPC in water	65.0	3.1	19.3	5.1	3.8	- 1.10	0.16	0.60
DMPC + ferroin[(a)] in water	-	-	18.8	3.1	4.6	- 0.90	-	-
DMPC in BZ/water	-	-	21.0	3.1	4.2	- 0.70	-	-
DMPC + myr A in water	63.5	7.5	19.3	2.3	2.3	- 0.98	0.09	0.35
DMPC + myrA + STS in water	-	-	19.5	2.3	4.0	- 0.68	-	-

(a) ferroin = 2.5 10^{-3} M
(b) MA 0.15 M, BrO^{3-}, 0.18 M, H_2SO_4 0.35 M, ferroin 2.5 10^{-3} M
(c) DMPC : myrA = 0.8 : 0.2 molar ratio
(d) DMPC : myrA :STS = 0.80 : 0.15 :0.05 molar ratio

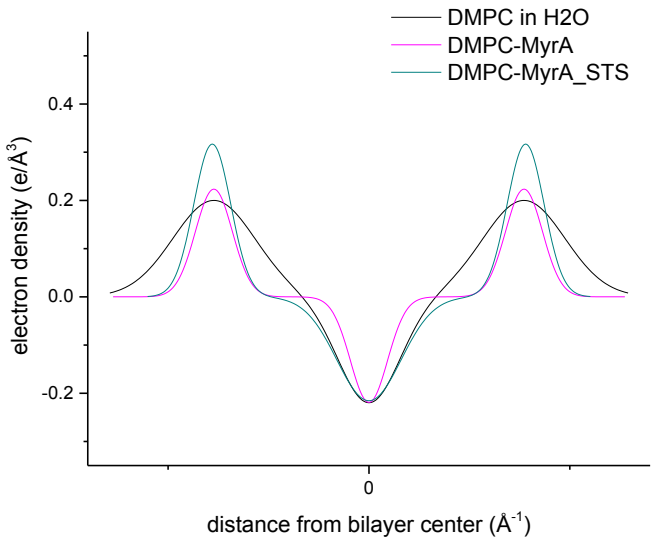

Figure SI1. Comparison among the electron density profile of bilayers containing pure DMPC, DMPC + myr A (0.8/0.2 mol fraction) and DMPC + myr A + STS (0.80/0.15/0.05 mol fraction).

ZETA POTENTIAL AND EXTRUDED LIPOSOMES:

The surface charge of extruded liposomes (having the same composition as the samples used for the SAXS experiments) was measured by electrophoretic light scattering with a Coulter DELSA 440 SX appartus (Coulter Corporation, Miami, FL, USA). Homemade hemispherical electrodes covered by a thin gold layer were used in the measurement cell. This variant was necessary in the present study, since samples containing BZ solutions would oxidize the silver electrodes typically used in this kind of instruments. The obtained Zeta potential values are reported in Table SI2 and refers to the average over 5 runs with detection at different angles (7.5°, 15°, 22.5° and 30°).

For liposome preparation, mixtures of dry lipids were dissolved in chloroform/methanol 2/1 and the solvent was evaporated under vacuum overnight. The resulting mixed lipid film was then swollen at room temperature with MilliQ grade water. Upon vortexing, multilamellar vesicles were obtained, which were then submitted to eight freeze/thaw cycles and subsequently downsized by extrusion through 100 nm polycarbonate membranes.Twenty-seven extrusions were performed with the LiposoFast apparatus, Avestin, Ottawa, Canada. Zeta potentials was measured not later than 5-6 hours after liposome prepration, since extruded suspension were a

little less stable than the spontaneous dispersions used for the SAXS experiments.

Table SI2. Zeta potential of liposomes*

pure DMPC in water	- 5 ± 2 mV
DMPC in water + ferroin	+ 11 ± 2 mV
pure DMPC in H_2SO_4	+ 11 ± 3 mV
DMPC in BZ/water	+ 18 ± 2 mV
DMPC + myr A in water	+ 18 ± 1 mV
DMPC + myrA + STS in water	- 14 ± 3 mV

* reproducilibily was observed to be within experimental error (by 2-3 replica measurements for each sample).

It is to be noted that in the presence of BZ reactant liposomes bear a positive charge, which is attributed to the protonation of the phospate groups of DMPC in the extremely acidic pH given by H_2SO_4 0.35 M.

CHOLESTEROL BROMINATION:

The bromination of olefins and ring-substituted compounds in polar solvents can be a rather complex mechanism depending on the substituents and on the presence of high concentration of Br^- in solution. However, when the analytic concentrations of the reactants $[olefin]_0$ and $[Br_2]_0$ are equal, the process can be described by a second order rate law, being the addition of the second bromine atom the rate determining step.[4] Therefore, for the cholesterol bromination

$$Br_2 + CHOL \xrightarrow{K} Br_2\text{-}CHOL \qquad (2)$$

when $[Br_2]_0 = [CHOL]_0$ the rate law can be written as

$$\frac{d[\mathrm{Br_2}]_t}{dt} = -\mathrm{K}[\mathrm{CHOL}]_t[\mathrm{Br_2}]_t \tag{3}$$

and, given the stoichiometry of the reaction, relation (4) holds

$$[\mathrm{CHOL}]_0 - [\mathrm{CHOL}]_t = [\mathrm{Br_2}]_0 - [\mathrm{Br_2}]_t \tag{4}$$

therefore, equation (3) can be rewritten as

$$\frac{d[\mathrm{Br_2}]_t}{dt} = -\mathrm{K}[\mathrm{Br_2}]_t^2 \tag{5}$$

which, integrated between $[Br_2]_0$ and $[Br_2]_t$ and 0 and t, yields the operative equation to calculate K as the slope of

$$\frac{1}{[\mathrm{Br_2}]_t} = \mathrm{K}t + \frac{1}{[\mathrm{Br_2}]_0} \tag{6}$$

In order to study the kinetics of equation (2) through the formula (6), we performed a series of experiments by following spectrophotometrically $[Br_2]_t$ at l = 400 nm, where the molar extinction coefficient of bromine is about 230 M^{-1} cm^{-1}, and we plotted data according to equation (6).

Experiments were performed in Methyl-*tert*-butyl ether (MTBE), in order to avoid the precipitation of Br_2-CHOL and to work with higher concentration of cholesterol, which solubility in MTBE is higher than that in water. We mixed equal concentrations of the reactants (1.3 mM) and a typical spectorphotometric recording is reported in Figure SI2. From the fitting of experimental data a value ok K = 0.129 $M^{-1}s^{-1}$ has been found.

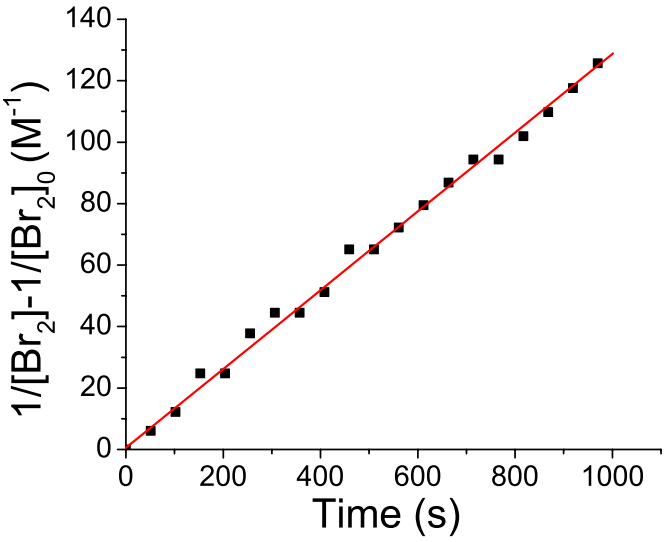

Figure SI2. Second order kinetics for the bromuration of Cholesterol.

NUMERICAL SIMULATION OF THE BZ REACTION:

Below is listed the complete reaction scheme used for the numerical simulation performed using the CO.PA.SI. software for the ferroin catalyzed BZ reaction. Table SI2 shows the related kinetic constants.

$$HOBr + Br^- + H^+ \rightleftharpoons Br_2 + H_2O \quad \text{(R1)}$$

$$Br^- + HBrO_2 + H^+ \rightarrow 2HOBr \quad \text{(R2)}$$

$$2HBrO_2 \rightarrow BrO_3^- + HOBr + H^+ \quad \text{(R3)}$$

$$Br^- + BrO_3^- + 2H^+ \rightleftharpoons HOBr + HBrO_2 \quad \text{(R4)}$$

$$BrO_3^- + HBrO_2 + H^+ \rightleftharpoons Br_2O_4 + H_2O \quad \text{(R5)}$$

$$Br_2O_4 \rightleftharpoons 2BrO^\bullet \quad \text{(R6)}$$

$$Fe(phen)_3^{2+} + BrO_3^- + 2H^+ \rightarrow Fe(phen)_3^{3+} + BrO_2^{\bullet} + H_2O \quad \text{(R7)}$$

$$Fe(phen)_3^{2+} + BrO_2^{\bullet} + H^+ \rightarrow Fe(phen)_3^{3+} + HBrO_2 \quad \text{(R8)}$$

$$Fe(phen)_3^{3+} + BrCH(COOH)_2 \rightleftharpoons Fe(phen)_3^{2+} + {}^{\bullet}CBr(COOH)_2 + H^+ \quad \text{(R9)}$$

$$BrCH(COOH)_2 \rightleftharpoons (HOOC)CBr{=}C(OH)_2 \quad \text{(R10)}$$

$$(HOOC)CBr{=}C(OH)_2 + Br_2 \rightarrow Br_2C(COOH)_2 + Br^- + H^+ \quad \text{(R11)}$$

$$(HOOC)CBr{=}C(OH)_2 + HOBr \rightarrow Br_2C(COOH)_2 + H_2O \quad \text{(R12)}$$

$$2\,{}^{\bullet}CBr(COOH)_2 + H_2O \rightarrow BrCOH(COOH)_2 + BrCH(COOH)_2 \quad \text{(R13)}$$

$$BrCOH(COOH)_2 \rightarrow Br^- + CO(COOH)_2 + H^+ \quad \text{(R14)}$$

Table SI2. Values of rate constants for reactions R1 – R14.

reaction	$k_{forward}$	$k_{inverse}$
R1	8×10^9 mol^{-2} dm^6 s^{-1}	80 s^{-1}
R2	2.5×10^6 mol^{-2} dm^6 s^{-1}	
R3	3×10^3 mol^{-1} dm^3 s^{-1}	
R4	10 mol^{-3} dm^9 s^{-1}	3.2 mol^{-1} dm^3 s^{-1}
R5	48 mol^{-2} dm^6 s^{-1}	3.2×10^3 s^{-1}
R6	7.5×10^4 s^{-1}	1.4×10^9 mol^{-1} dm^3 s^{-1}
R7	0.38 mol^{-3} dm^9 s^{-1}	
R8	1×10^9 mol^{-2} dm^6 s^{-1}	
R9	13 mol^{-1} dm^3 s^{-1}	6×10^8 M^{-2} s^{-1}
R10	0.012 s^{-1}	800 s^{-1}
R11	3.5×10^6 mol^{-1} dm^3 s^{-1}	
R12	6.6×10^4 mol^{-1} dm^3 s^{-1}	
R13	1×10^8 mol^{-1} dm^3 s^{-1}	
R14	1.5 s^{-1}	

1. S. T.-N. J.F. Nagle, *Structure and interaction of lipid bilayers: role of fluctuations*, 2001.
2. G. PABST, *Biophysical Reviews and Letters*, 2006, 01, 57-84.
3. R. K. G. Pabst, B. Pozo-Navas, M. Rappolt, K. Lohner, P. Laggner, *J. Appl. Cryst*, 2003, 36, 1379-1388.
4. K. Yates, R. S. McDonald and S. A. Shapiro, *The Journal of Organic Chemistry*, 1973, 38, 2460-2464.

Chapter III: Tuning the Chemical Communication of Oscillating Microdroplets by Means of Membrane Composition

III.1. Introduction

Following the bottom-up approach towards encapsulating the BZ-reaction in liposomes, one task is to seek a BZ-composition compatible with the microfluidics viscosity modulator. For the latter, polyvinyl alcohol (PVA) was the choice, as will be reported in later chapters. Here, the oscillatory behaviour of different BZ-compositions in the presence of PVA is investigated, in order to find a sustainable system suitable for the study of chemical communication between BZ-encapsulating liposomes. Analysing the suggested BZ-composition encapsulated in a simple emulsion droplet network, stabilized by phospholipids, provided insight on the effect of a lipid interface as a barrier-to-cross for the pertinent BZ-messenger molecules. By doping the interface, various synchronized behaviours were obtained. Finally in this chapter, an attempt to govern the BZ-reaction photochemically is described.

III.2. Influence of polyvinyl alcohol on the oscillatory behaviour of the Beluosov-Zhabotinsky reaction –A preliminary study for the choice of system

Polyvinyl alcohol (PVA) is often used as a viscosity modulator in microfluidics,[1-5] in particular for the generation of double emulsions serving as templates for liposomes. In the context of encapsulating the Belousov-Zhabotinsky (BZ) reaction in liposomes, for the study of communication between networks of the latter, the influence of PVA on the Belousov-Zhabotinsky (BZ) reaction is of interest. Since the BZ reaction constitutes a diffusion-reaction system, the main influence will be that changing the diffusion of the activatory and inhibitory species governing the oscillating dynamics. However, since each monomer unit of PVA include an alcohol group, other effects such as chemical oxidation by the BZ reaction component bromate, might influence the oscillation dynamics. In this preliminary chapter, the influence of PVA on the BZ reaction (the oscillation periods and frequency) in bulk solution is investigated by means of UV-vis spectroscopy in order to find a suitable system to be used for encapsulating the BZ reaction in liposomes. The main criteria for such a system is sustainable oscillations over a time span suitable for observing mutual activatory or inhibitory synchronization between liposomes in networks. Furthermore, the oscillation periods within each encapsulating unit must be at least that of the time of diffusion, of the activatory and inhibitory species, between each unit, in order to detect any mutual effects on the synchronization of the units in a network.[6]

In the following, three different BZ-compositions were chosen, and the graphs displaying the influence of PVA at various concentrations on the oscillatory behaviour in bulk solution are shown. In general, the BZ-systems described in Table 1-3, were monitored in the absence and presence of 1-5 % (w/w) PVA under mechanically stirring. The BZ components *i.e.,* malonic acid (MA), sulphuric acid (H_2SO_4) and ferroin (Fe^{2+}), except for the bromate (BrO_3^-), were introduced to a 1 cm quartz cuvette. After stirring, bromate was added and recording of the absorbance at 512 and 598nm, *i.e.,* the wavelength of maximum absorbance by ferroin (Fe^{2+}, red) and ferriin (Fe^{3+}, blue), were initiated immediately hereafter. Upon stirring, the BZ-reaction oscillated homogeneously in the cuvette, i.e., the colour changes due to oxidation/reduction of ferroin/ferriin occurred rapidly over the entire solution, see Figure 1. Figures 2, 4, and 6 show the absorbance-time plots. From these plots, the induction period, determined as the time from addition of bromate to the first

detectable oscillation as well as the time between two subsequent oscillations at various selected times of the experiment were deduced, see Figures 3, 5, and 7. In these plots, the development in

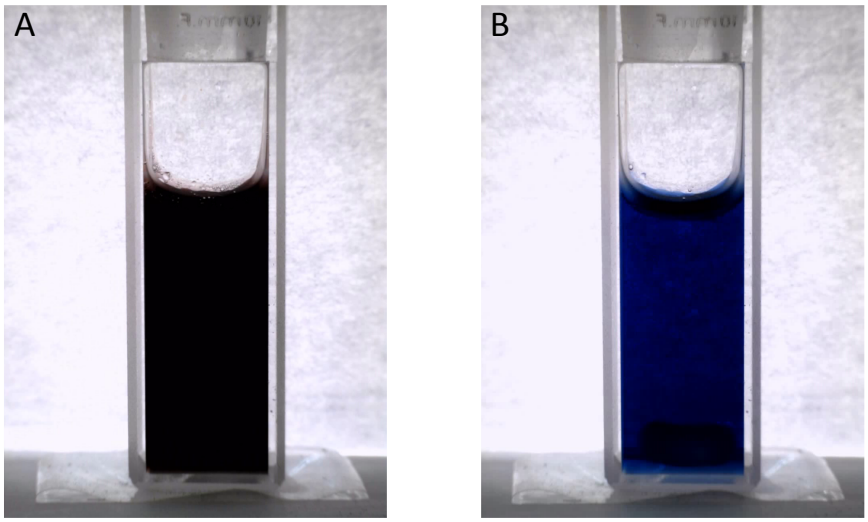

Figure 1. Images of the cuvette containing the the BZ-reaction, showing the homogeneity of the solution upon oscillation. (A) ferroin (Fe^{2+}, red)and (B) ferriin (Fe^{3+}, blue)

oscillation periods with time is displayed. The conversion efficiency of the system, *i.e.,* the degree of oxidation of ferroin to ferriin, was calculated by plotting the normalized absorbance, defined as

$$(\delta A_{red}/\delta A_{ox})/(\varepsilon_{ox}/\varepsilon_{red}) \qquad \text{Eq. 1}$$

for various times during the experiment. In *eq.* 1, δA_{red} and δA_{ox} represents the change in absorbance during one oscillatory cycle for ferroin and ferriin, respectively, and ε is the corresponding extinction coefficients. This was done in order to find a system providing the highest optical contrast for the BZ-system, monitored using optical microscopy, as *Eq.* 1 would take the value of unity for a total conversion of ferroin to ferriin during each oscillatory cycle, see Figure 8. However, this was only possible for the BZ-systems described in Table 3, since the absorbance spectra recorded at 598nm are too noisy to deduce values of δA_{ox} for the remaining BZ-systems. The values of the extinction coefficients were obtained by recording the absorbance at different concentrations of the two redox forms of ferroine, and derived by applying the Beer-Lambert law, $A = \varepsilon\ c\ l$, where A is the absorbance, ε the extinction coefficient ($Lmol^{-1}cm^{-1}$), c the concentration ($molL^{-1}$) and l the cuvette length (cm), see Figure 9. Values of 1.08 x 10^4 and 502 $Lmol^{-1}cm^{-1}$ were

found for ferroin and ferriin, respectively. These values are in good accordance with literature values.[7] Finally, the viscosity of aqueous solutions containing various concentrations was measured, as reported in Figure 10.

In the following, the investigated BZ-systems and their respective oscillatory behaviour in bulk solutions are presented.

Table 1. Concentrations of the BZ-system shown in Figure 1.

specie	conc./M
H_2SO_4	0.30
$NaBrO_3$	0.12
MA	0.03
ferroine	0.0005

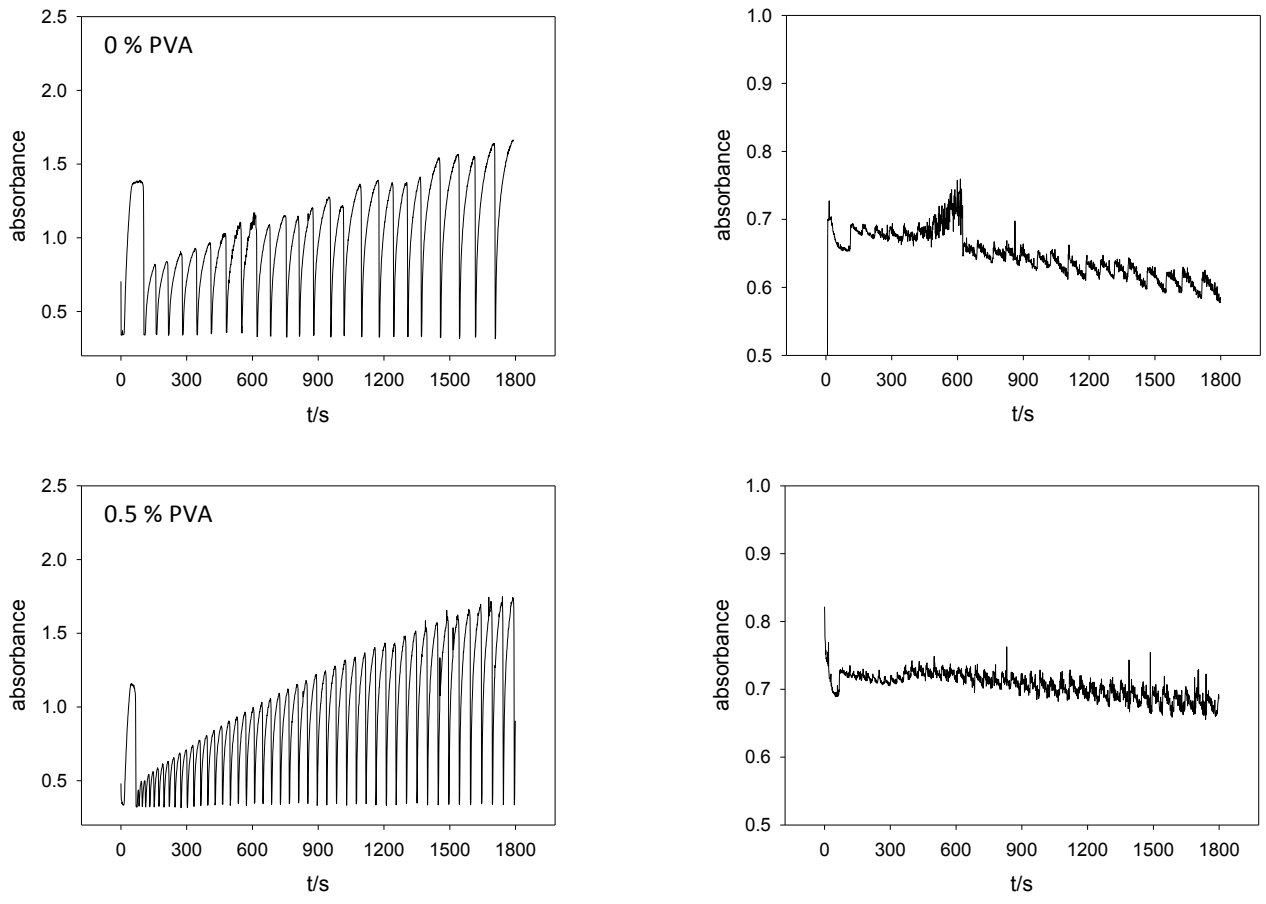

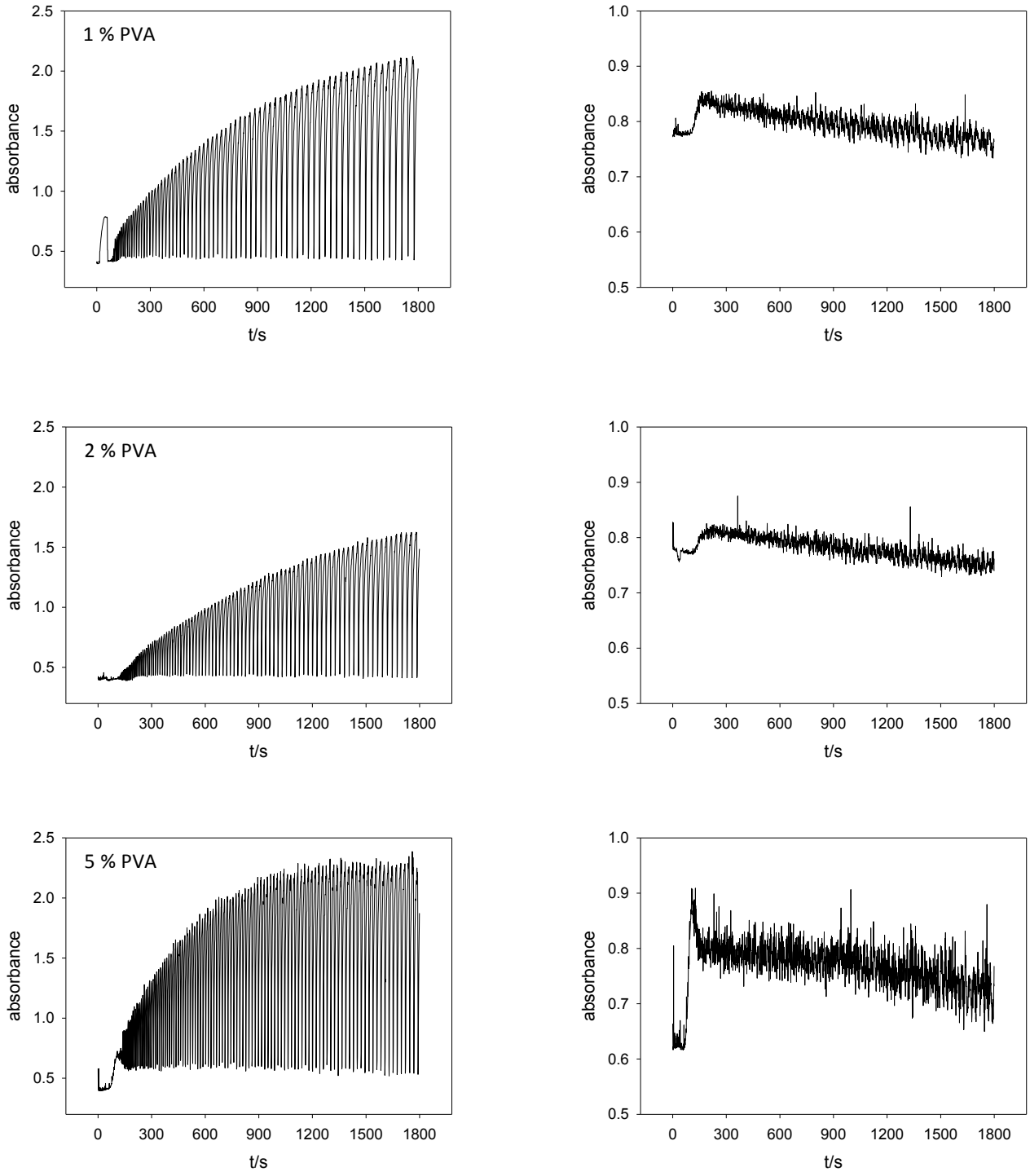

Figure 2. Absorbance-time plots recorded at 512 (left) and 598 nm (right) for various PVA concentrations. BZ composition as tabulated in Table 1.

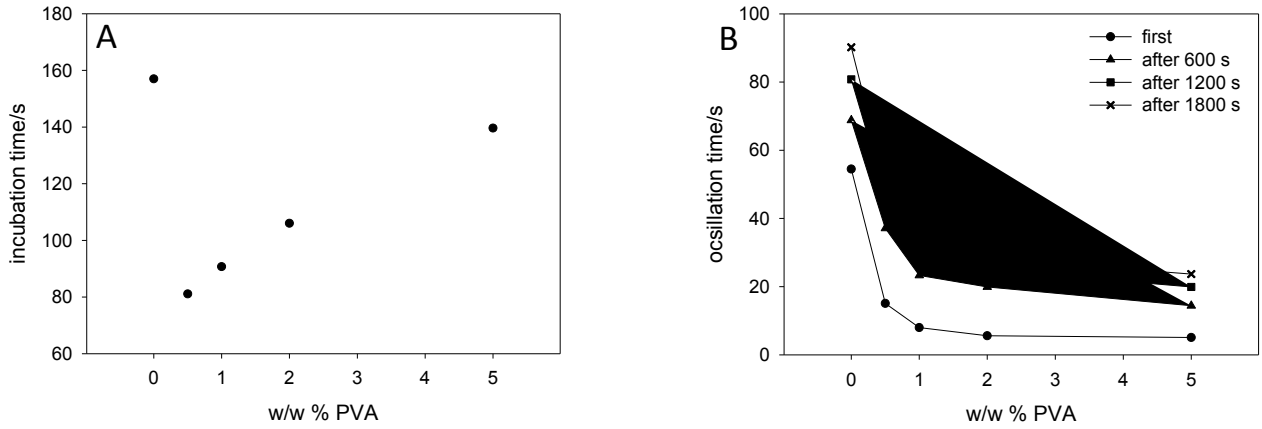

Figure 3. (A) Induction period, defined as the onset of oscillation in the BZ reaction measured from the addition of bromate, for various concentrations of PVA. (B) Development in oscillation time for various PVA concentrations as the BZ reaction proceeds. BZ composition as tabulated in Table 1.

Table 2. Concentrations of the BZ-system shown in Figure 4.

specie	conc./M
H_2SO_4	0.080
$NaBrO_3$	0.300
MA	0.100
ferroin	0.003

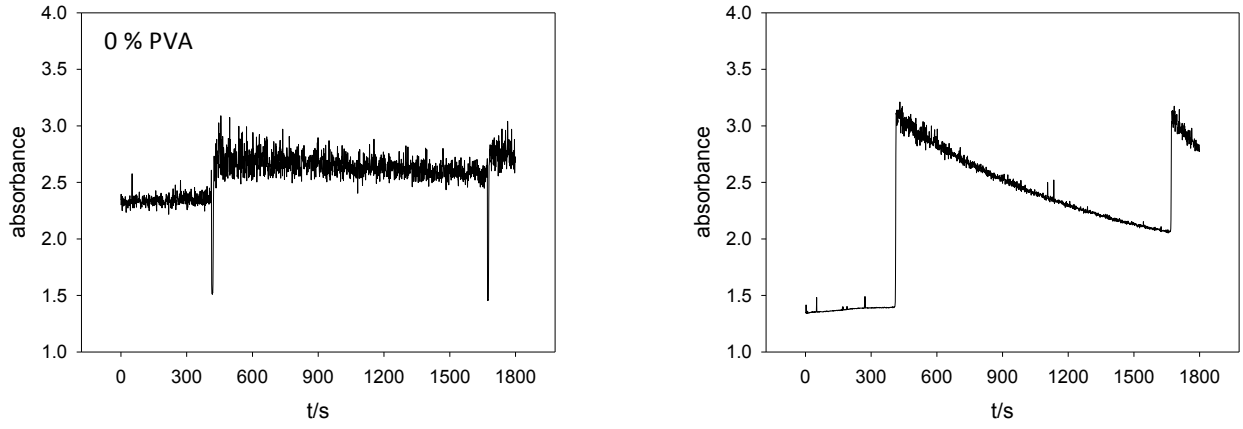

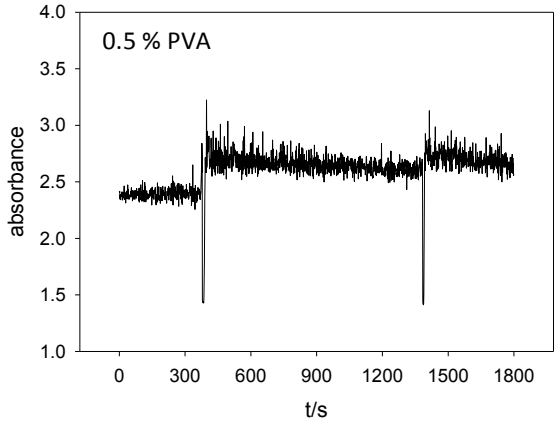
0.5 % PVA
absorbance
t/s
4.0
3.5
3.0
2.5
2.0
1.5
1.0
0
300
600
900
1200
1500
1800

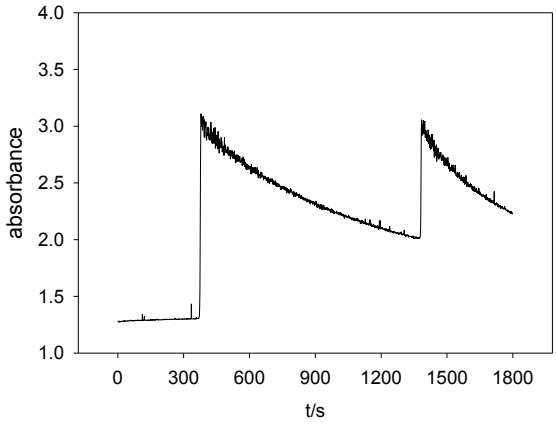
absorbance
t/s
4.0
3.5
3.0
2.5
2.0
1.5
1.0
0
300
600
900
1200
1500
1800

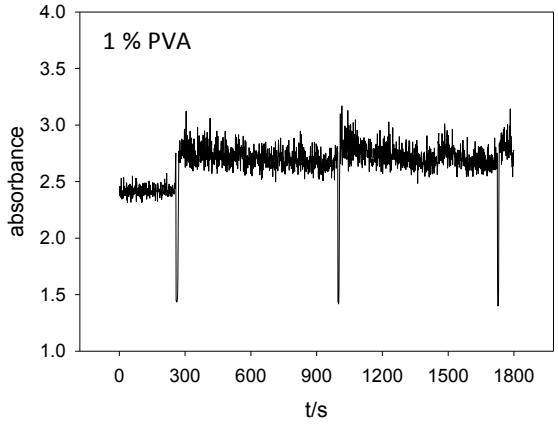
1 % PVA
absorbance
t/s
4.0
3.5
3.0
2.5
2.0
1.5
1.0
0
300
600
900
1200
1500
1800

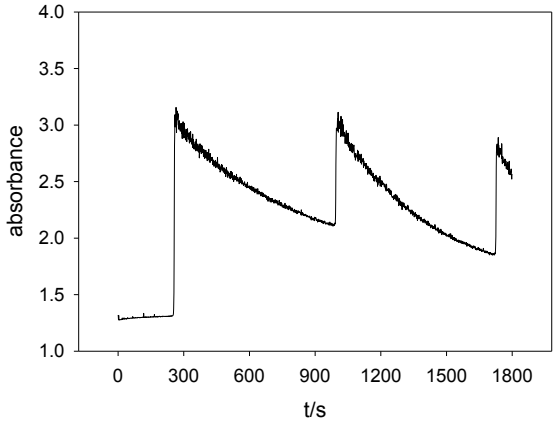
absorbance
t/s
4.0
3.5
3.0
2.5
2.0
1.5
1.0
0
300
600
900
1200
1500
1800

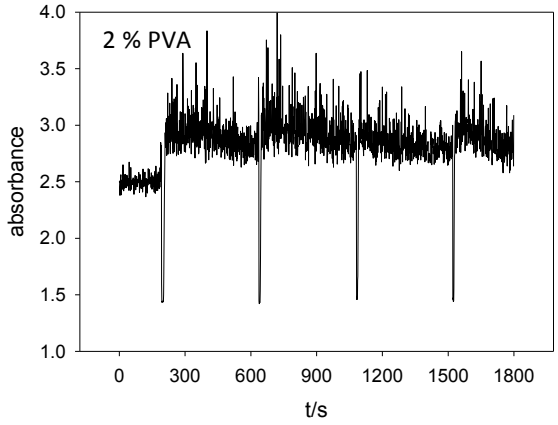
2 % PVA
absorbance
t/s
4.0
3.5
3.0
2.5
2.0
1.5
1.0
0
300
600
900
1200
1500
1800

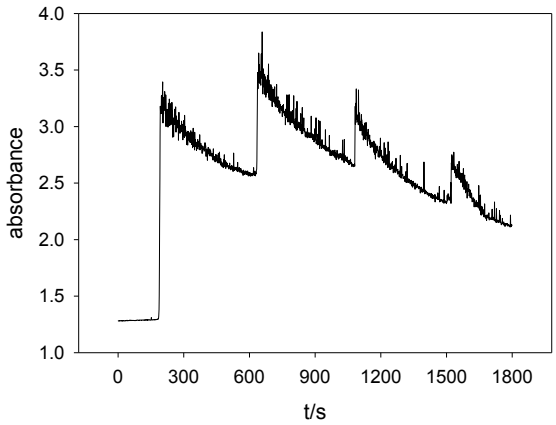
absorbance
t/s
4.0
3.5
3.0
2.5
2.0
1.5
1.0
0
300
600
900
1200
1500
1800

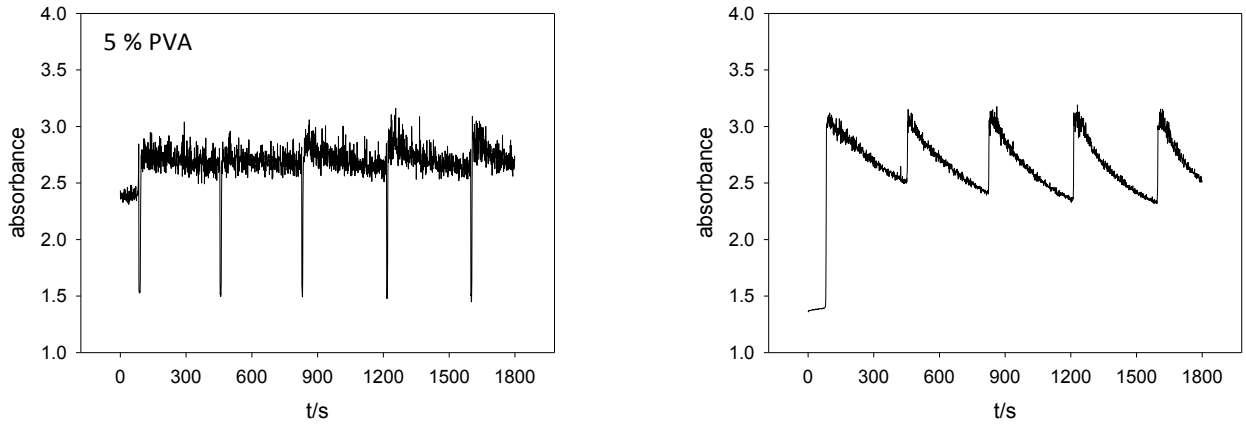

Figure 4. Absorbance-time plots recorded at 512 (left) and 598 nm (right) for various PVA concentrations. BZ composition as tabulated in Table 2.

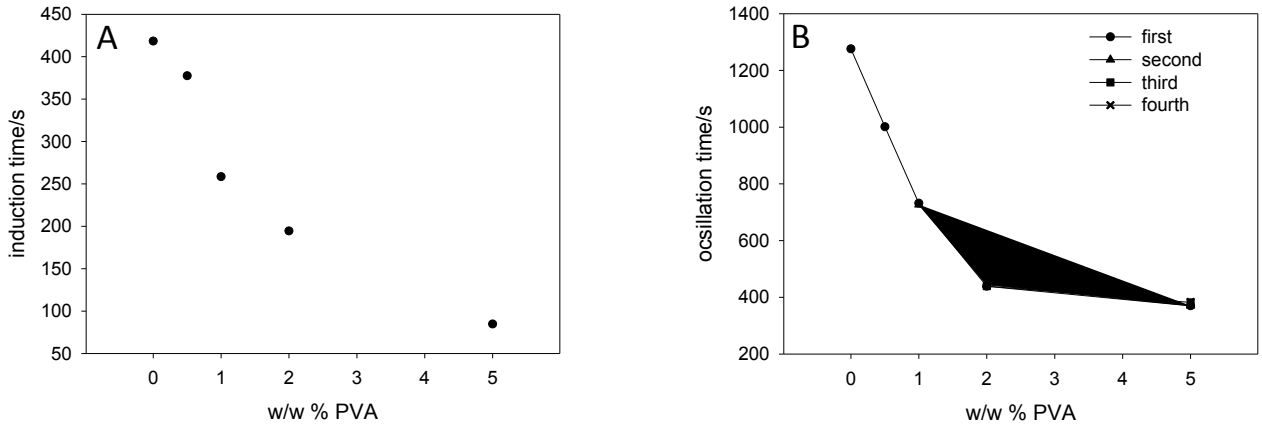

Figure 5. (A) Initiation time, defined as the onset of oscillation in the BZ reaction measured from the addition of bromate, for various concentrations of PVA. (B) Development in oscillation time for various PVA concentrations as the BZ reaction proceeds. BZ composition as tabulated in Table 2. Note, that in Figure 5B, the oscillation period is assigned to the number of oscillation instead of time.

Table 3. Concentrations in the BZ-system shown in Figure 6.

specie	conc./M
H_2SO_4	0.30
$NaBrO_3$	0.12
MA	0.30
ferroin	0.0005

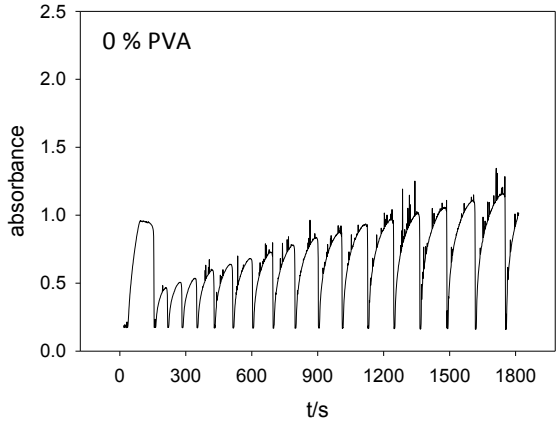
0 % PVA
absorbance
t/s
2.5
2.0
1.5
1.0
0.5
0.0
0
300
600
900
1200
1500
1800

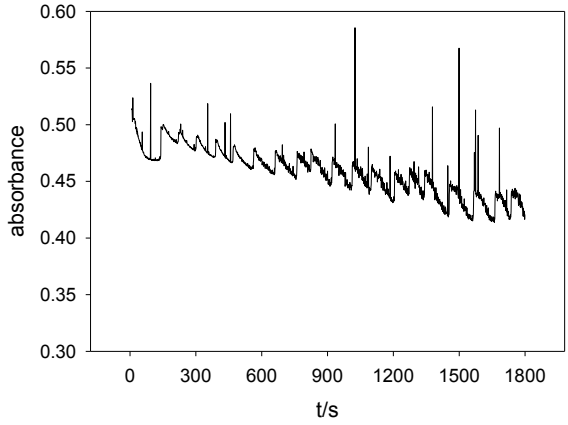
absorbance
t/s
0.60
0.55
0.50
0.45
0.40
0.35
0.30
0
300
600
900
1200
1500
1800

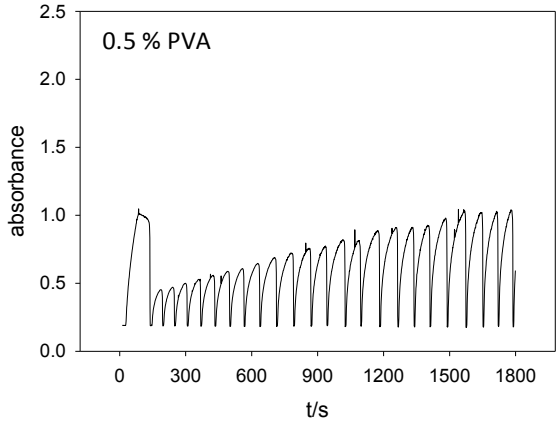
0.5 % PVA
absorbance
t/s
2.5
2.0
1.5
1.0
0.5
0.0
0
300
600
900
1200
1500
1800

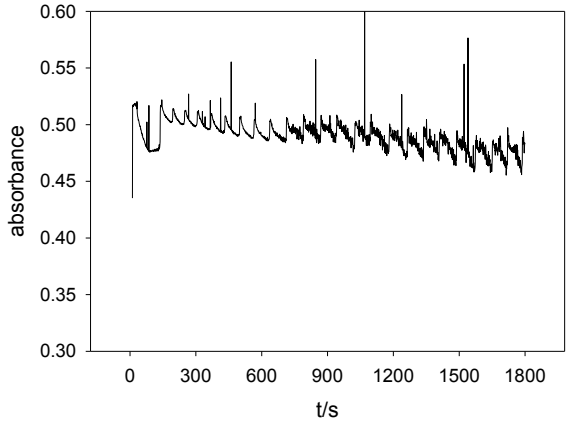
absorbance
t/s
0.60
0.55
0.50
0.45
0.40
0.35
0.30
0
300
600
900
1200
1500
1800

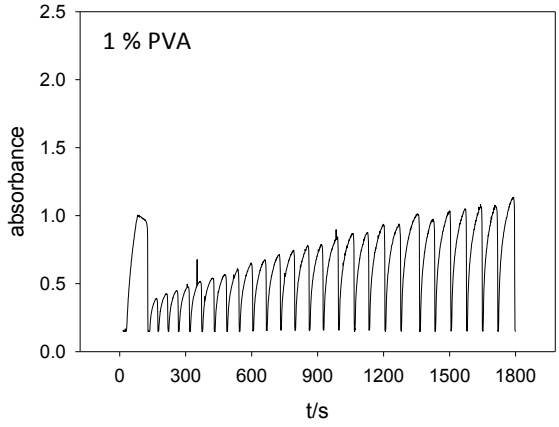
1 % PVA
absorbance
t/s
2.5
2.0
1.5
1.0
0.5
0.0
0
300
600
900
1200
1500
1800

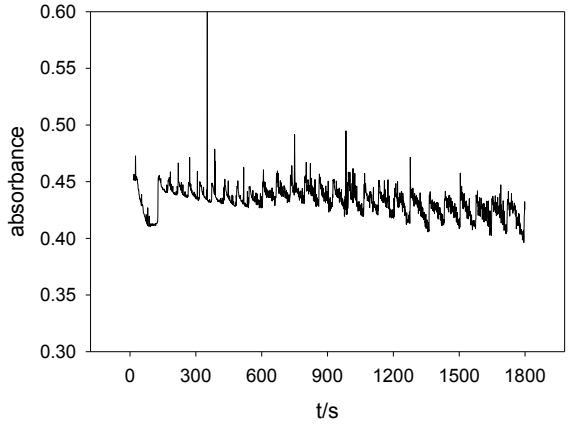
absorbance
t/s
0.60
0.55
0.50
0.45
0.40
0.35
0.30
0
300
600
900
1200
1500
1800

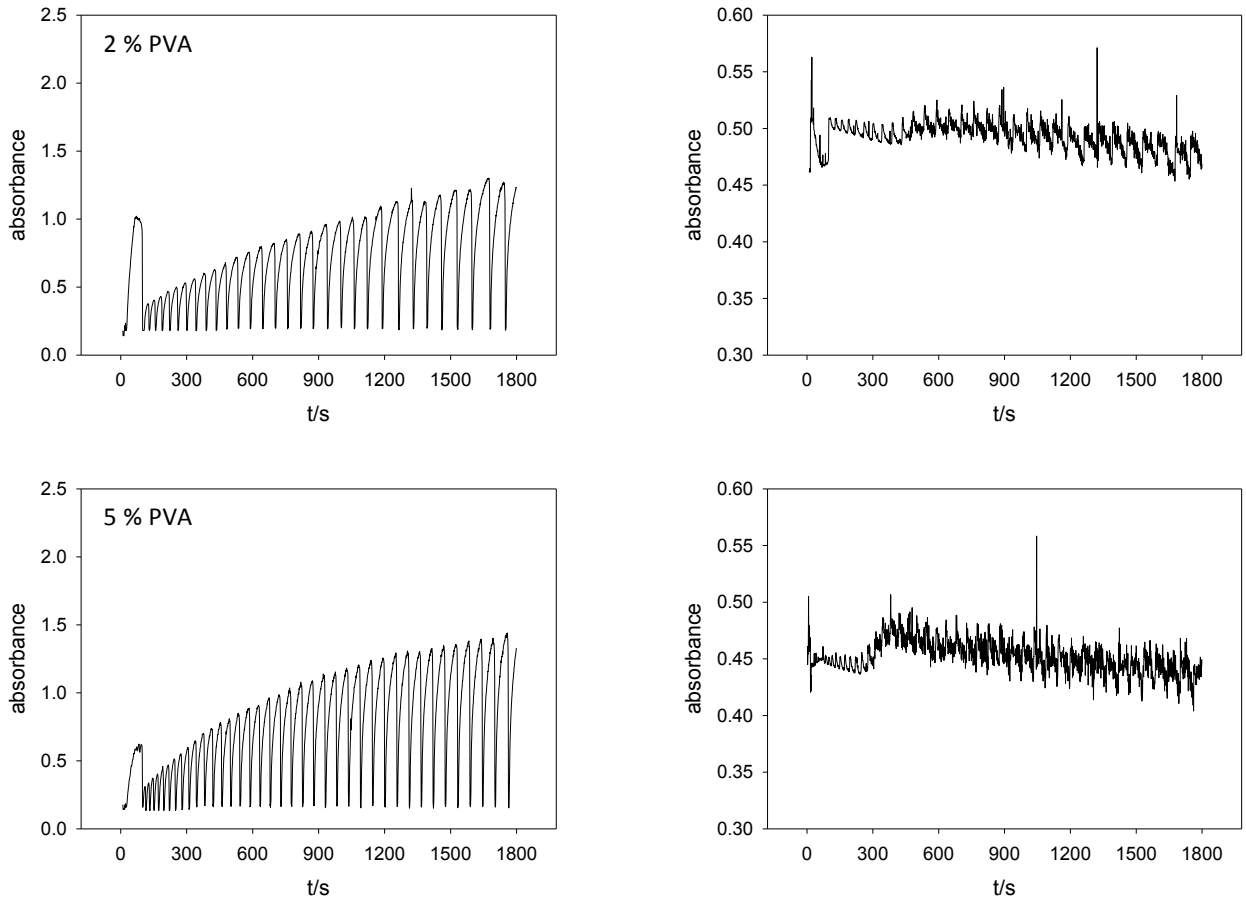

Figure 6. Absorbance-time plots recorded at 512 (left) and 598 nm (right) for various PVA concentrations. BZ composition as tabulated in Table 3. Note that the scale was changed in the graphs recorded at 598 nm for 2 and 5% PVA.

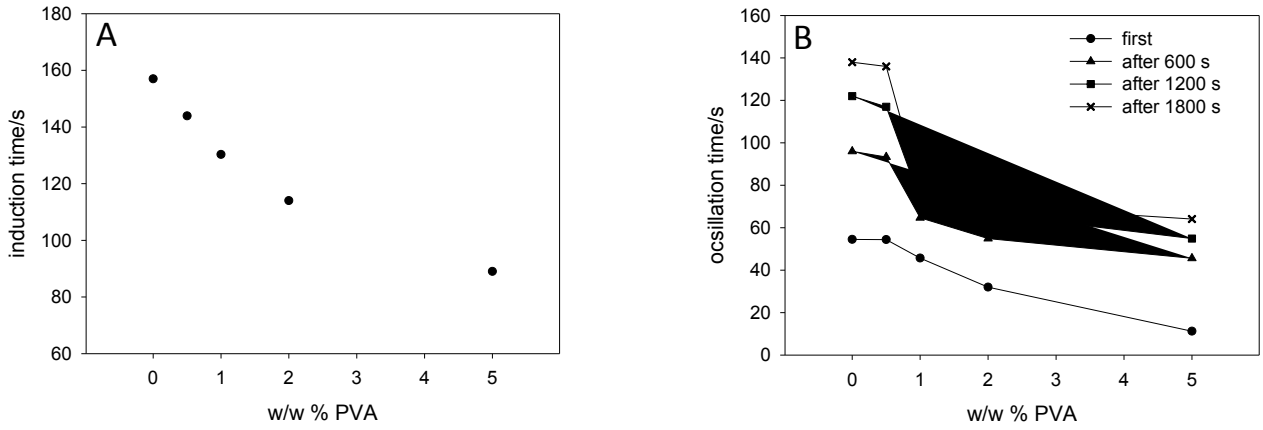

Figure 7. (A) Induction period, defined as the onset of oscillation in the BZ reaction measured from the addition of bromate, for various concentrations of PVA. (B) Development in oscillation time for various PVA concentrations as the BZ reaction proceeds. BZ composition as tabulated in Table 3.

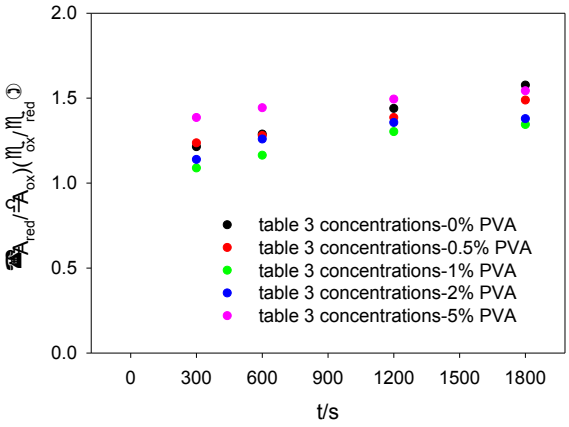

Figure 8. Development in normalized absorbance of the reduced and oxidized ferroin as a function of time for the BZ reaction. Concentrations as tabulated in Table 3

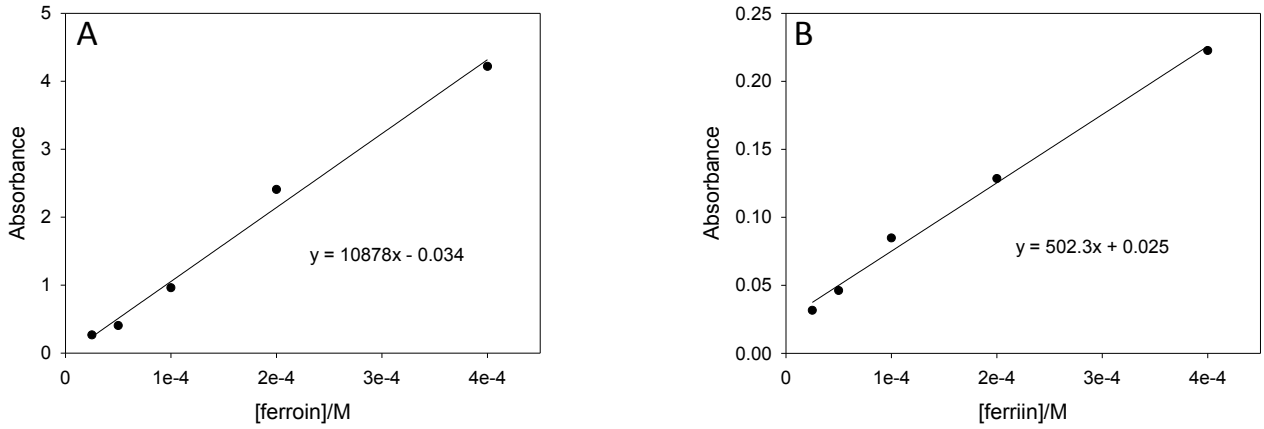

Figure 9. Extinction coefficients for (A) ferroin and (B) ferriin, derived as the slope of the line in the absorbance-concentration plots.

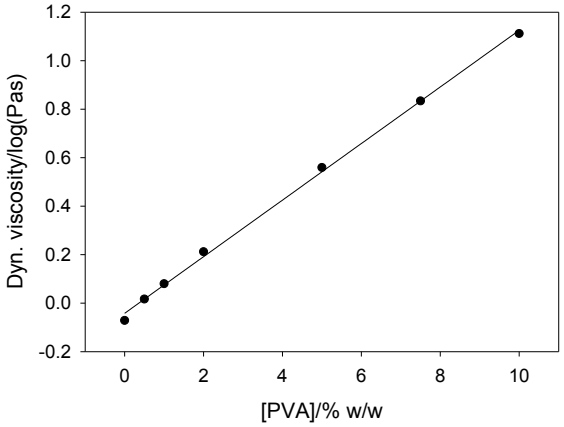

Figure 10. Dynamic viscosity of aqueous solutions containing various concentrations of PVA.

Of the various BZ-systems investigated here, only those of Table 2, 4 and 5 shows sustainable oscillations over the entire time span recorded, and for all the applied concentrations of PVA. The BZ-systems of Table 2 and 5 show relative fast oscillation periods, with minimum values of 5 and 30s respectively, except for the first oscillations of the system of Table 5 for 5% (w/w) PVA. Defining the diffusion length of small ionic species in aqueous solutions as $x = (t/2D)^{0.5}$, where t is the time of diffusion and D the Einstein-Stokes diffusion constant with a typical value of 5×10^{-5} cm^2s^{-1}, species will be able to diffuse between 100 and 250 μm between each oscillation cycle for the systems of Table 2 and 5, respectively. Hence, these BZ-systems will be suitable for the investigation of mutual communication between confined oscillating microsystems over a short range, *i.e.,* below the lengths of diffusion mentioned above. For the BZ-system of Table 5, with a minimum oscillation period of ~400s, and hence a diffusion length close to 900μm, long range communication might be studied. In the following, the BZ composition of Table 5 was chosen as a model system of chemical information to be encapsulated inside simple emulsions and double emulsions. The following part, which has been submitted for publication in the Journal of Physical Chemistry Letters, presents the dynamic behavior of simple water-in-oil emulsions encapsulating the BZ-system of Table 3.

REFERENCES:

1. K. Torbensen and A. Abou-Hassan, *Journal of Flow Chemistry*, 2015, **5**, 234-240.
2. H. C. Shum, E. Santanach-Carreras, J.-W. Kim, A. Ehrlicher, J. Bibette and D. A. Weitz, *J. Am. Chem. Soc.*, 2011, **133**, 4420-4426.
3. H. C. Shum, D. Lee, I. Yoon, T. Kodger and D. A. Weitz, *Langmuir*, 2008, **24**, 7651-7653.
4. L. R. Arriaga, S. S. Datta, S.-H. Kim, E. Amstad, T. E. Kodger, F. Monroy and D. A. Weitz, *Small*, 2014, **10**, 950-956.
5. F. Kong, X. Zhang and M. Hai, *Langmuir*, 2014, **30**, 3905-3912.
6. M. Toiya, V. K. Vanag and I. R. Epstein, *Angewandte Chemie International Edition*, 2008, **47**, 7753-7755.
7. Y. Hasegawa, K. Takahashi, S. Kume and H. Nishihara, *Chemical Communications*, 2011, **47**, 6846-6848.

III.3. Tuning the Chemical Communication of Oscillating Microdroplets by Means of Membrane Composition

Kristian Torbensen,[a] Sandra Ristori,[b] Federico Rossi,[c] and Ali Abou-Hassan[a]**

[a]Sorbonne Universités, UPMC Univ Paris 06, UMR 8234, Laboratoire Physico-chimie des Electrolytes, Nanosystèmes InterfaciauX (PHENIX), 4 place Jussieu - case 51, 75252 Paris cedex 05 – France

[b]Department of Earth Sciences & CSGI, University of Florence, Via della Lastruccia 3, 50019 Sesto Fiorentino, Firenze, Italy

[c]Department of Chemistry and Biology, University of Salerno, Via Giovanni Paolo II 132, Fisciano (SA), Italy

ABSTRACT:

Synchronization of dynamic elements *via* chemical communication is a widespread phenomenon in nature, and in many relevant fields such as in biology, physics and chemistry, where systems capable of giving and receiving information exist. In these systems, coupling and synchronization is achieved by messenger molecules diffusing from one element to others, by triggering and spreading a chemical reaction. An excellent example in nature of chemical communication and synchronicity, can be found in cell populations where the plasma membrane governs the crossing of ions or molecules (among other mechanisms), into and out of the cells, thus dictating their collective behavior. In a biomimetic approach, herein we used a microfluidic system to confine a "chemical information generator", consisting of the far-from-equilibrium Belousov-Zhabotinsky (BZ) reaction in the aqueous core of monodisperse simple emulsion microdroplets. These were surrounded by an oil phase containing the phospholipid 1,2-dimyristoyl-sn-glycero-3-phosphocholine (DMPC), and other dopants. Stabilized by a boundary lipid layer, the drops could be brought in closest contact and arranged in a 1D array, using the microfluidic device. The DMPC-based membrane, at the contact surface, provided a diffusion path between drops for the chemical species governing the dynamical behavior of the BZ oscillating reaction. We show, that by tuning the chemical composition of the lipid layer, different coupling patterns can be obtained, which spans from inhibitory to excitatory coupling. Numerical simulations suggest that the hydrophobic

properties and the lipid packing at the interface are of paramount importance for the trans-membrane crossing of the pertinent chemical species.

INTRODUCTION:

Cooperative and synchronized behavior in networks of biological oscillating systems is a widespread phenomenon in nature. Usually, synchronization phenomena proceeds *via* diffusive coupling of individual microreactors, *e.g.,* cells and neuron/receptor couples, by mutual exchange of chemical messenger species capable of triggering a chemical reaction or an electrochemical response. Specifically, living cells communicate through semipermeable barriers constituted by lipid-based membranes. The importance of these barriers in cell signaling has long been recognized, and was recently reasserted[1] by the discovery of the crucial role played by extracellular vesicles, *i.e.,* signal carriers structured as lipid-surrounded aqueous domains. Reaction-diffusion systems have been modelled by chemically coupled microdrops containing the Belousov-Zhabotinsky oscillating reaction.[2-9] The overall reaction is driven by the oxidation of an organic substrate, *e.g.,* malonic acid, by bromate in acidic solution in the presence of a catalytic specie in the form of an organo-metal complex, such as ferroin (a phenanthroline-iron(II) complex). The oscillatory dynamics however, is governed by the amount of the inhibitory intermediate bromine and the excitatory intermediate bromous acid present in the microdrops, *i.e*., the fluctuation of their concentrations governs the oscillatory behaviour of the microdrops. These BZ intermediates might diffuse between individual microdrops, thus affecting the overall oscillatory synchrony of multiple drop arrays. As such, the intermediates serve as messenger molecules between individual drops. By tuning the concentrations of the BZ components within the microdrops, the geometrical configurations of the drops and the physico-chemical properties of the diffusive pathway, both inhibitory and excitatory coupling could be achieved. One way of controlling the coupling between microdrops suspended in an oil phase, is by modification of the drop-stabilizing surfactant present in the oil phase. For drops separated by an oil gap, the BZ intermediates must diffuse through this gap to reach other drops. Any chemical reaction between the intermediates and species present in the oil phase will thus diminish the impact on the surrounding drops.[5] For drops in contact, one or more surfactant layers are formed at the boundary region between adjacent drops.[10] Such layers, if partially permeable to the BZ intermediates, then open a second communication pathway.[11-14]

Here, we analyse the coupling patterns obtained in BZ containing microdrops, brought into contact in a 1D array, suspended in a DMPC containing oil phase. DMPC is known to form stable

bilayers in water, and to self-assemble spontaneously at the water-oil interface.[15] The exact structure of DMPC, at this latter interface, is difficult to assess since with respect to the air/water case, the solubility of phospholipids in organic solvents represents an additional parameter, which influences the equilibrium conditions. However, at concentration higher than the critical value of surface coverage, the building up of a three dimensional structure at the boundary between the organic phase and water has been demonstrated.[15] We thus expect, that in our experimental conditions a multimolecular DMPC layer with internal arrangement is present at the water drop surface, possibly with the structure of a loose Y-type Langmuir-Blodgett film.[15] It is also well known, that the membrane properties of both mono- and bilayers of lipids can be altered by doping the lipid layer with molecules having similar amphiphilic characteristics, but different packing properties. We here investigated the influence of the membrane composition on the communication pathways in arrays of touching oscillating microdroplets, surrounded by an oil phase containing phospholipids, with or without the dopants cholesterol, myristic acid, sodium tetradecyl sulfate and tetradecylamine. 1D arrays of microdroplets were fabricated by encapsulating an oscillatory ferroin catalyzed BZ mixture into the microdroplets by means of a microfluidic system.

RESULTS AND DISCUSSIONS:

To generate the droplets encapsulating the BZ reaction, a homemade microfluidic system was used, as illustrated in Figure 1A. It is based on coaxial flow geometry (details in the experimental section) with two separated inner capillaries centered in the middle of an outer capillary. This configuration allows for mixing only in the microfluidic system, thus avoiding problems related to chemical reactions occurring prior to monitoring. At the exit of the microfluidic system, BZ simple emulsions coated with phospholipids are parked inside Teflon capillaries; see Figure 1B, sealed with both sides with wax and monitored using an optical microscope.

Figure 2A shows a simple emulsion array of six oscillating droplets loaded with BZ and surrounded by the mixture of cyclohexane/chloroform containing 1,2-dimyristoyl-*sn*-glycero-3-phosphocholine (DMPC). On the right of the array, the space-time (ST) plots display the oscillating dynamics of each droplet. Herein, the vertical dark lines correspond to a firing (oxidized catalyst) of the oscillator, whilst the bright regions represent the recovery period (reduced catalyst) between single oscillations.

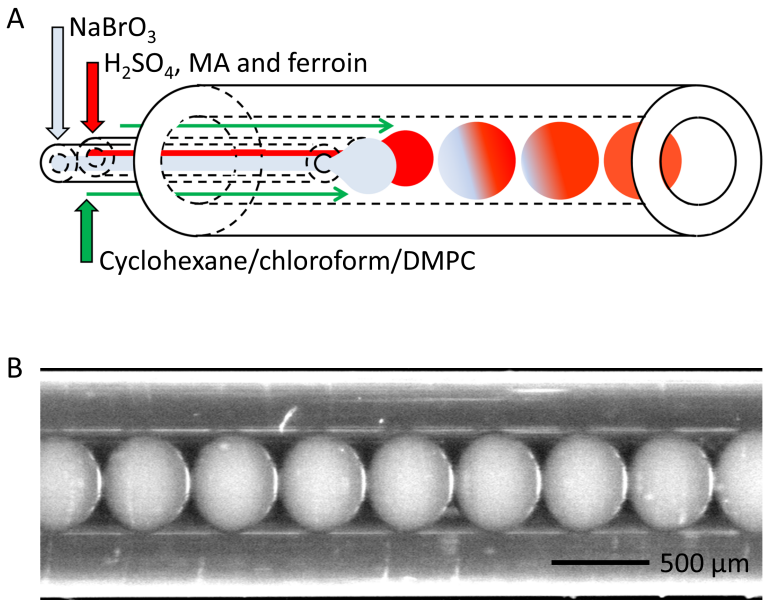

Figure 3. (A) Sketch of the microfluidic device used to generate the droplet arrays, showing the principal of the coaxial flow of the BZ reactants prior to the drop formation. (B) 1D array of BZ containing droplets as collected in a PTFE tube for monitoring.

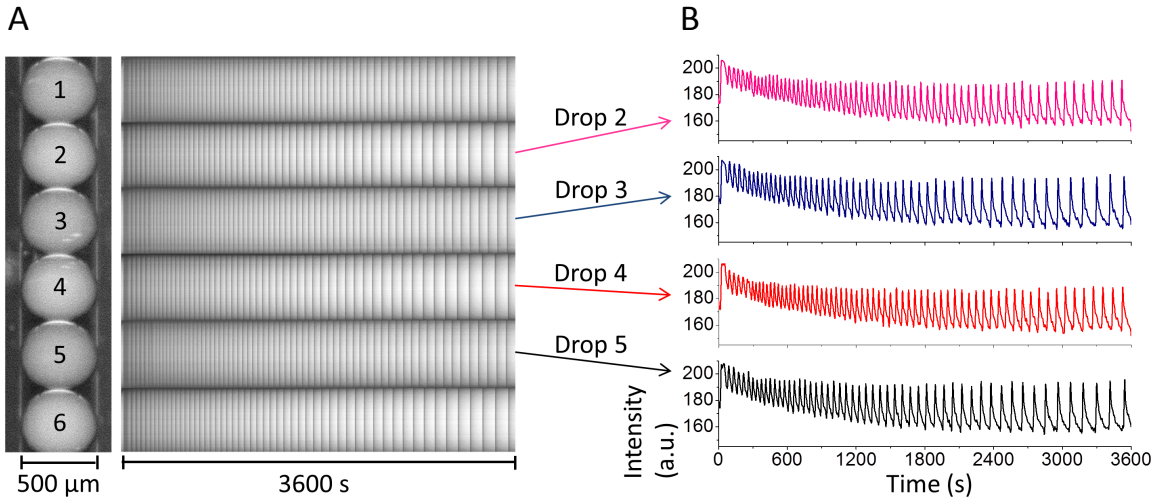

Figure 2. (A) Array of six oscillating droplets in a BZ/DMPC simple emulsion system. Space-Time plots of each droplet were reconstructed from the movie frames (sampling time 1 s). (B) Time-series extracted from the Space-Time plots by converting the pixels in grey scale values.

From the ST plots of four droplets (D2 – D5), the time-series were extracted by converting the pixels along a horizontal line, parallel to the time axis, in grey scale values; the corresponding time-series are reported in Figure 2B. By analyzing the phases and the periods of the selected droplets, it was possible to seek for emerging coherent dynamics due to the coupling between

neighboring oscillators. In fact, each oscillator is able to exchange reaction intermediates through the lipid membranes and hence influence the dynamical evolution of the array: Thus, each oscillator, in turn, is influenced by messenger molecules released by droplets within close vicinity. Several works[2, 5, 16, 17] showed that the most important intermediates governing the global behavior of a network of diffusively coupled BZ chemical oscillators are the inhibitors (Br^- and Br_2) and the activators ($HBrO_2$, $BrO_2^\bullet$ and the organic substrates MA or BrMA). Oscillation periods (τ) were calculated from the time-series as the time difference between two successive maxima, while the oscillation frequency (ω), measured in Hz, is calculated as the reciprocal of τ ($\omega = 1/\tau$). The oscillators array is thermodynamically closed; therefore, oscillations have a transitory nature that causes a continuous drift in the oscillating parameters. This fact makes it difficult to determine whether the changes in the oscillation dynamics of coupled droplets are the result of random fluctuations or a consequence of the mutual entrainment. To reduce this uncertainty, we here analyze the oscillating parameters by following different methodological approaches.

At a first glance, Figure 2 suggests a coherent behavior of the type *a-b-a-b*, by which next neighbor droplets oscillate with similar periods. Figure 3 shows a more thorough analysis of τ, as extrapolated from the time-series of the droplets 2 - 5. These droplets were chosen in the array, since they all have the same boundary conditions (*i.e.,* each droplet is in contact with its two neighbors). In Figure 3A, the oscillation periods of each droplet are plotted as a function of the oscillatory cycles. During the first 7 oscillations, periods are distributed quite evenly around 40 seconds, without any evidence of a coherent behavior. However, after this initial stage, a clear differentiation occurs, and couples of alternate droplets begin to oscillate with the same periodicity. In particular, the couple 2 - 4 oscillates faster with period times increasing from ~35 s to ~90 s whilst the couple 3 - 5 oscillates with a period that increases from ~35 s to ~130 s. As expected from Figure 2A, the ratio between the periods of alternate oscillators is stable around 1, while the ratio between the periods of adjacent droplets (2 - 3 and 4 - 5) decreases progressively in time, tending toward a value of ~0.5, as highlighted by Figure 3B. This phenomenon resembles that of the period halving of two pulse-coupled oscillators with time delay when the inhibitory coupling is dominant.[18]

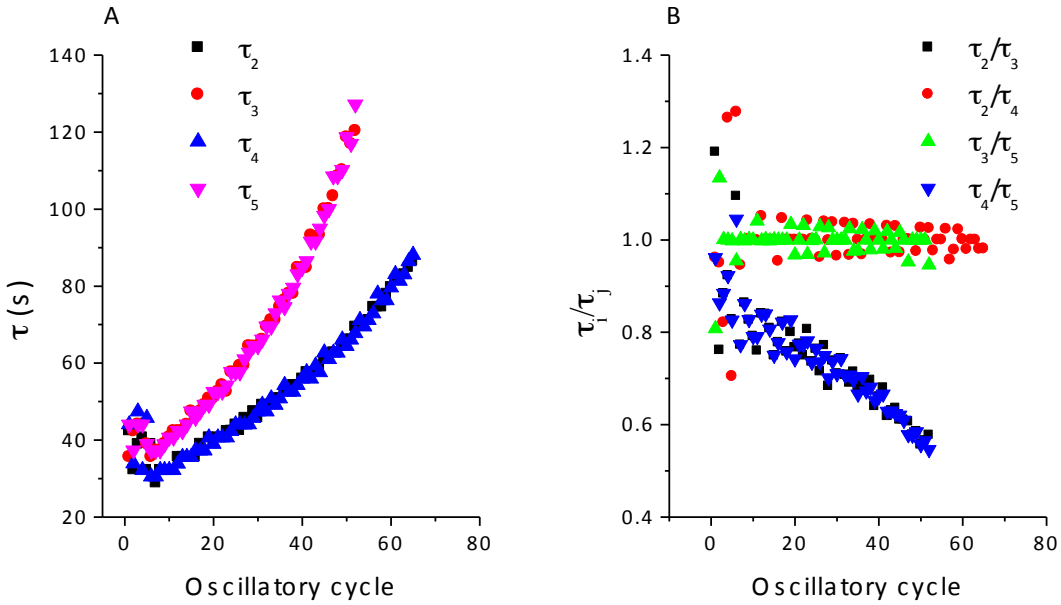

Figure 3. (A) Oscillation periods, derived from the ST-plots of the droplets 2 – 5 in Figure 2, plotted vs. the oscillatory cycle. (B) Ratio of oscillation periods between the same droplets.

To confirm that coupling is actually driving the global dynamics of the oscillators array, we calculated the instantaneous unwrapped phase of the four droplets by means of equation (1.1) as reported in Figure 4A

$$\phi_i = 2\pi \frac{t - t_k}{t_{k+1} - t_k} + 2k\pi \qquad t_k < t < t_{k+1} \qquad (0.0)$$

where t_k is the time of the k-th peak of the oscillatory time series of the i-th oscillator. As in the case of τ, the unwrapped phases cluster into two distinct groups of alternate oscillators (D2 - D4 and D3 - D5), meaning that these droplets are both phase and period coupled. This is also showed by the trend of the phase difference ($\Delta\phi_{i,j}$) as depicted in Figure 4B and C. In general, a diagonal trend of $\Delta\phi_{i,j}$ corresponds to a phase difference which is not constant over time, while horizontal trends indicate that both oscillators have the same period and oscillate with a constant phase difference. This latter situation represents a "phase lock" state (*i.e.,* a coherent behavior of the elements constituting the couple).

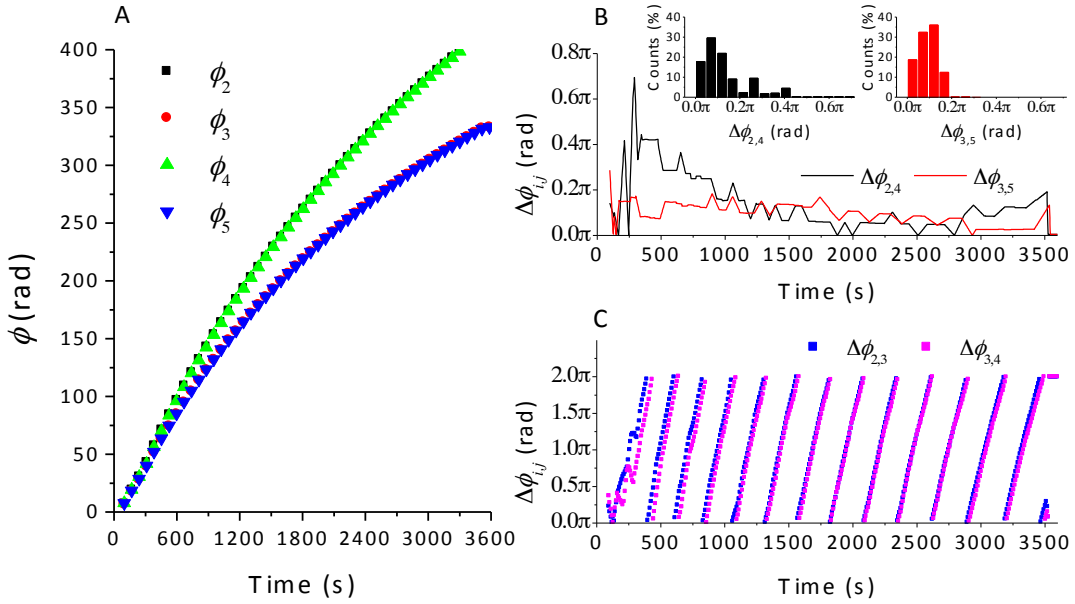

Figure 4. (A) Unwrapped phase, as calculated by *eq.* (1.1), for the droplets 2 - 5 of Figure 2, showing two distinct clusters of oscillating droplets. (B) Phase difference of the same droplets as a function of time. The insert in (B) show the count distribution for various intervals of phase differences. (C) Phase differences of the droplet couples 2,3 and 3,4 vs. time, displaying the progressive phase shift for these adjacent droplets.

Figure 4C clearly shows that adjacent droplets never oscillate in-phase, since a progressive shift from 0 to 2π takes place for every oscillatory cycle. On the contrary, Figure 4B shows that the phase difference between alternate droplets is embedded in a defined range, 0 - 0.8π for the couple D2 - D4, and 0 - 0.3π for the couple D3 - D5. The frequency distribution of $\Delta\phi_{i,j}$ (inserts of Figure 4B), shows that the phase difference is narrowly distributed in the interval 0 - 0.2π for both the couples, meaning that the alternate droplets tend to oscillate in-phase. As observed for τ, an initial time lag is observed, where phases are randomly distributed before the synchronization due to the coupling affects the oscillatory dynamics. During the course of the reaction the phase difference undergoes small adjustments (small diagonal intervals in Fig.4B) in response to the variation of the oscillation period.

A phase lock state between the alternate droplets can also be evidenced by the phase-plane reconstruction of the interval 700 - 3600 s (synchronous behavior) in Figure 5A and B, where a limit cycle is obtained by plotting the time-series of droplet D2 (or D3) with respect to the time-series of droplet D4 (or D5). Figure 5C and 5D report the non-structured attractors in the phase-space obtained from adjacent droplets.

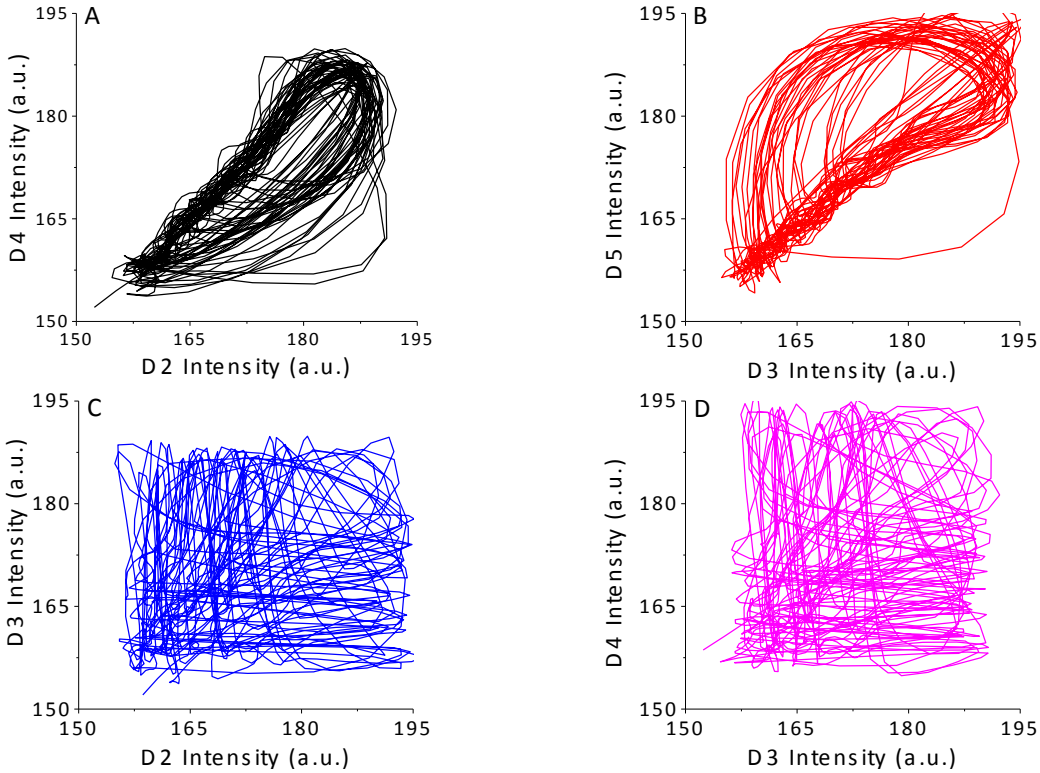

Figure 5. (A) and (B) Phase-plane reconstructions for the droplet couples D2 (or D3) and D4 (or D5) showing the synchronous behavior of these alternate couples. (C) and (D) displays the non-structured coupling between the adjacent droplet couples D2 (or D3) and D3 (or D4).

Cholesterol as membrane interactor:

Figure 6A shows a simple-emulsion (cyclohexane/chloroform-BZ) array of six oscillating droplets coated by 1,2-dimyristoyl-*sn*-glycero-3-phosphocholine (DMPC) and cholesterol (20% w/w). Similarly to Figure 2, the time-series of four droplets (D2 - D5) were extracted from the ST plots and converted in grey scale values (Figure 2B). The same analysis as for the pure DMPC system was applied here to seek for differences in the global behavior induced by the membrane composition. In a previous work,[19] we investigated the influence of several dopants on the oscillatory dynamics of bulk BZ systems: It was found that the interaction of brominated species, Br_2 in particular, with the double bonds of cholesterol caused some differences in the oscillation period and frequency. We expect that such chemical interaction might influence the global behavior of the droplet array by changing the communication pathways among single oscillators. In particular, we expect cholesterol to act as a barrier for Br_2, thus preventing, or at least mitigating, inhibitory coupling.

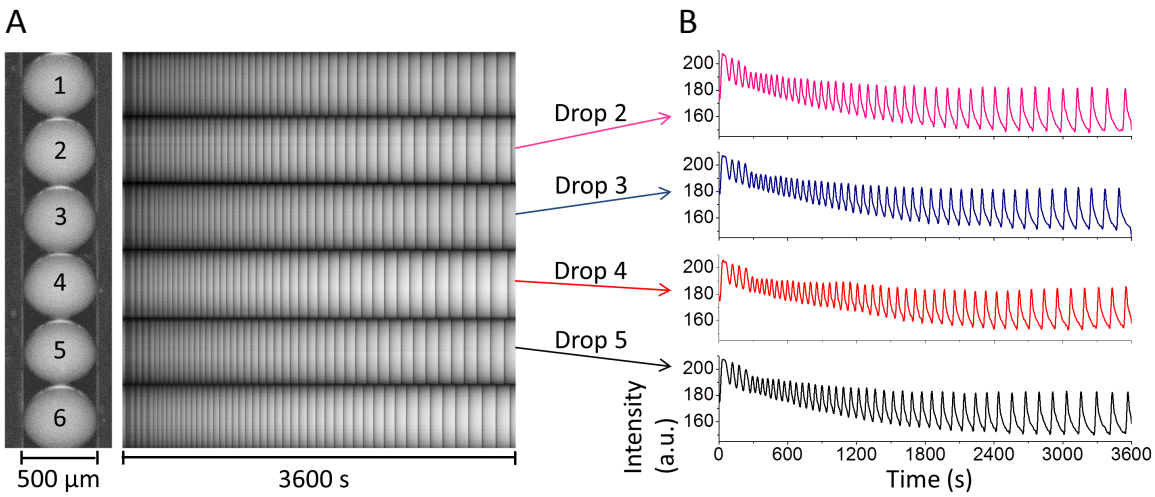

Figure 6. (A) Array of six oscillating droplets in a BZ/DMPC-CHOL simple emulsion system. Space-Time plots of each droplet were reconstructed from the movie frames (sampling time 1 s). (B) Time-series extracted from the Space-Time plots by converting the pixels in grey scale values.

The period analysis of the DMPC-CHOL system reveals a less defined behavior with respect to the pure DMPC system. In Figure 7A, the oscillation periods of each droplet are plotted as a function of the oscillatory cycles. As in the case of DMPC, during the first oscillations, periods are distributed quite evenly around a mean value of 50s, without any evidence of a coherent behavior. However, after this initial stage, a differentiation seems to take place and the couples D2 - D5 and D3 - D4 begin to oscillate with similar periods, making the difference in clusters periods smaller with respect to the case of pure DMPC. This is confirmed also by Figure 7B, where the ratio among the periods of droplet pairs is reported against the oscillatory cycles, showing values of τ_i/τ_j confined between 0.8 and 1.2. Furthermore, the phase analysis highlights a weak coupling of the two couples D2 - D5 and D3 - D4, as reported in Figure 8. As for the oscillation periods, the phases of the droplets cluster in two couples (Figure 8A, D2 - D5 and D3 - D4), but with a small phase difference between the two groups. A smaller phase-coupling, with respect to the pure DMPC system, is well described by Figure 8B, where $\Delta\phi_{i,j}$ of the two couples of droplets span a large range of frequency with long periods of uncorrelated oscillations, as, for example, shown by the long diagonal interval in the red trace of Figure 3B between ~1000 s and ~2500 s. A slightly stronger correlation is present in the couple D3 - D4 where two main phase lock values can be detected around 0.5π and 0.7π. The oscillation dynamics of the other permutated droplet couples are generally uncorrelated, as showed in Figure 8C.

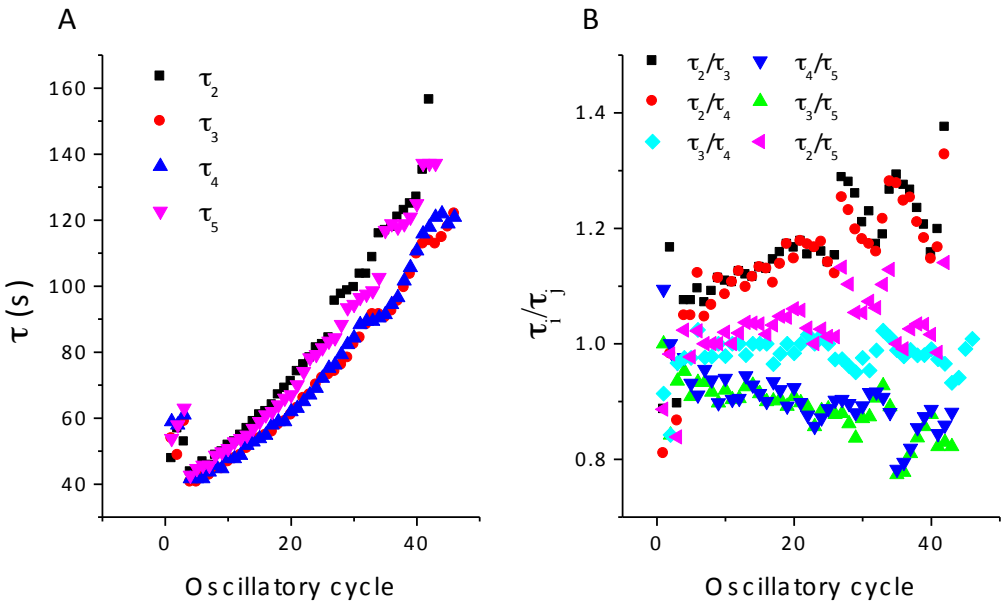

Figure 7. (A) Oscillation periods, derived from the ST-plots of the droplets 2 – 5 in Figure 6, plotted vs. the oscillatory cycle. (B) Ratio of oscillation periods between the same droplets.

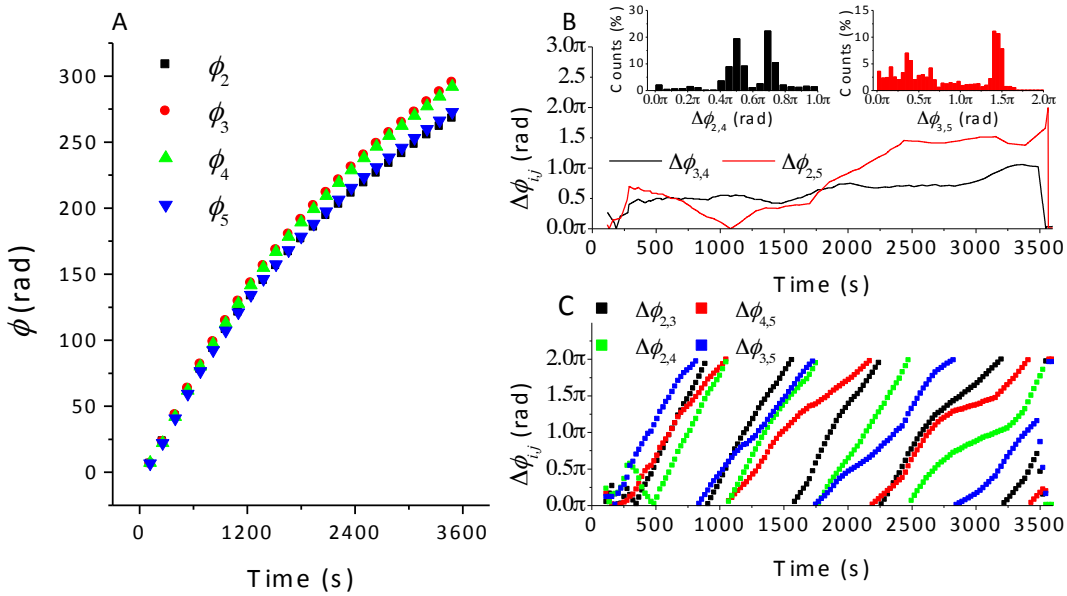

Figure 8. (A) Unwrapped phase, as calculated by *eq.* (1.1), for the droplets 2 - 5 of Figure 6, showing two clusters, albeit with a small phase difference, of oscillating droplets. (B) Phase difference of the droplet couples 3,4 and 2,5 as a function of time. The insert in (B) show the count distribution for various intervals of phase differences. (C) Phase differences of the droplet couples 2,3, 2,4, 4,5 and 3,5 vs. time, displaying an uncorrelated coupling for these adjacent droplets.

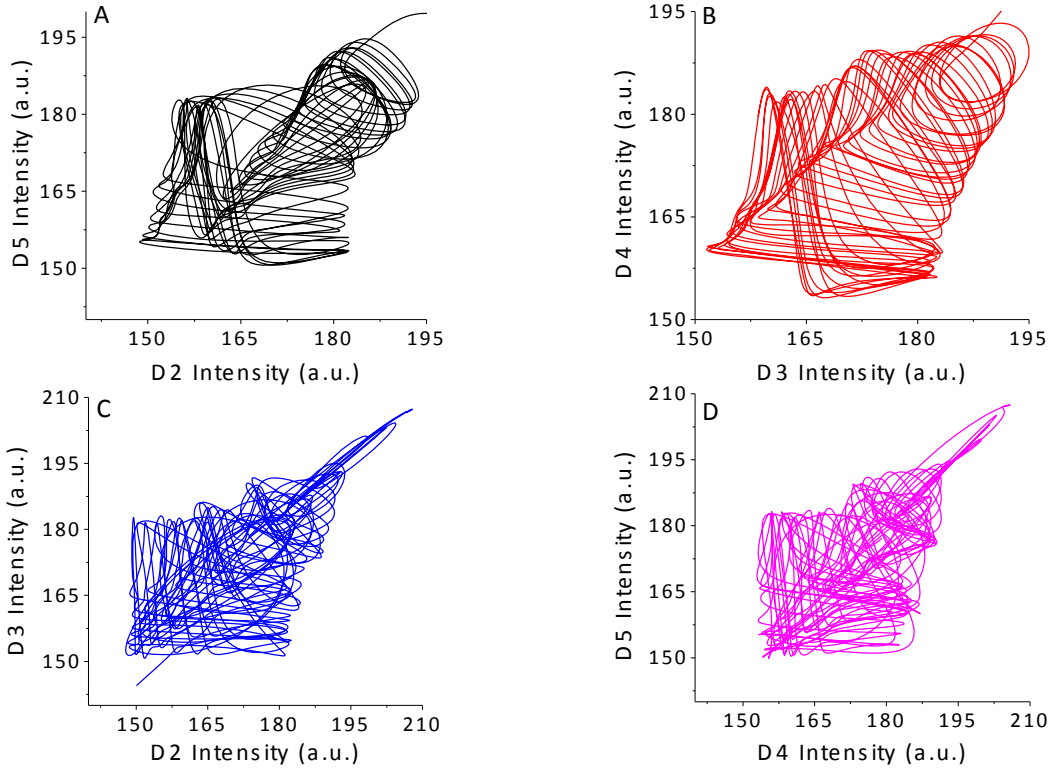

Figure 9. (A) and (B) Phase-plane reconstructions for the droplet couples D2 (or D3) and D5 (or D4) showing the limited oscillating cycles of both long-range and adjacent couples. (C) and (D) displays the coupling between the adjacent droplet couples D2 (or D3) and D3 (or D4).

Other bilayer interactors:

In addition to cholesterol, three more amphiphilic molecules (dopants) were intercalated in the DMPC layers to change the structural and physical properties of the membranes, and to study the influence on the communication dynamics in the droplet network. The dopants employed were myristic acid (Myr-A), sodium tetradecyl sulfate (STS) and tetradecylamine (TA), all with a C14 aliphatic chain, but different polar heads. As in the case of cholesterol, the influence of these dopants on the structure of DMPC liposomes and on the BZ kinetics was investigated in a previous paper.[19] Myr-A, STS and TA are neutral, negatively and positively charged, respectively, in our experimental conditions.

The dynamical behavior of the BZ array did not significantly differ from the DMPC case upon the addition of Myr-A and TA, *i.e.,* a phase and period synchronization took place among alternated droplets with uncorrelated oscillations characterizing the adjacent oscillators (*a-b-a-b* synchronization (data not shown), even though an accelerated kinetics favored a faster

communication with respect to the DMPC case. This was an indication that defects created by guest molecules in the bilayers and/or in the packing of the phosphoholine head layer are able to increase the exchange of small molecules between different compartments. On the contrary, when STS was used as dopant, even adjacent droplets showed a complete period synchronization (Figure 10A) and a phase-lock state (Figure 10B), with alternate droplets that tend to oscillate in-phase ($0 < \Delta\phi < 0.5\pi$) and adjacent droplets that seem to reach a plateau between π and 1.5π. It is worth noticing at this point that STS is the only negative lipid component at the low pH of the BZ system, therefore it probably act as a selective barrier for anions to cross the bilayer.

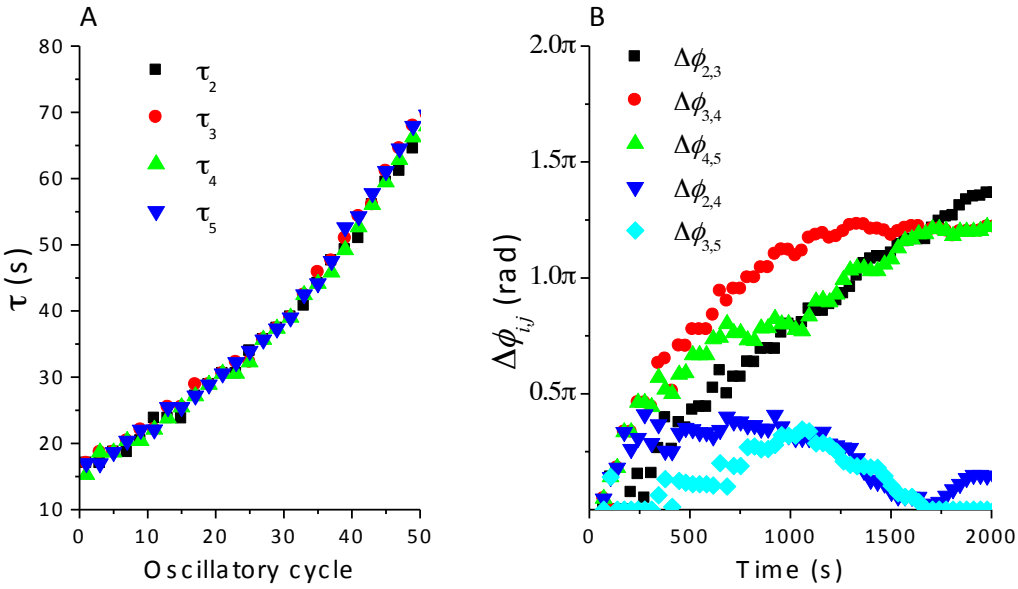

Figure 10. (A) Oscillation periods, derived from the ST-plots of the DMPC-STS system, plotted vs. the oscillatory cycle. (B) Ratio of oscillation periods between the same droplets.

Recently, we investigated several aspects connected with the nature of the messenger molecules transducing chemical signals in a network of oscillating liposomes and we demonstrated, by means of electrochemical techniques, that nonpolar brominated or oxy-brominated species can be responsible for signal transduction across DMPC membranes.[16] In a previous work,[13] we studied the communication among droplets in a double emulsion system (water/oil/water) at high concentration of bromate and sulfuric acid. In this configuration, the production of the autocatalytic species $HBrO_2$ was favored and the resulting activatory type of coupling led the system to a synchronous in-phase oscillating dynamics.

In this work, the comparison between two of the analyzed systems (DMPC and DMPC+CHOL) indicated a prominent role of an inhibitory coupling in the communication pathways between droplets in the array. In a previous paper,[19] we investigated the influence of the membrane composition on the oscillatory dynamics of the BZ reaction: One of the most relevant result was the assessment of the role of cholesterol in interacting with some of the intermediates produced during the oscillatory cycles of the reaction. In particular it was demonstrated how the double bond present in the structure of the cholesterol could be saturated by Br_2, thus altering the oscillation period and the frequency of the oscillations by the removal of Br_2. In the specific case of the droplet arrays, cholesterol directly influences the communication pathways between droplets by mitigating the passage of Br_2 from one droplet to another through the phospholipids membranes. In the case of pure DMPC, small nonpolar species, both with activatory ($BrO_2^{\bullet}$, $HBrO_2$, etc.) and inhibitory (Br_2) properties, can cross the membranes. It is unlikely that larger polar molecules ($CH_2(COOH)_2$, $CHBr(COOH)_2$, etc.), ionic species (Br^-, BrO_3^-, etc.) and the catalyst can cross the phospholipid layer.[20] Therefore, we focused our attention on the exchange of two species, $HBrO_2$ and Br_2, responsible for activatory and inhibitory coupling, respectively.[3, 5, 13, 16, 17]

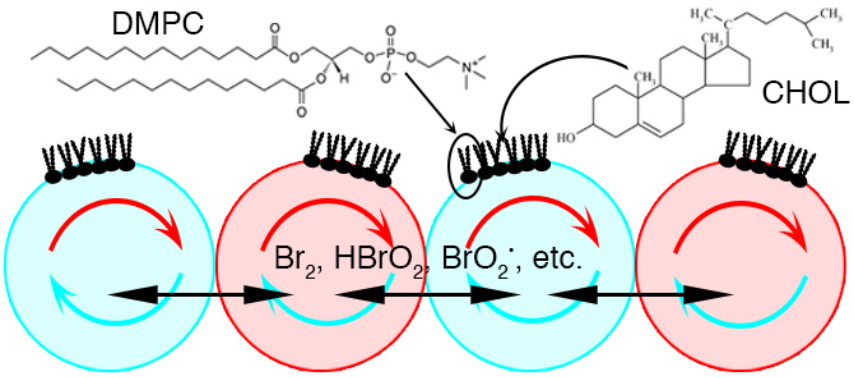

Figure 4. Illustration of the possible pathway of species governing the communication between droplets.

Numerical simulations can be useful to understand the influence of the membrane composition on the global dynamics of the droplets array. The system can be modeled as sketched in Figure 11: Four droplets, each of them containing the BZ reaction, are free to exchange $HBrO_2$ and Br_2 through a simple equilibrium reaction following mass action kinetics

$$Br_2(d_i) \underset{k_{-c}^1}{\overset{k_c^1}{\rightleftharpoons}} Br_2(d_j) \qquad (0.0)$$

$$HBrO_2(d_i) \underset{k^2_{-c}}{\overset{k^2_c}{\rightleftharpoons}} HBrO_2(d_j) \qquad (0.0)$$

where d_i and d_j represent adjacent droplets, and $k^i_c = k^i_{-c}$ (s^{-1}) are the transfer kinetic constants related with the permeability of the i-th species, P^i_m (cm/s), towards the phospholipid membranes by the relation $k^i_c = P^i_m A_c / V_d$, where V_d is the droplet volume (6.5×10^{-5} cm^3) and A_c is the contact surface area between two droplets (1.37×10^{-4} cm^2). The values for V_d and A_c were determined from our experiments being the diameter of the droplets (~ 500 μm) and the diameter of the contact area, assumed to be circular, ~ 130 μm, respectively. The value for P^1_m was measured by electrochemical techniques for a Langmuir monolayer of different phosphatidylethanolamines and was found to be 0.07 cm/s at a low surface pressure.[21] The value for P^2_m was chosen as 1×10^{-4} cm/s,[13, 16, 22, 23] so that $k^1_c = 0.15$ s^{-1} and $k^2_c = 2 \times 10^{-4}$ s^{-1}. The BZ system inside each droplet was modeled according to the following reaction scheme with relative kinetic constants reported in Table 1.

$$HOBr + Br^- + H^+ \rightleftharpoons Br_2 + H_2O \qquad (R1)$$

$$Br^- + HBrO_2 + H^+ \rightarrow 2HOBr \qquad (R2)$$

$$2HBrO_2 \rightarrow BrO_3^- + HOBr + H^+ \qquad (R3)$$

$$Br^- + BrO_3^- + 2H^+ \rightleftharpoons HOBr + HBrO_2 \qquad (R4)$$

$$BrO_3^- + HBrO_2 + H^+ \rightleftharpoons Br_2O_4 + H_2O \qquad (R5)$$

$$Br_2O_4 \rightleftharpoons 2BrO^{\bullet} \qquad (R6)$$

$$Fe(phen)_3^{2+} + BrO_3^- + 2H^+ \rightarrow Fe(phen)_3^{3+} + BrO_2^{\bullet} + H_2O \qquad (R7)$$

$$Fe(phen)_3^{2+} + BrO_2^{\bullet} + H^+ \rightarrow Fe(phen)_3^{3+} + HBrO_2 \qquad (R8)$$

$$Fe(phen)_3^{3+} + BrCH(COOH)_2 \rightleftharpoons Fe(phen)_3^{2+} + {}^{\bullet}CBr(COOH)_2 + H^+ \qquad (R9)$$

$$BrCH(COOH)_2 \rightleftharpoons (HOOC)CBr{=}C(OH)_2 \qquad (R10)$$

$$(HOOC)CBr{=}C(OH)_2 + Br_2 \rightarrow Br_2C(COOH)_2 + Br^- + H^+ \qquad (R11)$$

$$(HOOC)CBr{=}C(OH)_2 + HOBr \rightarrow Br_2C(COOH)_2 + H_2O \quad \text{(R12)}$$

$$2^{\bullet}CBr(COOH)_2 + H_2O \rightarrow BrCOH(COOH)_2 + BrCH(COOH)_2 \quad \text{(R13)}$$

$$BrCOH(COOH)_2 \rightarrow Br^- + CO(COOH)_2 + H^+ \quad \text{(R14)}$$

When cholesterol was intercalated in the DMPC membranes, a fast bromination reaction was added to the scheme, similarly to the bulk systems we investigated in our previous work[19]

$$Br_2 + Chol \xrightarrow{K} Br_2 - Chol \quad \text{(R15)}$$

with a kinetic rate constant K = 340 $M^{-1}s^{-1}$.

Numerical simulations were performed by integrating the reactions (1.2), (1.3) and (R1) - (R15) by means of the CO.PA.SI. software.[24] All data used in simulations reflected the real experimental parameters, and the different initial conditions of the droplets were reproduced by introducing a small delta in the concentration of the reactants (± 0.1 %).

Table 1.

reaction	$k_{forward}$	$k_{inverse}$
R1	8×10^9 mol^{-2} dm^6 s^{-1}	80 s^{-1}
R2	2.5×10^6 mol^{-2} dm^6 s^{-1}	
R3	3×10^3 mol^{-1} dm^3 s^{-1}	
R4	10 mol^{-3} dm^9 s^{-1}	3.2 mol^{-1} dm^3 s^{-1}
R5	48 mol^{-2} dm^6 s^{-1}	3.2×10^3 s^{-1}
R6	7.5×10^4 s^{-1}	1.4×10^9 mol^{-1} dm^3 s^{-1}
R7	0.38 mol^{-3} dm^9 s^{-1}	
R8	1×10^9 mol^{-2} dm^6 s^{-1}	
R9	100 mol^{-1} dm^3 s^{-1}	6×10^8 M^{-2} s^{-1}
R10	0.012 s^{-1}	800 s^{-1}
R11	3.5×10^6 mol^{-1} dm^3 s^{-1}	
R12	6.6×10^4 mol^{-1} dm^3 s^{-1}	
R13	1×10^8 mol^{-1} dm^3 s^{-1}	
R14	1.5 s^{-1}	

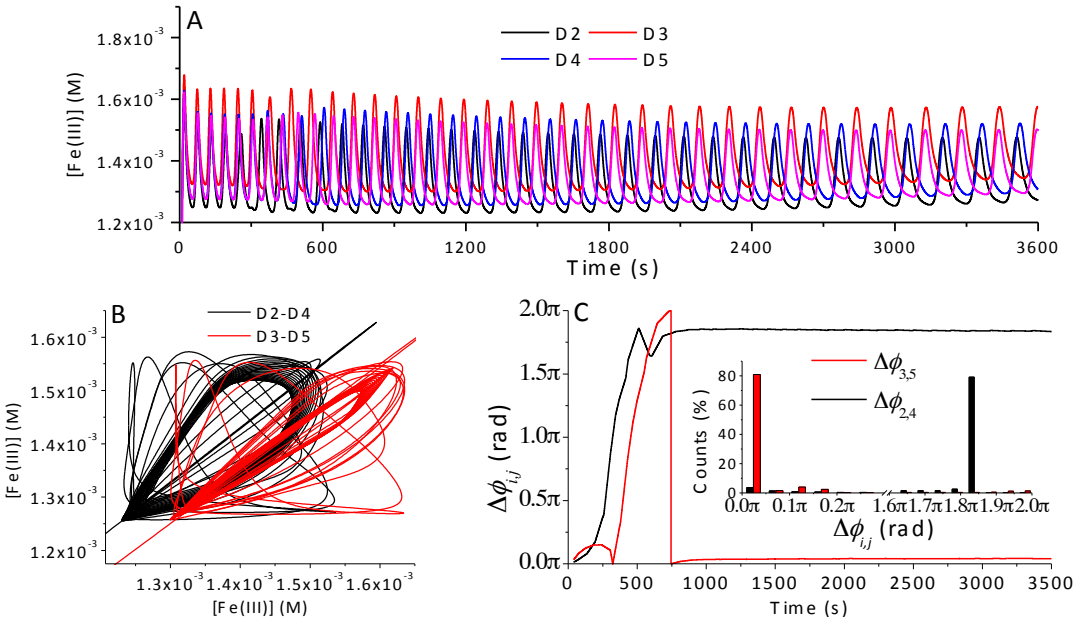

Figure 12. (A) Simulation of the ferriin concentration without the interaction of cholesterol. (B) phase-space graph of the alternate droplet couples, D2 - D4 and D3 - D5, showing two limited cycles. (C) phase difference of the synchronized droplets.

Figure 12 reports the simulations relative to the system of pure DMPC, where reaction (R15) was not taken into account and the concentration of cholesterol in the membranes was set to 0. Panel A show how, after a few oscillatory cycles between 0 and 600 s, a clear *a-b-a-b* configuration begins to take place, where alternate droplets start to oscillate with the same period and phase. Panel B shows the phase-space of the two alternate couples of droplets, where two limit cycles describe the dynamics in time of the droplets D2 - D4 and D3 - D5. Finally, Panel C depicts the phase difference behavior of the synchronized droplets; the couple D2 - D4 locks on a $\Delta\phi_{2,4} = 1.8\ \pi\ (-\ 0.2\ \pi)$ while the couple D3 - D5 locks on a $\Delta\phi_{3,5} = 0.02\ \pi$, as highlighted in the inset of Figure 12.

Simulations show a good matching with experimental data, even though they fail in reproducing the period halving observed between adjacent droplets (Figure 3B). The period halving is responsible for the uncorrelated phase difference relation between adjacent droplets observed in the experiments (Figure 4c), that cannot be reproduced in our model. Actually, the phase difference between adjacent droplets in our simulations locks on a value close to π (data not shown), *i.e.,* they are mainly out-of-phase, as can be easily inferred by the time-series reported in Figure 11A. This fact can be explained with a delayed inhibitory effect, not included in our model, like in the case of the coupled CSTR BZ systems described by Horvat *et al.*[18] In our experimental conditions, the

delayed inhibition can be due to the diffusion of bromine into the oil phase, and from there into the different droplets.

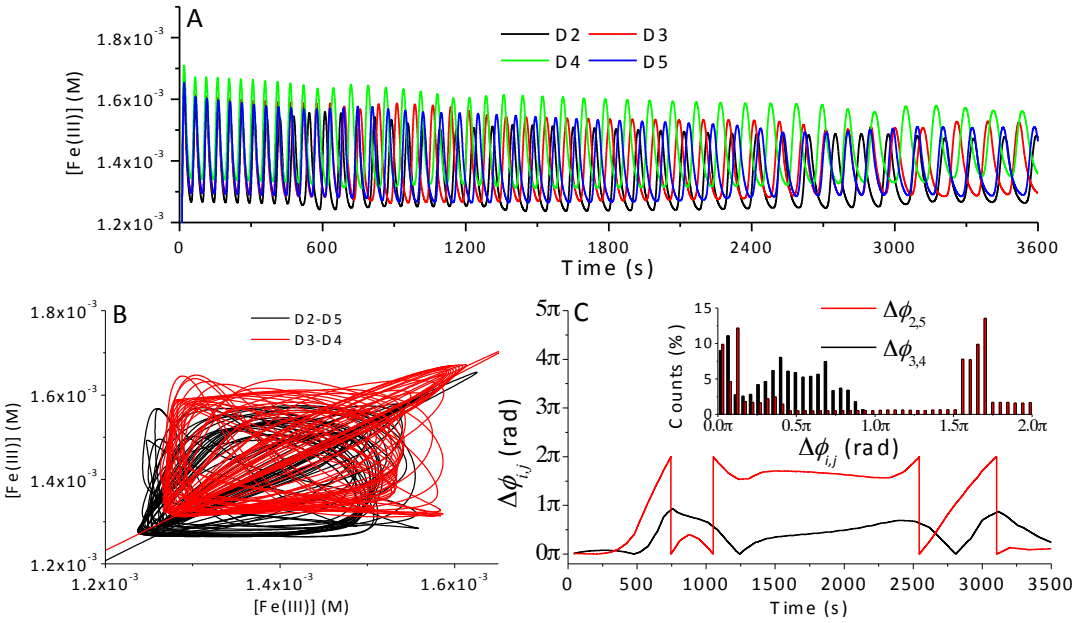

Figure 13. (A) Simulation of the ferriin concentration with the interaction of cholesterol according to eq. (R15). B) phase-space graph of the alternate droplet couples, D2 – D5 and D3 – D4, showing a less structured behavior with respect to the pure DMPC system. (C) phase difference of the synchronized droplets, spanning a broader frequency range with respect to the pure DMOC system.

When the cholesterol is intercalated into the membranes, the model takes into account the reaction (R15) with a concentration of cholesterol [CHOL] = 6 × 10^{-3} M. As in the case of experiments, simulations show a weakly coupled system with a configuration *a-b-b-a*. The time-series reported in Figure 13A shows a more complex behavior with respect to the pure DMPC system, however starting from ~2400 s an overlapping of the oscillations in droplets couples D2 - D5 and D3 - D4 is evident. Similar to the Figures 8 and 9, the simulated phase behavior show a less structured phase space with respect to pure DMPC, and the phase difference between droplet couples spans a broader range of frequencies over time, as observed experimentally.

From experiments we observed that the presence of neutral (Myr-A) or positively charged (TA) species did not change the dynamical behavior of the system with respect to the pure DMPC case. In a previous work, by means of SAXS investigations,[19] we demonstrated that these two dopants act on the packing properties and on the lamellarity of the lipid membranes, however a clear chemical interaction did not take place with the BZ intermediates. The same structural

influence was found for the case of the anionic surfactant STS. However, from the communication point of view, a different synchronization pathway was found with respect to DMPC membranes. At this stage it is difficult to interpret how the dopant charge influences the type of messenger molecules exchanged among the oscillators, but it is well known that amphiphiles with structural and chemical properties different from phospholipids can influence the permeability properties of the membranes.[25, 26] A general inhibitory-type coupling with *a-a*-a-a** (same periods but different phases) can be inferred from experimental data, but further investigations are needed to have a better assessment of the surfactant influence on the dynamical behavior of oscillators array.

CONCLUSION:

In this paper we investigated the influence of the lipid membrane composition on the communication pathways in arrays of touching oscillating microdroplets surrounded by an oil phase containing phospholipid monomers The arrays of micro-droplets were fabricated by encapsulating an oscillatory ferroin catalyzed BZ mixture into microdroplets by means of microfluidics. With respect to previous works, here the array configuration allowed for better controlled experimental conditions, and for a longer lifespan of the droplets. For these experimental conditions, the communication between adjacent droplets mainly exhibits an inhibitory character, governed by the prominent role of Br_2. Molecular bromine, has in fact a higher permeability towards phospholipid membranes with respect to the activator $HBrO_2$, resulting in an out-of-phase oscillatory regime between adjacent droplets and in an in-phase regime between alternating droplets (*a-b-a-b* configuration). With cholesterol intercalated in the membrane structure, the global dynamics resulted in a weakly coupled array, with adjacent droplets oscillating almost with the same period but with a less coherent phase with respect to the pure DMPC system. The primary role of cholesterol was to inhibit the Br_2 molecules to pass from one droplet to another, thus allowing for a weak activatory coupling.

Experiments with other dopants showed that by manipulating the droplet surrounding membranes, we can tune the communication properties of the oscillator network. However, without a chemical interaction with some of the BZ intermediates, the type of coupling remains mainly inhibitory for the reactant concentrations applied. Further experiments are planned to extend our findings from the simple emulsions system to double emulsion systems (water/oil/water) and finally to a real liposome (water-in-water) network.

EXPERIMENTAL DETAILS:

1,2-Dimyristoyl-sn-glycero-3-phosphocholine (DMPC) was purchased by Lipoids, Inc. Sodium bromate, malonic acid (MA), cholesterol (CHOL), myristic acid (Myr-A), sodium tetradecylsulfate (STS), tetradecylamine (TA) and sulfuric acid (96 %) were all purchased from Sigma-Aldrich and used without further purification. Ferroin was synthesized by adding 1.10-phenanthrolin to an aqueous (Milli-Q grade) solution of iron(II) sulfate in the stoichiometric ratio 3:1. Both chemicals were purchased from Sigma-Aldrich. Chloroform and cyclohexane (both analytical grade) were purchased from Sigma-Aldrich. The microfluidic device consisted of two fused (using epoxy resin) polyimide coated 150/50 μm (outer diameter (OD)/ inner diameter (ID)) glass capillary tubes (Polymicro) inserted into a cylindrical 1200/485 μm (OD/ID) polytetrafluoroethylene (PTFE) tube (UpChurch Scientific) using a T-junction with ferules (UpChurch Scientific, ref. P-728). Sulfuric acid, malonic acid and ferroin were pumped through one of the fused glass capillary tubes, while sodium bromate was pumped through the other using syringe pumps (kd Scientific) with a volumetric flow = 10 $\mu Lmin^{-1}$. Thus, no reactions occur prior to mixing of the two aqueous phases in the PTFE tube. The final concentrations of the BZ components in the drops were 0.3 M, 0.3 M, 5 mM, and 0.12 M for H_2SO_4, MA, ferroin and sodium bromate, respectively. The suspending oil phase, consisting of a mixture of chloroform/cyclohexane (1:2) and DMPC (1% w/w), was injected into the PTFE tube *via* the T-junction, as sketched in Figure 1 with a volumetric flow = 15 $\mu Lmin^{-1}$. Once an array of drops (at least 50 drops) were formed, the PTFE was removed from the T-junction and sealed in both ends with syringes (OD if 500 μm) filled with epoxy resin. Recordings (1 frame/s) of the oscillating drops were performed with a Zeiss Discovery V8 microscope mounted with a Dasla CCD camera. An induction period of the BZ reaction of approximately 2 min. was sufficient enough to initiate the recordings prior to the first BZ oscillation.

REFERENCES:

1. G. Raposo and W. Stoorvogel, *The Journal of Cell Biology*, 2013, **200**, 373-383.
2. J. Delgado, N. Li, M. Leda, H. O. Gonzalez-Ochoa, S. Fraden and I. R. Epstein, *Soft Matter*, 2011, **7**, 3155-3167.
3. M. Toiya, H. O. González-Ochoa, V. K. Vanag, S. Fraden and I. R. Epstein, *The Journal of Physical Chemistry Letters*, 2010, **1**, 1241-1246.
4. A. F. Taylor, M. R. Tinsley, F. Wang, Z. Huang and K. Showalter, *Science*, 2009, **323**, 614-617.
5. M. Toiya, V. K. Vanag and I. R. Epstein, *Angewandte Chemie International Edition*, 2008, **47**, 7753-7755.
6. B. T. Ginn, B. Steinbock, M. Kahveci and O. Steinbock, *The Journal of Physical Chemistry A*, 2004, **108**, 1325-1332.
7. H. Fukuda, N. Tamari, H. Morimura and S. Kai, *The Journal of Physical Chemistry A*, 2005, **109**, 11250-11254.
8. N. Tompkins, N. Li, C. Girabawe, M. Heymann, G. B. Ermentrout, I. R. Epstein and S. Fraden, *PNAS*, 2014, **111**, 4397-4402.
9. V. K. Vanag and I. R. Epstein, *Physical Review E*, 2011, **84**, 066209.
10. Y. Elani, X. C. I. Solvas, J. B. Edel, R. V. Law and O. Ces, *Chemical Communications*, 2016, DOI: 10.1039/C6CC01434H.
11. S. Thutupalli, S. Herminghaus and R. Seemann, *Soft Matter*, 2011, **7**, 1312-1320.
12. J. Guzowski, K. Gizynski, J. Gorecki and P. Garstecki, *Lab on a Chip*, 2016, **16**, 764-772.
13. A. Z. F. Rossi, S. Ristori, J-M. Noel, V. Cabuil, F. Kanoufi and A. Abou-Hassan, *Int. J. Unc. Comp.*, 2015, **11 (1)**, 23-36.
14. S. Thutupalli and S. Herminghaus, *The European Physical Journal E*, 2013, **36**, 1-10.
15. G. Cevc, *Phospholipids Handbook*, Marcel Dekker Inc., New York, 1993.
16. R. Tomasi, J.-M. Noel, A. Zenati, S. Ristori, F. Rossi, V. Cabuil, F. Kanoufi and A. Abou-Hassan, *Chem. Sci.*, 2014, **5**, 1854-1859.
17. N. Li, J. Delgado, H. O. Gonzalez-Ochoa, I. R. Epstein and S. Fraden, *Phys. Chem. Chem. Phys.*, 2014, **16**, 10965-10978.
18. V. Horvath, P. L. Gentili, V. K. Vanag and I. R. Epstein, *Angewandte Chemie International Edition*, 2012, **51**, 6878-6881.
19. K. Torbensen, F. Rossi, O. L. Pantani, S. Ristori and A. Abou-Hassan, *The Journal of Physical Chemistry B*, 2015, **119**, 10224-10230.
20. R. B. Gennis, *Biomembranes*, Springer Advanced Texts in Chemistry, 1989.
21. J. Zhang and P. R. Unwin, *Physical Chemistry Chemical Physics*, 2003, **5**, 3979-3983.
22. A. Walter and J. Gutknecht, *The Journal of Membrane Biology*, 1986, **90**, 207-217.
23. T. X. Xiang and B. D. Anderson, *Biophysical Journal*, 1997, **72**, 223-237.
24. S. Hoops, S. Sahle, R. Gauges, C. Lee, J. Pahle, N. Simus, M. Singhal, L. Xu, P. Mendes and U. Kummer, *Bioinformatics*, 2006, **22**, 3067-3074.
25. O. Ortona, V. Vitagliano, D. Fessas, P. Del Vecchio and G. D'Errico, *Journal of Colloid and Interface Science*, 2010, **343**, 401-407.
26. H. Heerklotz, *Quarterly Reviews of Biophysics*, 2008, **41**, 205-264.

III.4. Photochemical effect of ruthenium bipyridine on the Belusov-Zhabotinsky oscillatory behaviour

In the previous part, the composition of the applied BZ-reaction had an inherent induction period of ~120s, allowing for arrangement of the BZ encapsulating in a 1D array before the oscillations initiated. For other studies, *e.g.,* using a different BZ-composition or for arrangement of the droplets in more complex arrays, control over the induction period is required. One way of governing the initiation of the oscillation of the ferroin catalysed BZ-reaction is by illuminating the BZ-reaction mixture in the presence of the organometallic complex ruthenium bipyridine, $Ru(bipy)_3^{2+}$.[1-4] In general, $Ru(bipy)_3^{2+}$ can be excited upon illumination (with a maximum absorbance wavelength of 450nm), producing an excited triplet state that can be described as a Ru^{3+} complex containing a $bipy^-$ ligand. This ligand is a strong reducing agent, capable of reducing any ferriin formed upon reaction between ferroin and bromate, see equation (R7) of the FKN-model[5, 6] below, and thus inhibits the oscillation cycle.

$$Fe(phen)_3^{2+} + BrO_3^- + 2H^+ \rightarrow Fe(phen)_3^{3+} + BrO_2^{\cdot} + H_2O \qquad \text{(R7)}$$

To investigate the effect of adding the photosensitive ruthenium complex $Ru(bipy)_3Cl_2$ to microreactors encapsulating the BZ-reaction, simple water-in-oil emulsions were generated, using the same microfluidic setup as described in the previous part. The oil phase consisted of a 2:1 cyclohexane/chloroform mixture, and the aqueous drops contained the BZ-reaction with a composition as tabulated in Table 1 below.

Table 1:

Specie	C/M
H_2SO_4	0.300
$NaBrO_3$	0.120
MA	0.300
ferroin	0.005
$Ru(bipy)_3Cl_2$	0, 0.0001 or 0.0005

Three different concentrations of $Ru(bipy)_3Cl_2$ were employed, as tabulated in Table 1. In each case, the drops were collected in a capillary tube (inner diameter of 500μm) in an arrangement separating the drops, in order to observe the isolated oscillatory behaviour of the individual drops, as shown in Figure 1A. The drops were monitored for a time of 1800s using optical microscopy. Figure 1B-D shows the space-time plots deduced from the image sequences as vertical projections of a single drop in the case of 0, 0.1 and 0.5mM $Ru(bipy)_3Cl_2$, respectively.

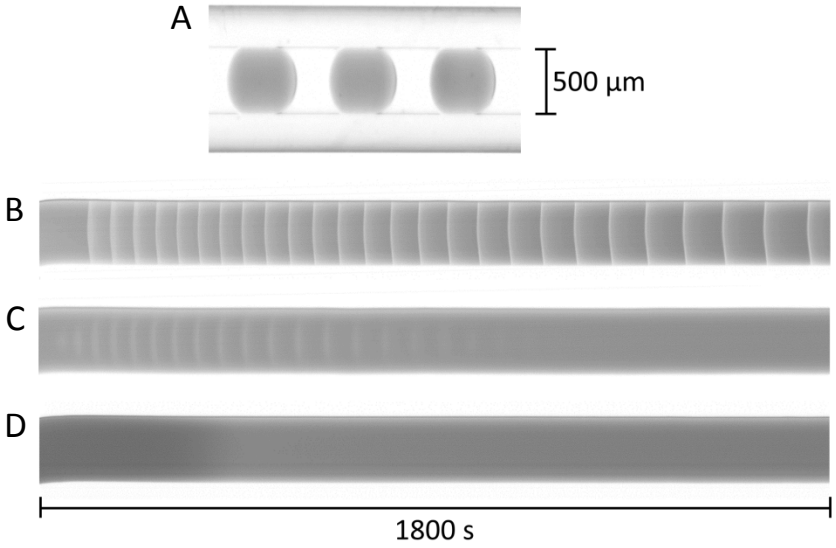

Figure 1. (A) image of the BZ containing drops as collected in the tube for monitoring. (B-D) space-time plots representing the vertical projection of the images (one frame per second), recorded over 1800s, of an individual drop containing the BZ composition as tabulated in Table 1, with 0, 0.1 and 0.5 mM $Ru(bipy)_3Cl_2$, respectively.

The only illumination employed was that of the microscope light source (white light) needed to record images/video sequences with an acceptable contrast, *i.e.,* level 3 on the light-control panel. The effect of adding small amounts (0.1 and 0.5mM) of $Ru(bipy)_3Cl_2$ to the BZ reaction is illustrated in the profile plots shown in Figure 2A. The profiles were deduced from the space-time plot presented in Figure 1. Figure 2A clearly shows, that even small amounts $Ru(bipy)_3Cl_2$ has an effect on the oscillatory behaviour, albeit the only light source was that of the microscope. Upon addition of 0.1 mM $Ru(bipy)_3Cl_2$, the oscillation amplitude is diminished, and the oscillation eventually ceases after ~900s. For 0.5 mM $Ru(bipy)_3Cl_2$, no oscillatory behaviour was observed. The general decrease in intensity with increasing concentration of $Ru(bipy)_3Cl_2$ stems from a higher absorbance as the amount of $Ru(bipy)_3Cl_2$ increases.

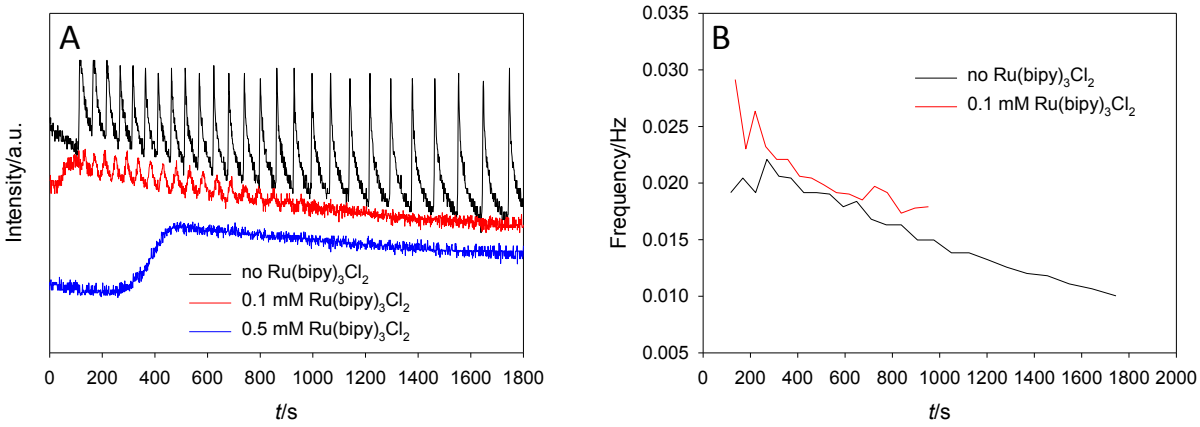

Figure 2. (A) profile plots displaying the oscillation dynamics of individual drops containing the BZ reaction in concentrations a tabulated in Table 1, together with (black line) 0, (red line) 0.1 and (blue line) 0.5 mM $Ru(bipy)_3(Cl)_2$. (B) frequency of the oscillations derived from the plots in (A) for (black line) 0 and (red line) 0.1mM $Ru(bipy)_3(Cl)_2$.

The diminished amplitude and ceasure of the oscillation after ~900s when 0.1mM $Ru(bipy)_3Cl_2$ is present in the drop, and total abcense of oscillations in the case 0.5mM $Ru(bipy)_3Cl_2$, are most likely due to the chloride ions of the ruthenium salt. Chloride, having similar chemical properties as bromide, the BZ inhibitor intermediate, thus seem to have an undesired impact on the overall BZ kinetics. However, this has not been adressed in works employing $Ru(bipy)_3Cl_2$ as photosensitizing agent for the ferroin catalyzed BZ-reaction.[1, 3, 4] Figure 2B shows the frequency of the oscillations for the drops containing 0 and 0.1mM $Ru(bipy)_3Cl_2$, displaying only minor changes in the oscillation frequency when $Ru(bipy)_3Cl_2$ is present in the drop.

To verify that the chloride ions of the $Ru(bipy)_3Cl_2$ are responsible for the effects on the BZ reaction dynamics described above, the sulfate salt ($Ru(bipy)_3(SO_4)_2$) was employed instead, as sulfate is already present in the BZ mixture, stemming from the ferroin salt. The ruthenium bipyridinesulfate was made by extracting $Ru(bipy)_3Cl_2$ with stoichiometric amounts of $AgSO_4$, to percipitate chloride as AgCl according to equation 1:

$$2AgSO_{4(aq)} + Ru(bipy)_3Cl_{2(aq)} \rightarrow 2AgCl_{(s)} + Ru(bipy)_3(SO_4)_{2(aq)} \qquad (1)$$

With $K_{sp,AgCl} = 1.77 \times 10^{-10}$, only traces of chloride ions will be present in the remaining solution.

The same experiment as described above was conducted with $Ru(bipy)_3(SO_4)_2$. Figure 3 shows the space-time plots deduced from the recordings of the oscillating drops in the presence of various concentrations of $Ru(bipy)_3(SO_4)_2$.

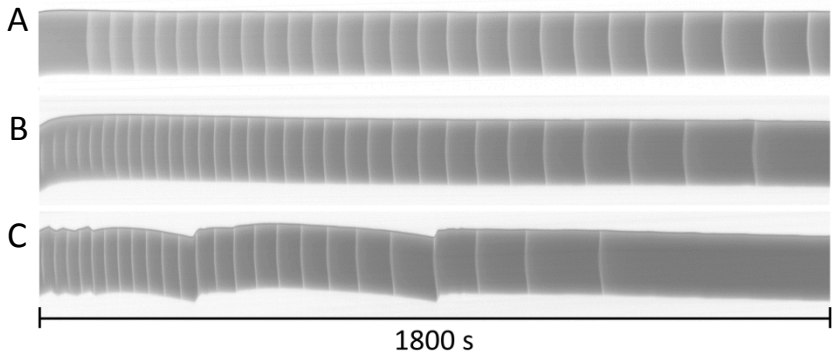

Figure 3. (A-C) space-time plots representing the vertical projection of the images (one frame per second), recorded over 1800s, of an individual drop containing the BZ composition as tabulated in Table 1, with 0, 0.1 and 0.5 mM $Ru(bipy)_3(SO_4)_2$, respectively.

The corresponding profile plots displaying the oscillatory behaviour of individual drops are shown in Figure 4A. Here, the effect of $Ru(bipy)_3(SO_4)_2$ manifests in absence of an induction period, and in an decrease in oscillation period, the latter giving rise to an increase in the oscillation frequency, Figure 4B, compared to the oscillation frequency in the absence of $Ru(bipy)_3(SO_4)_2$ in the system. This can be explained by $Ru(bipy)_3(SO_4)_2$ itself being a catalyst, like ferroin, for the BZ-reaction.[7] Figure 4A clearly shows, that this system exhibits sustainable oscillations for at least 1200s. Hence, the photosensitizing effect of $Ru(bipy)_3(SO_4)_2$ on the BZ reaction could be investigated further. An attempt to totally inhibit the oscillatiory behaviour of the BZ-reaction was made using the microscope light source. Drops containing 0.1 and 0.2mM $Ru(bipy)_3(SO_4)_2$, was illuminated for 900s using the maximum level of light providable by the microscope light source. Then the light was adjusted to level 3, and recordings of the drops were continued for further 900s. The space-time plots obtained hereby are shown in Figure 5. The profile plots shown in Figure 6, obtained from the space-time plots of Figure 5, shows the oscillatory behaviour under strong illumination and under the normal light level for our optical microscopy recordings. In the case of 0.1mM $Ru(bipy)_3(SO_4)_2$, some initial oscillations, emerging without induction period, appears, but ceases after 600s.

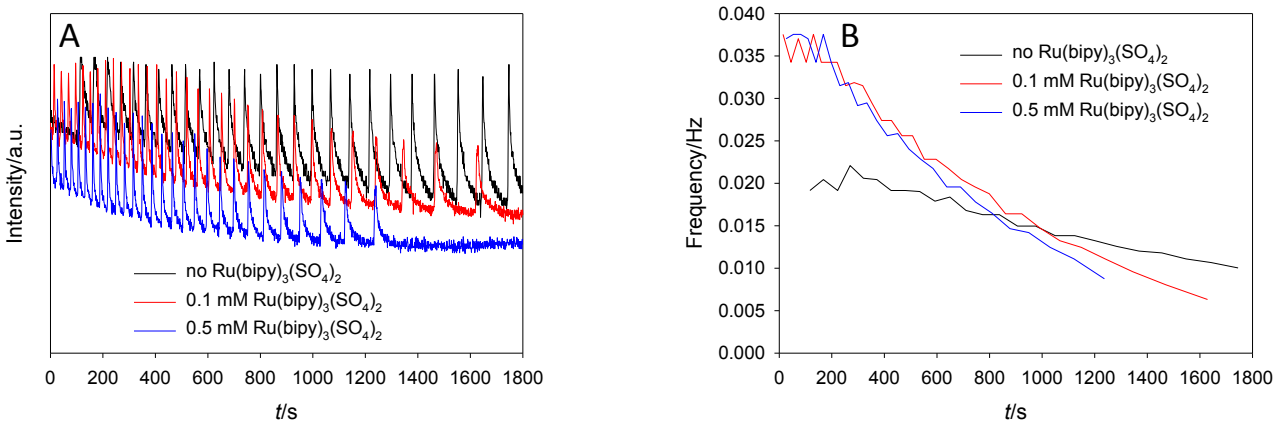

Figure 4. (A) profile plots displaying the oscillation dynamics of individual drops containing the BZ reaction in concentrations a tabulated in Table 1, together with (black line) 0, (red line) 0.1 and (blue line) 0.5 mM $Ru(bipy)_3(SO_4)_2$. (B) frequency of the oscillations derived from the plots in (A) for (black line) 0, (red line) 0.1 and (blue line) 0.5mM $Ru(bipy)_3(SO_4)_2$.

These initial experiments on inhibiting the BZ-reaction using the photosensitizing complex $Ru(bipy)_3^{2+}$ shows, that the chloride salt had a dramatic negative effect on the BZ-reaction, even under low illumination. Hence, under our experimental conditions, this compound is not suitable for the use of inhibiting the BZ-reaction.

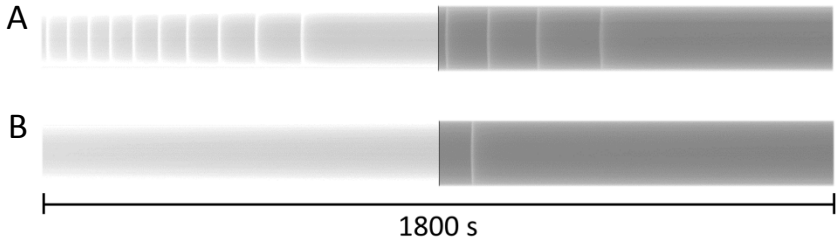

Figure 5. (A and B) space-time plots representing the vertical projection of the images (one frame per second), recorded over 1800s, of an individual drop containing the BZ composition as tabulated in Table 1, with 0.1 and 0.5 mM $Ru(bipy)_3(SO_4)_2$, respectively.

These furthermore appears with a lower frequency compared to the system without $Ru(bipy)_3(SO_4)_2$, indicating that the BZ-reaction to some extent is inhibited. Leveling down the light after 900s results in oscillations to emerge again, however the oscillations do not sustain for more than a few cycles. A concentration of 0.5mM $Ru(bipy)_3(SO_4)_2$ totally inhibits the BZ-reaction

under strong illumination. After adjusting down the light, only a single oscillation was observed. One reason for this could be, that heat induced by the strong illumination causes undesirable side reactions, removing or degrading one or more of the BZ-components.

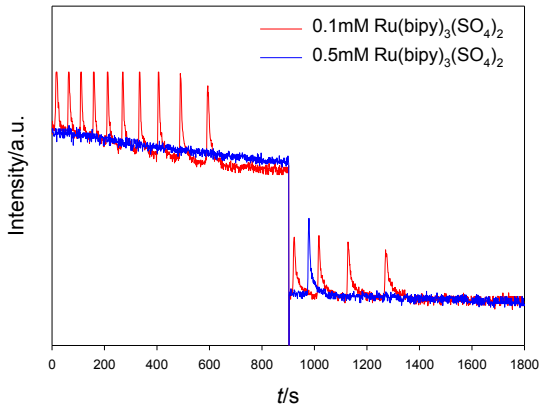

Figure 6. Profile plots displaying the oscillation dynamics of individual drops containing the BZ reaction in concentrations a tabulated in Table 1, together with (red line) 0.1 and (blue line) 0.5 mM $Ru(bipy)_3(SO_4)_2$. The illumination strength is decreased at t = 900s.

The use of the sulfate salt of the ruthenium complex showed more promising results, with partly or total inhibition under strong illumination for concentrations of 0.1 and 0.5mM, respectively. However, only a sparce oscillatory behaviour was observed under normal light. By optimizing of the concentration of $Ru(bipy)_3(SO_4)_2$, and utilizing a stronger light source, *i.e.,* stronger illumination near the absorbance wavelength of $Ru(bipy)_3(SO_4)_2$, improved inhibitory control over the BZ-system can be achieved.In this context, control over the temperature is also required.

REFERENCES:

1. M. Toiya, V. K. Vanag and I. R. Epstein, *Angewandte Chemie International Edition*, 2008, **47**, 7753-7755.
2. V. K. Vanag, A. M. Zhabotinsky and I. R. Epstein, *The Journal of Physical Chemistry A*, 2000, **104**, 8207-8215.
3. J. Delgado, N. Li, M. Leda, H. O. Gonzalez-Ochoa, S. Fraden and I. R. Epstein, *Soft Matter*, 2011, **7**, 3155-3167.
4. N. Li, J. Delgado, H. O. Gonzalez-Ochoa, I. R. Epstein and S. Fraden, *Phys. Chem. Chem. Phys.*, 2014, **16**, 10965-10978.
5. R. M. Noyes, R. Field and E. Koros, *J. Am. Chem. Soc.*, 1972, **94**, 1394-1395.
6. R. J. Field, E. Koros and R. M. Noyes, *J. Am. Chem. Soc.*, 1972, **94**, 8649-8664.
7. R. Toth and A. F. Taylor, *Progress in Reaction Kinetics and Mechanism*, 2006, **31**, 59-115.

Chapter IV: Microfluidics: A platform for generating BZ-encapsulating double emulsions towards templating communicative liposome networks

IV.1. Introduction

In this chapter, a novel design for a microfluidic device for producing encapsulating double emulsions is reported. The first part, describing the microfluidic device, is publiched in *Journal of Flow Chemistry*. BZ-encapsulating double emulsions can, upon solvent removal from the oil shell, serve as a template for liposomes with the BZ-reaction confined in the core drops. This route is however far from trivial, and some of the obstacles encountered, such as double emulsion instability and solvent removal, are reported in the following parts of this chapter.

IV.2: Easy-to-assemble and adjustable coaxial flow focusing microfluidic device for-generating controllable water/oil/water double emulsions: toward templating giant liposomes with different properties

Kristian Torbensen[a] and Ali Abou-Hassan[a]*

[a] *UPMC Univ Paris 6, Laboratoire Physico-chimie des Electrolytes et Nanosystèmes InterfaciauX (PHENIX), UMR 8234, équipe Colloïdes Inorganiques, Université Paris 6 (UPMC) Bat F(74), case 51, 4 place Jussieu, F-75252 Paris Cedex 05, France*

** Corresponding author:* ali.abou_hassan@upmc.fr

ABSTRACT:

Herein, an optimized microfluidic device for manufacturing encapsulating water-in-oil-in-water (w/o/w) double emulsions is reported. The adjustability of the microfluidic device allows on-demand formation of oil shells with different thicknesses during the w/o/w double emulsion formation while maintaining the same core size. This was achieved by manipulation of the separation distance between the cylindrical tubes constituting the flow focusing part of the device and the outer flow rate of the continuous phase at the same time. By incorporating lipids in the oil shell, the w/o/w double emulsions serve as templates for the formation of monodisperse encapsulating liposomes. Thus, liposomes with different shell properties can be generated after evaporation of the oil that can be collected either separately or pooled together in a single sample batch using only one experimental step. The w/o/w double emulsions are highly monodisperse, generated with a throughput of more than 10 Hz, having water core diameters ranging from 130 to 290 µm and different oil shell thicknesses varying from 5 to 13 µm. Moreover, double emulsions with diameters down to 10 µm are reported, however at this size the dispersity is less controllable. The microfluidic device is composed of commercially available parts with only minor modifications required, thus facilitating the manufacturing of encapsulating w/o/w double emulsions.

INTRODUCTION:

The study of complex biological systems such as living cells has been subject to research for more than a century, resulting in a profound understanding of transport phenomena across cell membranes and cell metabolism, etc. The complexity of biological systems, often having a nonlinear response to external and internal manipulation, and the handling of living cells had led to the search for more simple and manageable model systems. In this context, giant unilamellar vesicles (GUVs) composed of self-assembled amphiphiles have proven invaluable in mimicking cellular structures.[1] In particular, the use of phospholipids as amphiphiles in the construction of artificial cellular membranes, i.e. liposomes,[2,3] constitutes an important class of structures as these membranes are easily doped, e.g. with proteins,[4,5] providing model systems for biological pathways of signal transduction and membrane transport.[6] Moreover, GUVs not only serves as synthetic model systems mimicking biological cells,[7] but also plays a major role in recent developments of carriers of active material in drug delivery systems[8-10] and as encapsulating agents in the food industry.[11] These versatile applications of GUVs have motivated researchers to develop different methodologies to control their elaboration.

Traditionally, GUVs are generated by hydration of dried lipid films - with (electroformation) or without a voltage potential[12-14] - or in bulk solutions followed by membrane extrusion.[15, 16] However, the as formed vesicles often lack monodispersity and/or the product yield is relative low. More recently, new techniques such as pulsed jet flow[17,18] and, with the development of soft lithographic methods,[19] microfluidic devices have been applied in the formation of lipid vesicles. In particular, microfluidics, i.e. the manipulation of fluids on the micrometric scale, has proven an excellent technique for generating double emulsion for GUV encapsulation. The drawbacks of previous techniques are here overcome by using flow focusing microfluidic devices with high channel resolution achieved either by a lithographic approach[4,20] or by coaxial assemblies of capillary tubes.[5, 10, 21-23] However, limitations to present designs still exist since the geometry of these devices is fixed once the cast or assembly is completed. Although some variations in the vesicle size and lamellarity can be obtained by changing the volumetric flow rates and the radius of the capillary dimensions,[5,21] these devices have no inherent option for changing the geometry of the flow focusing part which is a crucial parameter for optimization of the vesicle design. It is important to note here that the initial products formed by the aforementioned microfluidic devices is in fact water-in-oil-in-water (w/o/w) double emulsion drops that only constitute a template for the actual vesicles. Only upon dewetting or evaporation of the volatile oil phase is the liposome membrane formed.[22,24] In this context, controlling the thickness of the oil film in the double

emulsion drops is crucial for governing the final lamellarity of the vesicle, i.e. formation of uni- or multilamellar shells or shells comprised of aggregated material.[5,24-26]

Herein, we present an optimized microfluidic device combining all together the different technical advantages reported separately for droplet,[27] double emulsion[21,28] and vesicle[5,29] formation. We added, in a combining design, the ability of adjusting the device geometry *during* (i.e. under continuous flow) w/o/w double emulsion formation. This adds a new degree of freedom to accompany volumetric flow rate variations in order to increase control over the vesicle formation and characteristics, e.g. size, monodispersity and lamellarity. On one hand, we demonstrate the ability of generating monodisperse encapsulating liposomes from w/o/w double emulsion templates, having the same water core size but different oil shell thicknesses. We assume that after evaporation of the oil shells of different thicknesses, and at the same phospholipid concentration, increasing (respectively decreasing) the thickness of the oil layer will result in liposomes of different membrane properties (lamellarity, permeability,etc). Such a control on the membrane properties can be ideal for a broad variety of studies, e.g. on the effect of membrane on chemical communication[30] and membrane sequestering and membrane permeation of bioactive molecules for modelling drug delivery systems.[31] In a biomimetic approach, e.g. modelling living cells, indeed a unilamellar structure is preferred. However, for compartmentalizing purposes, it might be desirable to increase the vesicle stability by generating multilayered membranes. Although the sizes of the generated vesicles are too large for real drug delivery applications, for the aforementioned purposes the size of the generated vesicles might come in handy as individual vesicles can be monitored optically and spectroscopically. On the other hand, the adjustability enables on-demand change of the liposome lamellarity, resulting in monodisperse vesicles with different shell properties within the same batch. This provides a versatile and reliable platform for screening trials for investigation of membrane transport phenomena, release conditions of delivery systems, etc. Furthermore, our device enables mixing of liquid phases prior to the vesicle encapsulation process thus preventing premature aging of chemical reactions intended to occur solely within the vesicles.

RESULTS AND DISCUSSION:

Our device is constituted of coaxially aligned glass tubes of various dimensions and geometry. First, a single or two fused (using epoxy resin) polyimide coated 150/50 μm (outer diameter (OD)/ inner diameter (ID)) glass capillary tubes (Polymicro) are inserted into a cylindrical 1/0.5 mm

(OD/ID) borosilicate tube (Drummond Scientific). The borosilicate tube was narrowed in one end for enhanced flow focusing (see below) by exposing the tube orifice to a butane flame while rotating the tube. The inner wall and the orifice of this tube were rendered hydrophobic using 2% (v/v) trichloro(1*H*,1*H*,2*H*,2*H*-perfluorooctyl)silane (Sigma Aldrich) in toluene, rinsed with toluene and dried overnight at 70°C to obtain desired wetting properties. These tubes are in turn inserted into a square borosilicate tube 1.25 x 1 mm (outer/inner side length, Vitrocom), the principal illustrated in Figure 1A. Depending on the solution(s) to encapsulate one or more tubes can be used. However the use of two tubes (or more) is mandatory when there's a need to separate chemicals, preventing them from premixing and reacting before encapsulation inside the double emulsions. A second cylindrical borosilicate tube, likewise flame treated and serving as the vesicle collector tube, was inserted from the opposite end of the square tube and the two cylindrical tubes were positioned with the narrowed orifices in close position followed by positioning of the two inner most fused capillary tubes close to the orifice of the left cylindrical tube, see Figure 1B. All glass tubes were assembled using T-crosses (P-727, Upchurch Scientific), ferrules (F-331, Upchurch Scientific) and pieces of 1/3 mm (OD/ID) silicon tubing (Tygon Versilic Silicon Tubing, Sigma Aldrich) and mounted on a Plexiglas stand as displayed in Figure 1C. All parts required for the device are shown in Figure S1 (see Supplemental Material). The setup allows injection of fluids into the inner most capillary tubes, the left most cylindrical tube and from both ends of the square tube as illustrated in Figure 2. Additionally, the separation distance between the cylindrical tubes, d, and thus the geometry of the flow focusing part, can be varied by turning the left most ferrule fitting as illustrated by the red arrow in Figure 1C. The soft silicon tube sealing allows for changing reversibly, and without any leakage, the distance by several hundreds of micrometers, which can be done in a controlled manner when monitored by optical microscopy. The close joining of the two inner most capillary tubes results in instantaneous merging of the aqueous phases upon forming a coherent aqueous flow engulfed by the oil phase. In principal, this protocol enables insertion of several fused inner tubes allowing mixing of multiple phases prior to emulsification. As stated previously, flow-focusing devices reported so far have been described to control the size of the final vesicles by controlling the size of the w/o/w double emulsions. This was achieved by varying the ratio of the volumetric flow rate of the outer flow (Q_3) to the oil middle flow rate (Q_2), which not only varied the thickness of the oil layer but also affected the size of the inner aqueous core. Similar results were obtained in our device for a fixed geometry; the size of the double emulsions (core and oil shell) decreased when Q_3/Q_2 increased. However our main objective is to prepare double

emulsions with same core sizes but with variable oil shell thicknesses, which may result, after evaporation, in different membrane lamellarity. Our work is mainly motivated by our recent work on chemical communication between vesicles encapsulating chemical information.[30]

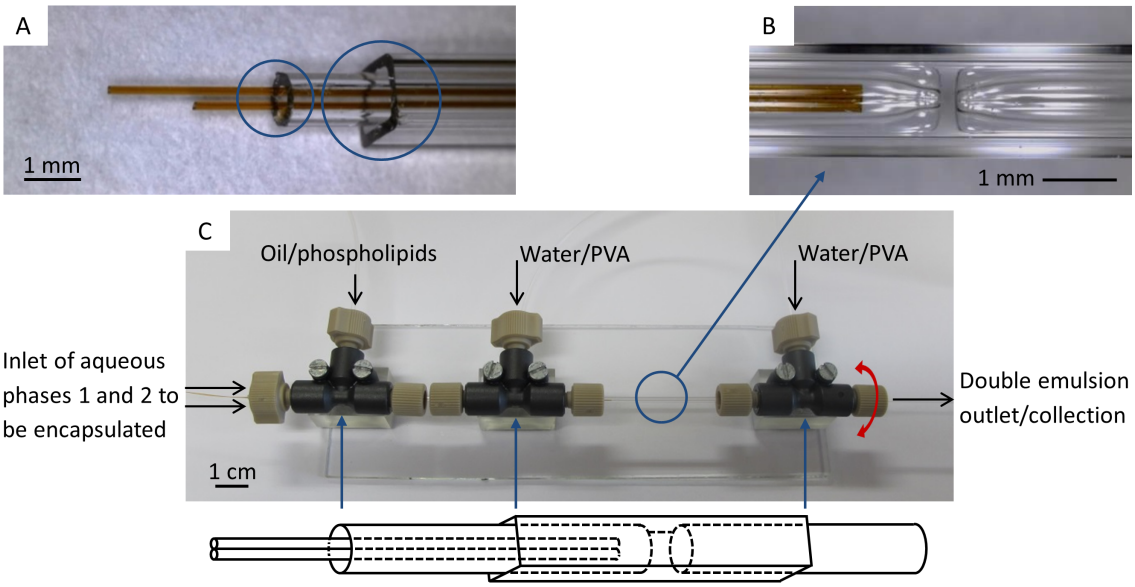

Figure 1. (A) Image demonstrating the concept of coaxial alignment of tubes with various diameters and geometries. The circles highlights the flow entries enclosed in the T-crosses enabling the coaxial flow of the oil phase along the two inner most capillaries and the aqueous solution of polyvinyl alcohol (PVA, 2% wt, Mw 18 kDa) solution in the corners of the square tube, the latter from both ends. (B) Close-up of the flow focusing part of the microfluidic device showing the two inner most fused capillary tubes and the narrowed cylindrical tubes enclosed in the outer square tube and (C) the complete assembled microfluidic device mounted on a Plexiglas stand, together with a sketch of the assembled tubes.

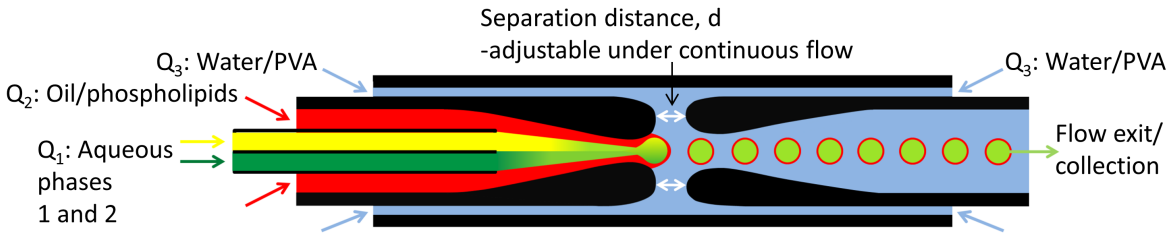

Figure 2. Schematic illustration of the microfluidic device for generating w/o/w double emulsions. A simple emulsion (w/o middle phase, light green) of two mixed aqueous phases (yellow and green, total volumetric flow Q_1) is being formed in the oil containing phospholipids (red, volumetric flow rate Q_2) in the left inner capillary tube just prior to the encapsulation. Breakup and re-emulsification of the w/o middle phase is effectuated upon encountering the outer aqueous phase, flowing in from the corners of the square tube with

total volumetric flow rate Q_3, forming monodisperse w/o/w double emulsion drops (light green in red circles) in the right capillary tube. The white arrows indicate the geometric adjustability of the device.

To demonstrate the versatility of the microfluidic device in varying the thickness of the oil shell, and thus the lamellarity of the final liposomes, while maintaining the size dispersity (same core size) of the liposomes, we generated w/o/w double emulsions with different geometric configurations of the device, i.e. different distances, d, separating the orifices of the cylindrical tubes, as displayed for two cases by the optical micrographs in Figure 3 (Multimedia view). The left row, Figure 3A-C and the right row, Figure 3D-F, shows the device with d =122 μm and 276 μm, respectively. The inner aqueous phase was injected with a volumetric flow rate Q_1 = 15 μL/min and was formed *in situ* by mixing two aqueous solutions containing 2% (w/w) polyvinyl alcohol (PVA), with a dynamic viscosity (η) at 20°C of 1.63 mPas (measured with an automated micro viscometer, Anton Paar), of which one contained 10 mM ferroin as a dye marker. The middle oil phase was injected with different volumetric flow rates of Q_2, and was composed of a solution of the phospholipid 1,2-dimyristoyl-*sn*-glycero-3-phosphocholine (DMPC; 1% (w/w)) dissolved in a mixture of the volatile solvents cyclohexane/chloroform (volume ratio 2:1). The experiments were performed at 20° C, thus maintaining the DMPC in the gel state.[30] The outer phase was an aqueous solution containing 2% (w/w) PVA and was injected at different volumetric flow rates of Q_3. All volumetric flows were controlled using syringe pumps (KD Scientific). The PVA serves both to increase the viscosity for enhanced flow focusing and to increase the stability of the double emulsions.[5] When the viscosity ratio of the outer phase to the inner phase was below 1, only laminar flow can be observed and no jetting or dripping occurred. However when the viscosity ratio was ≥1 double emulsion are observed due to Rayleigh-Plateau instabilities. The instantaneous merging of the co-flow of the two inner most capillaries is driven by a decrease in surface tension upon encountering the hydrophobic oil phase, thus forming a simple water-in-oil emulsion, as displayed in Figure 3A and 3D. The drop-shaped inner aqueous phase is clearly seen engulfed by the coaxially flowing oil phase, the latter forming a meniscus at the hydrophobic orifice of the left capillary tube, just prior to formation of the w/o/w double emulsion in the right capillary tube. The addition of a dye in one of the inner most capillary tubes clearly demonstrates the instant merging of the two aqueous phases. Figure 3B and 3E displays the w/o emulsion just after breakup of the inner aqueous phase, now entirely engulfed by the oil meniscus, and just prior to entering the left collection tube. The natural hydrophilic character of the borosilicate glass ensures wetting of the left capillary tube by the outer aqueous phase, thus facilitating the w/o/w emulsification. Figure 3C and

3F shows the final breakup of the oil phase forming the w/o/w double emulsion. The increased orifice separation, with concomitant increased flow rate of the outer aqueous phase, causes the oil phase to break up in the dripping regime more rapidly and closer to the orifice of the left tube, thus generating a much thinner oil film separating the encapsulated and the outer aqueous phases. An increase of the outer aqueous flow rate, without changing the separation distance (d), not only resulted in a larger separation of the double emulsions in the collection tube but also decreased the size of the w/o/w double emulsions, thus disrupting the overall size dispersity. When the flow rate of the outer aqueous phase was kept constant and the separation distance was increased the size of the double emulsions decreased and a transition to laminar regime can be observed for $d \geq 350$ μm thus leading to non-formation of double emulsions. Thus it is clear that to prepare double emulsions of same inner core size and different oil thicknesses the orifice separation and the flow rates of the middle oil phase and the outer aqueous phase have to be changed simultaneously. The throughput, i.e. the generation frequency, of the w/o/w double emulsions is 14 and 16 Hz for the setup shown in Figure 3A-C and Figure 3D-E, respectively.

The effect of changing the geometry of the flow focusing part of the device on the resulting oil shell thickness was investigated by optical and fluorescence microscopy using the organic soluble fluorophore rhodamine B (Sigma Aldrich). The w/o/w double emulsions were generated in a microfluidic device mounted with a single inner most capillary tube. The volumetric flow rates of the different flows were Q_1 = 30 μL/min for the inner aqueous phase composed only of an aqueous PVA solution (2% (w/w)), Q_2 = 3-10 μL/min for the middle phase composed of DMPC (1% (w/w)) in a mixture of cyclohexane/chloroform solvents (2:1 (v:v) and containing 0.5% (w/w with respect to DMPC) rhodamine B) and Q_3 = 10-50 μL/min for the outer aqueous PVA solution (2% (w/w)). The separation distance, d, between the orifices of the cylindrical tubes was varied between 100-300 μm. Different types of w/o/w double emulsions were collected on a glass slide mounted with a 65 μL frame reservoir and left for 10 min. This resulted in the double emulsions to settle in one layer on the glass slide due to the density of the oil phase being slightly higher than the outer aqueous matrix. The degree of oil phase evaporation is expected to be rather low at the experimental temperature of 20º C at this time scale, thus the membranes are believed to contain a considerable amount of the organic solvents. Figure 4A-D displays optical and fluorescent micrographs of four examples of such batches of double emulsions, generated with orifice separations, d, of 276, 201, 162 and 122 μm, middle fluid volumetric flow rates, Q_2, of 3, 5, 7 and 10 μL/min and outer fluid volumetric flow rates, Q_3, of 50, 30, 20 and 10 μL/min, respectively. As

can be seen from Figure 4A-D the spatial density of the double emulsions increases with decreasing values of Q_3, and due to their high monodispersity double emulsions tend to organize into hexagonal packed clusters. The average diameters of the double emulsion measured on at least 100 double emulsions for the different conditions are 286.4 ± 2.4, 285.0 ± 1.6, 290.6 ± 2.1 and 287.5 ± 2.0 µm, respectively, which confirm the versatility of the system to produce double emulsions with same core sizes and with high monodispersity.

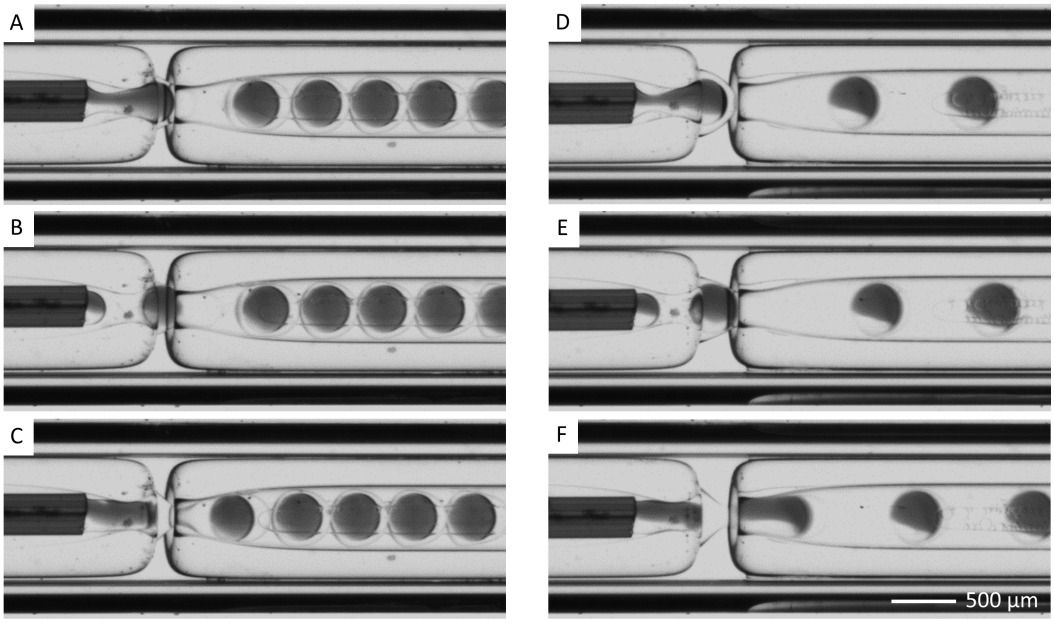

Figure 3. Snapshots showing w/o/w double emulsions generation in the flow focusing part of the adjustable microfluidic device obtained at same Q_1 = 30 µL/min for the inner phase while changing at the same time the orifice separation (d), Q_2 of the oil phase and Q_3 of the outer aqueous phase. (A-C): d =122 µm, Q_2 = 10 µL/min and Q_3 =10 µL/min, resulting in a thick oil shell in the generated w/o/w double emulsions. (D-F): d = 276 µm, Q_2 = 3 µL/min and Q_3 = 50 µL/min resulting in a barely visible oil shell separating the encapsulated and the outer aqueous phases. (Multimedia view)

Figure 5 displays magnified optical and fluorescent micrographs along with membrane profile plots of the double emulsions displayed in Figure 4. The observed oil shell thickness, defined as the full-width-at-half-maximum of the profile plots, provides thicknesses of 5.3 ± 0.9, 8.9 ± 1.1, 10.1 ± 0.8 and 12.7 ±1.2 µm for the double emulsions shown in Figure 5A-D, respectively (based on measurements of at least 25 double emulsions for each oil shell thickness). This gives an oil shell thickness-to-diameter ratio between 0.019 to 0.044 on going from the ultrathin shell of the double emulsion depicted in Figure 5A, to the thickest shell in Figure 5D. These values are several orders of magnitude higher than what is expected for unilamellar

membrane structures and probably caused by the considerable amount of organic solvents left in the membrane. The resulting liposomes obtained after complete solvent evaporation are under current investigation.

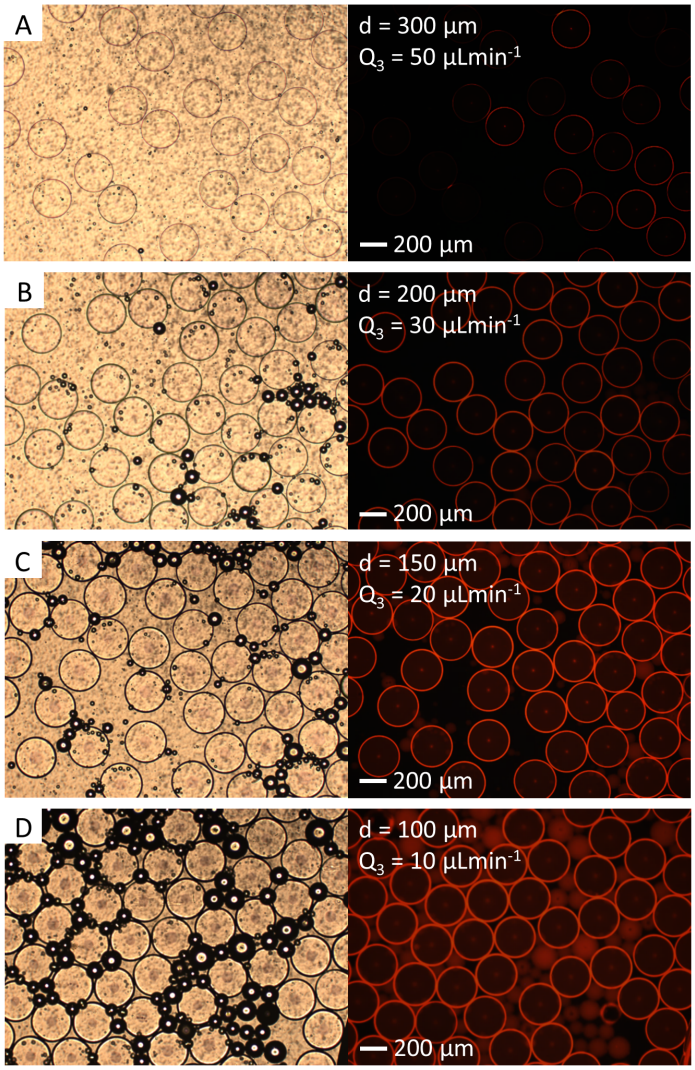

Figure 4. Optical (left) and fluorescence micrographs (right) of w/o/w double emulsions with various oil shell designs generated using constant flow rates of Q_1 = 30 µL/min for the inner aqueous solution (2% (w/w) PVA solution), varying flow rates of Q_2, the middle oil layer (DMPC/cyclohexane/chloroform phase, 1% (w/w), 2:1 (v/v)) and Q_3, the outer aqueous solution (2% (w/w) PVA solution) and varying separation distances, d, between the two cylindrical capillary orifices. The latter three parameters were Q_2 = 3, 5, 7 and 10 µL/min, Q_3 = 50, 30, 20 and 10 µL/min and d = 276, 201, 162 and 122 µm for A-D, respectively. The DMPC was mixed with 0.5% (w/w) rhodamine B.

The ability of generating double emulsions of equal core radius, R, with different oil shell thicknesses, t, is illustrated by plotting R and t as a function of the parameters changed during the

generation, i.e. the middle and outer fluid volumetric flow rates, Q_2 and Q_3, and the separation distance, d, between the two inner capillaries. Figure 6A shows the core radius as a function of Q_3 and d for the four different oil shell designs described above. The small size variation shows overall high size dispersity for all four types of double emulsions. The changes in the oil shell thickness as a function of the total volumetric flow, Q_{tot}, and Q_2 are shown in Figure 6B.

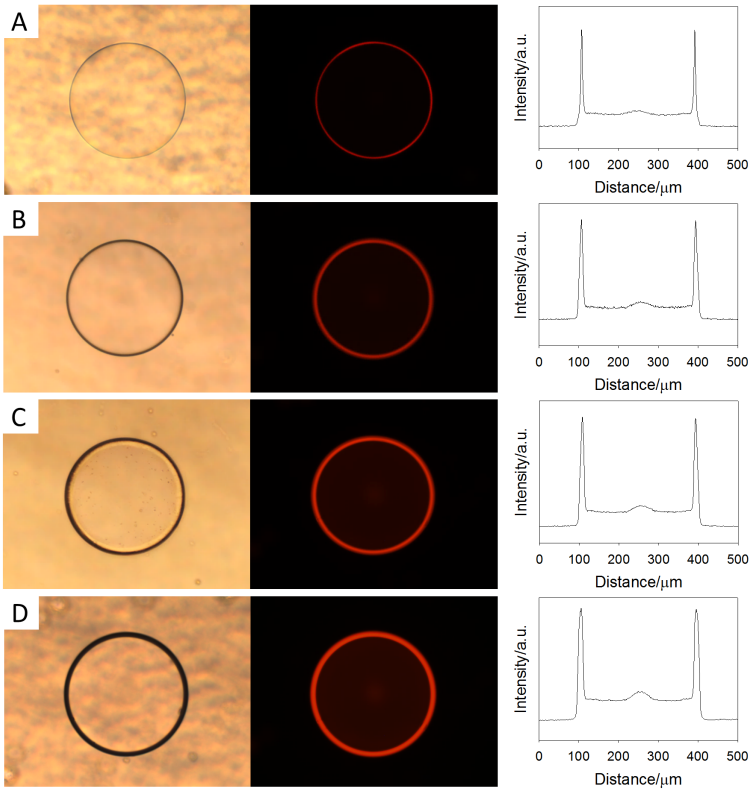

Figure 5. Optical and fluorescence micrographs and membrane profile plots (from left to right) of w/o/w double emulsions with various membrane designs collected individually. Generated using the same conditions as described in Figure 4.

Here, a linear relationship between the oil shell thickness and both the outer fluid volumetric flow rate divided by the orifice separation distance, and the flow rate, Q_2, of the middle oil phase are observed. A theoretical model for predicting both R and t can be generated by using the frequency with which the double emulsions are formed. The mean flow velocity, U, in the left capillary can be calculated as the total volumetric flow, Q_{tot} (= $Q_1 + Q_2 + Q_3$) divided by the cross section, S: $U = Q_{tot}/S$. The frequency of formation, f, is then defined as the ratio U/d, where d is the

orifice separation distance. From mass balance considerations, the core radius of the double emulsions is then defined as equation 1:

$$R = (Q_1/f * 3/4\pi)^{1/3} \quad (1)$$

From equation 1, a constant value for R, close to the experimentally obtained values, can be obtained by using the experimental flow rates and values for d close to the experimental ones, as shown in Figure 6A. Similar considerations can be used to evaluate theoretical values for the oil shell thickness, equation 2:

$$t = (Q_1 + Q_2/f * 3/4\pi)^{1/3} - R \quad (2)$$

Again, as shown in Figure 6B, a good correlation is observed between the experimental values and the values predicted by the theoretical model. This displays the ability with which the oil shell can be designed in a controlled manner while maintaining the same core size.

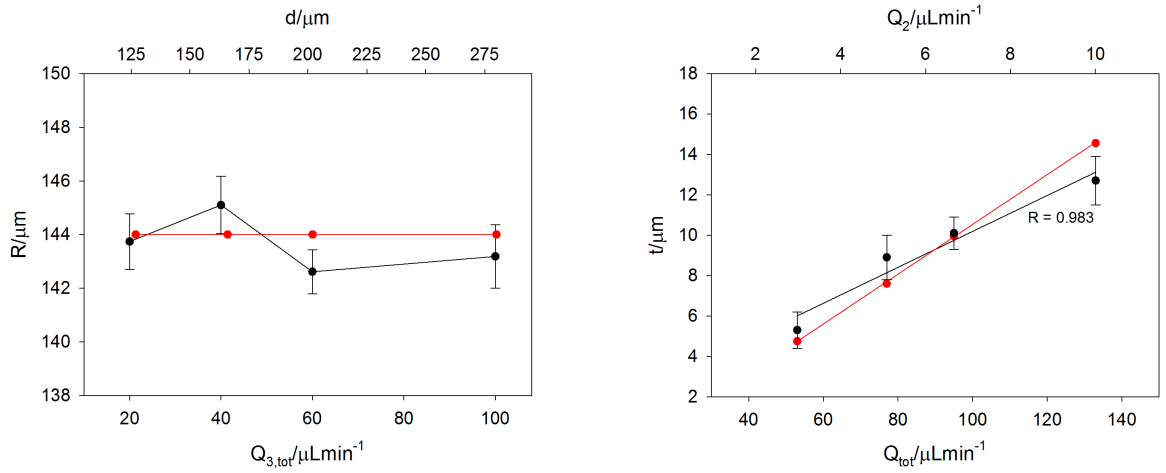

Figure 6. Plots of (A, black trace) the double emulsion size and (B, black trace) the oil shell thickness as a function of the total outer volumetric flow rate, $Q_{3,tot}$, and the orifice separation distance, d. Values deduced from the double emulsions depicted in Figure 4 and 5. Red traces in both Figures shows theoretical calculations based on equation 1 and 2.

As reported in literature, the size of the double emulsions and the membrane thickness can be tuned by changing the outer fluid flow rate and the ratio between the inner and middle fluid flow rates, respectively.[23] However, we experienced that simultaneously maintaining control over both the size dispersity and membrane thickness by adjusting the flow rates proved difficult. Instead, we

took advantage of the possibility to easily exchange the individual parts of the device. By decreasing the inlet diameter of the inner left capillary, i.e. the inlet of the collection capillary, the double emulsion size was reduced. Examples of monodisperse double emulsions with diameters of 130 µm are shown in Figure 7. By further decreasing the inlet diameter, double emulsions with diameters down to 10 µm could be generated, however with less control over the dispersity, as shown in Figure 8. We are currently working on optimizing the geometry of the device in order to generate monodisperse double emulsions with sizes below 10 µm.

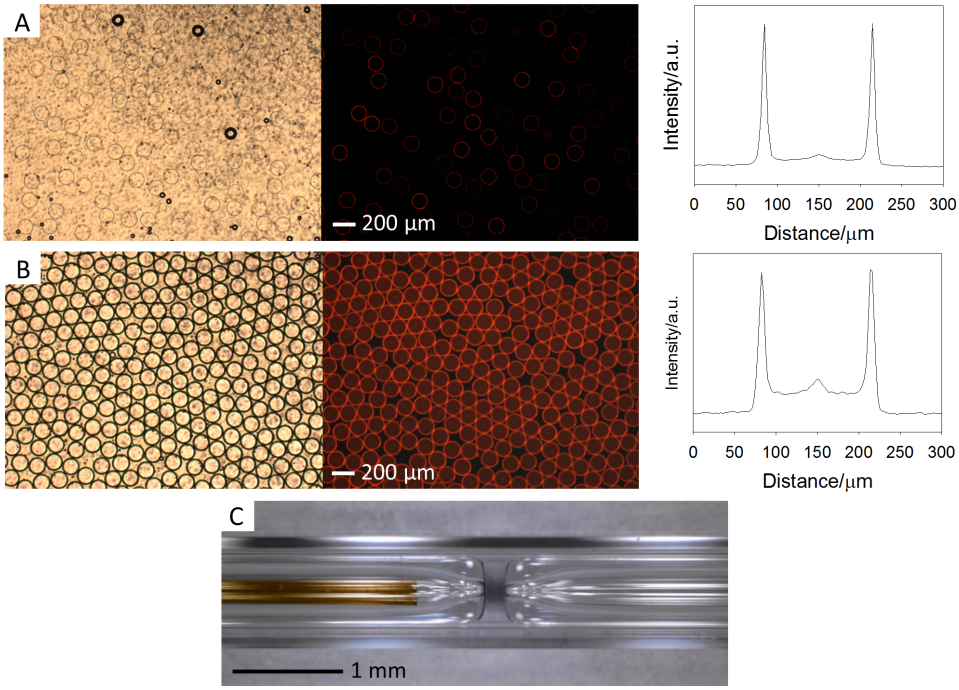

Figure 6. Optical, fluorescence micrographs and profile plots (from left to right) of w/o/w double emulsions with various oil shell designs. The double emulsion core sizes are 130.4 ± 1.7 and 132.1 ± 2.1 µm with membrane thicknesses of 6.0 ± 0.9 and 10.1 ± 0.8 µm in (A) and (B), respectively. Generated using flow rates of 30 µL/min for the inner aqueous/2% (w/w) PVA solution, 10 µL/min for the DMPC/cyclohexane/chloroform phase (1% (w/w), volume ratio 2:1) while the flow rate of the outer aqueous/2% (w/w) PVA solution were 50 and 10 µL/min and the separation distance between the two cylindrical capillary orifices were 300 and 100 µm in (A) and (D), respectively. The DMPC was mixed with 0.5% (w/w) rhodamine B. Close-up of the flow focusing part of the microfluidic device used here is shown in (C).

Finally, the versatility of the device was demonstrated by the ease with which, *during* the w/o/w double emulsion formation, batches of monodisperse double emulsions with different oil shell thicknesses can be generated by simply sliding back and forth the left capillary tube, by

turning the left most ferrule fitting in Figure 1, while adjusting the outer aqueous volumetric flow rate, as described above. The double emulsions were collected on a glass slide and left to settle for 10 min. at 20º C. Figure 8 shows optical and fluorescent micrographs of an assembly of double emulsions with monodisperse size but different oil thicknesses. The ability of elaborating such assemblies enables monitoring various properties originating from the different membrane compositions, e.g. membrane transport phenomena and release properties, within the same batch in a screening approach.

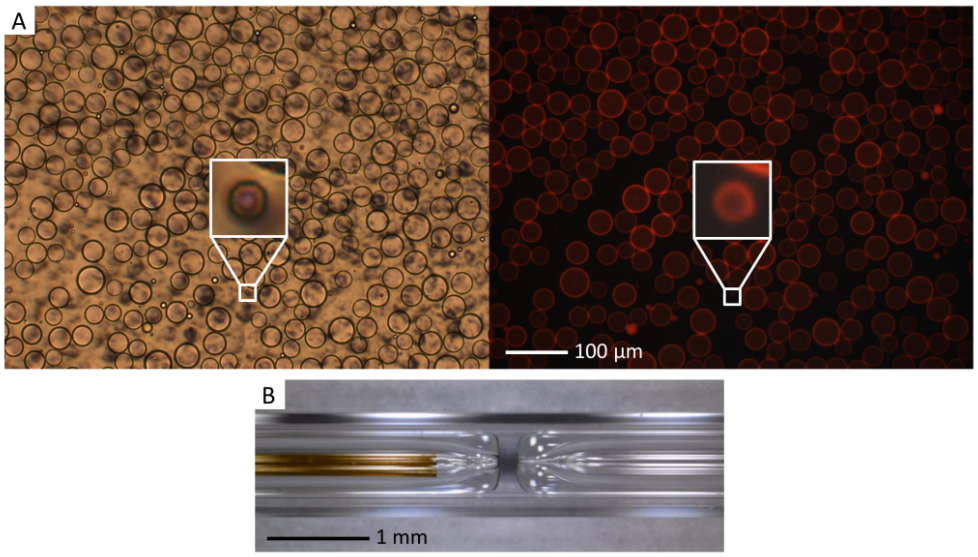

Figure 7. (A) Optical and fluorescence micrographs (from left to right) of w/o/w double emulsions with various oil shell designs. The double emulsion core sizes are generally 28 to 50 µm, however few double emulsions of below 10 µm are observed (see insert in (A). Generated using flow rates of 30 µL/min for the inner aqueous/2% (w/w) PVA solution, 10 µL/min for the DMPC/cyclohexane/chloroform phase (1% (w/w), volume ratio 2:1) while the flow rate of the outer aqueous/2% (w/w) PVA solution were 50 µL/min and the separation distance between the two cylindrical capillary orifices was 200 µm. The DMPC was mixed with 0.5% (w/w) rhodamine B. Close-up of the flow focusing part of the microfluidic device used here is shown in (B).

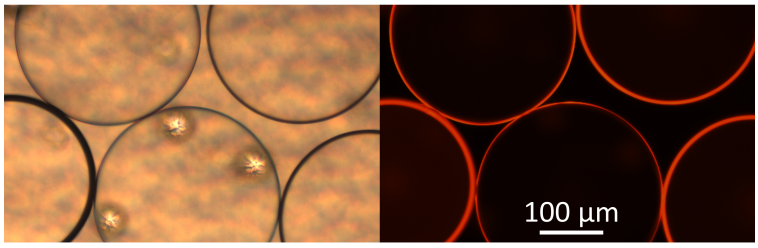

Figure 8. Optical and fluorescence micrographs of various lipid membrane designs formed continuously in the device and collected in one batch. The vesicles were generated by varying the flow rates and geometry as described in Figure 4.

CONCLUSION:

We have demonstrated a new easy to assemble/disassemble and robust design for a microfluidic device with adjustable geometry for generating monodisperse w/o/w double emulsion templates for encapsulating liposomes with a diameter range of 130 to 290 µm with a throughput of more than 10 Hz. Double emulsions down to 10 µm was generated, however at this size the dispersity was lower. The oil shell thickness of the double emulsions can be varied from ultrathin shells, herein reported down to 5.3 µm. The ease of adjusting the geometry of the coaxial design enables the formation of encapsulating liposomes with different membrane properties and high monodispersity either to be collected separately or within the same batch. The latter provides the opportunity of monitoring various effects of the membrane composition in a single sample batch, thus facilitating the experimental procedure and enhancing reproducibility. Furthermore, since the device is based on commercially available parts with low tolerance, the reproducibility of the device itself is high.

REFERENCES:

1. Blain, J. C.; Szostak, J. W. *Annual Review of Biochemistry* **2014,** 83, (1), 615-640.
2. Zagnoni, M. *Lab on a Chip* **2012,** 12, (6), 1026-1039.
3. Matosevic, S. *BioEssays* **2012,** 34, (11), 992-1001.
4. Karamdad, K.; Law, R. V.; Seddon, J. M.; Brooks, N. J.; Ces, O. *Lab on a Chip* **2015**.
5. Arriaga, L. R.; Datta, S. S.; Kim, S.-H.; Amstad, E.; Kodger, T. E.; Monroy, F.; Weitz, D. A. *Small* **2014,** 10, (5), 950-956.
6. Ikonen, E. *Current Opinion in Cell Biology* **2001,** 13, (4), 470-477.
7. Stano, P.; Carrara, P.; Kuruma, Y.; Pereira de Souza, T.; Luisi, P. L. *Journal of Materials Chemistry* **2011,** 21, (47), 18887-18902.
8. Allen, T. M.; Cullis, P. R. *Advanced Drug Delivery Reviews* **2013,** 65, (1), 36-48.
9. Herranz-Blanco, B.; Arriaga, L. R.; Makila, E.; Correia, A.; Shrestha, N.; Mirza, S.; Weitz, D. A.; Salonen, J.; Hirvonen, J.; Santos, H. A. *Lab on a Chip* **2014,** 14, (6), 1083-1086.
10. Kong, F.; Zhang, X.; Hai, M. *Langmuir* **2014,** 30, (13), 3905-3912.
11. Skeie, S. *International Dairy Journal* **1994,** 4, (7), 573-595.
12. Rodriguez, N.; Pincet, F.; Cribier, S. *Colloids and Surfaces B: Biointerfaces* **2005,** 42, (2), 125-130.
13. Angelova, M. I.; Dimitrov, D. S. *Faraday Discussions of the Chemical Society* **1986,** 81, (0), 303-311.
14. Mathivet, L.; Cribier, S.; Devaux, P. F. *Biophysical Journal* **1996,** 70, (3), 1112-1121.
15. Hope, M. J.; Bally, M. B.; Webb, G.; Cullis, P. R. *Biochimica et Biophysica Acta (BBA) - Biomembranes* **1985,** 812, (1), 55-65.
16. Darszon, A.; Vandenberg, C. A.; Schönfeld, M.; Ellisman, M. H.; Spitzer, N. C.; Montal, M. *Proceedings of the National Academy of Sciences* **1980,** 77, (1), 239-243.
17. Funakoshi, K.; Suzuki, H.; Takeuchi, S. *Journal of the American Chemical Society* **2007,** 129, (42), 12608-12609.
18. Stachowiak, J. C.; Richmond, D. L.; Li, T. H.; Brochard-Wyart, F.; Fletcher, D. A. *Lab on a Chip* **2009,** 9, (14), 2003-2009.
19. Xia, Y.; Whitesides, G. M. *Annual Review of Materials Science* **1998,** 28, (1), 153-184.
20. Rossi, F.; Budroni, M. A.; Marchettini, N.; Cutietta, L.; Rustici, M.; Liveri, M. L. T. *Chemical Physics Letters* **2009,** 480, (4–6), 322-326.
21. Utada, A. S.; Lorenceau, E.; Link, D. R.; Kaplan, P. D.; Stone, H. A.; Weitz, D. A. *Science* **2005,** 308, (5721), 537-541.
22. Shum, H. C.; Lee, D.; Yoon, I.; Kodger, T.; Weitz, D. A. *Langmuir* **2008,** 24, (15), 7651-7653.
23. Kim, S.-H.; Kim, J. W.; Cho, J.-C.; Weitz, D. A. *Lab on a Chip* **2011,** 11, (18), 3162-3166.
24. Foster, T.; Dorfman, K. D.; Ted Davis, H. *Journal of Colloid and Interface Science* **2010,** 351, (1), 140-150.
25. Whitesides, G. M.; Grzybowski, B. *Science* **2002,** 295, (5564), 2418-2421.
26. Nishimura, K.; Suzuki, H.; Toyota, T.; Yomo, T. *Journal of Colloid and Interface Science* **2012,** 376, (1), 119-125.
27. Benson, B. R.; Stone, H. A.; Prud'homme, R. K. *Lab on a Chip* **2013,** 13, (23), 4507-4511.
28. Shang, L.; Cheng, Y.; Wang, J.; Ding, H.; Rong, F.; Zhao, Y.; Gu, Z. *Lab on a Chip* **2014,** 14, (18), 3489-3493.
29. Duncanson, W. J.; Lin, T.; Abate, A. R.; Seiffert, S.; Shah, R. K.; Weitz, D. A. *Lab on a Chip* **2012,** 12, (12), 2135-2145.

30. Tomasi, R.; Noel, J.-M.; Zenati, A.; Ristori, S.; Rossi, F.; Cabuil, V.; Kanoufi, F.; Abou-Hassan, A. *Chem. Sci.* **2014,** 5, (5), 1854-1859.
31. Walde, P.; Cosentino, K.; Engel, H.; Stano, P. *ChemBioChem* **2010,** 11, (7), 848-865.

Supplementary Information (ESI) for

Easy-to-assemble/disassemble and adjustable coaxial flow focusing microfluidic device for elaboration of giant uni- and multilamellar encapsulating liposomes

Kristian Torbensen[a] and Ali Abou-Hassan[a]*

[a] *UPMC Univ Paris 6, PHENIX, UMR 8234, équipe Colloïdes Inorganiques, Université Paris 6 (UPMC) Bat F(74), case 51, 4 place Jussieu, F-75252 Paris Cedex 05, France*
* *Corresponding author:* ali.abou_hassan@upmc.fr

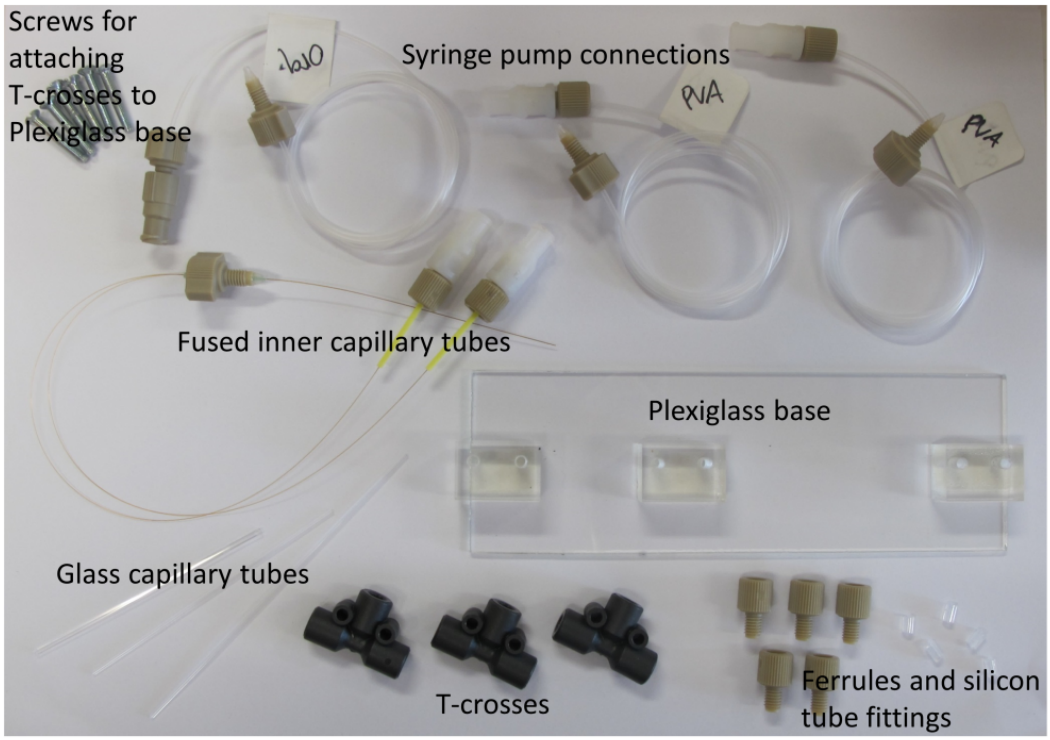

Figure S1. Image displaying all hardware required to assemble the microfluidic device.

IV.3. The BZ-reaction and double emulsions: Towards templating BZ encapsulating liposomes

A biomimetic model of chemical and electrical activity in neurons can be found in non-equilibrium chemical systems such as the Belousov–Zhabotinsky (BZ) oscillating reaction.[1] When encapsulated or confined in microcompartments or microreactors,[2-6] the BZ-reaction has shown to be a mean for studying long- and short-range communication between individual micro environments. The generation of pertinent intermediates governing the oscillatory dynamics of the BZ-system, *e.g.,* the inhibitory and activatory species bromide and bromous acid, was addressed as the messenger molecules, and, when capable of diffusing between the individual microreactors, allowed for spatio-temporal propagation of chemical information.[7-9] Observing collective behaviours such as coupling and synchronization between the individual microreactors, this approach to generate communicating droplet-based networks thus seem promising.

An approach to mimic communication between biological cells, is to encapsulate the BZ-reaction in giant unilamellar vesicles (GUVs, or liposomes), where aqueous drops are compartmentalized by phospholipid membranes. When dispersed in an aqueous medium, GUVs provide a reliable and biomimicking artificial cell-like platform.[10-14] Such encapsulating GUVs can be templated using coaxial microfluidics; in a first step, encapsulating w/o/w (water-in-oil-in-water) double emulsions are formed, which, in a second step, are transformed into GUVs by solvent removal from the oil shell.[15-17] Although controlling the formation of well characterized GUVs (lamellarity, shells without oil residues, etc), encapsulating the BZ reaction still remains a challenge.

In the following, the encapsulation of the BZ-reaction in double emulsions, with the eventual purpose of templating BZ encapsulating GUVs, is described. Also, before proceeding to the second step in the GUV formation, the oscillatory behaviour of the BZ confining double emulsions were investigated. Using the microfluidic device developed in our group,[18] the formation step of the BZ encapsulating double emulsions proved easily feasible. However, obtaining long term stability of the as formed double emulsions, in order to proceed to the second step, *i.e.,* the solvent removal from the oil shell, proved more challenging. An attempt to overcome shell instability is described.

For the generation of the encapsulating double emulsions, the microfluidic device was mounted with two inner capillaries (as described in chapter IV), thus allowing for splitting up the BZ solutions in two phases in order to prevent oscillations to occur prior to the encapsulation: One phase contained the BZ species ferroin, sulfuric acid and malonic acid, the other phase sodium bromate. The final concentrations after encapsulation were 5mM ferroin, 0.3M sulfuric acid, 0.12M sodium bromate, and 0.3M malonic acid. Both the inner phases contained 2% w/w PVA. The middle phase, *i.e.,* the oil phase, consisted of chloroform/cyclohexane (1:2 v/v) containing 1% w/w of the phospholipid 1,2-Dimyristoyl-sn-glycero-3-phosphocholine (DMPC). In a first attempt, the outer phase was an aqueous 2% w/w PVA solution. This was later adjusted by adding sucrose and increasing amounts of PVA, *vide infra*. Figure 1 shows the flow focusing part of the microfluidic device, displaying the encapsulation process.

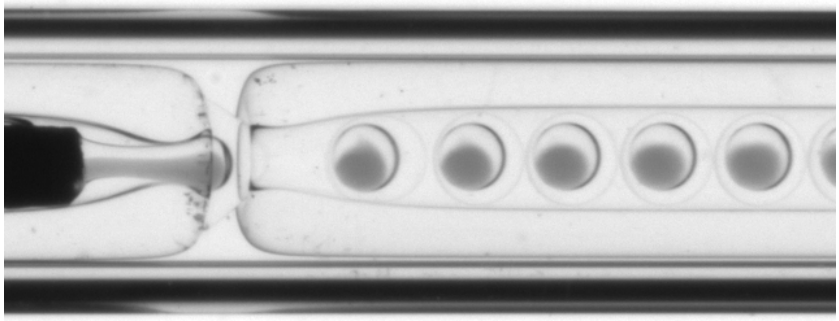

Figure 1. Image showing the encapsulation of the BZ-reaction in w/o/w double emulsions. The two inner phases are merging as they flow from the two inner capillaries (from left) and the mixing proceeds as the double emulsions flow through the collection tube (right). For a more thorough description of the microfluidic device, see ref. 18. Flow rates were: $Q_1 = 5\mu Lmin^{-1}$ (for both inner capillaries), $Q_2 = 10\mu Lmin^{-1}$ (middle phase) and $Q_3 = 10\mu Lmin^{-1}$ (outer phase).

The double emulsions were collected in a 10mm glass capillary tube (ID of 500µm). When the tube was filled with double emulsions, constituting a 1D array, see Figure 2, it was sealed in both ends with wax, and the double emulsions were monitored using optical microscopy for a time period of 1800s. An induction period for the employed BZ-reaction of ~120s made it possible to initiate the recordings before the first oscillation set in. From the recorded image sequence, a space-time plot was constructed as shown in Figure 3A. The remaining part of the induction period is observed for ~45s. Then a period of ~240s sets in with broad oscillations, followed by periods of faster

oscillations. However, after a period if ~1100s, some of the double emulsions rupture, due to shell instability.

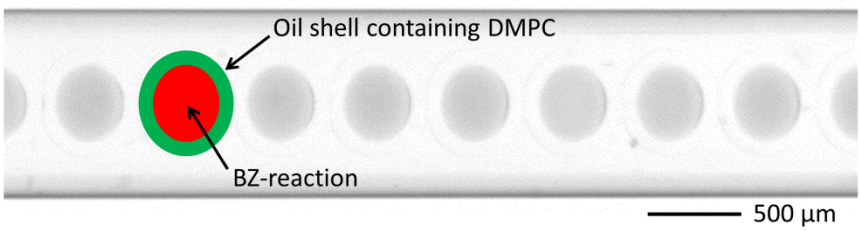

Figure 2. Micro emulsions, in a glass capillary tube, arranged in a 1D array. The double emulsions were suspended in a 2% w/w PVA aqueous solution.

This instability can arise for several reasons. Ferroin ($Fe(phen)^{2+}$) is known to adsorb at lipid containing interfaces,[19] which is present between the inner drop and the oil shell. As oscillations proceed, ferroin is oxidized to ferriin ($Fe(phen)^{3+}$). Hence, a change in electrochemical potential at the interface occurs. Since the oxidation (and subsequent reduction) does not occur absolutely uniformly around the interface, gradients in surface tension can arise, which may provoke Marangoni flow in the lipid interface resulting in destabilization of the interface.

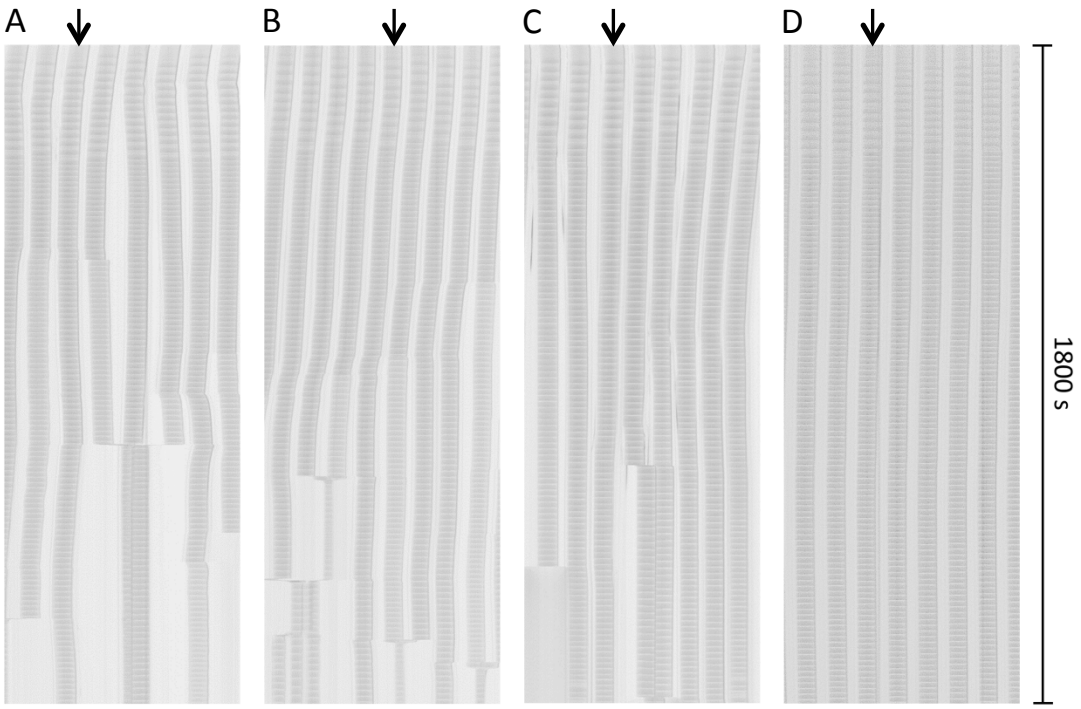

Figure 3. Space-time plots obtained by taking vertical projections of the recorded image sequences of double emulsion 1D arrays, as illustrated in Figure 2. The BZ composition was 0.5mM ferroin, 0.3M H_2SO_4, 0.18M $NaBrO_3$ and 0.3M malonic acid. The outer suspending phase was (A) 2% w/w PVA, (B) 2% w/w PVA and 1.445M sucrose, (C) 5% w/w PVA and 1.445M sucrose and (C) 10% w/w PVA and 1.445M sucrose.

It has also previously been shown, that the electron density of phospholipid bilayers in liposome changes in the presence of ferroin, towards a more narrow localization,[18] leading to less stable lipid-lipid interactions. This effect will be enhanced by the additional positive charge introduced at the interface upon ferroin oxidation. Another reason for the rupturing of the double emulsions can be found in the difference in osmotic pressure across the oil shell, due to the presence of the BZ-components in the inner drop. This will tend water to diffuse from the outside towards the inside of the double emulsion. In this process, water molecules are squeezed in between the lipid assembly at the interface, weakening the lipid-lipid interaction. To equilibrate osmotic stress in double emulsions, sucrose has been used to adjust the osmolarity of the inner drop and the outer phase.[16] In our case, the osmotic pressure, Π, in the inner drop was calculated to be 3532kPa, using van´t Hoof´s equation, stating $\Pi = \Sigma RTci$, where R is the gas constant ($8.315 JK^{-1}mol^{-1}$), $T = 293K$, c is the concentration of the individual BZ-components and i is the respective van´t Hoof´s factors. The contribution to the osmotic pressure by the PVA is ~0.1% of the total pressure inside the drop, and will be neglected in the following. The concentration of sucrose to be added to the outer phase was then calculated to be 1.445M. With this amount present in the outer phase, the space-time plot shown in Figure 3B was obtained. The oscillatory behaviour is similar to that of Figure 3A, *i.e.,* without sucrose in the outer phase, whereas the life time of the double emulsions was prolonged, suggesting that sucrose has a positive effect on the osmotic balance between the inner and outer phases. However, one common feature observed in Figure 3A and B is the horizontal shift in position of the individual space-time plots. This means that the double emulsions move over time in the tube, and is hence exerted to some mechanical stress, contributing to the overall instability. This mechanical stress could be caused by pressure waves induced to the system upon rupturing of nearby double emulsions. To circumvent this problem, the viscosity of the outer phase was increased by using higher concentrations of the viscosity modulator PVA. Figure 3C and D shows the effect on the system upon adding 5 and 10% w/w PVA to the sucrose containing outer phase, respectively. A clear positive effect on the overall stability and fixation of the double emulsions is observed; in the case of 10% w/w PVA, Figure 3D, all double emulsions sustain the 1800s recording time, and almost straight space-time plots are obtained. Regarding the oscillatory

behaviour, a closer inspection of the different systems, presented in Figure 3, reveals not significant effects exerted by the sucrose and increased amounts of PVA present in the outer phase. Figures 4A-D presents the oscillation profiles extracted from the space-time plots in Figure 3, marked by the arrows. Similar induction periods, periods of broad oscillation waves, and subsequent sharper oscillation peaks was observed for all systems; the total numbers of oscillations were counted to be 107, 104, 103 105 for the double emulsions suspended in 2% PVA, 2% PVA and 0.1445M sucrose, 5% PVA and 0.1445M sucrose and 10% PVA and 0.1445M sucrose, respectively. Compared to the bulk study of the same BZ-composition, this gives an oscillation frequency almost three times faster for the BZ-reaction confined in the double emulsions, probably due to the small volume of core drop.[20]

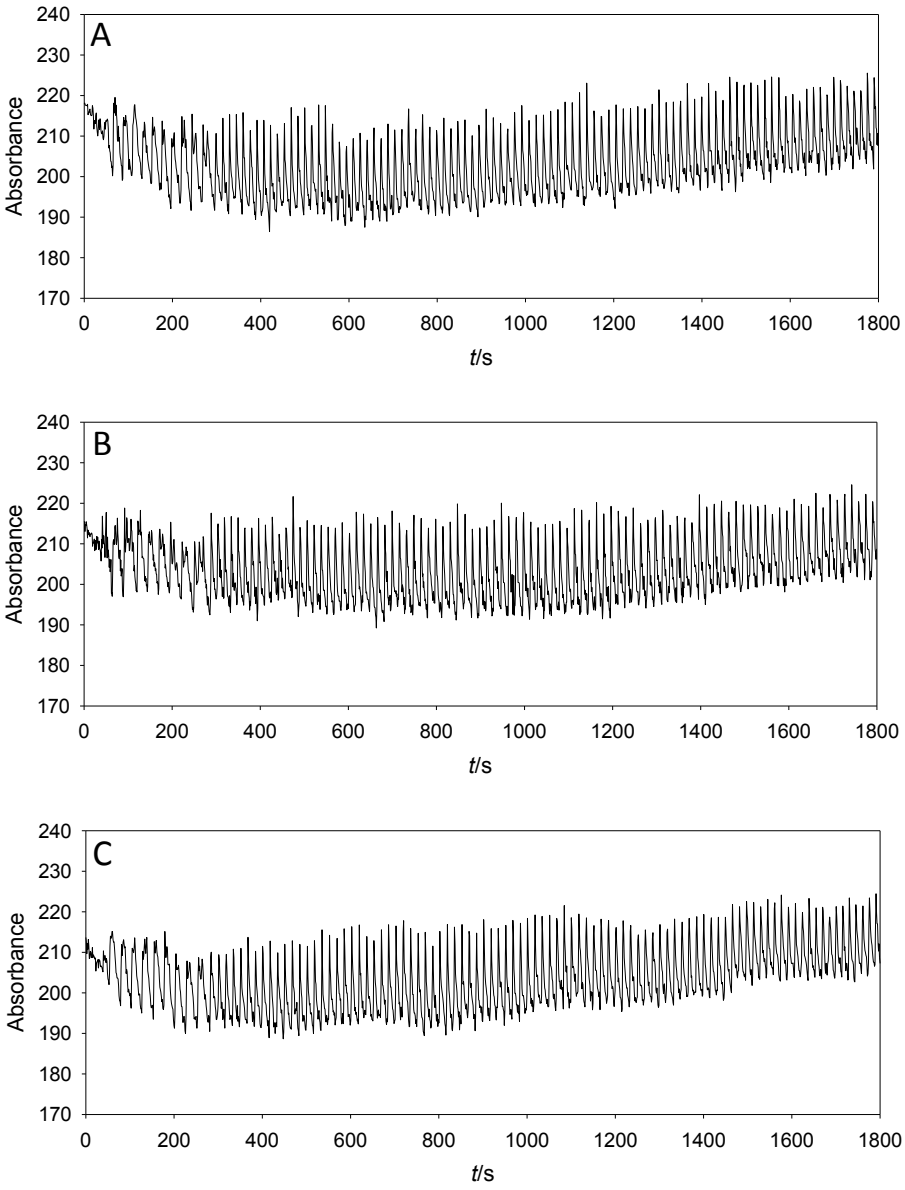

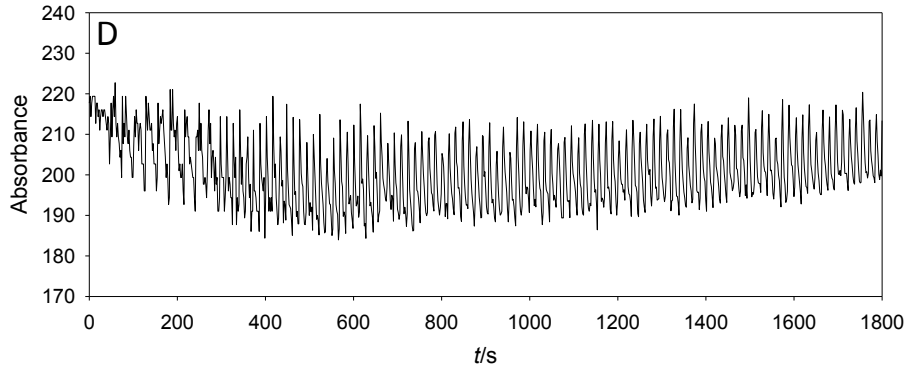

Figure 4. Profile plots, deduced from the space-time plots presented in Figure 3, showing similar oscillatory behaviour for the BZ-encapsulating double emulsions suspended in (A) 2% w/w PVA, (B) 2% w/w PVA and 1.445M sucrose, (C) 5% w/w PVA and 1.445M sucrose and (D) 10% w/w PVA and 1.445M sucrose.

In this part, the stability of BZ confining double emulsions was investigated. When suspended in a 2% w/w PVA solution, the double emulsions exhibited low stability and movement of the double emulsions over time was observed. The low stability was attributed to interaction of the charged specie ferroin and the phospholipids stabilizing the interface between the inner drop and the oil shell, an osmotic pressure gradient across the oil shell caused by the encapsulated BZ components and mechanical stress exerted on the double emulsions by fluctuations in the suspending phase. Whereas the first reason is difficult to circumvent, the latter two was addressed by adding sucrose to the suspending phase to equilibrate the inner and outer osmotic pressure of the double emulsions, and by increasing the viscosity of the suspending phase by elevating the concentration of the viscosity modulator PVA. Stable, for more than 1800s, and fixated oscillating double emulsions were obtained when suspended in a 10% w/w PVA/1.445M sucrose solution. These modifications seemed to have no significant impact on the oscillatory behaviour of the double emulsions. Further studies on the possibility of solvent removal from the oil shell under these conditions are to be conducted for the purpose of generating BZ encapsulating GUVs.

REFERENCES:

1. A. F. Taylor, *Progress in Reaction Kinetics and Mechanism*, 2002, **27**, 247-325.
2. V. Horvath, P. L. Gentili, V. K. Vanag and I. R. Epstein, *Angewandte Chemie International Edition*, 2012, **51**, 6878-6881.
3. A. F. Taylor, M. R. Tinsley, F. Wang, Z. Huang and K. Showalter, *Science*, 2009, **323**, 614-617.
4. M. Toiya, V. K. Vanag and I. R. Epstein, *Angewandte Chemie International Edition*, 2008, **47**, 7753-7755.
5. J. Delgado, N. Li, M. Leda, H. O. Gonzalez-Ochoa, S. Fraden and I. R. Epstein, *Soft Matter*, 2011, **7**, 3155-3167.
6. R. Tomasi, J.-M. Noel, A. Zenati, S. Ristori, F. Rossi, V. Cabuil, F. Kanoufi and A. Abou-Hassan, *Chem. Sci.*, 2014, **5**, 1854-1859.
7. I. R. Epstein, V. K. Vanag, A. C. Balazs, O. Kuksenok, P. Dayal and A. Bhattacharya, *Accounts of Chemical Research*, 2012, **45**, 2160-2168.
8. I. R. Epstein, *Science*, 2007, **315**, 775-776.
9. J. Holley, A. Adamatzky, L. Bull, B. De Lacy Costello and I. Jahan, *Nano Communication Networks*, 2011, **2**, 50-61.
10. G. Cevc, *Phospholipids Handbook*, 1994.
11. E. V. Skorb and H. Möhwald, *Advanced Materials*, 2013, **25**, 5029-5043.
12. A. S. Utada, E. Lorenceau, D. R. Link, P. D. Kaplan, H. A. Stone and D. A. Weitz, *Science*, 2005, **308**, 537-541.
13. Y.-C. Tan, K. Hettiarachchi, M. Siu, Y.-R. Pan and A. P. Lee, *J. Am. Chem. Soc.*, 2006, **128**, 5656-5658.
14. A. Seth, G. Béalle, E. Santanach-Carreras, A. Abou-Hassan and C. Ménager, *Advanced Materials*, 2012, **24**, 3544-3548.
15. H. C. Shum, D. Lee, I. Yoon, T. Kodger and D. A. Weitz, *Langmuir*, 2008, **24**, 7651-7653.
16. L. R. Arriaga, S. S. Datta, S.-H. Kim, E. Amstad, T. E. Kodger, F. Monroy and D. A. Weitz, *Small*, 2014, **10**, 950-956.
17. F. Kong, X. Zhang and M. Hai, *Langmuir*, 2014, **30**, 3905-3912.
18. K. Torbensen and A. Abou-Hassan, *Journal of Flow Chemistry*, 2015, **5**, 234-240.
19. K. Torbensen, F. Rossi, O. L. Pantani, S. Ristori and A. Abou-Hassan, *The Journal of Physical Chemistry B*, 2015, **119**, 10224-10230.
20. O. Steinbock and S. C. Müller, *J. Phys. Chem. A*, 1998, **102**, 6485-6490.

IV.4. Removal of the solvent from w/o/w double emulsions by evaporation/dewetting of the middle oil layer

The terms solvent evaporation and dewetting have been used to describe in literature the removal of excess solvent from the middle oil phase of w/o/w double emulsions, stabilized by amphiphiles such as phospholipids[1-4] or block copolymers,[5-7] resulting in the formation of giant unilammelar vesicles (GUVs), liposomes or polymersomes. In the general case of phospholipids, it was assumed that these amphiphilic molecules are arranged in monolayers at the two oil/water interfaces of the double emulsion, *via* self-assembly. The evaporation of the oil (a mixture of chloroform/cyclohexane or toluene) is reported to occur spontaneously. As solvent is removed from the middle layer, this eventually becomes so thin that the hydrophobic tails of the amphiphiles of the two monolayers, present at the interfaces, touch at one point. Van der Waals forces drive the monolayers together, like fastening a zipper, resulting in the formation of a double layer of phospholipids. The remaining oil then flows between the interfaces, by dewetting, into a localized pocket. Upon evaporation of the remaining oil, the liposome is then formed. These processes were reported to occur at room temperature in both open and closed containers.

Since the perspective of this thesis is to generate liposomes encapsulating the Belousov-Zhabotinsky reaction, a reliable protocol for liposome formation must be at hand. In the following, two approaches to obtain liposomes are reported. In a first attempt, since solvent removal did not occur spontaneously, double emulsions, with a middle oil layer constituted by a chloroform/cyclohexane (1:2) mixture, were heated in order to promote the solvent evaporation. In the second attempt, only chloroform was used as the oil phase. Since chloroform has a higher vapor pressure than cyclohexane, the evaporation process is expected to occur at a faster rate.

The double emulsions were generated using the microfluidic device developed in our group.[8] The inner and outer aqueous phases were 2% w/w PVA solutions, while the oil phase was a chloroform/cyclohexane (1:2) mixture containing 1% w/w of the phospholipid 1,2-Dimyristoyl-sn-glycero-3-phosphocholine (DMPC, gel/sol transition temperature of ~23°C), together with 0.02% w/w rhodamine B labelled DMPC as a fluorescent marker. The double emulsions were collected on a microscope slide, suspended in the outer fluid phase. The microscope slide was mounted with a silicon frame, serving as a reservoir. When the evaporation process was followed at room temperature, it took more than 24h to observe the evaporation of only 20% of the organic shell.[9] We

have thus decided to follow the effect of temperature on the evaporation process. The microscope slide was placed on a Peltier element, mounted on a microscope, as shown in Figure 1A. To avoid heat loss, or temperature gradients across the sample, Styrofoam sheets were placed on top of the Peltier element, the latter having a pre-set temperature of 25°C. Optical and fluorescent images of this initial stage were recorded, *vide infra*. Heating of the double emulsions were initiated immediately hereafter, using a heating ramp of 5°C min^{-1}, to a maximum temperature of 70°C, see Figure 1B.

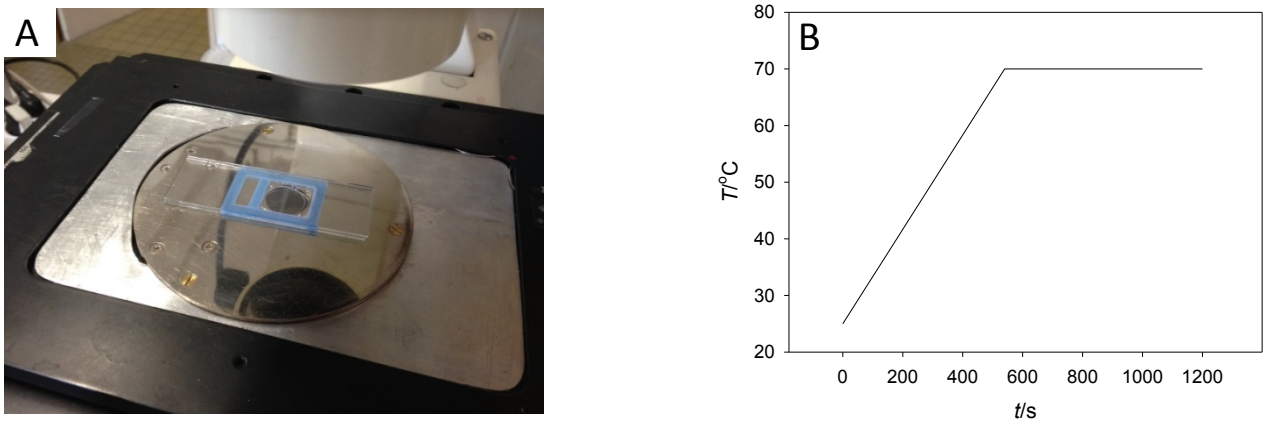

Figure 1. (A) The Peltier element mounted on the microscope. (B) The heating ramp employed.

The double emulsions were monitored optically during the heating process. A decrease in the oil shell thickness was observed after 5 min. of heating, *i.e.,* one minute, and this trend continued till a temperature of ~55°C, *i.e.,* after ~360s of heating, after which no visible changes in oil shell thickness was observed, see Figure 2. From profile plots taken across the oil shell, *i.e.,* along the white lines in Figure 2, the oil shell thickness could be deduced. Taking the full width at half maximum (FWHM) as a measure for the oil shell thickness (Figure 3), values of 16.4, 14.2, 12.1 and 10.0µm were obtained. The oil shell volume can be calculated as $V = (4/3)\pi(R_O^3 - R_I^3)$, where R_O and R_I are the outer and inner radius of the shell. The initial volume for a shell thickness of 16.4 µm and an outer radius of 142.5µm then becomes 3.72 x 10^{-6} cm^3. Similar, the shell volume after heating for 360s can be calculated to 2.38 x 10^{-6} cm^3. This correspond to a decrease in volume of 36%, only slightly more than the amount of chloroform initially present in the middle oil phase, indicating that the chloroform (boiling point of 61.2°C at 1atm) has evaporated completely from the oil shell.

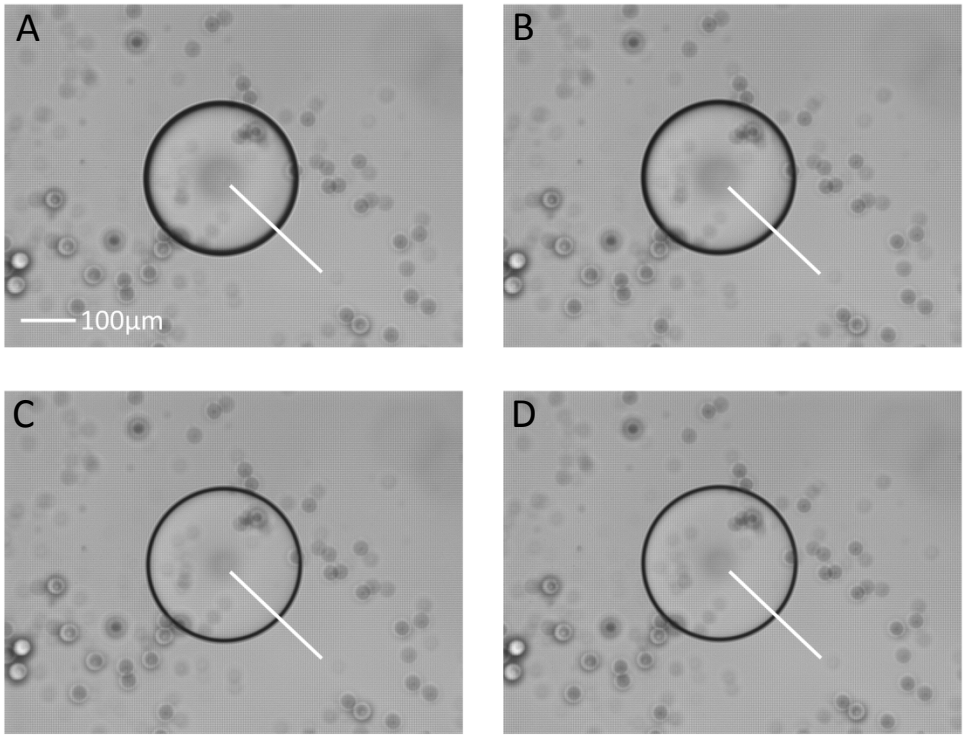

Figure 2. Optical images of the double emulsions recorded during heating. Heating times and temperatures: (A) 0s and 25°C (B) 120s and 35°C, (D) 240s and 45°C and (C) 360s and 55°C.

After 1049s, at the 70°C plateau (close to the boiling point of cyclohexane; 80.74°C at 1atm), an abrupt transformation of the double emulsion occurs, as shown in Figure 4, which may look very similar to the dewetting process described in ref.,[3] that results in the formation of an oil pocket. This structure remained stable for at least 120s, without any further transformation. An oil pocket formed by dewetting should be rich in phospholipids, since the concentration of the latter by far exceeds that necessary for the formation of a lipid bilayer. Hence, since rhodamin B labelled lipids are present in the oil phase, high fluorescence intensity should be observed here. That this is not the case can be seen from the fluorescence images presented in Figure 5. Optical and fluorescence images of the double emulsions before and after heating are shown in Figure 5A and B, respectively, showing a thinner oil shell, but no local accumulation of lipids. This is made even more clear in Figure 5C, which displays the profiles taken across the fluorescence images in A and B. Figure 5C also shows a slight difference in the drop size, from R_O = 142.5µm to R_O = 146.7µm, due to thermal expansion. However, this increase is 5-6 times higher than that calculated for a 2% w/w PVA solution, having a measured thermal volumetric expansion coefficient of 2.53 x $10^{-3}K^{-1}$.

It should here be noted, that the interpretation of the graphs is not straight forward, as the fluorescence intensity is temperature dependent due to a decrease in the rotational correlation time at elevated temperatures.

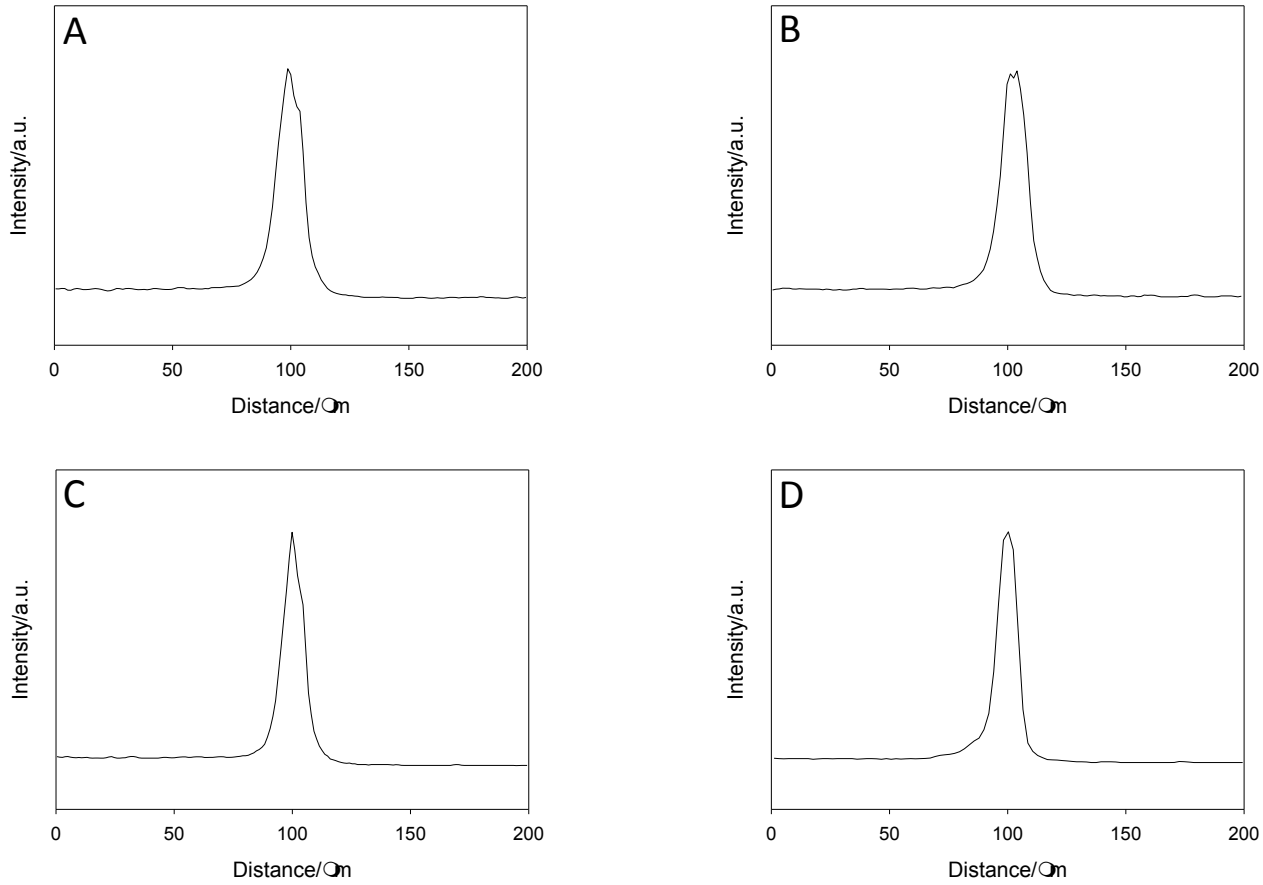

Figure 3. Profile plots taken along the white lines in Figure 2, across the oil shells of the double emulsions. Heating times and temperatures: (A) 0s and 25°C (B) 120s and 35°C, (D) 240s and 45°C and (C) 360s and 55°C.

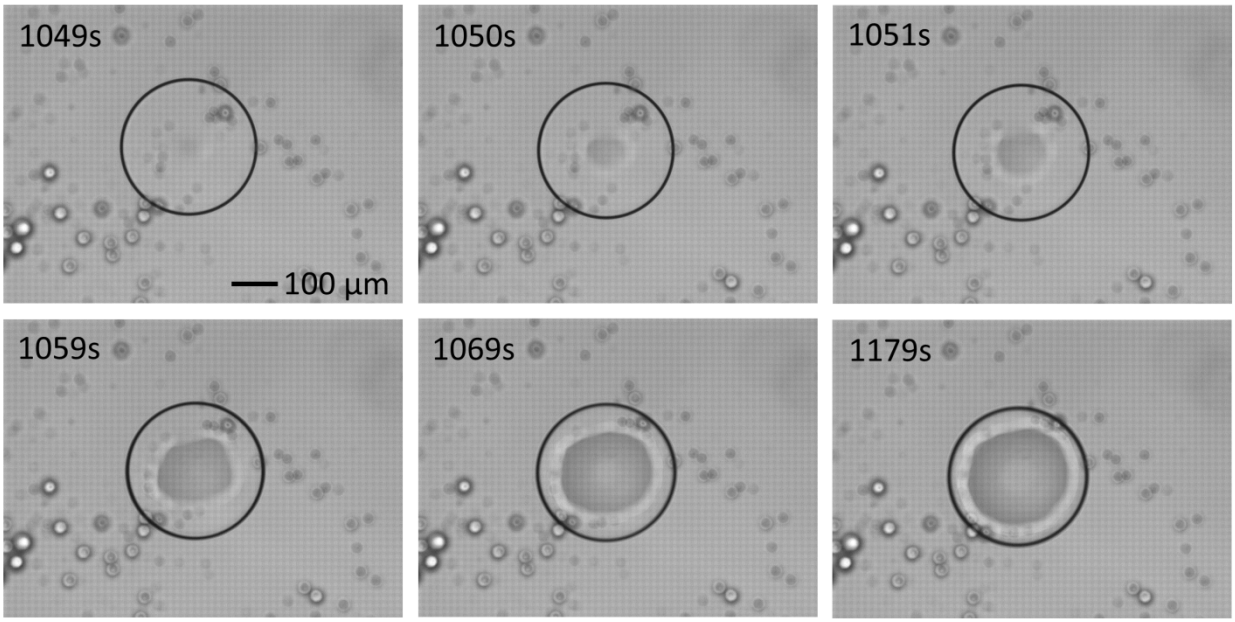

Figure 4. Image sequence displaying the shell transformation occurring at the 70°C plateau after 1049s to 1179s.

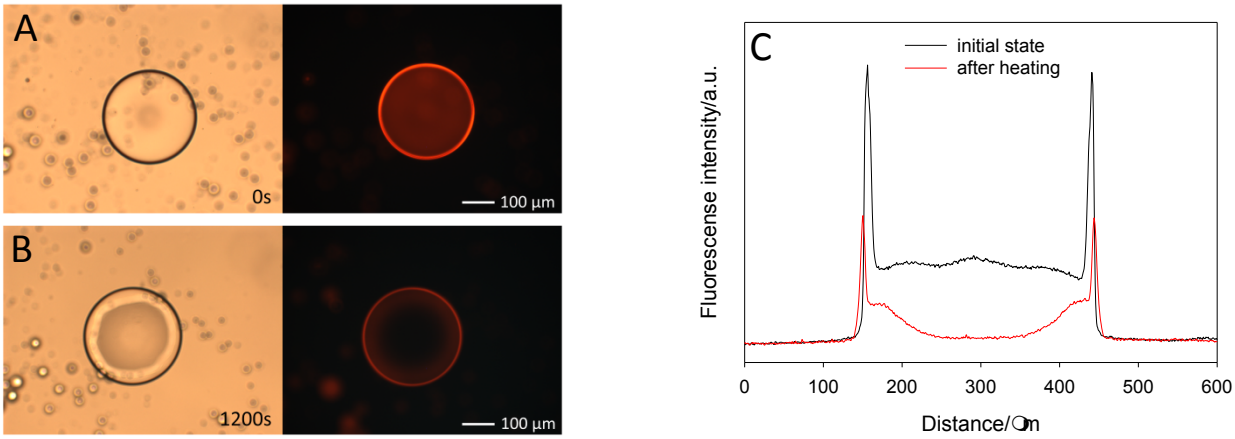

Figure 5. (A and B) Optical and fluorescens images showing a double emulsion at (A) 25°C and after heating to 70°C. (C) Profile plots, displaying the fluorescence intensity across the double emulsion, at (black line) 25°C and at (red line) 70°C.

Although it might be possible to remove chloroform by heating, with this method it seems very difficult to eliminate cyclohexane. Moreover, heating a double emulsion encapsulating a BZ

reaction might have an influence on the BZ-composition, *e.g.,* degradation of malonic acid in the presence of Fe^{2+},[10] in a way that will affect the oscillatory behavior. Thus we have decided, in a in a second attempt to obtain liposomes by solvent removal, by using only chloroform/DMPC as the oil phase. With this setup, as described elsewhere in this thesis, tip streaming from the double emulsions occur under flow. This generates daughter double emulsions, thus removing solvent from the oil shell of the mother double emulsion. The remaining structure of the mother double emulsions was investigated at room temperature by optical and fluorescence microscopy. As in the previous experiment, the double emulsions were collected on a microscope slide. After ~30s of observation, the oil shell changes its shape gradually into what appears as a ring formed structure surrounding the core drop, as shown in Figure 6. This image sequence is similar to the dewetting process described by Duncanson *et at*.[11] A slight difference though, is that in our experiment, the detachment of the oil drop vas not visible. In our case, the oil drop appears to sink below the core drop. This seems reasonable, as chloroform has a higher density ($1.49 g/cm^{-3}$) compared to the suspending aqueous phase. If the dewetting initiates from the top of the double emulsion, and proceeds downwards, a temporary ring shaped structure would show, as observed. Images of the as formed structure are shown in Figure 7. One striking observation from Figure 7A and B is the non-spherical shape of the structure. Whereas the spherical shape of a double emulsion is a result of interfacial tension, liposome bilayers, without any middle oil phase, are less rigid. However, from the observed non-uniformity of the surfaces, this points to a thicker lipid aggregation, rather than a lipid bilayer. Addition of the fluorescent labelled DMPC to the oil phase, and encapsulating fluorescein in the core drop, allowed for recording fluorescence images of the structure after dewetting. Figure 8A and B shows the rhodamin B labelled DMPC in the oil shell, and the fluorescein in the core drop, confirming that the structure still remains a core-shell structure. The structures remained stable for at least 2h.

The results obtained here shows promising for obtaining stable liposomes upon solvent removal of w/o/w double emulsions. In the first attempt however, no evidence on having obtained liposomes was observed. Furthermore, problems with thermal expansion and heat induced perturbations of the lipid self-assembly at the interfaces might arise. In the second attempt, having only chloroform in the oil phase, solvent removal seemed more feasible. Non-spherical shell-core structures with aggregated matter in the shell were obtained. By decreasing the amount of phospholipids in the oil phase, less aggregation should occur. For further studies of these structures, small angle x-ray scattering (SAXS) and Raman spectroscopy could prove valuable.

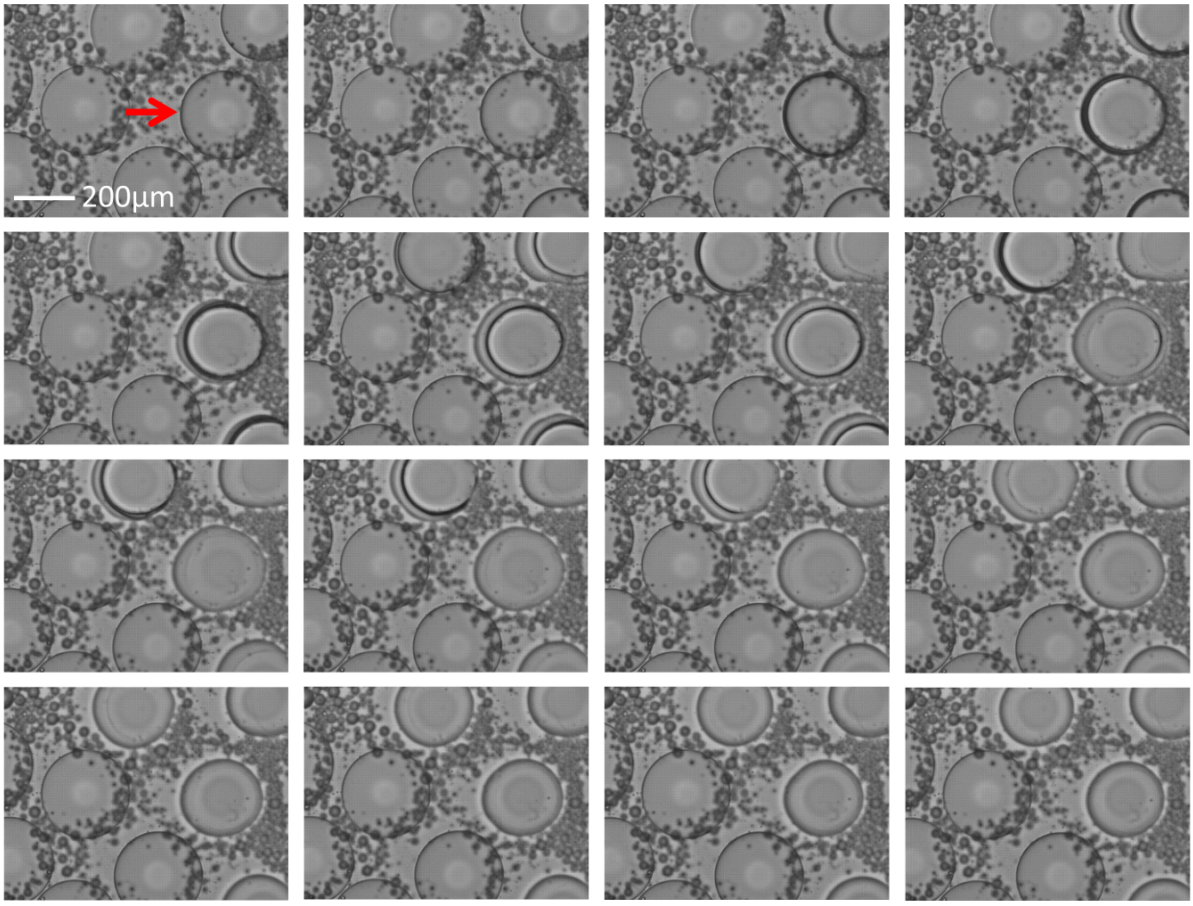

Figure 6. Image sequence showing the removal of the oil phase from the double emulsion indicated by the red arrow. Images were recorded with intervals of 0.5s, from upper left corner to the lower right corner.

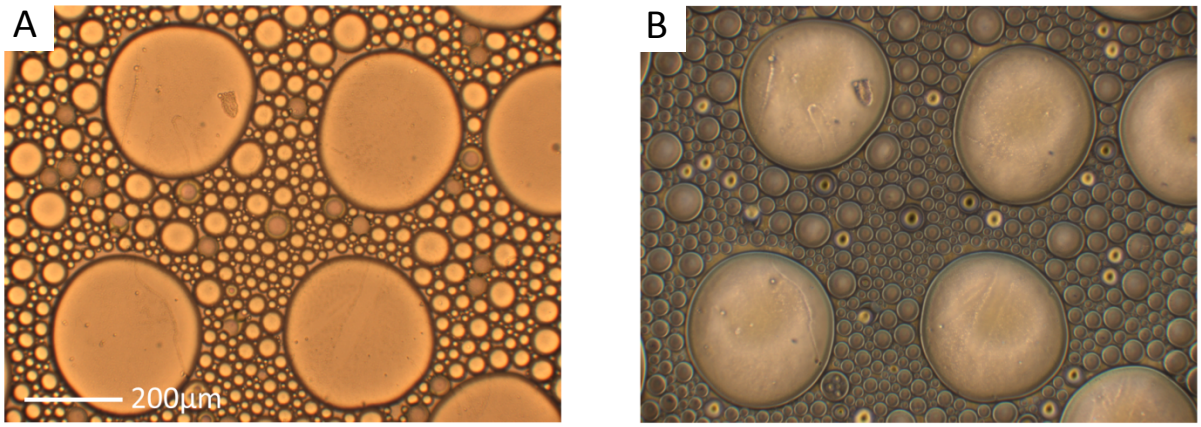

Figure 7. Optical images of the structures formed upon solvent removal, and suspended in the outer 2% w/w PVA phase. (A) Image recorded without bypass filter. (B) image recorded with bypass filter.

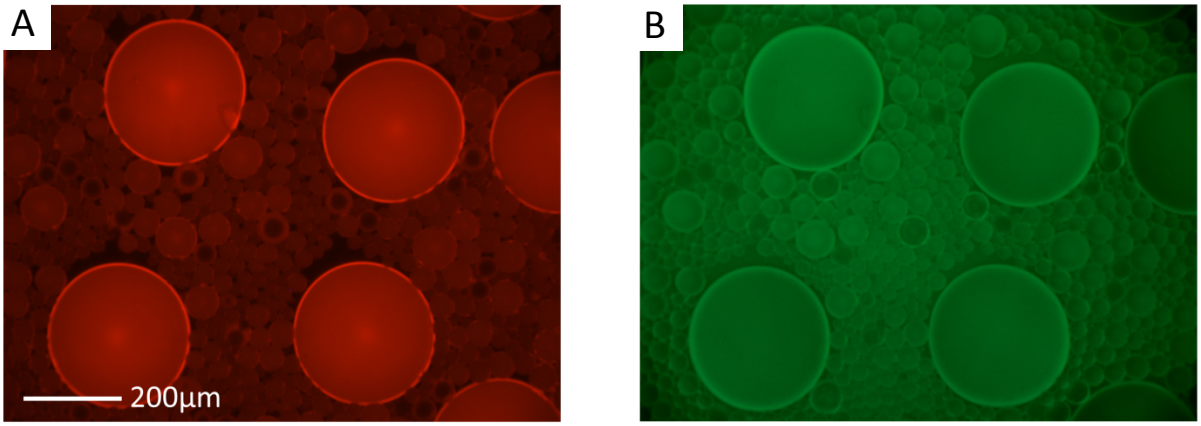

Figure 8. Fluorescens images of the structures formed upon solvent removal, and suspended in the outer 2% w/w PVA phase. (A) Image showing the rhodamin B labeled phospholipids, appearing red, in the shell structure (B) Image showing the fluorescein, appearing green, encapsulated in the core drop.

REFERENCES:

1. L. R. Arriaga, S. S. Datta, S.-H. Kim, E. Amstad, T. E. Kodger, F. Monroy and D. A. Weitz, *Small*, 2014, **10**, 950-956.
2. F. Kong, X. Zhang and M. Hai, *Langmuir*, 2014, **30**, 3905-3912.
3. H. C. Shum, D. Lee, I. Yoon, T. Kodger and D. A. Weitz, *Langmuir*, 2008, **24**, 7651-7653.
4. H. C. Shum, E. Santanach-Carreras, J.-W. Kim, A. Ehrlicher, J. Bibette and D. A. Weitz, *J. Am. Chem. Soc.*, 2011, **133**, 4420-4426.
5. R. C. Hayward, A. S. Utada, N. Dan and D. A. Weitz, *Langmuir*, 2006, **22**, 4457-4461.
6. H. C. Shum, J.-W. Kim and D. A. Weitz, *J. Am. Chem. Soc.*, 2008, **130**, 9543-9549.
7. T. Foster, K. D. Dorfman and H. Ted Davis, *J. Colloid Interface Sci.*, 2010, **351**, 140-150.
8. K. Torbensen and A. Abou-Hassan, *Journal of Flow Chemistry*, 2015, **5**, 234-240.
9. A. Seth, G. Béalle, E. Santanach-Carreras, A. Abou-Hassan and C. Ménager, *Advanced Materials*, 2012, **24**, 3544-3548.
10. F. J. Caires, D. J. C. Gomes, A. C. Gigante, L. S. Lima, C. T. Carvalho and M. Ionashiro, *Braz. J. Therm. Anal.*, 2013, **2**, 12-16.
11. W. J. Duncanson, T. Lin, A. R. Abate, S. Seiffert, R. K. Shah and D. A. Weitz, *Lab on a Chip*, 2012, **12**, 2135-2145.

Chapter V: Tip-streaming of double emulsions under flow: A novel approach for templating liposomes**?**

V.2. Introduction

This chapter reports on a peculiarity observed on generating double emulsions with chloroform as the only liquid constituent of the oil phase. After being formed, the double emulsions started deforming under flow, which eventually resulted in the formation of a tube extruding from the rear or the double emulsion. Pinching, or tip-streaming, of the tube generated daughter double emulsions with similar core-shell properties as the mother double emulsion. By removal of solvent from the originally formed double emulsions, is suggested that this process might be a new approach for templating liposomes.

V.2. Deformation and Tip-streaming of Water/Oil/Water Double Emulsions Induced by Interfacial Shearing in a Microfluidic Device

Kristian Torbensen[a] *and Ali Abou-Hassan*[a]*

[a]Sorbonne Universités, UPMC Univ Paris 06, UMR 8234, Laboratoire Physico-chimie des Electrolytes, Nanosystèmes InterfaciauX (PHENIX), 4 place Jussieu - case 51, 75252 Paris cedex 05 – France

ABSTRACT:

Herein we study the behavior of w/o/w (water/oil/water) double emulsions (DE) generated in a microfluidic device, formulated using 1,2-dimyristoyl-sn-glycero-3-phosphocholine (DMPC) as phospholipid and chloroform as the oil phase, in an attempt to template giant liposomes. We show, that for such a composition of the oil phase, a rich dynamic behavior of the DEs is observed under flow, giving rise to different rich phenomena such as deformation and tip-streaming. To the best of our knowledge, this has never reported previously for DEs. When the DEs were generated using the same composition and viscosity in the core as well in the outer continuous flowing phase, the concentration of DMPC showed to have significant impact on the nature and degree of deformation of the middle phase. While the shape of the core remained practically unperturbed under these conditions, increasing the viscosity of the continuous phase resulted in the DEs adapting a pear-like shape. Due to the interfacial shearing, tubes were gradually extruded at the rear of the DEs. These eventually reached a *Rayleigh-Plateau* instability condition, resulting in pinch off, or tip-streaming, at the tube extremity, by which smaller (daughter) DE were formed. The deformation and tip-streaming were monitored by optical fluorescence microscopy; the latter enabled by incorporating rhodamine B labelled phospholipids in the middle phase, and encapsulating fluorescein in the core drop, which showed that the daughter droplets generated by tip-streaming from the mother DE are also w/o/w DE. Tip-streaming may open new possibilities related to the release of encapsulated substances from a cargo under flow. As a proof of concept we show the generation of magnetic daughter DEs with different sizes (5-32 um) from a magnetic mother DE under flow.

INTRODUCTION:

Over the past decades, the field of droplet microfluidics has witnessed a very rapid evolution. In particular, due to many achievements in soft lithography[1] and in engineering of simple and versatile devices built for example from simple capillaries such as coaxially aligned capillary tubes.[2] With high control over flow rates and both channel geometry and dimensions, monodisperse multi-compartment droplet, *e.g.,* water-in-oil-in-water (w/o/w) DEs with single or multiple cores can be generated with high frequency. Such emulsions have broad potential in several applications as drug delivery systems,[3-5] modelling of bioreactors,[6, 7] in food industry[8] and cosmetics.[9] Understanding the dynamics of such emulsions under flow in microchannels are thus important for the further development and optimization of microfluidic devices.

Several studies on the deformation, breakup and/or tip-streaming of single emulsions in flow systems have been reported,[10-22] but less on multiple emulsions and compound droplets. Whereas the hydrodynamics of single emulsions can be described by the interfacial tension and the viscosity ratio between the droplet and the continuous flowing supporting matrix, the flow dynamics of multiple emulsions are complicated by the additional interfaces that arise, when core droplets are encapsulated by liquid shell films. In general, under static conditions, the geometrical configuration of both single and higher ordered compartment emulsions are concentric due to surface energy considerations. However, when subject to stress, such as under shear flow conditions in microfluidic channels, deformation of both the core droplet and the shell might occur, either independently or simultaneously. Three different conformations of compound droplets have been described by Johnson *et al*:[23] Complete engulfing of the core droplet in the shell, where only the two interfaces between the core and the shell, and the shell and the matrix solution exist. Partial engulfing, where the shell is partly detached from the core (Janus droplets), and interfaces between all three phases exist, and finally a non-engulfing configuration where the core and shell completely detaches to form individual droplets. The adapted conformation of the compound emulsion is governed by the interfacial tensions between the three liquid phases, and the nature of the stress induced by the external conditions, such as flow velocity and channel geometry. This approach was applied by Guzowski *et al*.[24] in order to investigate the structure and stability of multiple microdroplets.

The dynamics of DEs under shear flow has been investigated numerically by Hua *et al*.[25] and both numerically and experimentally by Chen *et al*.[26, 27] in a Couette geometry, *i.e.,* DEs suspended in a liquid matrix between two parallel solid boundaries moving in opposite directions. The deformation of the outer droplet (*i.e.,* the middle phase) was shown to be governed by competition between viscous shear stress and interfacial tensions, together with the ratio between the core and outer droplet radii. The deformation of the core was demonstrated to be mainly induced by a vorticity flow within the outer droplet, generated by the shear stress between the middle phase and the supporting matrix. It was furthermore demonstrated,[26] that at critical capillary numbers, a transformation from a steady shape to a transient deformation eventually resulted in breakup of the outer droplet. Shaohua *et al*.[28] investigated the core deformation of w/o/w DEs under sheath flow focusing. They emphasized the significance of core and shell viscosity on core deformation, whereas the type of surfactant present at the interfaces apparently was of minor importance. Chunfeng *et al*. and Tao *et al*.[29] studied numerically the flow dynamics of compound drops in contracting tubes. Similarly, Chen *et al*.[30] investigated the deformation and breakup mechanism of DEs in a tapered nozzle.

Microfluidics is largely used for the formation of w/o/w DEs, which are the templates of other materials such as giant phospholipid vesicles, polymersomes, capsules, etc.[2, 31-37] The oil phase is usually composed of a mixture of two or more organic solvents, with chloroform as one of the frequent components. This due to its excellent ability of solvating alkane tailed amphipliles including phospholipids, widely employed as stabilizing surfactants, or polymers with the purpose of engineering polymersomes. However, due to its high density, the chloroform is mixed with lower density solvents such as tetrahydrofuran, toluene or cyclohexane, in order to match the density of the supporting matrix, thus preventing sedimentation of the DEs.[2, 33, 35, 38-41] Reports on formulating w/o/w DEs as templates of other materials are numerous in microfluidics, including our previous report (using a 1:2 (v:v) mixture of chloroform/cyclohexane) on the formulation of giant liposomes.[42] However to the best of our knowledge, none of these reports observed the deformation or tip-streaming of w/o/w DEs. Herein, we show that by employing 1,2-dimyristoyl-sn-glycero-3-phosphocholine (DMPC) as the phospholipid with pure chloroform as the oil phase, a different dynamic behavior of the DEs under flow was be observed, giving rise to different phenomena such as deformation and tip-streaming of w/o/w DEs.

EXPERIMENTAL SECTION:

The DEs were generated using a microfluidic flow focusing device,[42] consisting of coaxially aligned glass capillary tubes assembled using commercial available fittings, *i.e.,* T-crosses and ferules. The absence of any glued sealing enables not only a fast assembly procedure, but also provides the opportunity of fast replacement of clogged or damaged capillary tubes. The microfluidic device consists of coaxially aligned glass tubes of various dimensions and geometry. First, polyimide coated 365/75 μm (outer diameter [OD]/inner diameter [ID]) glass capillary tubes (Polymicro) are inserted into a cylindrical 1/0.5 mm (OD/ID) borosilicate tube (Drummond Scientific). The borosilicate tube was narrowed in one end for enhanced flow focusing by exposing the tube orifice to a butane flame while rotating the tube. The inner wall and the orifice of this tube were rendered hydrophobic using 2% (v/v) trichloro(1H,1H,2H,2H-perfluorooctyl) silane (Sigma-Aldrich) in toluene, rinsed with toluene and dried overnight at 70 °C to obtain the desired wetting properties. These tubes are in turn inserted into a square borosilicate tube 1.25 × 1 mm (outer/inner side length, Vitrocom). A second cylindrical borosilicate tube, likewise flame treated and serving as the DE collector tube, was inserted from the opposite end of the square tube, and the two cylindrical tubes were positioned with the narrowed orifices within close distance, followed by positioning of the two inner most fused capillary tubes close to the orifice of the left cylindrical tube. All glass tubes were assembled using T-crosses (P-727, Upchurch Scientific), ferrules (F-331, Upchurch Scientific), and pieces of 1/3 mm (OD/ID) silicon tubing (Tygon Versilic Silicon Tubing, Sigma-Aldrich), and mounted on a Plexiglas stand. A more thorough description of this microfluidic device has been published elsewhere.[42] Chloroform, polyvinyl alcohol (PVA, Mw 18 kDa), and fluorescein were supplied by Sigma-Aldrich. DMPC was supplied by Lipoids, Inc. L-α-Phosphatidylethanolamine-N-(lissamine rhodamine B sulfonyl) (Ammonium Salt) was supplied by Avanti Polar Lipids. All chemicals were used as received. A Zeiss Axiovert 200 microscope mounted with a NeoFluar objective (2.5x magnification and field depth of 62.4 μm) and a Dasla CCD camera, was employed for monitoring the DEs. For monitoring the fluorescent probes, a FluoArc laser was connected to the microscope, and the appropriate wavelengths selected with optical band pass filters (532 nm for rhodamine B and 445 nm for fluorescein). The optical images were recorded with 300 frames/s and an exposure time of 3000 μs. Fluorescence images were

recorded with 100 frames /s and an exposure time of 9000 μs. The freely available software ImageJ was used for image processing. A interfacial tensiometer (DSA100, Krüss GMBH), mounted with a 0.516 or a 1.837 mm needle, was used for measuring the interfacial tension between oil and aqueous phases, empolying the pendant drop method with the oil phase suspended in the aqueous phase. Viscosities of the PVA solutions were measured using an Anthon Paar Automated Micro Viscometer, employing the rolling ball method, using a 1.6 mm for the 2% PVA solution, and a 1.8 mm capillary tube for 5-10% solutions. Rolling time was 10s. The measured viscosity values were found to be 1.63, 3.62, 6.97 and 12.94 mPas for 2, 5, 7.5 and 10% PVA, respectively. The magnetic nanoparticles are citrated maghemite nanoparticles (iron concentration =1.07M) suspended in water, synthesized according to Massart's protocol.[43] For the encapsulation studies, magnetic nanoparticles were diluted in a 2% (w/w) PVA solution to a final iron concentration of 0.107M

RESULTS AND DISCUSSION:

The DEs investigated here were generated using flow-focusing microfluidics. Figure 1 shows a schematic illustration of the microfluidic device, displaying the concept of the one-step encapsulation process: The setup allows injection of fluids into the innermost capillary tube, the left most cylindrical tube and from both ends of the square tube. Additionally, the separation distance between the cylindrical tubes, *d*, and thus the geometry of the flow-focusing part, can be varied. This feature enables high control over the size ratio between the core and the oil film thickness.[42] The DE formation occurs *via* dripping,[44, 45] as the simple emulsion (as Q_1 flows into Q_2) reaches the *Rayleigh-Plateau* instability upon encountering the outer phase Q_3 in the gap between the two inner tubes. This is facilitated by modulating the viscosity of the aqueous phases with PVA: In fact, we found that for concentrations of PVA below 1% (w/w), the DE formation occurs only for specific ratios of the flow rates, whereas for concentrations above 2% (w/w), a wide range of flow rate combinations can be employed, thus expanding the window of the overall size distribution of the DEs. Figure 2 shows optical and fluorescence images of the w/o/w DE formation process, by which a fluorescein containing core droplet is engulfed in the phospholipid containing oil film. Figure 2A show an optical image of the flow focusing part of the microfluidic device. In the center left, the inner aqueous phase forms a coaxial flow with the middle phase, which flows around the inner phase. At the hydrophobic outer part of the left capillary tube, the oil phase forms a meniscus,

which is being gradually filled with the inner phase. As this drop-in-a-drop reaches the approximate size of the right capillary orifice, it is eventually pinched off by the outer viscous phase, thereby generating the DE. Since the fluorescent probes employed here are only soluble in either the oil or the aqueous phase, they are excellent markers for outlining the different phases.

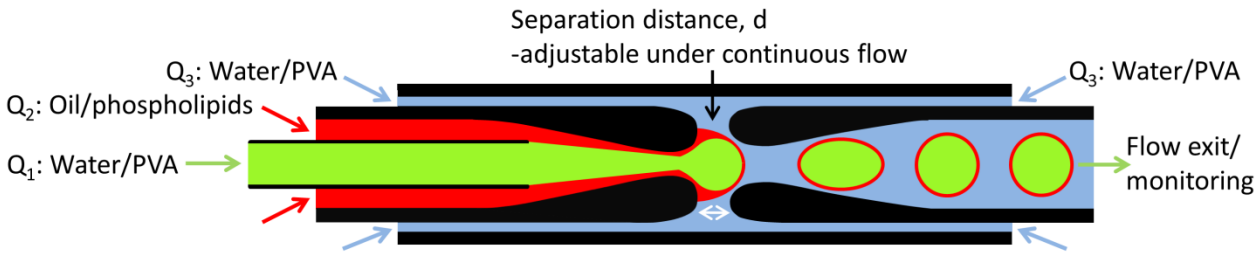

Figure 1. Schematic illustration of the microfluidic device for generating w/o/w double emulsions. A simple emulsion (w/o middle phase, green) of an aqueous phase (volumetric flow rate Q_1) is being formed in the oil containing phospholipids (red, volumetric flow rate Q_2) in the left inner capillary tube just prior to the encapsulation. Breakup and emulsification of the w/o middle phase is effectuated upon encountering the outer aqueous phase, flowing in from the corners of the outer square tube with total volumetric flow rate of Q_3, forming monodisperse w/o/w double emulsion drops (green core in red circles) in the right capillary tube. The white arrow indicates the geometric adjustability of the device.

Figure 2B illustrates this by displaying a superimposition of images recorded individually for the two fluorescent probes. The oil phase containing the rhodamine B labelled phospholipid is clearly seen as red colored areas, while the fluorescein containing inner phase appears green.

The as formed DEs were monitored optically in the cylindrical capillary tube down-stream the flow focusing part of the microfluidic device. The geometrical constrictions of the microfluidic device only allowed monitoring the DEs over a flow distance of 22 mm. However, this geometric window was sufficient to provide a significant evidence of the impact on droplet deformation exerted by various concentrations of DMPC present in the oil phase. Figure 3 shows DE droplets monitored at various positions down-stream the point of formation. For each image series of Figure 3A - D, the number annotation corresponds to identical points at the tube. Thus, by keeping the flow parameters unchanged between each series, images with same numbers thus display the DEs after being exposed to identical length (and time) of flow. The topological changes of the DEs within each series can then be directly compared with respect to the different concentrations of DMPC. In Figure 3A - D, the DMPC concentration was increased from 0 over 0.1 and 0.5 to 1% w/w, respectively. In the following, the small amount, *i.e.,* 0.02% w/w, of the fluorescent probe present in all cases, was considered to have no significant impact on the interfacial properties of the DEs. It is

furthermore assumed, that the continuous flow profile adapts a parabolic shape, as outlined in Figure 4A. As the DEs travels the capillary tube with a velocity higher than the continuous phase, the resulting shearing exerted by the latter will take the shape of an inverted parabola with respect to the flow velocity profile.

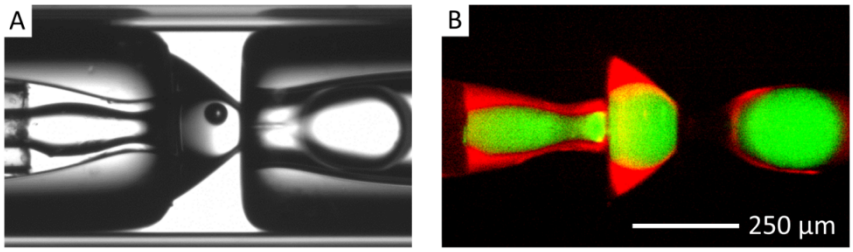

Figure 2. (A) Optical image showing the formation of w/o/w double emulsions. (B) Same formation recorded with a fluorescence microscope showing the inner aqueous phase with 0.02% (w/w) fluorescein (green), surrounded by the chloroform/1% (w/w) DMPC/0.02% (w/w) rhodamin B labelled phospholipid (red) oil phase.

Thus, the viscous forces acting on the DE will be largest at the perimeter closest to the tube walls. Starting with Figure 3A, *i.e.,* the case of no DMPC present in the oil phase, only minor changes in the drop topology are observed. Since no surfactant is present at the interphases, the interfacial tension tends to overcome the viscous forces exerted by the continuous phase; hence the DE remains fairly spherical. As the concentration of DMPC is increased, the interfacial surface tension decreases, and viscous forces become more dominant. Figure 3B, representing the case of 0.1% DMPC present in the oil phase, clearly display the deformation of the middle drop, as the DE travels down-stream the capillary tube. This trend becomes even more pronounced, as the concentration of DMPC is increased further throughout Figure 3C and 3D. Here, the outer drop of the DE not only deforms more rapidly, but eventually forms a thin tube at the rear of the DE. In Figure 3C-5 and 3D-5, capillary instabilities results in breakup of this tube, resulting in the formation of small drops of chloroform suspended in the continuous phase.

To quantify the extent of deformation, approximated as the transformation of a sphere to an ellipsoid, we adapt the dimensionless index D,[46] defined as in equation 1:

$$D = \frac{B-L}{B+L} \qquad \text{Eq. 1}$$

where B and L are the axial and transverse dimensions of the middle droplet, respectively, as outlined in Figure 4A.

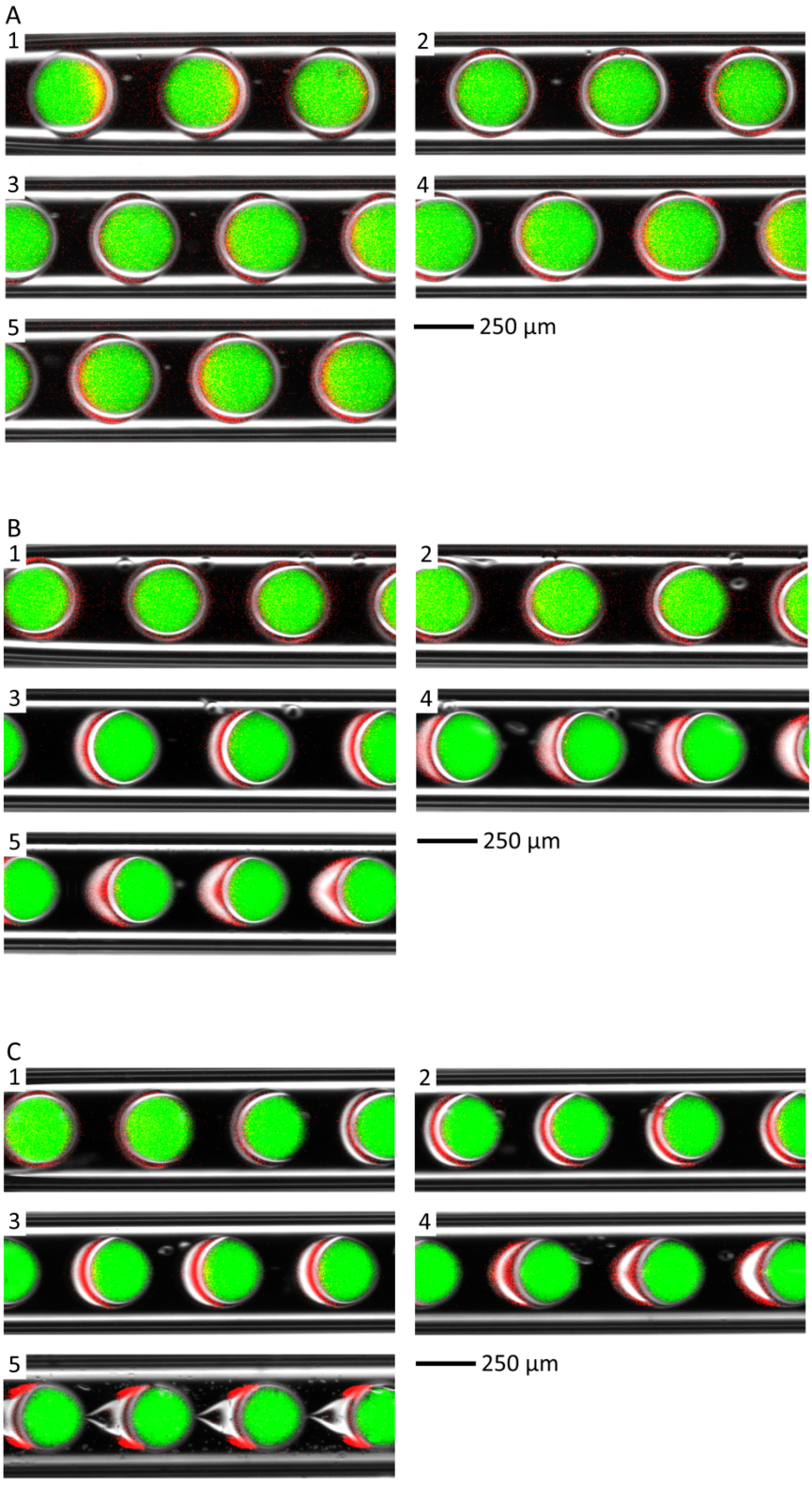

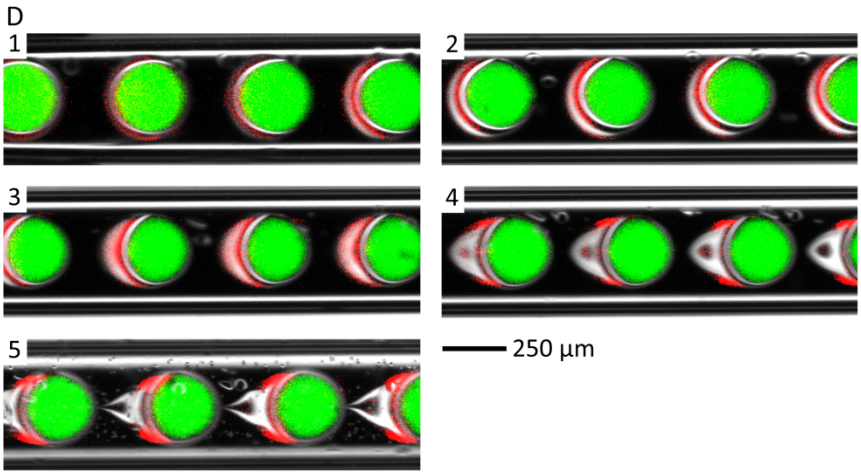

Figure 3. Superimposed optical and fluorescence images recorded along the exit tube of the microfluidic device, at distances of (1) 0.2 mm, (2) 5.5 mm, (3) 11 mm, (4) 16.5 mm and (5) 22 mm from the flow focusing part (*i.e.,* the point of formation, and corresponding to flow times of 0.026, 0.724, 1.447, 2.171 and 2.985s, respectively). The images show the deformation of the double emulsions along the tube, induced by the interfacial shearing between the continuously flowing outer aqueous phase, and the oil shell of the double emulsion. The concentrations of DMPC in the oil phase are 0, 0.1, 0.5 and 1% (w/w) in (A), (B), (C) and (D), respectively. Inner diameter of the tube is 500µm. Flow rates applied: Q_1 (H_2O/2% w/w PVA and 0.02% w/w fluorescein) = 4.17 x 10^{-4} cm^3s^{-1}, Q_2 (chloroform/various concentrations of DMPC and 0.02% w/w rhodamin B labelled phospholipids) = 1.67 x 10^{-4} cm^3s^{-1} and Q_3 (H_2O/2% w/w PVA) = 4.17 x 10^{-4} cm^3s^{-1} (that is, an average velocity of the continuous flowing phase of 0.21 cms^{-1}). Velocity of double emulsions = 0.76 cms^{-1}.

From the images of Figure 3, values for B and L were determined, and a linear relationship between D and the distance travelled by the DEs was observed for all the applied concentrations of surfactant, see Figure 5A. Within the geometric frame monitored, this means that for each concentration of surfactant, a gradual deformation occurs. However, for the highest concentrations of surfactant, and thus for the lowest values of interfacial tension, the viscous forces eventually governs the dynamics of the middle droplet in such a way as to invert the convex curvature of the ellipsoid, turning the shape into that of a hanging drop. Taking the slope of each line as an expression for the impact of the surfactant concentration on the extent of deformation, it appears that a saturation concentration of the surfactant exists. In Figure 5B, a plot of the slope *vs*. the

surfactant concentration reaches a plateau at [DMPC] ~0.5% (w/w), above which viscous forces are dominant. This is in line with the measured interfacial tension for the water/PVA-chloroform/DMPC system, in which the interfacial tension only decreases slightly for DMPC concentrations above 0.5%, as shown in Figure 6A.

Similar considerations regarding the capillary number of the system can be made. The capillary number, defined as $Ca = \mu v/\gamma$, where μ is the dynamic viscosity, v the flow velocity and γ the interfacial tension, expresses the relative effect between viscous forces and interfacial tension, and is thus directly related to the surfactant concentration. Figure 6B displays the effect of the surfactant concentration on the capillary number; above ~0.5% w/w DMPC present in the oil phase, the capillary number reaches a maximum value of ~0.03, at which viscous forces dominates the dynamic behaviour of the DEs in shear flow.

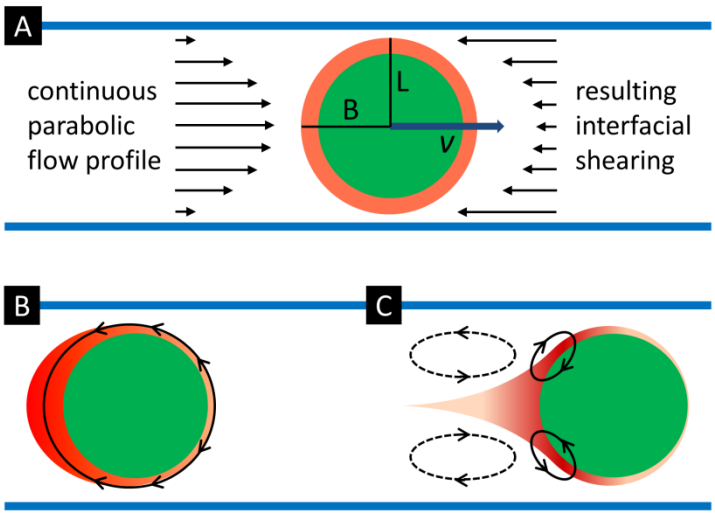

Figure 4. Sketch illustrating the deformation of the middle drop, and the transport of surfactant herein. (A) B and L are the axial and transverse dimensions, respectively, of the double emulsion moving in the capillary tube with velocity v. As v is larger than the mean velocity of the continuous phase, the double emulsion moves with a positive net velocity through the continuous phase, the latter exerting a shearing stress on the double emulsion in the opposite direction of v. (B) Intermediate drop deformation, illustrating the rearrangement of the oil phase, and accumulation of surfactant, at the rear of the double emulsion. (C) Drop shape deformation of the oil phase caused by a vortex flow (dashed elliptic arrows) in the continuous phase emerging at the rear of the double emulsion. Solid elliptic arrows illustrate the vortices within the middle phase, causing a local accumulation of surfactants.

A closer inspection of the fluorescent signal stemming from the rhodamine B labelled phospholipid present in the oil phase, as displayed in Figure 3, provides a more detailed insight on the surfactant distribution in the outer droplet of the DEs. Figure 7 shows the fluorescence intensity

profiles in the flow direction across individual DEs, recorded at various distances as presented in Figure 3A-1-5, and thus flow times, from the point of formation. Figure 7A represents the profiles in the case of no surfactant present in the oil phase, *i.e.,* [DMPC] = 0% (w/w). Initially, *i.e.,* 0.026s after formation, the main part of the oil is situated at the front of the DE.

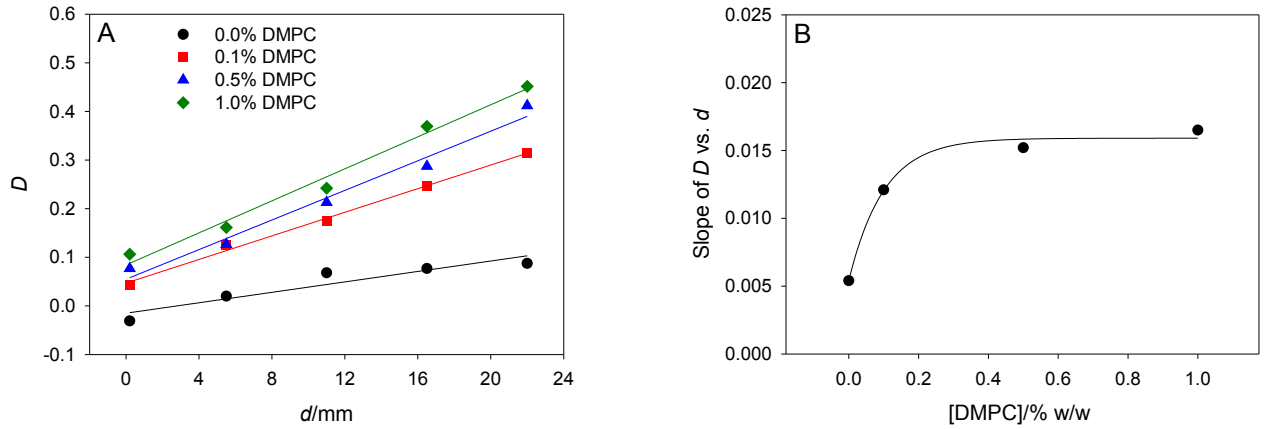

Figure 5. (A) Plot of the deformation parameter D, as defined in eq. 1, vs. the distance travelled by the double emulsion, showing a linear relationship. (B) Extent of deformation, expressed as the slope of the lines in (A), *vs*. the surfactant concentration. A saturation point is reached around 0.5% w/w DMPC, above which viscous forces are dominant. The solid line is added as a guide to the eye.

This is due to the geometry of the capillary tube, which expands over a short distance from its narrow orifice. In this case, where surface tensions are high, the surface energy of the outer droplet is then minimized by the higher curvature at the front of the DE. The gradual displacement from front to rear of the oil phase engulfing the core droplet, as it travels down-stream the tube, is clearly

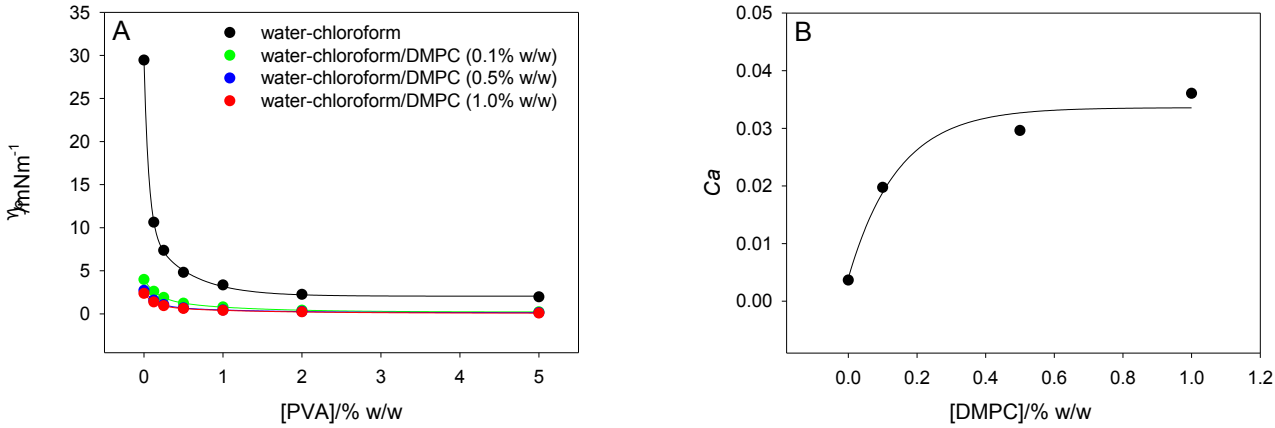

Figure 6. (A) Plot showing the interfacial tension, γ, of the water/chloroform system for various concentrations of PVA and DMPC. (B) Capillary number as a function of surfactant concentration. For capillary numbers above ~0.03, viscous forces dominate over interfacial effects. The solid line is added as a guide to the eye.

displayed as the fluorescence profiles shifts its position with respect to the core center at x = 0 µm. Due to the high surface tension, the DE appears to reach a steady-state topology, where viscous shearing forces are balanced by interfacial effects. Figure 7B shows the case where [DMPC] = 0.1% (w/w). The effect of the surfactant is here clearly displayed, as the deformation of the outer droplet occurs more rapidly due to the decreased surface tension. Also, the displacement of the oil phase extends in this case further away from the core center, as the width of the oil phase continues to increase. This can be explained by an increased drag exerted on the DE; due to a surfactant build up at the rear, and thus a local decrease in surface tension, a *Marangoni* force[47] acts in a direction opposing the flow, *i.e.,* from regions of low to high surface tension, and thus increases the drag acting on the DE. This phenomenon is, as expected, even more pronounced for higher surfactant concentrations, as displayed in Figure 3C and 3D. In fact, the drag here becomes so strong that the outer droplet, as mentioned above, transforms from an ellipsoid into a drop-like shape. Furthermore, the surfactant enriched moiety of the outer droplet shift to positions closer to the poles of the DE. As illustrated in Figure 4C, this is caused by the hydrodynamic flow topology of the continuous phase, which at this stage can no longer be assumed to have the profile of the classic *Poiseuille* flow.

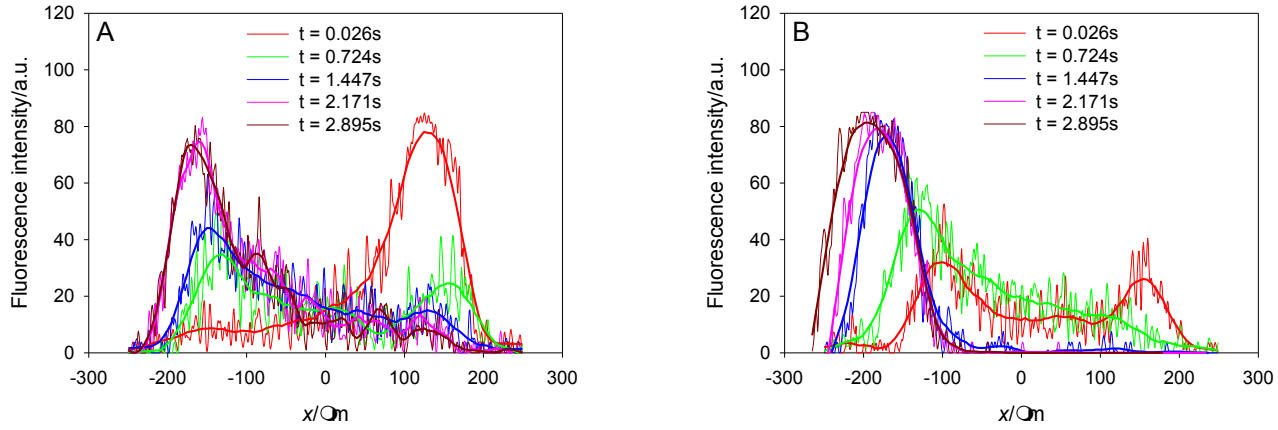

Figure 7. Fluorescence intensity profiles, stemming from the rhodamine B labeled phospholipids confined in the outer oil droplet of the double emulsion, recorded at various flow times. The abscissa refers to the axial position with respect to the center of the core drop. (A) With no surfactant present, *i.e.,* [DMPC] = 0%, in the oil phase, a gradual displacement of the oil from the front to the rear of the double emulsion occurs, until a steady-state topology is reached. (B) With [DMPC] = 0.1% (w/w), the displacement occurs more rapidly, and the middle droplet deformation extents further away from the center of the core drop. Thick lines represent the raw data smoothed using second-degree polynomials.

Instead, bearing in mind that the DE still moves faster than the average velocity of the continuous phase, a pressure drop behind the DEs will cause the continuous phase to accelerate. As the pressure drop is larger at the boundary walls of the tube, *i.e.,* where the velocity difference between the droplet and the continuous phase is largest, the continuous phase will respond by forming vortices resembling the dashed elliptic arrows in Figure 4C. These will in turn induce a vortex flow within the middle droplet, as illustrated by the solid elliptic arrows in Figure 4C, causing a build-up of surfactant at the stagnatio displayed by the change in the fluorescence intensity 0.5% (w/w), as shown in Figure 8. Here, the intensi , plotted with respect to the transverse axis of the capi e middle droplet superseded by localized surfactant bui he later stage.

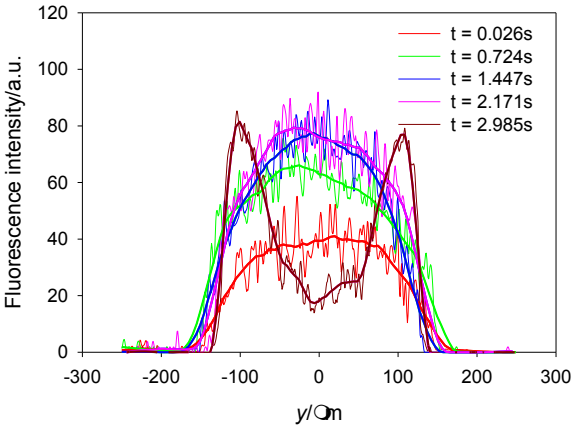

Figure 8. Fluorescence intensity profiles, stemming from the rhodamine B labelled phospholipids confined in the outer oil droplet of the double emulsion, recorded at various flow times. The abscissa refers to the transverse position with respect to the center of the core drop. For [DMPC] = 0.5% (w/w), the initial displacement of the middle droplet is superseded by localized surfactant build-up induced by vortices within the middle droplet. Thick lines represent the raw data smoothed using second degree polynomials.

The tip-streaming observed at high surfactant concentrations, and hence at high capillary numbers, was further investigated by increasing the concentration of the viscosity modulator PVA in the continuous phase. This not only increases the shearing force between the oil phase and the continuous phase, but simultaneously lowers the interfacial tension. In fact, for [PVA] = 5% (w/w), the interfacial tension was measured to 0.09 mNm^{-1}, and no detectable decrease in the interfacial tension was observed for the water-PVA-chloroform/DMPC system for higher concentrations of PVA (see Figure 6A). Hence, the change in droplet topology under these conditions becomes isolated to a matter of viscous forces only. Figure 9 show this effect as the PVA concentration is increased from 5 over 7.5 to 10% (w/w). In the formation process, the decrease in viscosity ratios between the inner and outer aqueous phases, μ_I/μ_O, (0.45, 0.23 and 0.13 for 5, 7.5 and 10% PVA, respectively), causes the drops to break up at higher frequencies, thus generating DEs of gradually smaller dimensions. Compared with the case of $\mu_I/\mu_O = 1$, the lower viscosity ratios changes the nature of deformation of the DEs dramatically. Instead of a displacement of the outer droplet to the rear of the core, the oil phase maintain to completely engulf the core droplet as the latter is deformed into a drop-like shape. This deformation of the DE continues until tubes are extruded at the rear, which eventually reach its *Rayleigh-Plateau* instability where smaller droplets are formed by tip-streaming; see Figure 9A-3, B-3 and C-3. These images are recorded at different positions, and thus different flow times, after the formation, with the tip-streaming occurring at an earlier stage for higher PVA concentrations: Plotting the flow time as a function of the viscosity ratio μ_I/μ_O, a linear relationship is obtained, as shown in Figure 10A. The deformation parameter D as defined in Eq.1, calculated using values of B and L obtained just prior to the tip-streaming, show a similar trend, as displayed in Figure 10B.

The viscosity ratio not only affects the size of the as formed DEs, but also influences the relative velocity of the DEs with respect to the continuous phase. As the DEs travel the capillary tube, they push the continuous phase against the capillary walls since the *Laplace* pressure in the drop being higher than the pressure of the external phase. Simultaneously, the DEs push the continuous phase in the direction of the flow due to viscous entrainment.

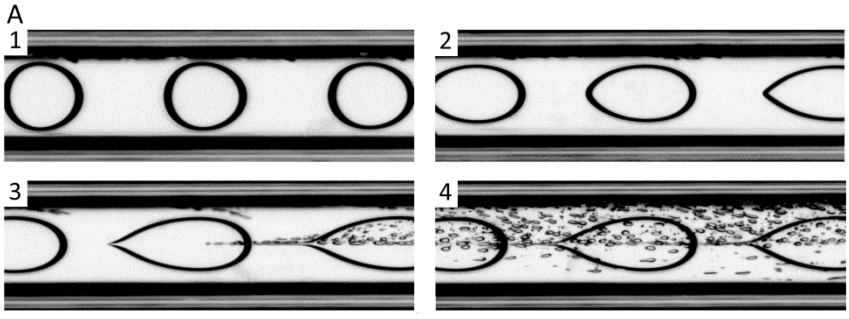

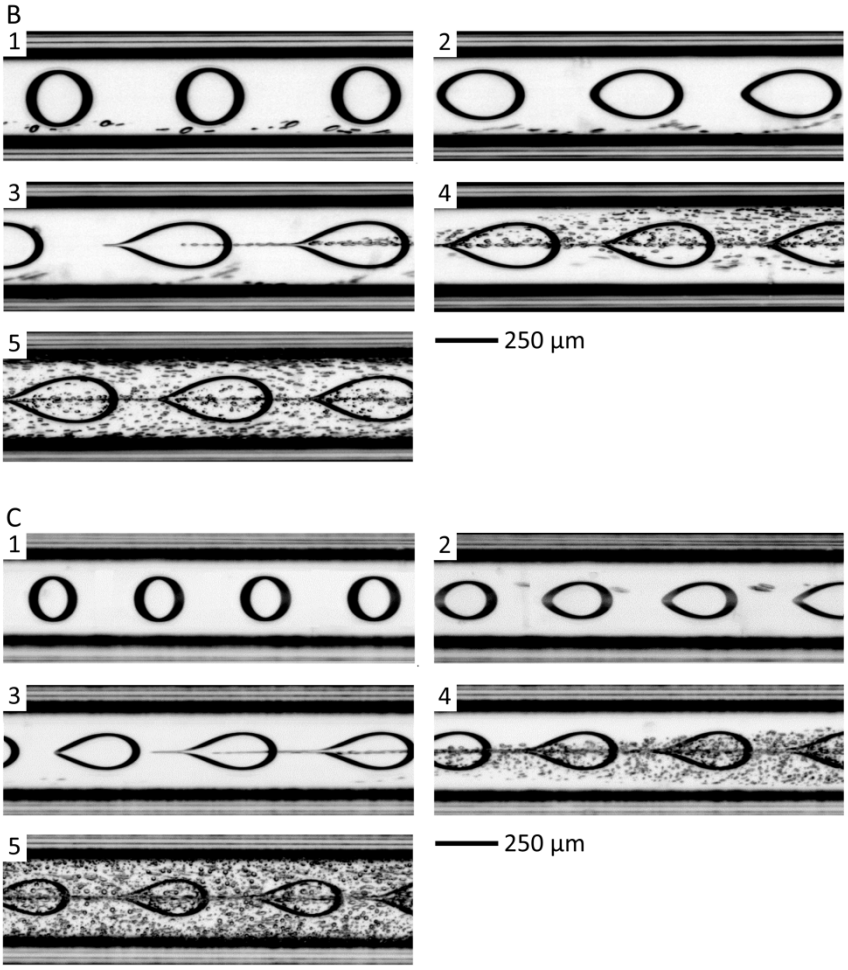

Figure 9. Optical images showing the effect of the viscosity of the continuous flowing phase. The increasing viscosity, obtained by changing the concentration of PVA in the continuous phase (5, 7.5 and 10% w/w for (A), (B) and (C), respectively) results in a decrease in size of the double emulsions. The shape of the double emulsions changes to a more drop-like conformation compared to the observations obtained at 2% PVA. The numbering of the images does in this case not refer to identical positions of the capillary tube. Flow rates applied: Q_1 (H_2O/2% w/w PVA) = 4.17 x 10^{-4} cm^3s^{-1}, Q_2 (chloroform/1% w/w DMPC) = 1.67 x 10^{-4} cm^3s^{-1} and Q_3 (H_2O/various concentration of PVA) = 4.17 x 10^{-4} cm^3s^{-1} (that is, an average velocity of the continuous flowing phase of 0.21 cms^{-1}). Velocity of double emulsions = 0.62, 0.80 and 1.01 cms^{-1} for (A), (B) and (C), respectively.

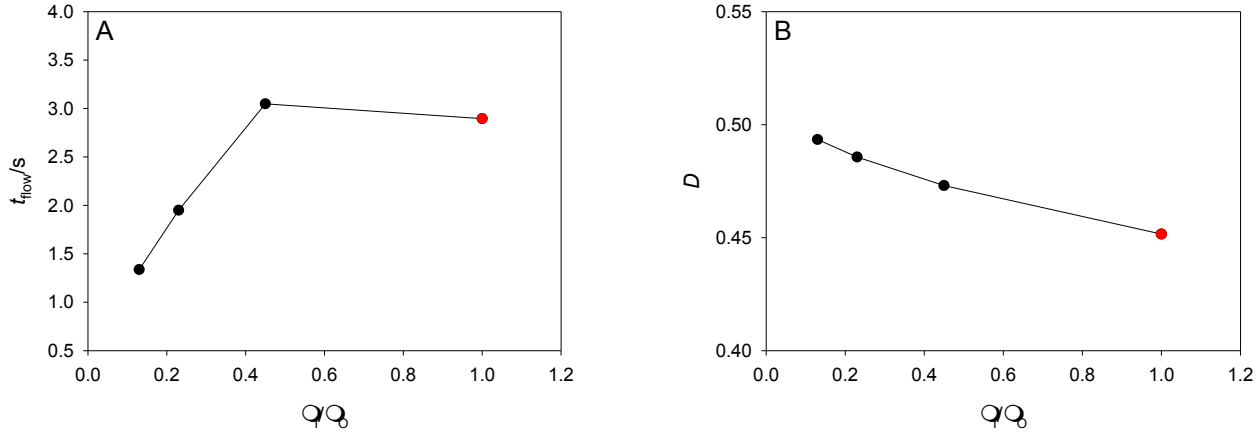

Figure 10. (A) Effect of the viscosity ratio between the core and the continuous phase on the time to establish tip-streaming as a result of capillary instability. A linear relationship is found for double emulsions with μ_I/μ_O below 0.5, all adapting the same drop-like topology upon interfacial shearing. The red point corresponds to Figure 3D-5, and is included for comparison. (B) The deformation parameter D shows a linear relationship spanning all values of μ_I/μ_O investigated.

Due to the viscous drag exerted by the tube walls on the continuous phase, a stagnant film is formed, which thickness depends on the viscosity of the external phase and, thus, the droplet capillary number, Ca_d. It has been reported, that for small capillary numbers, a nonlinear relation for the ratio of film thickness e and the tube diameter H is given by $e/H \propto Ca_d^{2/3}$. In our case however, for capillary numbers closer to unity, we find from the slope in Figure 10A the exponent to be quite smaller, namely 0.14, thus yielding the expression

$$\frac{e}{H} \propto Ca_{de}^{0.14} \qquad \text{Eq. 2}$$

with Ca_{de} being the capillary number of the DE. In the reference frame of the DE, the difference between the mean velocity of the continuous phase, v_{cont}, and the velocity of the DE, v_{de}, results in a

net flux of the continuous phase expressed as $Q_{cont} = S(v_{cont} - v_{de})$, where S is the cross sectional area of the capillary tube. Our findings suggest that Q_{cont} scales nonlinearly with the droplet capillary number and the droplet velocity v_{de}, as $Q_{cont} \propto -Ca_{de}^{0.14} S v_d$. In the reference frame of the DE, the liquid phase surrounding the DEs is advected backwards with a velocity of $-v_{de}$. Hence, the DE should move faster than the continuous phase by an amount of

$$\frac{v_{de} - v_{cont}}{v_{de}} \propto Ca_{de}^{0.14} \qquad \text{Eq. 3}$$

which is in good accordance, see Figure 11B, with the experimental results obtained from Figure 9.

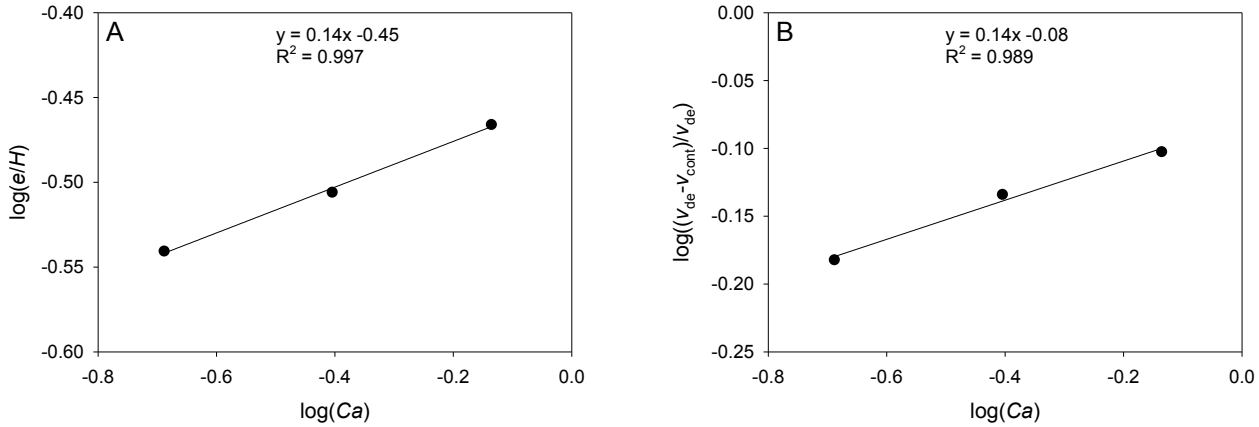

Figure 11. (A) A plot of log(e/H) vs. log(Ca) provides the exponent for eq. 2. (B) A plot of $\log((v_{de}-v_{cont})/v_{de})$ vs. log(Ca), derived from eq. 3, with the same exponent as in eq. 2 fits the experimental data obtained from Figure 9.

Considering the extruded tube as an coaxial fluid cylinder, the time of formation of the daughter drops formed by the tip-streaming, t_{pinch}, has been reported to be proportional to the tube radius, R_t, the viscosity-to-interfacial tension ratio, and a constant C, which depends on the viscosity ratio between the inner and outer liquid phases, μ_I/μ_O:[2]

$$t_{pinch} = \frac{C R_t \mu_O}{\gamma} \qquad \text{Eq. 4}$$

For the range of viscosity ratios considered here, C has a value of ~0.2.[48] From Figure 9A-3, B-3 and C-3, the values of R_t just prior to the first drop pinch-off can be found, and thus provide calculated values of t_{pinch}. Experimental values of t_{pinch} were likewise deduced from the recordings

of the tip-streaming. Figure 12 show both the calculated and the experimental values of t_{pinch}, with the experimental values being 1.4 to 3.3 times higher than the calculated. The discrepancy between the two values of t_{pinch} can be explained by a local variation in surface tension: According to *eq*. 4, γ must be smaller than the value measured for a static drop. This is in line with the observed accumulation of surfactant at the rear of the outer droplet of the DEs, of which is the part feeding the tube extrusion. Hence, the local capillary number will be smaller, facilitating the droplet pinching.

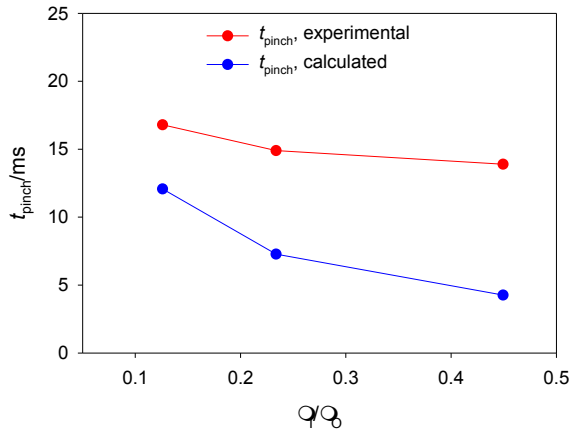

Figure 12. Plot of the droplet pinching time, t_{pinch}, as a function of the viscosity ratio μ_I/μ_O between the core drop and the continuous phase. The calculated values of t_{pinch} are from *eq*. 4, using values of γ measured for steady pendant drop systems.

The change in topology of the DEs, for viscosity ratios below unity, is as mentioned above, quite different from the case where the viscosity of the core and the continuous phase are identical. In the former case, the core droplet apparently extends into the tube extruded from the outer droplet. Thus, it would be expected that the daughter droplets formed by the tip-streaming are DEs also. That this is indeed the case was demonstrated by encapsulating fluorescein in the core drop and rhodamine labelled phospholipids in the oil phase. Figure 13 shows optical and fluorescence images of the tip-streaming of DEs at two different positions in the capillary tube. Figure 13A-1 and A-2 display the tube extrusion just prior to the tip-streaming, the latter clearly showing the surfactant rich part of the outer droplet by its red colour. Figure 13B-1 and B-2 show DEs a short distance down-stream the position where the tip-streaming is initiated. The daughter droplets clearly appear as green moieties in the fluorescent image. This is only possible if they are engulfed in an oil film, preventing them from merging with the continuous phase, thus showing that these are in fact DEs. The absence of red colour in the oil film are due to the small amount of rhodamine B present here,

not being sufficient for detecting under the applied dynamic experimental conditions. However, when collected on a microscope slide, and thus monitored under static conditions enabling longer exposure times, the red colour stemming from the rhodamine B labelled phospholipids are clearly visible, see Figure 14.

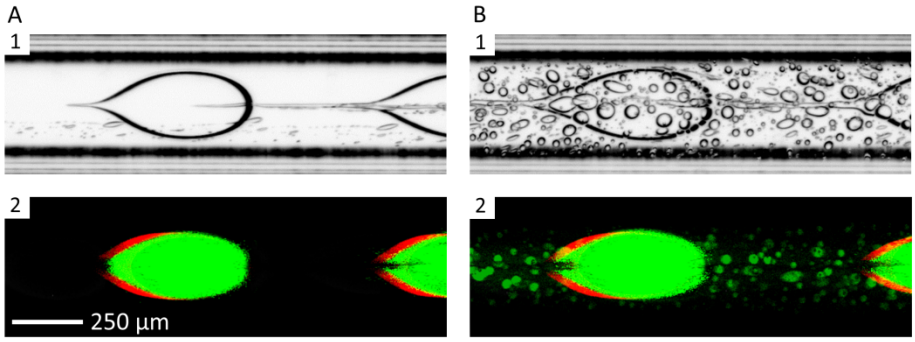

Figure 13. Optical and fluorescence images of (A) prior to tip-streaming and (B) at a position where tip-streaming has been initiated. Flow rates applied: Q_1 (H_2O/2% w/w PVA and 0.02% w/w fluorescein) = 4.17 x 10^{-4} cm^3s^{-1}, Q_2 (chloroform/various concentrations of DMPC and 0.02% w/w rhodamin B labelled phospholipid) = 1.67 x 10^{-4} cm^3s^{-1} and Q_3 (H_2O/2% w/w PVA) = 1.67 x 10^{-4} cm^3s^{-1} (that is, an average velocity of the continuous phase of 0.09 cms^{-1}). Velocity of double emulsions = 0.44 cms^{-1}.

The phenomenon of tip-streaming of DEs observed under shear flow resulting in the generation of smaller DEs may open new perspectives and possibilities in the field of encapsulation and release of cargos encapsulated inside a mother DE. After having evidenced that the daughter droplets are true DEs, we have decided as a proof of concept to demonstrate the generation of magnetic daughter DEs with different sizes (5-32 µm) from a mother DE encapsulating magnetic nanoparticles. The as formed DEs, and the daughter droplets formed by tip-streaming, were collected on a microscope slide and exposed to an external magnetic. Figure 15 display the droplets before and after being exposed to the magnetic field, showing the movement of both mother and daughter drops that tend to align parallel to the direction of the magnetic field, thus confirming that the magnetic nanoparticles were indeed encapsulated in daughter DEs formed by the tip-streaming.

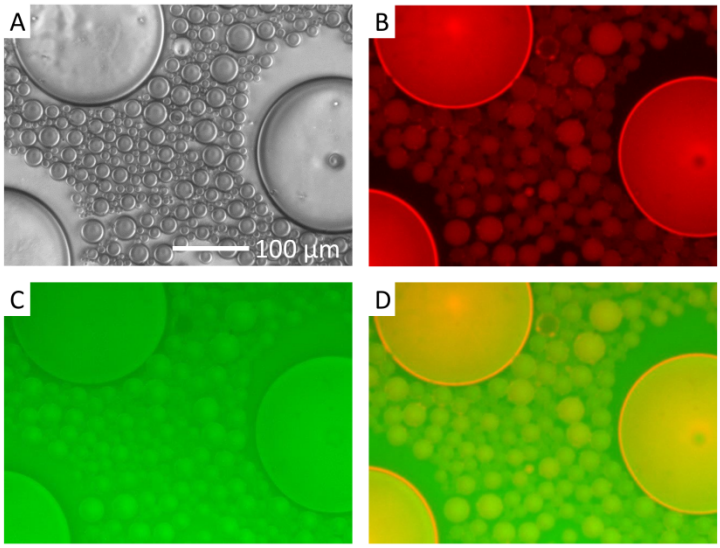

Figure 14. (A) Optical and (B and C) fluorescent images showing the double emulsions, generated under the same conditions as in Figure 13, and collected on a microscope glass slide. This enabled long exposure recordings showing both (B) the rhodamine B contained in the oil shell, and (C) the encapsulated fluorescein of the small double emulsions. (D) display a superimposition of the images (B) and (C).

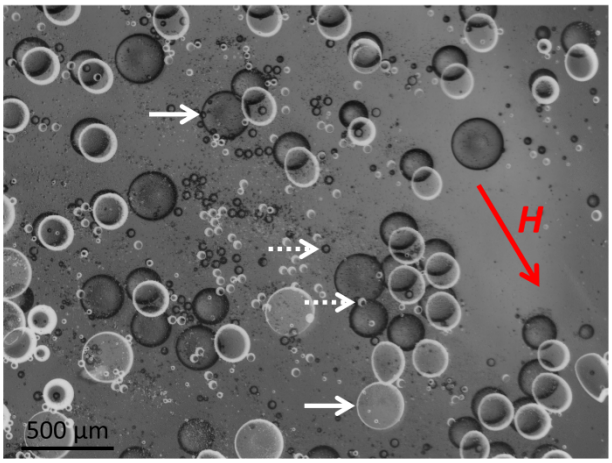

Figure 15. A further evidence of the formation of double emulsions upon the tip-streaming was provided by adding magnetic nanoparticles to the inner phase (and thereby being encapsulated in the double emulsions). By collecting the large and small double emulsions formed under the same conditions as in Figure 14, but here diluted in a 5% PVA solution, it was possible to monitor the motion of the double emulsions under the influence of a magnetic field. The white arrow/dark circular structure shows a large double emulsion before applying the magnetic field (direction indicated by the red arrow). The white arrow/white structure shows the position of the same double emulsion after 10s. The dashed white arrow/dark structure and dashed white arrow/dark structure shows the same scenario for a small double emulsion as formed by the tip-streaming.

CONCLUSION:

The behavior of w/o/w double emulsions (DE) generated in a microfluidic device, using the phospholipid 1,2-dimyristoyl-sn-glycero-3-phosphocholine (DMPC) as surfactant and chloroform as the oil phase, was herein reported. We showed, with this composition of the oil phase, that the dynamic behavior of the DEs under flow gives rise to different phenomena such as deformation and tip-streaming. To the best of our knowledge, this has never reported previously for DEs. When the DEs were generated using the same composition and viscosity in the core as well in the outer continuous flowing phase, the concentration of DMPC showed to have significant impact on the nature and degree of deformation of the middle phase. For DEs with the same viscosity of the core and the outer continuous phase, the shape of the core remained practically unperturbed, while increasing the viscosity of the continuous phase resulted in the DEs adapting a pear-like shape. In the latter case, due to the interfacial shearing, tubes were gradually extruded at the rear of the DEs. These eventually reached a *Rayleigh-Plateau* instability condition, resulting in pinch off, or tip-streaming, at the tube extremity, by which smaller (daughter) DEs were formed. The deformation and tip-streaming were monitored by optical fluorescence microscopy; the latter enabled by incorporating rhodamine B labelled phospholipids in the middle phase, and encapsulating fluorescein in the core drop. This furthermore provided evidence for the fact that the daughter droplets, generated by tip-streaming from the mother DEs, are also w/o/w DEs, as the former exhibited the same core-shell behavior. Tip-streaming may open new possibilities related to the release of encapsulated substances from a cargo under flow. As a proof of concept, we generated magnetic daughter DEs with different sizes (5-32 um) from a magnetic mother DE under flow.

REFERENCES:

1. R. S. Kane, A. D. Stroock, N. Li Jeon, D. E. Ingber and G. M. Whitesides, in *Optical Biosensors*, eds. F. S. Ligler and C. A. R. Taitt, Elsevier Science, Amsterdam, 2002, DOI: http://dx.doi.org/10.1016/B978-044450974-1/50018-5, pp. 571-595.
2. A. S. Utada, E. Lorenceau, D. R. Link, P. D. Kaplan, H. A. Stone and D. A. Weitz, *Science*, 2005, **308**, 537-541.
3. C. Martino, S.-H. Kim, L. Horsfall, A. Abbaspourrad, S. J. Rosser, Cooper, J. and D. A. Weitz, *Angew. Chem. Int. Ed.*, 2012, **51**, 6416–6420.
4. S.-H. Kim, H. C. Shum, J. W. Kim, J.-C. Cho and D. A. Weitz, *Journal of the American Chemical Society*, 2011, **133**, 15165-15171.
5. F. Meng, G. H. M. Engbers and J. Feijen, *Journal of Controlled Release*, 2005, **101**, 187-198.
6. M. Marguet, L. Edembe and S. Lecommandoux, *Angewandte Chemie*, 2012, **124**, 1199-1202.
7. J. Thiele, V. Chokkalingam, S. Ma, D. A. Wilson and W. T. S. Huck, *Materials Horizons*, 2014, **1**, 96-101.
8. S. Skeie, *Int. Dairy J.*, 1994, **4**, 573-595.
9. D. J. McClements, *Current Opinion in Colloid & Interface Science*, 2012, **17**, 235-245.
10. C. D. Eggleton, T.-M. Tsai and K. J. Stebe, *Physical Review Letters*, 2011, **87**, 048302-048301 - 048302-048304.
11. P. Fischer, S. F. M. Kaufmann, N. Maag, K. Maruyama, C. Cramer and E. J. Windhab, *Chemie Ingenieur Technik*, 2001, **73**, 740-741.
12. S. L. Anna, N. Bontoux and H. A. Stone, *Applied Physics Letters*, 2003, **82**, 364-366.
13. D. R. Link, S. L. Anna, D. A.Weitz and H. A. Stone, *Physical Review Letters*, 2004, **92**, 054503-054501 - 054503-054504.
14. X. Li and K. Sarkar, *Journal of Rheology*, 2005, **49**, 1377-1394.
15. X. Zhao, *Journal of Rheology (1978-present)*, 2007, **51**, 367-392.
16. C. Cramer, P. Fischer and E. J. Windhab, *Chemical Engineering Science*, 2004, **59**, 3045-3058.
17. F. Abbassi-Sourki, M. Bousmina and M. A. Huneault, *Rheologica Acta*, 2012, **51**, 111-126.
18. A. Ramachandran, K. Tsigklifis, A. Roy and G. Leal, *Journal of Rheology*, 2012, **56**, 45-97.
19. C.-X. Zhao and A. P. J. Middelberg, *Chemical Engineering Science*, 2011, **66**, 1394-1411.
20. N. Boruah and P. Dimitrakopoulos, *Journal of Colloid and Interface Science*, 2015, **453**, 216-225.
21. C. N. Baroud, F. Gallaire and R. Dangla, *Lab on a Chip*, 2010, **10**, 2032-2045.
22. H. A. Stone, *Annual Review of Fluid Mechanics*, 1994, **26**, 65-102.
23. a. R E Johnson and S. S. Sadhal, *Annual Review of Fluid Mechanics*, 1985, **17**, 289-320.
24. J. Guzowski, P. M. Korczyk, S. Jakiela and P. Garstecki, *Soft Matter*, 2012, **8**, 7269-7278.
25. H. Hua, J. Shin and J. Kim, *International Journal of Heat and Fluid Flow*, 2014, **50**, 63-71.

26. Y. Chen, X. Liu and M. Shi, *Applied Physics Letters*, 2013, **102**, 051609.
27. Y. Chen, X. Liu and Y. Zhao, *Applied Physics Letters*, 2015, **106**, 141601.
28. S. Ma, W. T. S. Huck and S. Balabani, *Lab on a Chip*, 2015, **15**, 4291-4301.
29. J. Tao, X. Song, J. Liu and J. Wang, *Chemical Engineering Science*, 2013, **97**, 328-336.
30. H. Chen, J. Li, H. C. Shum, H. A. Stone and D. A. Weitz, *Soft Matter*, 2011, **7**, 2345-2347.
31. M. Zagnoni, *Lab on a Chip*, 2012, **12**, 1026-1039.
32. S. Matosevic, *Bioessays*, 2012, **34**, 992-1001.
33. J. Thiele, A. R. Abate, H. C. Shum, S. Bachtler, S. Förster and D. A. Weitz, *Small*, 2010, **6**, 1723-1727.
34. T. M. Allen and P. R. Cullis, *Adv. Drug Deliver Rev.*, 2013, **65**, 36-48.
35. B. Herranz-Blanco, L. R. Arriaga, E. Makila, A. Correia, N. Shrestha, S. Mirza, D. A. Weitz, J. Salonen, J. Hirvonen and H. A. Santos, *Lab on a Chip*, 2014, **14**, 1083-1086.
36. F. Kong, X. Zhang and M. Hai, *Langmuir*, 2014, **30**, 3905-3912.
37. W. J. Duncanson, T. Lin, A. R. Abate, S. Seiffert, R. K. Shah and D. A. Weitz, *Lab on a Chip*, 2012, **12**, 2135-2145.
38. S. A. Nabavi, G. T. Vladisavljević, S. Gu and E. E. Ekanem, *Chemical Engineering Science*, 2015, **130**, 183-196.
39. L. R. Arriaga, S. S. Datta, S.-H. Kim, E. Amstad, T. E. Kodger, F. Monroy and D. A. Weitz, *Small*, 2014, **10**, 950-956.
40. H. C. Shum, J.-W. Kim and D. A. Weitz, *J. Am. Chem. Soc.*, 2008, **130**, 9543-9549.
41. S.-H. Kim, J. W. Kim, J.-C. Cho and D. A. Weitz, *Lab on a Chip*, 2011, **11**, 3162-3166.
42. K. Torbensen and A. Abou-Hassan, *Journal of Flow Chemistry*, 2015, **5**, 234-240.
43. R. Massart, *IEEE Transactions on Magnetics*, 1981, **17**, 1247-1248.
44. A. S. Utada, L.-Y. Chu, A. Fernandez-Nieves, D. R. Link, C. Holtze and D. A. Weitz, *MRS Bulletin*, 2007, **32**, 702-708.
45. A. S. Utada, A. Fernandez-Nieves, H. A. Stone and D. A. Weitz, *Physical Review Lettters*, 2007, **99**, 094502-094501 - 094502-094504.
46. G. I. Taylor, *Proceedings of the Royal Society of London A: Mathematical, Physical and Engineering Sciences*, 1934, **146**, 501-523.
47. D. T. Papageorgiu, *Interfacial Phenomena and the Marangoni Effect*, Springer-Verlag, New York, 2002.
48. H. A. STONE, B. J. BENTLEY and L. G. LEAL, *J. Fluid Mech.*, 1986, **173**, 131-158.

Conclusion and Perspectives

CONCLUSION:

The final objective of this thesis is to develop a reliable platform for generating communicative networks of liposomes, encapsulating the Belousov-Zhabotinsky reaction as source of information or a transmitted signal, and to study the dynamics of such a system. To reach this goal, several issues were addressed by following a bottom-up and multi-scale approach.

We investigated the interaction between both bulk DMPC liposomes and liposomes doped with cholesterol, myristic acid, tetradecylsulfate, tetradecylamine, and the species involved in the BZ-reaction by using small angle X-ray scattering (SAXS) and UV-visible spectrophotometry. Structural data on the liposome membranes evidenced a partial penetration of the BZ species within the lipid bilayers, in particular ferroin. However, the DMPC liposomes showed to exert only small perturbations to the BZ oscillating behaviour. When introduced to the lipid membrane, cholesterol showed to perturb the oscillatory behaviour, due to chemical interactions between the BZ inhibitor bromine and the double bond in cholesterol.

A reliable BZ-system, compatible with the viscosity modulator polyvinyl alcohol was chosen for studying chemical communication of simple emulsions, stabilized by lipid membranes with different composition. 1D arrays of micro-droplets were fabricated by encapsulating the BZreaction into microdroplets by means of microfluidics. The communication between adjacent droplets mainly exhibited an inhibitory character, governed by the prominent role of Br_2, thus exhibiting a higher permeability towards phospholipid membranes with respect to the activator

$HBrO_2$. With cholesterol present in the lipid membrane, bromine was suppressed to pass from one droplet to another, thus allowing for a weak activatory coupling.

We demonstrated an easy to assemble/disassemble and robust design for a microfluidic devise with adjustable geometry for generating monodisperse water-in-oil-in-water double emulsions. The adjustability of the flow focusing part of the device, allowed for varying the oil shell thickness, while maintaining the core size. These features are of paramount importance for using double emulsions as a model of microreactors in aqueous solution, and later as templates for liposomes.

Finally, the behaviour of w/o/w double emulsions generated in a microfluidic device, using phospholipids as surfactant and chloroform as the oil phase, was reported. We showed, with this composition of the oil phase, that the dynamic behavior of the double emulsions under flow gave rise to different phenomena, such as deformation and tip-streaming. The latter resulted in the formation of smaller daughter droplets, exhibiting the same core-shell features as the mother drops. Tip-streaming may open new possibilities related to the release of encapsulated substances from a cargo under flow. As a proof of concept, we generated magnetic daughter double emulsions with from a magnetic mother double emulsion under flow. Furthermore, since oil is removed from the double emulsion middle layer, this method might proof valuable for the generation of liposomes.

PERSPECTIVES:

Having obtained a fair insight into the interaction and dynamics of the BZ-reaction with lipid interfaces, both in bulk solution and when confined in networks of simple emulsion droplets stabilized by lipid layers, and with the development of a reliable microfluidic platform for generation of BZ-encapsulating double emulsions, a route to produce and understand the dynamics of BZ-encapsulating liposomes has been established. The remaining tasks to fulfil this objective will be the development of a protocol for solvent removal from the oil shell of the double emulsions. Based on results obtained in this thesis, the use of chloroform as the only liquid constituent of the oil shell seems promising. The “tip-streaming approach” provides an alternative route for solvent removal from double emulsions, and should be investigated further for a more profound insight on the dynamics governing this process. To avoid lipid aggregation in the resulting membranes, optimization of the original lipid concentration is needed. The inhibition of the BZ-

reaction during the solvent removal is of paramount importance, and a reliable experimental platform must be developed. When these tasks are fulfilled, the generation and investigation of BZ-encapsulating liposomes in networks can be conducted.